Interpolation et rééchantillonnage de données spatiales et application à la cartographie urbaine et à la détermination du fond cosmique primordial

Svitlana Zinger

Thèse

présentée pour obtenir le grade de docteur
de l'Ecole Nationale Supérieure des Télécommunications

Spécialité: **Signal et Images**

Svitlana Zinger

Interpolation et rééchantillonnage de données
spatiales et application à la
cartographie urbaine et à la détermination
du fond cosmologique primordial

Composition du Jury:
Bernard Chalmond   Rapporteur
Annick Montanvert   Rapporteur
Laure Blanc-Féraud   Examinateur
Jacques Delabrouille   Examinateur
Michel Roux   Examinateur
Henri Maître   Directeur de thèse

Acknowledgements

I would like to express my gratitude to the director of my thesis, Professor Henri Maître who provided me this great opportunity to work towards a Ph.D. degree at one of the best institutes of France. I appreciate very much his constant support and attention during all my time in ENST. His help and encouragement were crucial for my thesis. I am also thankful to Michel Roux, the co-director of my thesis, for all his help and practical advices that made my progress faster and easier.

I would like to thank to the members of the jury of my thesis. I thank Professors Bernard Chalmond and Annick Montanvert for writing reports on my thesis and their suggestions. The comments of Annick Montanvert helped me very much to improve the text of my thesis. I appreciate her help very much. I thank very much to Laure Blanc-Féraud and to Jacques Delabrouille for accepting to participate in the jury of my thesis. I am especially thankful to Jacques Delabrouille for providing me the cosmic microwave background data, for discussions and suggestions on this topic.

I am thankful to Olivier de Joinville for providing me the laser scanning data and for helping me to understand it. Many discussions with Mila Nikolova, Evgeniy Pecherskiy, Yann Gousseau made me realize the theoretical issues of cost function based methods and minimization problems. I thank them very much.

I would like to convey my feelings to all the TSI faculty members, postdoc fellows, Ph.D. students (Jasmine, Yong, Céline, Carlos, Eve, Daniel, Alejandro, Tony, Dalila, Saeid, David, Antonio and others). It was my pleasure to work and communicate with them.

Abstract

In this thesis we study interpolation methods for irregularly distributed spatial data. We consider the resampling problem applied to the altimetry measures on an irregular grid obtained by airborne laser scanning. This type of data is irregularly spaced and a resampling on a regular grid is necessary in order to generate a digital elevation model (DEM). Some well-known methods are considered: linear triangle-based interpolation, nearest neighbor interpolation, and kriging. We propose an energy minimization approach which allows to avoid the drawbacks of the methods mentioned above. This approach imposes a model of a surface that corresponds to urban areas. The energy function is adapted for irregularly distributed data. The methods are tested on two sets of irregularly distributed spatial points acquired by a laser scanner on Brussels and Amiens. These data sets have different sampling patterns and therefore let us better analyse the performance of the methods. We also applied these methods as well as binning for determination of cosmic microwave background.

Résumé

Les problèmes d'interpolation sont fondamentaux dans de nombreux domaines des sciences appliquées, en particulier en traitement du signal et des images. L'avènement des technologies numériques a en effet contribué au développement de techniques de mesure fournissant des valeurs discrétisées des signaux à acquérir. Il apparaît capital de disposer de méthodes d'interpolation adaptées à la physique du signal, et donc à l'éventuelle irrégularité spatiale des grilles discrètes représentant ces mesures. Dans ce cadre, un modèle a priori du signal est souvent utile.

Si de nombreuses méthodes de traitement d'image sont bien connues pour les traitements de données construites sur une grille régulière, il n'en est pas de même pour les données sur grille irrégulière et sur grille avec gigue. Ces types de grilles se rencontrent en particulier en télédétection : bien que, dans le meilleur des cas, les mesures soient régulièrement échantillonnées dans le référentiel du capteur, les points 3D géoréférencés correspondants sont irrégulièrement espacés dans le référentiel terrestre. L'interpolation et le rééchantillonnage des données originales sur une grille régulière permettent de les traiter et de les analyser. En effet, des traitements tels que la visualisation, la segmentation, la fusion, etc. nécessitent souvent d'avoir une grille régulière.

Le nombre important de techniques d'interpolation disponibles aujourd'hui se réduit considérablement lorsque l'on veut interpoler des valeurs distribuées sur une grille irrégulière. C'est la problématique que l'on considère dans le cadre de cette thèse. Nous traiterons en particulier la question complexe de l'interpolation d'un signal à bande non limitée et dont les mesures sont dispersées dans l'espace. Cette question est envisagée à partir de données du levé laser aéroporté acquises sur des zones urbaines. En effet, dans les zones urbaines, les bords des bâtiments forment des discontinuités conduisant à un signal à bande non limitée.

La création de modèles 3D de villes est importante pour plusieurs raisons. Elle permet par exemple la création et la mise à jour des systèmes d'information géographiques, la planification urbaine et les projets de développement censés empêcher la dispersion des substances polluantes, ou encore la planification de réseau de transport et le positionnement des antennes de télécommunication. La télédétection sur des zones urbaines est un des outils permettant de construire les représentations des villes en réalité virtuelle 3D. Cette technique autorise, par levé laser aéroporté, une acquisition rapide et précise de données en cours de test sur des zones urbaines. Dans la première partie de cette thèse, nous nous intéressons à cette technique en présentant l'état des recherches qui la concernent. Ceci nous permet de comprendre la nature des données

3

acquises, notamment en ce qui concerne le bruit et la précision des mesures. De tels paramètres sont également utiles au développement d'une méthode d'interpolation appropriée.

La deuxième partie de la thèse est consacrée à l'interpolation des données du fond cosmologique primordial (CMB - Cosmic Microwave Background). Ce type de données se caractérise également par une grille irrégulière et représente une surface à interpoler lisse en l'absence de déconvolution. L'acquisition et le traitement des données du fond cosmologique primordial est d'un grand intérêt scientifique. En effet, la cosmologie (science qui étudie l'origine de notre univers) a construit des modèles de l'univers, dont les paramètres peuvent déterminer son âge, sa forme et la matière qui la constitue. Ces paramètres, qui doivent être calculés à partir des cartes du CMB, nécessitent une grille régulière, ce que les mesures originelles ne fournissent pas. Nos travaux permettent de résoudre, de manière originale, cette difficulté.

La thèse s'organise plus précisément de la façon suivante. Dans le chapitre 1, on s'intéresse aux aspects théoriques d'échantillonnage. Avant de nous attaquer aux théories d'échantillonnage irrégulier, nous commençons ce chapitre par le théorème bien connu de Shannon, fondamental pour la recherche ultérieure sur l'échantillonnage. Nous mettons en évidence, parmi des problèmes d'échantillonnage irrégulier, celui de la taille optimale de grille. Ce problème difficile n'a pas été traité en profondeur dans cette thèse, et il pourrait constituer un axe de recherche à part. Cependant, certaines voies à envisager pour le résoudre sont possibles. Par exemple, on peut proposer les suivantes : les mesures de densité de l'information, l'étude des degrés de liberté ou encore l'approche en termes de minimum d'entropie. Dans ce chapitre, nous considérons une classification des grilles d'échantillonnage en prenant en compte une ou deux dimensions. Nous étudions également la théorie de l'échantillonnage non-uniforme et aléatoire qui correspond aux données dont nous disposons. Ceci constitue un domaine particulièrement important de la recherche actuelle en mathématiques pures et appliquées.

Dans le chapitre 2, nous étudions la technique du levé laser aéroporté : sa précision, ses propriétés, ainsi que les paramètres des systèmes existants de balayage à laser. Les applications pratiques de ce type de données sont aussi envisagées. De nombreux points techniques sont abordés dans ce chapitre dans la mesure où, dans les méthodes d'interpolation présentées et appliquées dans les chapitres suivants, nous voulons tenir compte non seulement de la forme et des propriétés de la surface balayée, mais également de la technique d'acquisition. Nous analysons également les sources de bruit. Nous montrons l'intérêt porté par la recherche à cette technique et son application à l'étude des zones urbaines.

Le chapitre 3 décrit les approches générales pour l'interpolation de données irréguliè-rement espacées et présente également les méthodes que nous employons dans les expérimentations sur les données réelles. Les deux premières méthodes décrites sont l'interpolation au plus proche voisin et l'interpolation linéaire basée sur le triangle. Ces méthodes présentent l'avantage d'être rapides et simples mais aussi certaines lim-ites. Nous les envisageons à travers des résultats obtenus afin de pouvoir proposer une approche mieux adaptée à nos données. La troisième méthode décrite est le krigeage.

Elle est développée en géostatistique pour l'interpolation de données irrégulièrement espacées. Nous montrons que ses hypothèses restent valides pour les anisotropies du fond cosmologique primordial. Nous présentons également les résultats de cette méthode sur des données de laser aéroporté. En effet le problème de l'interpolation de données irrégulièrement espacées peut être considéré comme un problème inverse mal-posé. Nous présentons enfin une méthode de minimisation d'énergie que nous adaptons aux données de laser. Nous utilisons les fonctions potentielles qui sont connues pour leur propriété de préservation des discontinuités. Nous proposons une définition du voisinage adaptée à notre problème, ainsi que l'expression de la fonction de coût et le choix de l'algorithme d'optimisation.

L'application de ces méthodes conduit à des résultats qui sont présentés dans le chapitre 4. Nous appliquons les méthodes sur deux ensembles de données réelles et évaluons ainsi les méthodes d'interpolation. En effet, les deux ensembles étant acquis par différents systèmes de balayage possèdent des propriétés différentes en termes d'échantillonnage. Cela nous permet, par comparaison des résultats avec les références, de conclure sur la performance des méthodes d'interpolation retenues.

Dans le chapitre 5, nous proposons une courte introduction à la théorie du CMB ainsi qu'à la technique d'acquisition de données de CMB. Cette technique sera utilisée en 2007 par l'Agence Spatiale Européenne, une fois le satellite Planck lancé. Cette mission fournira les données les plus précises et les plus complètes jamais acquises sur le CMB.

Le chapitre 6 présente quelques résultats sur les données simulées du CMB. Ces données respectent l'échantillonnage qui sera utilisé pour la mission Planck. Nous appliquons les méthodes d'interpolation présentées ci-dessus à ce type de données. Nous mettons également en application la technique de binning - technique utilisant une moyenne locale - souvent utilisée en astronomie. La différence principale entre les données d'anisotropies du CMB et les données de laser se situe non seulement dans le type de la surface qui est balayée mais également dans l'existence d'un bruit très fort dans les mesures d'anisotropies du CMB. Aussi ajoutons-nous un bruit blanc. Nous étudions alors les performances des méthodes retenues sur les données bruitées.

Enfin, le dernier chapitre présente les conclusions générales et propose quelques directions pour de futurs travaux.

Il existe actuellement de nombreux problèmes théoriques et appliqués qui utilisent des interpolation et échantillonnage de données spatiales irrégulièrement espacées. Dans le cadre de la thèse nous considérons certaines questions théoriques et pratiques pour deux applications dans le domaine de la télédétection :

- l'interpolation de données laser aéroporté sur des zones urbaines ;

- la détermination du fond cosmologique primordial (CMB - Cosmic Microwave Background).

L'échantillonnage de données irrégulièrement espacées constitue un champ parti-culièrement fécond de la recherche. Fondée sur les théorèmes de Shannon et de Pa-

poulis, la théorie de l'échantillonnage, ainsi que les méthodes d'interpolation actuelles, sont pour l'essentiel adaptées à des signaux et à des images à bande limitée.

Avant d'interpoler les données, nous étudions leurs techniques d'acquisition, leur précision et leurs propriétés. Cette étape est en effet essentielle puisque, même si les grilles d'échantillonnage sont semblables pour les données laser et les mesures d'anisotropies du CMB, les techniques d'acquisition diffèrent beaucoup.

Nous pouvons raisonnablement supposer que les données laser ont une bonne précision et n'ont pratiquement pas de bruit. Au contraire, les données de CMB sont très perturbées par le bruit et par les rayonnements. De plus, ces dernières sont le résultat de la convolution de la carte du ciel avec la réponse impulsionnelle du capteur.

Les propriétés de la surface à reconstruire ainsi que les techniques d'acquisition doivent donc être prises en compte. Pour l'interpolation de données laser, nous considérons que le problème est mal-posé et adaptons une fonction de coût pour les données irrégulièrement espacées. Les bords des bâtiments dans des zones urbaines formant de fortes discontinuités, nous utilisons des fonctions potentielles qui préservent les discontinuités. La minimisation d'une telle fonction de coût permet d'obtenir la surface recherchée. Les résultats de cette approche sont comparés à quelques méthodes bien connues pour l'interpolation de données irrégulièrement espacées, à savoir l'interpolation linéaire, l'interpolation au plus proche voisin et le krigeage. En utilisant la corrélation et l'erreur absolue moyenne, nous montrons que ces méthodes fournissent des résultats moins bons que la minimisation d'une fonction de coût, qui impose les propriétés désirées à la surface résultante. Quand on les compare visuellement avec l'image de référence, les images qui ont une faible erreur absolue moyenne sont plus satisfaisantes que celles avec une bonne corrélation. Les expérimentations sont faites sur deux ensembles de données réelles. Pour chacun d'entre eux, la stratégie de balayage et la densité des points étaient différentes.

Nous adaptons la fonction de coût à l'interpolation de données laser. Pour ce faire, nous avons défini un voisinage adéquat. Nous présentons et discutons les résultats obtenus avec différentes fonctions potentielles et en faisant varier le coefficient du terme de régularisation. Nous étudions de manière approfondie l'influence du choix des fonctions potentielles sur les propriétés de la surface reconstruite représentant des zones urbaines. Pour choisir la fonction potentielle d'attache aux données dans la fonction de coût, nous utilisons des résultats théoriques récents. Pour les données laser, le choix classique de la fonction quadratique pour le terme d'attache aux données ne mène pas à des résultats satisfaisants sur des zones urbaines.

En dehors de l'interpolation au plus proche voisin, de l'interpolation linéaire et du krigeage, nous essayons également la méthode de binning et la minimisation de fonction de coût pour les mesures simulées d'anisotropies du CMB. La surface composée par ces mesures est lisse si l'on ne fait pas la déconvolution. Dans ce cas, la régularisation de Tikhonov est appliquée aux données bruitées. Le krigeage n'avait pas été appliqué auparavant pour interpoler des données du CMB. Nous avons montré que cette méthode donne de bons résultats. Le krigeage sur un voisinage fixe permet l'exécution rapide sur de grands ensembles de données. C'est donc un avantage pour l'interpolation des données réelles. Cependant, bien que le krigeage surpasse la min-

imisation de fonction de coût, celle-ci peut être adaptée à la fois à la déconvolution et à l'interpolation. Il vaut alors mieux dans ce cas utiliser une fonction quadratique tronquée pour le terme de régularisation, afin de reconstruire les sources ponctuelles.

Les conclusions suivantes résultent de nos travaux sur les méthodes d'interpolation pour des données irrégulièrement espacées :

- l'interpolation au plus proche voisin convient quand la densité de la grille régulière imposée est inférieure à la densité des données originelles irrégulièrement espacées. Les données ne doivent cependant avoir aucun bruit. L'avantage de cette méthode est sa vitesse et simplicité ;

- l'interpolation linéaire basée sur triangle fonctionne bien quand la densité des points de grille est inférieure ou égale à la densité de données originale ;

- le krigeage est basé sur les paramètres de variogramme et nécessite leurs estimations avant d'employer cette méthode. L'évaluation des paramètres est souvent faite manuellement, même s'il est possible de la faire automatiquement. A la différence des deux méthodes précédentes, le krigeage peut supprimer le bruit, dans la mesure où le paramètre de pépite contient dans l'algorithme les informations sur le bruit ;

- le binning, souvent utilisé en astronomie, fait la moyenne des valeurs des données à l'intérieur de chaque pixel et peut ainsi diminuer le bruit. L'inconvénient de cette méthode est que la densité des points des données doit être au moins dix fois supérieure à la densité de la grille régulière pour obtenir de bons résultats. Il est également souhaitable d'avoir des points distribués de façon homogène ;

- l'approche par fonction de coût a l'inconvénient de faire intervenir un coefficient pour le terme de régularisation. Les avantages de la méthode sont sa flexibilité et sa capacité pour interpoler différents types de surfaces en utilisant différentes fonctions potentielles. Des gradients calculés sur les données originales pourraient être incorporés dans le terme d'attache aux données.

Grâce aux expérimentations utilisant la minimisation d'une fonction de coût pour les données laser, nous avons mis en évidence les résultats suivants :

- les valeurs du coefficient du terme de régularisation doivent être supérieures ou égales à 1 ou pour obtenir de bons résultats ;

- le voisinage d'un pixel de la grille a d'abord été défini comme étant l'ensemble des échantillons inclus dans le plus petit cercle contenant les huit plus proches pixels voisins du pixel ; les expérimentations ont prouvé qu'un tel voisinage est un bon choix quand :

  1) la densité des points de la grille régulière est approximativement égale à la densité des points des données ;

  2) les points des données sont espacés de façon homogène ;

- quand une des deux conditions, mentionnées ci-dessus n'est pas rencontrée, nous proposons une autre définition du voisinage qui doit inclure des points des données dans différentes directions par rapport au pixel. Cette stratégie est définie suite aux expérimentations faites sur les données laser d'Amiens, où les échantillons forment les lignes parallèles très espacées ;

- la taille recommandée du voisinage doit être approximativement égale à la distance entre les lignes de balayage. Cette distance peut être calculée avant même l'acquisition de données, en tenant compte des paramètres techniques du système de balayage et de la vitesse prévue de l'avion ou de l'hélicoptère employé.

Plusieurs directions sont envisageables pour améliorer les résultats sur l'interpolation de données laser. En ce qui concerne la technique de minimisation d'une fonction de coût, les travaux futurs suivants pourront être envisagées. La définition du voisinage peut d'abord être changée : nous pourrions ainsi choisir les points voisins du pixel selon le diagramme de Voronoi. Le premier avantage de ce choix serait l'anisotropie des données choisies. Le deuxième avantage serait d'avoir un paramètre en moins : il n'y aurait alors aucun besoin de fixer la taille du voisinage, puisque celui-ci changerait automatiquement à chaque fois selon la proximité des échantillons. Une autre amélioration consisterait à changer de fonction de coût pour que le choix des fonctions potentielles dépende de l'évaluation locale du gradient des échantillons. Nous pourrions également employer différentes fonctions potentielles dans différentes directions à l'intérieur d'une clique, en essayant de renforcer les discontinuités de la surface. Une forme et une taille différentes des cliques pourraient être envisagées pour tenir compte de quelques propriétés géométriques évidentes des zones urbaines, telles que les lignes droites. Indépendamment de l'interpolation basée sur la fonction de coût, nous pourrions étudier des fonctions d'ondelettes pour l'interpolation de la surface avec des discontinuités. Une autre possibilité reviendrait à tenir compte de la structure des grilles d'échantillonnage. Le filtrage itératif de médiane constitue également une perspective intéressante pour de futurs travaux. C'est une technique simple et rapide qui est connue pour avoir les propriétés de la diffusion anisotrope. Elle aiderait ainsi à préserver les discontinuités. Enfin, les résultats de l'interpolation linéaire sur les données laser pourraient être améliorées en utilisant la géométrie stochastique à la triangulation de Delaunay sur les bords des bâtiments.

Concernant les données du CMB, les recherches pourraient porter sur l'adaptation de la fonction de coût et sur quelques autres méthodes. La fonction de coût pourrait être adaptée à la déconvolution tout en interpolant les données. Cette modification pourrait prendre en compte la forme elliptique de la réponse, qui est importante pour les mesures réelles d'anisotropies du CMB. Les données du CMB pourraient être considérées comme somme de la surface lisse, représentant les anisotropies du CMB, et de la surface composée des sources ponctuelles. Les différentes contraintes, imposées à chacune des deux surfaces, pourraient ainsi améliorer les résultats. Plusieurs méthodes de reconstruction pour les signaux à bande limitée pourraient enfin être appliquées aux données du CMB. Cependant, dans ce cas, le signal devrait être échantillonné selon le critère de Nyquist à la moyenne.

Le but des expérimentations avec interpolation de données du CMB est d'obtenir une méthode qui fonctionne pour des coordonnées sphériques. Les données réelles du CMB sont en effet en coordonnées sphériques. Or, les méthodes présentées dans la thèse utilisent des voisinages locaux qui peuvent être considérés comme localement plans.

En conclusion, cette thèse nous aura permis de reposer le problème de l'échantillonnage sur des données irrégulièrement espacées et de montrer que celui-ci constituait un problème inverse mal posé. Nous avons également pu définir des modèles mathématiques adaptés aux données originales afin d'obtenir des résultats concluants. De plus, en analysant ceux-ci, nous avons pu proposer de nombreux perspectives visant à les améliorer.

Contents

Introduction

Interpolation problems have been widely considered in many areas of applied science, and one of them is signal and image processing. Development of digital technologies leads to the measurement techniques that provide discretized values of the signals one wants to acquire. These measurements may be obtained at odd positions and not on regular grids as expected. In this framework it is very important to have interpolation methods that correspond to the physics of the signal to measure. In other words, an a-priori model of the signal is often useful for its interpolation.

Nowadays a lot of methods allow different types of image processing. Most of these methods have been well studied both in theory and practice. But very often they can only be applied to the data on a regular grid. In the same time, some acquisition techniques are able to get the measurements either on a jittered or on an irregular grid. This is the case for many airborne or spaceborne remote sensing techniques. Even though sometimes the sampling is performed on the regular grid in the reference system of the sensor, the resulting georeferenced points are scattered. Therefore interpolation and resampling of the original data will produce the data on the regular grid and will enable us to perform further processing and analysis: visualization, segmentation, fusion, etc.

The wide range of the interpolation techniques, available at the present time, gets smaller when one wants to interpolate the values that are initially distributed on an irregular grid. It is the topic that we consider in the thesis. Moreover, interpolating a signal that is non-bandlimited and whose measurements are scattered in space is not a trivial problem and requires some studies to be done. This problem is considered in the thesis while working with airborne laser scanning data. The data has been acquired over the urban areas. Since the urban areas often consist of streets and buildings, the edges of the buildings form discontinuities and so the signal to interpolate is non-bandlimited.

Obtaining 3D city models is important for several reasons. They include creation and updating of Geographical Information Systems for towns, urban planning and development projects that are supposed to prevent distribution of polluting substances, or provide transport network planning, telecommunication antennas placements. 3D cities in virtual reality are also one of the possible applications of remote sensing on urban areas. Airborne laser scanning is a fast and precise data acquisition technique that has been tested over urban areas. This technique itself is still a subject of research and development. We present a review on the laser scanning acquisition technique since it leads to the understanding of the nature of the acquired data, for example the noise

and the precision of the measurements. Such parameters are helpful for developing the suitable interpolation method.

The second part of the thesis is devoted to cosmic microwave background (CMB) data interpolation. This kind of data is also on an irregular grid. The surface to interpolate is considered to be smooth as long as no deconvolution is made. Acquiring and treating the cosmic microwave background data has been an area of great scientific interest during the last decades. It is a topic of cosmology - the science about the origin of our Universe. There are models of the Universe, developed by astronomers, and it is considered that some parameters may determine the age, the shape and the matter of the Universe. However, these parameters are to be calculated from the maps of CMB. These maps must be on a regular grid, while the original measurements are not. So the problem of irregularly spaced data interpolation should be considered in this case.

The manuscript is organized in the following way. In Chapter 1 the theoretical aspects of sampling are considered. Though we are interested in the irregular sampling theories, we start this chapter by the well known theorem of Shannon, because it served as a starting point for most of the later research in sampling. We realize that among problems of irregular sampling there is a problem of the optimal grid size. It could be a subject of research of the thesis. Several approaches could be tried in this direction: information density measures, degrees of freedom or minimum of the entropy approach. In this chapter we pay attention to the theory of non-uniform and random sampling which is the case of the data we have. We consider a classification of sampling sets in one and in two dimensions. Random sampling of non-bandlimited signals is the area of interest in the current research in applied and pure mathematics.

In Chapter 2 we consider the laser scanning technique, its precision and properties, as well as the range of parameters for the existing laser scanning systems and practical applications of such kind of data. In the interpolation methods presented and implemented in the following chapters we would like to take into account not only the form and properties of the scanned surface, but also the acquisition technique. That is why many technical details are given in this chapter. For example, it would be interesting to simulate the airborne laser scanning acquisition. In this case the analysis of the sources of noise must be done. As we will see in this chapter, the performance of laser scanning is still a subject of research, especially when it concerns urban areas. In this chapter we also name the applications of the airborne laser scanning which explain why this technique has received so much attention of the remote sensing research community in recent years.

Chapter 3 describes the general approaches for scattered data interpolation and also contains the description of the methods to be used in experiments with the real data. The first two described methods are nearest neighbor and triangle based linear interpolation. These methods are fast and simple and we would like to know what results they give in order to be able to introduce a better approach more suited for our data. The third described method is kriging. It is developed in geostatistics for irregularly spaced data interpolation. The assumptions used by this method are valid for the cosmic microwave background anisotropies. Nevertheless, we will present the results of this method on airborne laser scanning data too. The problem of scattered

data interpolation can be regarded as an ill-posed inverse problem. Therefore we present an energy minimization method and we adapt it to laser scanning data. We will use the potential functions that are known for their edge preserving properties. We present the definition of the neighborhood for our problem, expression of the cost function as well as the choice of the optimization algorithm.

These methods are implemented and their results are presented in Chapter 4. We apply the methods to two real data sets. It will help us to evaluate the interpolation methods, because the two sets are acquired by different laser scanning systems and therefore have different properties: sampling patterns are very different. We compare the results with the reference and make conclusions about their performance.

In Chapter 5 there is a short introduction to the CMB theory as well as to the CMB data acquisition technique. The described technique will be used in 2007 by the European Space Agency when it launches the Planck satellite. This mission will provide the most precise and complete data ever acquired on the CMB.

Chapter 6 presents some results and their comparison over the simulated CMB data. The simulated data respects the sampling pattern as it is supposed to be for the Planck mission. We apply the interpolation methods presented above to this kind of the data and we also implement binning - an averaging technique, often used in astronomy. The main difference between the CMB anisotropies data and the laser data is not only in the type of the surface that is scanned but also in the fact of having very strong noise in the CMB anisotropies measurements. We simulate it as white noise and we study the performance of the methods on the noisy data.

The chapter of conclusions presents the summary and proposes some directions for the future work.

Chapter 1

Sampling theory

1.1 Introduction

This chapter presents some theoretical aspects of the sampling theory. This theory has received a lot of attention in the several recent decades. Especially is important if we take into account the fast development of digital technologies. When real world signals are acquired through digital devices, they are often sampled on the regular grids with equal distances between nodes. For images, the most widely used grid are square grids, though there are some cases when hexagonal ones are preferred. The theory of sampling is supposed to answer many questions on the optimal acquisition of data and its reconstruction and further processing afterwards. In this framework signals may be divided on bandlimited and non-bandlimited ones, and grids are divided on uniform and nonuniform.

The chapter contains three sections. In the first section we consider uniform sampling and the theorems of Shannon and Papoulis. These theorems are now considered as classical ones, and we present them in the text, because most of the later research and development of the sampling theory relies on them. The second section contains a classification of sampling sets from the theoretical point of view. It shows the possible variety of sampling sets, some of which are already applied in technology and allow reconstruction and resampling. It should be emphasized that after the regular square grids, one can consider hexagonal grids as quite well studied and applied ones. In the third section we consider nonuniform grids. Taken into account the classification made in the previous section, we notice, that most of the theories are developed either for jittered or for irregular sampling.

1.2 Uniform sampling

1.2.1 Shannon sampling theory

The basics of the sampling theory was developed in the beginning of the last century. It is often associated with names of Nyquist, Whittaker, Kotel'nikov and Shannon

[Jerri, 1977]. The sampling theorem given by Shannon is the following [Shannon, 1949]. If a function $f(t)$ contains no frequencies higher than W cps, it is completely determined by giving its ordinates at series of points spaced $1/2W$ seconds apart. The rate $1/2W$ is called Nyquist rate. Let x_n be the nth sample, then the function $f(t)$ is represented by

$$f(t) = \sum_{n=-\infty}^{\infty} x_n \frac{sin\pi(2Wt-n)}{\pi(2Wt-n)}.$$

Emphasizing that only stable sampling is meaningful in practice, Landau proved that it cannot be performed at a lower rate than the Nyquist rate [Jerri, 1977]. Considering the Shannon sampling theorem and using the Parseval equation, Landau gave an interpretation that relates the Nyquist rate with the stability of the sampling expansion.

1) Every signal $f(t)$ of finite energy, i.e. $\int_{-\infty}^{\infty} f^2(t)dt < \infty$, and bandwidth W may be completely recovered in a simple way, from the knowledge of its samples taken at the Nyquist rate of $2W$ per second. The recovery is stable in the sense of Hadamard, such that a small error in sample values produces only a correspondingly small error in the recovered signal.

2) Every square-summable sequence of numbers may be transmitted at the rate of $2W$ per second over an ideal channel of bandwidth W by being represented as the samples of an easily constructed band-limited signal of finite energy.

In relation to the required Nyquist rate for the transmitted sequence of samples or the recovered ones, Landau considered other configurations, besides the band-limited finite energy signals, in order to improve such rates. He proved the following two results.

1) Stable sampling cannot be performed at a lower rate than the Nyquist rate.

2) Data cannot be transmitted as samples at a rate higher than the Nyquist rate regardless of the location of sampling instants, the nature of the set of frequencies which the signal occupy, or the method of construction.

These results also apply to bounded signals besides finite energy signals.

For the multidimensional sampling theorem [Marks, 1991] let's consider

- $x(\vec{t})$ as a multidimensional bandlimited function;

- $X(\vec{u})$ as its spectrum; the function $x(\vec{t})$ is defined to be bandlimited if $X(\vec{u}) = 0$ outside of an N-dimensional sphere of finite radius;

- $S(\vec{u})$ as the replication of $|detP|X(\vec{u})$ as a result of sampling, where the periodicity matrix P must be chosen so that the spectral replications do not overlap and therefore alias.

The multidimensional sampling theorem can be summarized in the following way:

$$x(\vec{t}) = \sum_{\vec{m}} x(Q\vec{m}) f_c(\vec{t} - Q\vec{m}),$$

where

$$f_c(\vec{t}) = |detQ| \int_{\vec{u} \in C} exp(j2\pi \vec{u}^T \vec{t}) d\vec{u},$$

C is a periodicity cell for the spectrum, the Q matrix it the sampling matrix and it dictates the geometry of the uniform sampling. The sampling density (samples/unit area) corresponding to Q is

$$SD = \frac{1}{|detQ|} = |detP|.$$

The Nyquist rate can be generalized to higher dimensions. In this case it is called Nyquist density - the density resulting from maximally packed unaliased replication of the signal's spectrum. For the case of two dimensions the Nyquist density corresponds to the hexagonal sampling geometry.

There have been a number of significant generalizations of the sampling theorem [Marks, 1991, Jerri, 1977]. Some are straightforward variations on the fundamental cardinal series. Oversampling, for example, results in dependent samples and allows much greater flexibility in the choice of interpolation functions. It can also result in better performance in the presence of sample data noise. Kramer generalized the sampling theorem to signals that were bandlimited in other than the Fourier sense.

Bandlimited signal restoration from samples of various filtered versions of the signal is the topic addressed in Papoulis' generalization of the sampling theorem [Papoulis, 1977]. Included as special cases are recurrent nonuniform sampling and simultaneously sampling a signal and one or more of its derivatives.

New generalizations of the sampling theorem are still being developed [Unser, 2000, Vaidyanathan, 2001].

For example, in [Unser, 1994] the theoretical framework for a general sampling theory is given. The theory restates the theorem of Shannon. The main goal of the general sampling theory presented in the paper is to adapt the process of signal reconstruction to non-ideal acquisition devices. The matter is that on the theorem of Shannon the signal is considered to be sampled by Dirac functions, while on practice one has to deal with an impulse response of a sensor. The convolution with this impulse response function is performed before the signal is sampled. The paper proposes a reconstruction and a correction filters in order to reconstruct the signal. The signal may not be bandlimited. Lifting the condition of a bandlimited signal leads to the approximation of it. It is proved that in theory one can reconstruct a signal, sampled by non-ideal acquisition devices, and this reconstruction will be consistent. It means that if we reinject the reconstructed signal into the acquisition device, then the samples will be the same as the ones of the signal reconstructed previously. The presented theory

is developed only for 1D case, though it is supposed that it can be extended to more dimensions. Another remark concerns the fact that noise is not taken into account, and more development should be done to adapt the presented theory for a noise.

1.2.2 Papoulis generalization of the sampling theorem

There are a number of ways to generalize the manner in which data can be extracted from a signal and still maintain sufficient information to reconstruct the signal [Marks, 1991]. Shannon noted that one could sample at half the Nyquist rate without information loss of it, at each sample location, two sample values were taken: one of the signal and one of the signal's derivative. The details were later worked out by Linden who generalized the result to restoring from a signal sample and samples of its first $N-1$ derivatives taken every N Nyquist intervals. It is also possible to choose any N distinct points within N Nyquist intervals. If signal samples are taken at these locations every N Nyquist intervals, it is the question of restoration from interlaced (or bunched) samples.

All of these cases are subsumed in a generalization of the sampling theorem developed by Papoulis (1977). The generalization concerns restoration of a signal given data sampled at $1/N^{th}$ the Nyquist rate from the output of N filters into which the signal has been fed.

Let $\{H_p(u)|p = 1, 2, ..., N\}$ be a set of N given filter frequency responses and let $f(t)$ have bandwidth B. As shown in Figure 1.1, $f(t)$ is fed into each filter.
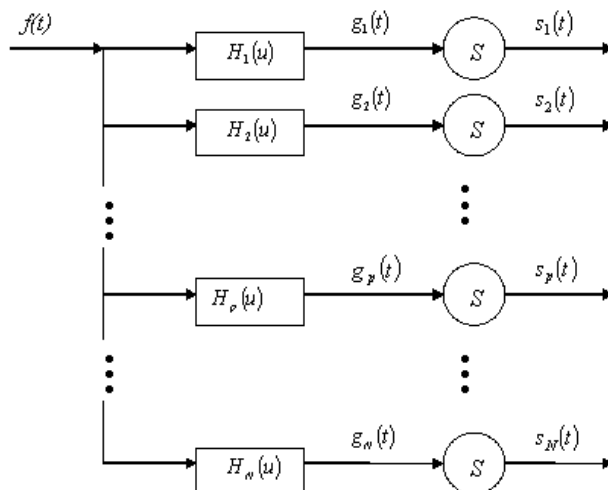

Figure 1.1: Generation of sample data from Papoulis' generalized sampling theorem. The encircled S is a sampler.

The outputs are

$$g_p(t) = f(t) * h_p(t); 1 \leq p \leq N.$$

Each output is sampled at $1/N^{th}$ the Nyquist rate. The signal of samples obtained from the pth filter are

$$s_p(t) = \sum_{n=-\infty}^{\infty} g_p(nT_N)\delta(t - nT_N),$$

where $T_N = 1/2B_N$ and $B_N = B/N$. The problem is to restore $f(t)$ from this set of functions or, equivalently, the sample set

$$g_p(nT_N|1 \le p \le N, -\infty < n < \infty).$$

According to Papoulis' theorem,

$$f(t) = \sum_{p=1}^{N} \sum_{n=-\infty}^{\infty} g_p(nT_N)k_p(t - nT_N)$$

where

$$k_p(t) = \int_{B-2B_N}^{B} K_p(u;t)e^{j2\pi ut}du$$

and the $K_p(u;t)$'s are the solutions of the simultaneous set of equations

$$2B_N \sum_{p=1}^{N} K_p(u;t)H_p(u - 2mB_N) = exp(-j2\pi mt/T_N)$$

over the parameter set $0 \le m \le N$, $B - B_N < u < B$ and $-\infty < t < \infty$. If $N = 1$ and $H_1(u) = 1$, then the Shannon sampling theorem results.

The theorem of Papoulis can be used for signal interpolation after recurrent nonuniform sampling. Let $\alpha_p|p = 1, 2, ..., N$ denote N distinct locations in N Nyquist intervals (Figure 1.2).
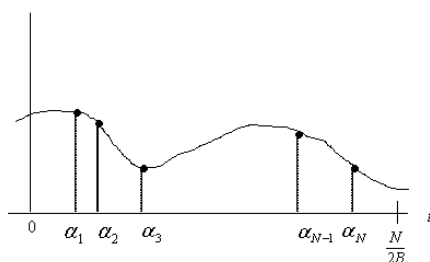
Figure 1.2: Illustration of Nth order recurrent nonuniform sampling. In each N Nyquist intervals, samples are taken at these same relative locations.

A signal is sampled at these points every N Nyquist intervals. Thus there is knowledge of the data

$$\{f(\alpha_p + \frac{m}{2B_N})|1 \le p \le N, -\infty < m < \infty\}.$$

Such sampling is also referred as interlaced (or bunched) sampling.

The generalized sampling theorem is applicable here if the filters are

$$H_p(u) = exp(j2\pi\alpha_p u); \ 1 \le p \le N.$$

On the interval $(0, T_N)$ the resulting interpolation functions are:

$$k_p(t) = sinc[2B_N(t - \alpha_p)] \prod_{q=1; \ q \ne p}^{N} \frac{sin[2\pi B_N(t - \alpha_q)]}{sin[2\pi B_N(\alpha_p - \alpha_q)]}.$$

By utilizing the Papoulis' generalized sampling expansion, it was demonstrated [Cheung, 1993] that there is a class of sampling theorems which are ill-posed. In particular, given the samples are contaminated with noise, the interpolation noise variance is unbounded for these ill-posed sampling theorems.

The multidimensional extension of Papoulis' theorem is utilized to reduce the sampling density of multidimensional band-limited functions. The reduction leads to the minimum sampling density, which is equal to the area of the support of the function's Fourier spectrum.

For the data we want to interpolate on this thesis, there are two limitations for using the theorem of Papoulis. At first, the signal to interpolate is non-bandlimited. It is true when we consider the airborne laser data over urban areas, which we will describe in the following chapter. At second, the sampling strategy in the real data cannot be modeled as recurrent nonuniform sampling. Especially it is valid for the areas where the scanning strips overlap. The cosmic microwave background anisotropies also can be described as non-bandlimited signals when we consider the point sources.

The theory of Papoulis has been extended for the case of non-bandlimited signals, but in this case it is possible to obtain an approximation of a signal instead of a reconstruction [Unser et al., 1998].

1.2.3 Extension of Papoulis theorem for non-bandlimited signals

In this section we describe the work of Unser and Zerubia on the generalized sampling theory [Unser et al., 1998]. The main point of the theorem of Papoulis is that there are many possible ways of extracting data from a signal for a complete characterization. The standard approach of taking uniform signal samples at the Nyquist rate is just one possibility among many others. Typical instances of generalized sampling that have been studied in the literature are interlaced and derivative sampling. Later, an interest has been strengthen in such alternative sampling schemes for improving image acquisition. For example, in high resolution electron microscopy there is an inherent tradeoff between contrast and resolution. It is possible, however, to compensate for these effects by combining multiple images acquired with various degrees of defocusing. Super-resolution is another promising application where a series of low resolution images that are shifted with respect to each other are used to reconstruct a higher resolution picture of a scene.

Papoulis' generalized sampling theory provides an attractive framework for addressing most restoration problems involving multiple sensors or interlaced sampling. However, the underlying assumption of a bandlimited input function $f(x)$ is very restrictive. It is because most of the real world analog signals are time or space limited which is in contradiction with the bandlimited hypothesis. Another potential difficulty is that Papoulis did not explicitly translate his theoretical results into a practical numerical reconstruction algorithm.

The main contributions of the work of Unser and Zerubia are as follows. First, they propose a much less constrained formulation where the analog input signal can be almost arbitrary, typically in the space of finite energy functions (Figure 1.3). This
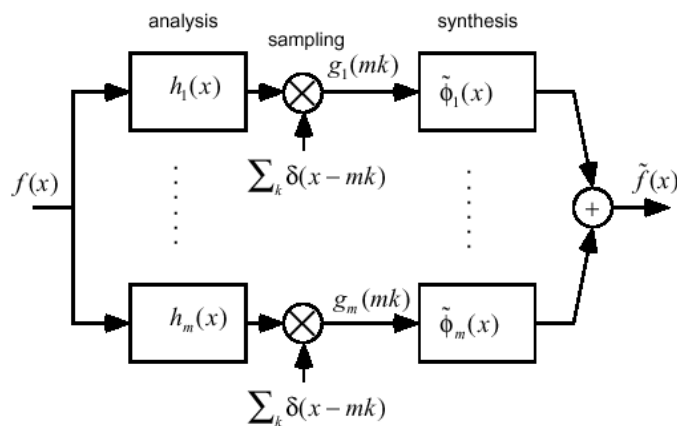
Figure 1.3: Generalized sampling procedure [Unser et al., 1998]. The left part of the block diagram represents the measurement process which is performed by sampling the output of an m channel analysis filterbank. The sampling operation is modeled by a multiplication with a sequence of dirac impulses. The right part describes the reconstruction process which involves the synthesis functions. The system produces an output function that is a consistent approximation of the input signal $f(x)$.

is only possible because the Papoulis and Shannon's principles of a perfect reconstruction are replaced by the weaker requirement of a consistent approximation. That means that the reconstructed signal provides exactly the same measurements as the input signal if it was reinjected into the system. The second contribution is the consideration of a more general form of the reconstruction subspace. In this way the results are applicable for non-bandlimited signal representation models. At third, the implementation issue is addressed explicitly and a practical reconstruction algorithm is proposed, though the results on the signals with discontinuities are not presented.

1.2.4 Sources of errors

Various errors may arise in the practical implementation of the sampling theorems [Jerri, 1977, Jerri, 1993, Feichtinger et al., 1993]. This includes the truncation error which results when only a finite number of samples are used instead of the infinite

samples needed for the sampling representation, the aliasing error which is caused by violating the band-limitedness of the signal, the jitter error which is caused by sampling instants different from the sampling points, the round-off error, and the amplitude error which is the result of the uncertainty in measuring the amplitude of the sample values.

For the band-limited signal

$$f(t) = \int_{-a}^{a} F(u)e^{iut}du$$

and its sampling representation

$$f(t) = \sum_{n=-\infty}^{\infty} f(\frac{n\pi}{a})\frac{sin(at-n\pi)}{(at-n\pi)}$$

the truncation error ϵ_T is the result of considering the partial sum $f_N(t)$ with only $2N+1$ terms of the infinite series,

$$\epsilon_T = f(t) - f_N(t) = \sum_{|n|>N} f(\frac{n\pi}{a})\frac{sin(at-n\pi)}{(at-n\pi)}.$$

In practice, the signals are not necessarily band-limited in the sense required by the Shannon sampling expansion. The aliasing error $\epsilon_A(t) = f(t) - f_s(t)$ is the result from applying the sampling theorem representation $f_s(t)$ to signals $f(t)$ with samples $f(n\pi/a)$ even when they are not band-limited or band-limited to different limits than those used in sampling expansion.

The amplitude error is caused by the uncertainty in the sample values due to either quantization or to some fluctuation where the round-off error may be considered as a special case.

The jitter error results from sampling at instants $t_n = nT + \gamma_n$ which differ in a random fashion by γ_n from the required Nyquist sampling instants nT.

1.3   Classification of sampling sets

1.3.1   One-dimensional sampling sets

For one-dimensional sampling sets the possibilities for creating different types of sets are not as large as they are in two dimensions. The following description of sampling geometries is sorted by the different steps of irregularity [Schmidt, 1997].

The geometry of the regular sampling sets depends on the length of the signal. If n is the length of the vector and k is the amount of sampling points (k is a divisor of n), then the difference between the regular sampling structures is determined only by the density k/n of the sampling points.

The periodic sampling sets are a more general way of creating geometries in the one-dimensional case. No strict regular periodicity is demanded, a sampling set may

be composed of some shifted subsets of it. Then the resulting set is periodic in the way that the shifted subsets are repeated periodically. So such a periodic sampling set is not regular, but has some properties left. In the two-dimensional case this form of sampling is called bunched sampling. The two-dimensional periodicity gives more information about the sampling set, than in irregular sampling, and can be used to improve the reconstruction.

Irregular (random) sampling sets mean just making a random sampling. There are different parameters which can be varied (as the density of the sampling set), but the structure of irregularity is granted.

1.3.2   Two-dimensional sampling sets

In the two-dimensional case the variability of different sampling sets is increasing rapidly in comparison with the one-dimensional case, because there are not only the product sampling sets of the corresponding one-dimensional possibilities, but also some new variations which do not have an equivalent in the 1-D problem (for example, spiral sampling). The following two-dimensional sampling sets are arranged by increasing irregularity and at the same time by increasing the number of possible sampling sets depending on the sampling method [Schmidt, 1997].

A square (or regular) sampling set in two dimensions (Figure 1.4) can be treated like a multiplication of two one-dimensional sampling sets. The square sets can be described in matrix form by multiplying two regular one-dimensional sets a, a', which have the same coordinates and where $'$ denotes the transpose: $C = a' * a$.
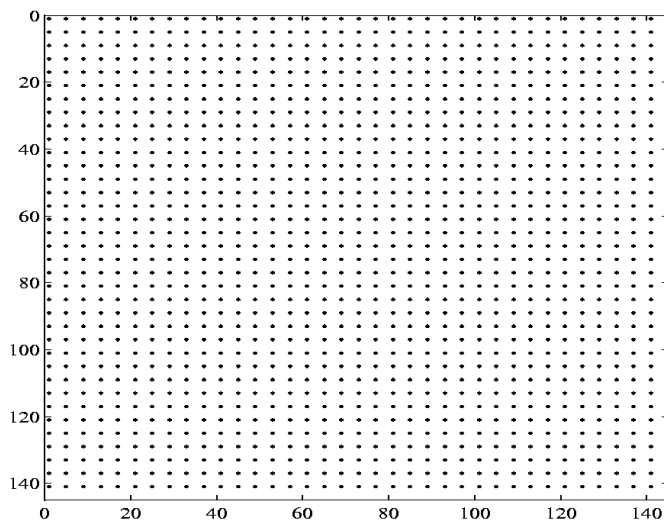
Figure 1.4: A square sampling set (regular geometry).

A rectangular sampling set (Figure 1.5) differs from a square set, because the multiplication is not done by two similar regular vectors but it is performed by two different regular vectors.
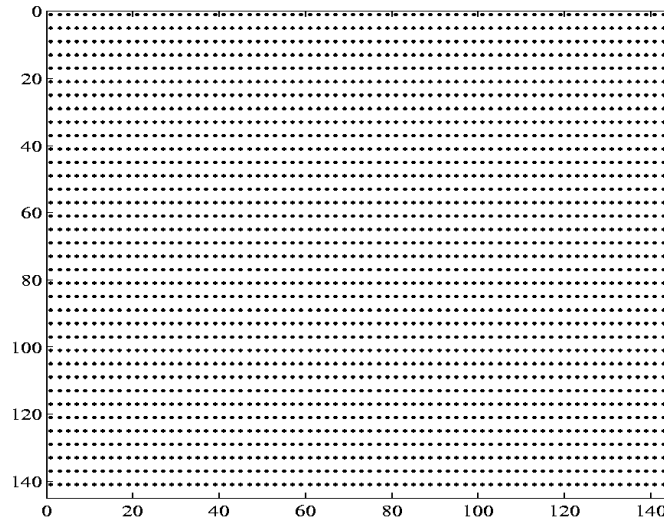
Figure 1.5: A rectangular sampling set.

As the result the grid has two different step widths. The rectangular sets are more general than the square sets.

The double periodic sampling sets (Figure 1.6) are created through multiplication of two one-dimensional periodic vectors.
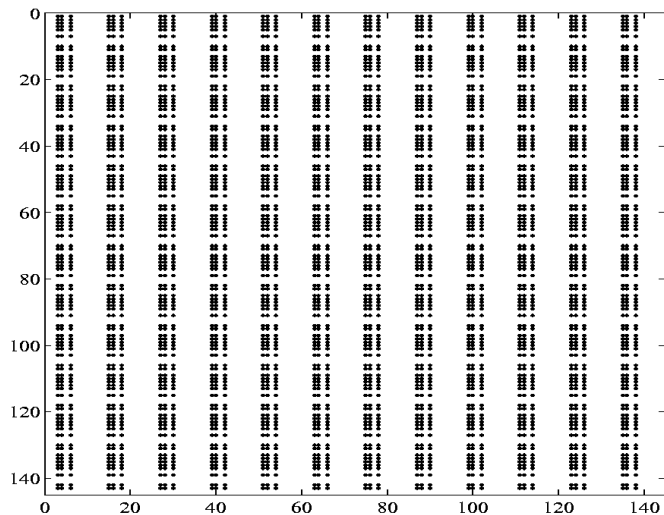

Figure 1.6: A periodic sampling set.

They are a special type of the product sampling sets because they need to be periodic in both directions.

Product sampling sets are the easiest way of getting a two-dimensional sampling geometry because they can be generated by just multiplying two arbitrary vectors. An example of image reconstruction from product sampling set is given in [Feichtinger et al., 1994]. Superposition of three different product sampling sets is used for RGB color coding

for some cameras. The grid received by this method is called Bayer mask.

Bunched sampling sets (Figure 1.7) can be obtained by first taking a sparse matrix with regular or periodic entries and then defining some shift vectors with components in both directions to define an overlay of two or more of these matrices.
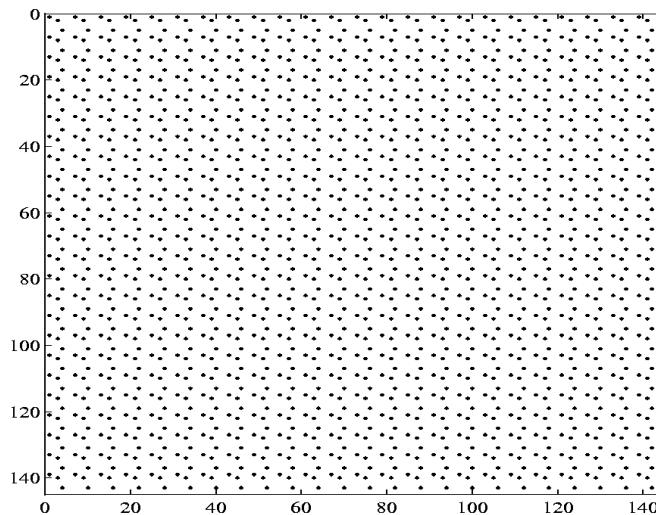
Figure 1.7: A bunched sampling set.

The bunched set can also be described as a form of irregular sampling because it is possible to look on it as a simple product set with missing points inside. But this description is less useful because of the loss of information about the structure of the set and way of generating it. Hexagonal sampling sets and octagonal sampling sets are examples of bunched sets.

Elliptic, polar or spiral sampling sets (Figure 1.8) occur in astronomical observations. When the astrophysical data acquisition is performed with the equipment installed on Earth, spiral sampling sets will be caused by the movement of the Earth. Polar sampling is used both in biomedical imaging (computer tomography) and in remote sensing (radar data).

There are interpolation methods developed for this kind of sampling sets [Stark, 1993].

Quasiregular sampling sets are generated by thinning out or filling in some amount of points (i.e. 10 percent) from a regular hexagonal, octagonal or product sampling set. Normally, a structure of a quasiregular sampling set is still visible for a human eye. Quasiregularity also means that regularly distributed sampling points may be distorted from their original position by a small amount. That is also not a regular set, but the irregularity is not too large.

Irregular sampling sets (Figure 1.9) have no internal structure to exploit and so all algorithms have to be kept generally.

In general, the classification of sampling sets, presented in this section, is mostly of a theoretical interest, because most of the real sampling sets have either jittered regular structure (like images taken in some remote sensing applications) or they are irregular, random. Considering the sampling pattern of airborne laser scanning, pre-
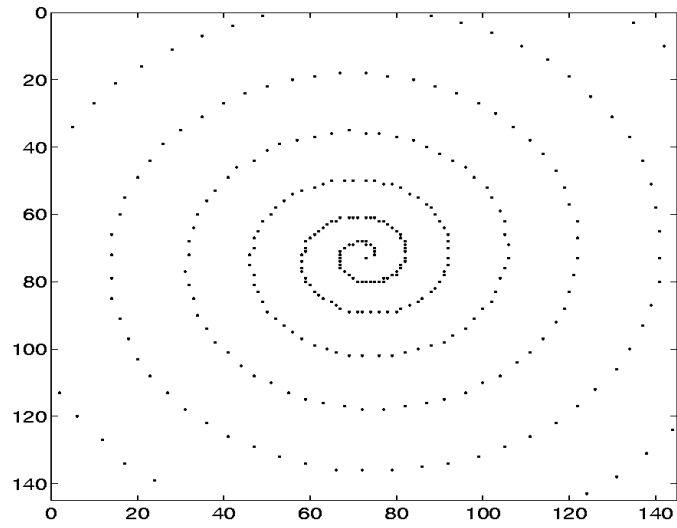
Figure 1.8: A linear expanding spiral sampling set.
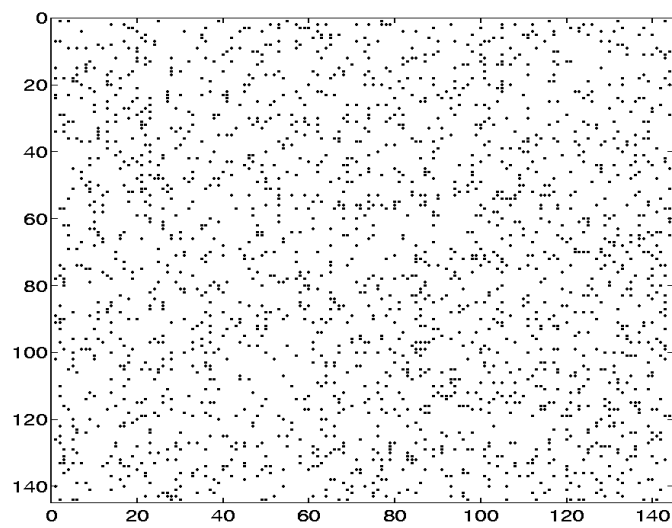
Figure 1.9: An irregular sampling set.

27

sented later in this thesis, we can say that the sampling set strongly depends on the scanning system. Airborne laser scanning in theory can be represented by a sampling set composed of circles, or by jittered hexagonal grid, or by a particular periodic set. But in practice scan lines overlap and then it is difficult to find a structure in the obtained data (Figure 1.10, 1.11). Recently it has been clear that for urban areas it
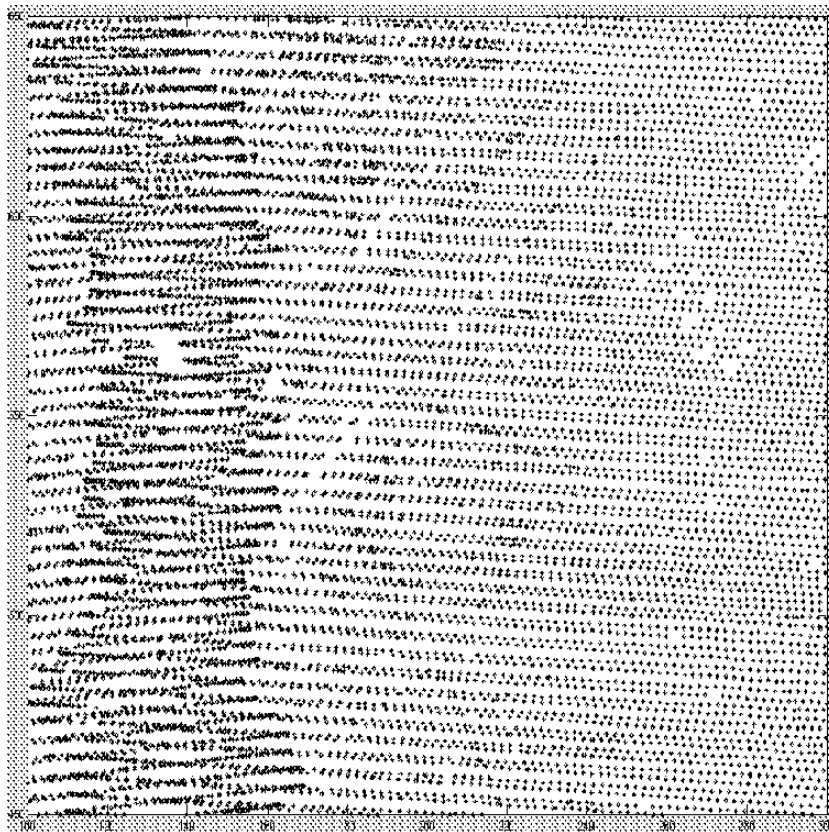
Figure 1.10: An irregular grid produceed by laser scanning over an area of 200×200 meters.

is necessary that large parts of scan lines overlap, because it will provide more dense data and therefore more information on the area to scan, especially on the edges of buildings.

1.3.3 Hexagonal sampling

The hexagonal sampling (Figure 1.12) offers substantial savings in machine storage and arithmetic computations [Schmidt, 1997]. There exist some methods for processing 2D signals sampled on 2D hexagonal arrays. The rectangular sampling set can be treated as a special case of the general non-orthogonal sampling strategy. Especially for bandlimited signals over a circular region of the Fourier plane the hexagonal setting seems to be fruitful and optimal since it reduces the necessary sampling density to the amount of almost 13%. This might lead to a very efficient implementation since this percentage might be won at each iteration of applied iterative algorithms.
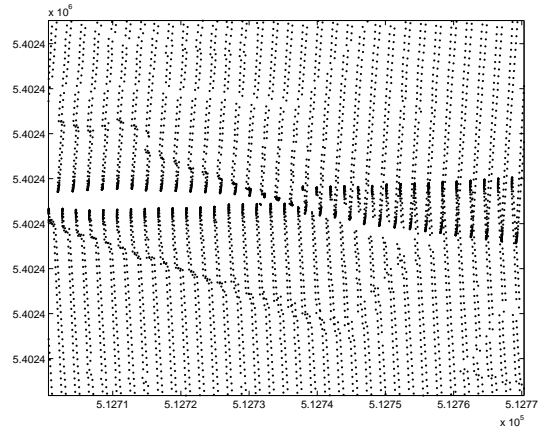
Figure 1.11: A sampling pattern of a real laser data: a gap in the data appears because two neighboring stips don't overlap.
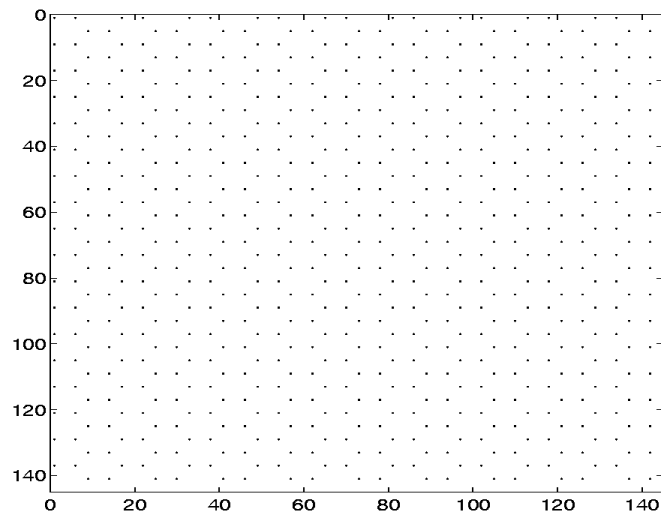

Figure 1.12: A hexagonal sampling set.

A review of hexagonal sampling is given in [Almansa, 2002]. The motivation of this study was the development of imaging systems, that would use hexagonal sampling grids, at the French Space Agency (CNES). In the conclusions of this review, two reasons are given that prevent the extensive use of hexagonal grids and algorithms: the fact that display, acquisition and processing hardware is most often better suited for square grids; and the increased complexity of the algorithms under certain circumstances.

1.4   Nonuniform sampling

There are some cases where there is no choice but to process nonuniform data. Some of the examples are:

- data measured in a moving vehicle with fluctuations in speed for applications in remote sensing, where random or uniform samples with jitter are often inevitable;

- data tracked in digital flight control;

- data read from and recorded on a tape or disk with speed fluctuations;

- data loss due to channel erasures and additive noise.

Interpolation techniques are developed to reconstruct the signal from nonuniform samples.

Unlike uniform sampling, there is no guarantee of the uniqueness of a band-limited signal reconstructed from arbitrary nonuniform samples [Marvasti, 1993]. This is true even when the average sampling rate is equal to the Nyquist rate. For example, let's suppose there is one solution to a set of nonuniform samples at instances $\{t_n\}$, and assume that it is possible to interpolate a band-limited function of the same bandwidth at the zero-crossings $\{t_n\}$. Now, if one adds this interpolated function to the first solution, one will get another band-limited function (of the same bandwidth) having the same nonuniform samples. Thus, nonuniform samples do not specify a unique band-limited signal. For a given bandwidth, this ambiguity is related to the set $\{t_n\}$. Therefore, the $\{t_n\}$ instances must be chosen such that the existence of a unique solution is guaranteed. A set of these sampling instances that assures unique reconstruction is called a sampling set.

The following lemma has been derived: if the nonuniform sample locations $\{t_n\}$ satisfy the Nyquist rate on the average, they uniquely represent a band-limited signal if the sample locations are not the zero-crossings of a band-limited signal of the same bandwidth. This lemma implies the following corollary: if the average sampling rate of a set of sample locations $\{t_n\}$ is higher than the Nyquist rate, the samples uniquely specify the signal and $\{t_n\}$ is a sampling set.

In general, the requirements [Feichtinger et al., 1992] for the reconstruction methods for irregularly sampled band-limited functions are:

- constructivity, i.e. a possibly iterative algorithm should allow numerical reconstruction;

- multidimensionality, so that it can be used in signal and image processing or for the interpolation of sequences of images;

- locality, so that the value of a band-limited function at a point is essentially determined by the adjacent sampling values, and more distant sampling values have no influence;

- stability, so that small perturbations of the parameters cause only small errors in the reconstruction.

1.4.1   Nonuniform sampling for bandlimited signals

The main question here is to recover a signal with a limited band-width and known spectral support from irregularly spaced sampling values. The irregular sampling problem for bandlimited 1D and 2D signals has found much interest during the last decade. Most of the results concern 1D case, though. For the case of irregular sampling values no simple formula for reconstruction, such as the one given by Shannon in the case of regular samples, can be expected. Nevertheless, it is still possible to recover a bandlimited irregularly sampled signal completely, if the sampling set is not too sparse.

There are various techniques to reconstruct signals [Strohmer, 1991], such as iterative algorithms, the frame method, direct methods (based on the solution of linear equations using pseudoinverse matrices) and others [Cenker et al., 1991, Feichtinger et al., 1995]. Iterative algorithms received a lot of attention recently [Almansa, 2002], and we will describe their idea.

Iterative algorithms use the irregularly spaced sampling information about the signal f and the information about the spectral support of f. Iterative two-step algorithms are typical for most of the methods. They are based on a recursion of the form:
$$f_{r+1} = P_B(Af_r),$$
where A is some approximation operator using only the original irregularly spaced sampling values, and P_B is mapping a given signal onto the space of bandlimited signals with spectrum B. One may think of this mapping as of a smoothing operation, which eliminates the discontinuity of Af. This projection P can be described as a low-pass filter or as a convolution using a $sinc$-type kernel with the spectrum defined over the set B.

There are several choices available for the approximation operator A [Strohmer, 1991, Feichtinger et al., 1991]. The Wiley-Marvasti method uses just the sampled signal multiplied by a global relaxation factor. The Sauer-Allebach algorithm takes classical interpolation methods in order to obtain the first approximation. Among these methods are: Voronoi method, Sample and Hold method, piecewise linear interpolation,

spline interpolation. The Voronoi method can also be called nearest neighbor interpolation. In higher dimensions the corresponding construction makes use of Voronoi regions, that is a step function is used, which is constant in the nearest neighborhood of the sampling points. The Sample and Hold method requires twice the Nyquist rate for a complete reconstruction [Strohmer, 1991]. For large gaps this method for constructing an approximation of the signal is divergent. Piecewise linear interpolation is suitable only when the gaps between samples are not much larger than the Nyquist rate [Strohmer, 1991]. Spline interpolation gives a good approximation of the signal but requires much more computational expenses comparing with the linear interpolation. The adaptive weights method is a more flexible version of the Wiley-Marvasti method and it derives different appropriate weights from the sampling geometry. In 1D case the distances between subsequent points are considered [Feichtinger et al., 1991].

1.4.2 Nonuniform sampling for non-bandlimited signals

There is a class of non-band-limited signals that can be represented uniquely by a set of nonuniform samples. If a band-limited signal goes through a monotonic non-linear distortion, $y(t) = f[x(t)]$, then, although $y(t)$ is a non-band-limited signal, it can be represented by nonuniform samples if t_n is a sampling set for the band-limited signal $x(t)$ [Marvasti, 1993]. The reconstruction scheme is shown in Figure 1.13.
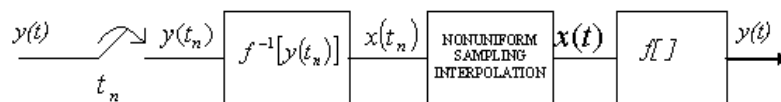

Figure 1.13: Reconstruction of a non-bandlimited signal from nonuniform samples.

Necessary and sufficient conditions for such non-band-limited signals have been established [Marvasti and Jain, 1986]. If a band-limited $y(t)$ is transformed into a non-band-limited $x(t)$ through an unknown analytic and monotonic nonlinear operation $f(\bullet)$, then $y(t)$ can be recovered from $x(t)$ within a constant factor, provided that one of the following conditions is satisfied:

1) $dy(t)/dt$ has only real zeros (zero crossings), but $f(\bullet)$ is only analytic and monotonic;

2) $dy(t)/dt$ may have any kind of zeros, but $f(\bullet)$ has the additional condition that df/dy is also monotonic.

Another example is a set of non-band-limited signals generated by a time varying filter when the input is a band-limited signal. If the system has an inverse, then the samples of the output (the non-band-limited signal) are sufficient to reconstruct the signal. This non-band-limited signal is essentially a time-warped version of the band-limited signal.

The results presented above in this section have not been extended for 2D signals and stay to be a purely theoretical setting for the 1D case, because no practical application was developed. It makes the use of these results impossible for the real data sets treated in this thesis, because the sampling sets we have are in two dimensions and demand a practically applicable algorithm.

1.4.3   Jittered sampling

Jittered samples are nonuniform samples that are clustered around uniform samples either deterministically or randomly with a given probability distribution. This random jitter is due to uncertainty of sampling at the transmitter end. For deterministic jitter, Papoulis has proposed a method for the recovery. The problem is recovery of $x(t)$ from the jittered samples, $x(nT - \mu_n)$, where μ_n is a known deviation from nT. The main idea is to transform $x(t)$ into another function $g(\tau)$ such that the nonuniform samples at $t_n = nT - \mu_n$ are mapped into uniform samples $\tau = nT$ (Figure 1.14).

Consequently, $g(\tau)$ can be reconstructed from $g(nT)$ if $g(\tau)$ is band-limited ($W \leq \frac{1}{2T}$). $x(t)$ can be found from $g(\tau)$ if the transformation is one-to-one [Marvasti, 1993]. Let's take the one-to-one transformation as $t = \tau - \theta(\tau)$, where $\theta(\tau)$ is a band-limited function defined as

$$\theta(\tau) = \sum_{n=-\infty}^{\infty} \mu_n sinc[\pi W_2(\tau - nT)],$$

where $W_2 \leq \frac{1}{2T}$ is the bandwidth of $\theta(\tau)$. Since the transformation is one-to-one, the inverse exists and is defined by $\tau = \gamma(t)$. If $\theta(nT) = \mu_n$ and $t_n = nT - \theta(nT)$, then $g(\tau) = x[\tau - \theta(\tau)]$ and $g(nT) = x[nT - \theta(nT)] = x(t_n)$. Using the uniform sampling interpolation for $g(\tau)$,

$$g(\tau) = \sum_{-\infty}^{\infty} g(nT)sinc[\frac{\pi}{T}(\tau - nT)].$$

Using the substitution $\tau = \gamma(t)$ gives

$$x(t) = g[\gamma(t)] \approx \sum_{n=-\infty}^{\infty} x(t_n)sinc[\frac{\pi}{T}(\gamma(t) - nT)].$$

When $x(t)$ is not band-limited, this approximation becomes an exact representation.

Satellite images, which are sampled on a slightly perturbed grid, are an example of jittered sampling. The sources of the grid perturbations include micro-vibrations of the satellite while it takes the image, and irregularities in the position of the sensors on the image plane [Almansa, 2002]. Physical models of the satellites exist, which allow to predict vibration modes, that can be activated at one time or another. This perturbation can be estimated with high accuracy, but it must be also corrected in the images for certain stereo and multi-spectral applications.

If the positions of the samples are

$$\Lambda = \{\lambda_k\}_{k \in Z^2} , \ \ \lambda_k \in R^2$$
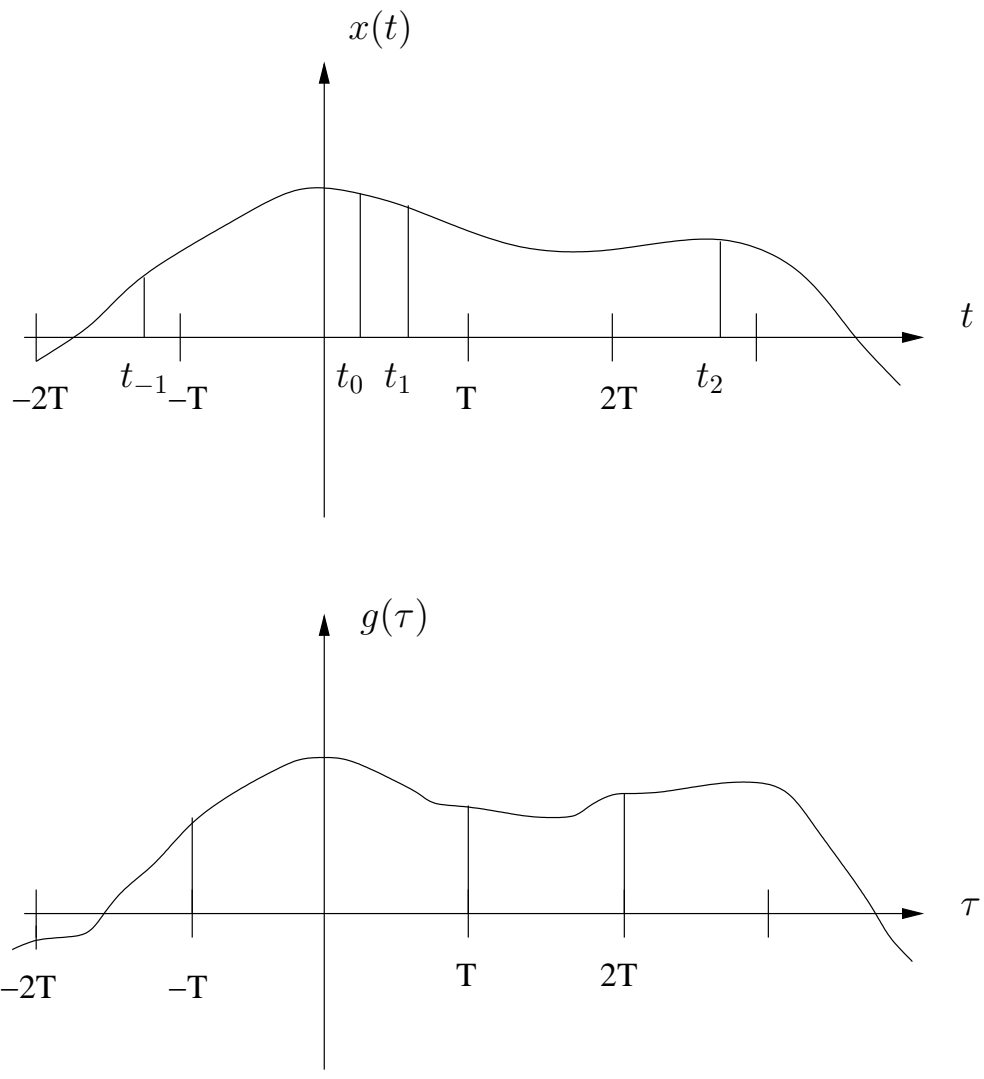
Figure 1.14: Jittered samples.

then in the perturbed (jittered) sampling case

$$\lambda_k = k + \mu(k),$$

where some properties may be assumed about the perturbation function μ, for example, about its amplitude. The main results on the limits of perturbed sampling were given by Kadec [Almansa, 2002, Almansa et al., 2001]. For the one-dimensional case the limit is the following. If there is a constant c such that

$$|\mu(k)| = |\lambda_k - k| \le c < \frac{1}{4},$$

then there exists a stable reconstruction formula of any band-limited function x from its irregular samples $x(\lambda_k)$.

For two dimensions: if the perturbation μ is such that

$$|\mu(k)| = ||\lambda_k - k|| \le 0.11,$$

then there exists a stable reconstruction formula of any band-limited function x from its irregular samples $x(\lambda_k)$.

There are two factors that limit the application of the results presented in this section. At first, as it is mentioned in [Almansa, 2002], the theorems of Kadec give the theoretical results for the acceptable bounds of jitter for 1D and 2D cases, but the practical algorithms consider only the 1D case. And the generalization for two dimensions is difficult for most of the cases and doesn't exist at the moment. The second factor is related to the framework of this thesis, because the data sets we have do not satisfy the theorems of Kadec. The sampling strategy used to acquire our data leads to irregular sampling and not to a jittered one.

1.4.4 Wavelets on irregular grids

The fundamental property of wavelets is that they allow representations which are efficient and which can be computed fast. Wavelets are capable of quickly capturing the essence of a data set with only a small set of coefficients. This is based on the fact that most data sets have correlation both in time (or space) and frequency. Because of the time-frequency localization of wavelets, efficient representations can be obtained. This is the key to applications.

Wavelet function are traditionally defined as the translates and dilates of one particular function, the "mother" wavelet. Such wavelets are called first generation wavelets. In [Sweldens, 1997] a more general setting is introduced where the wavelets are not necessarily translates and dilates of each other, but still enjoy all the powerful properties of first generation wavelets. These wavelets are referred to as second generation wavelets. The lifting scheme is presented in [Sweldens, 1997], this scheme is a simple, but powerful tool to construct second generation wavelets.

The construction of wavelets as initiated by Daubechies and co-workers essentially consists of three stages. The algebraic stage involves constructing the filters that are

used in the fast wavelet transform, which allows to pass between the function and its wavelet coefficients. In the analytic stage one shows that wavelets associated with these filters exist and that they form a basis for the proper function space. In the geometrical stage one checks the smoothness of the basis functions.

One of the applications, which illustrates the need of the second generation wavelets, is that many real life problems require algorithms adapted to irregularly sampled data, while first generation wavelets imply a regular sampling of the data. The basic idea of the lifting scheme is to start with a simple multiresolution analysis and gradually work one's way up to a multiresolution analysis with particular properties. The lifting scheme allows one to custom-design the filters, needed in the transform algorithms, to the situation at hand. In this sense it provides an answer to the algebraic stage of a wavelet construction. Whether these filters actually generate functions which form a stable basis (analytic stage) or have smoothness (geometric stage), remains to be checked in each particular case. In the lifting scheme, instead of using scaling functions on the finer level to build a wavelet, one uses an old, simple wavelet and scaling functions on the same level to synthesize a new wavelet [Sweldens, 1997].

In [Daubechies et al., 1999] there are some practical examples given for 1D and 2D cases. It is emphasized that in 1D case there are much more results obtained with semi-regular grids than with irregular ones. The key assumption made in this article for both 1D and 2D cases is the smoothness of the sought signal. The examples refers to simplification of meshes in computer graphics applications.

Wavelets can also be adapted for non-smooth functions. An example is the technique called wavelet probing [Sweldens, 1997]. The short description of it is the following. Consider a function which is smooth except for jump discontinuities at isolated points. We know that the decay of the wavelet coefficients is fast away from the jumps and slow in the neighborhood of the jumps. Suppose that we know the location of the jumps. If we use interval wavelets on each interval between two jumps, and thus segment the signal accordingly, we would get fast convergence everywhere. Wavelet probing is a technique which allows us to locate the jumps. It simply tries every location between two samples and checks whether it would pay off to segment at this location. The pay-off can be measured with, for example, the entropy of the wavelet coefficients. Wavelet probing allows quick localization of the edges in a image, and then builds wavelets on the segments defined by those edges.

1.5   Conclusion

The irregular sampling theory started as an extension of the Shannon sampling theorem. This theorem was at first proved for the one-dimensional signal and then extended for the multidimensional case. A powerful generalization of many sampling theorem extensions was given in 1977 by Papoulis. The Papoulis' theorem included the cases of sampling with derivatives and jittered sampling. However, this theorem treated only band-limited functions. So later there were generalizations of the Papoulis theory in order to treat the non-bandlimited signals [Unser et al., 1998]. Since the class

of admissible input functions is enlarged, one looks for an approximation instead of an exact reconstruction. This approximation is consistent in the sense that it produces exactly the same measurements as the input of the system. There are also some other approaches for nonuniform sampling of nonband-limited signals [Ferreira, 1995].

As for the classification of sampling sets, there are regularly spaced samples, structured sampling sets and irregular sampling sets. Regularly spaced samples normally mean equal distances between them in all directions. Structured sampling sets keep some periodicity. The number and complexity of such sets increases rapidly with increasing the dimension of the considered signal. Many methods are developed to reconstruct band-limited signals from irregularly spaced samples [Strohmer, 1997, Feichtinger et al., 1994]. These methods sometimes classified as iterative and non-iterative ones.

An important aspect of the theory of irregular sampling is a necessary density of sampling needed to recover the signal from its samples. The first results were obtained by Landau in 1967 and there is still research conducted in this area [Unser, 2000].

The theory of irregular sampling is applied in many areas, like geophysics, computer tomography, astronomy, control theory, missing data problem and others, and this theory is currently being developed [Martin, 1998, Almansa, 2002].

In this chapter we have considered the existing theories on the regular and irregular sampling. We conclude that in the present state of the sampling theory there are no practical methods on the reconstruction preserving discontinuities for randomly sampled signals. In the following chapters we describe the data to be interpolated as well as the methods we choose to apply.

Chapter 2

Airborne laser scanning

2.1 Introduction

Airborne laser scanning is a relatively new data acquisition technique regarding the start of its practical usage with high precision. It gives us the possibility to recover the information on the scanned area in the form of 3D coordinates of the scanned points. This scanning technique is a subject of research and a lot of interest has been shown to its performance over different types of surfaces. Also this technique is often compared with the other, more traditional, stereo photography methods. This chapter presents a short introduction to airborne laser scanning, discusses its accuracy and properties as well as the main fields of laser data application. We analyse laser scanning technology in detail because we believe that understanding of the nature of data is necessary for developing a suitable interpolation approach, which is the goal of this thesis.

2.2 Acquisition technique

Laser ranging instruments placed on aircraft or spacecraft platform are capable of high resolution altimetry measurements of the topography of earth, lunar, and planetary surfaces [Bufton, 1989]. First laser altimeters appeared in 1970 [de Joinville, 2003]. The first measurements didn't have the same precision as now. With the development of GPS and INS (Inertial Navigation System) technologies, airborne laser scanning is used more widely in remote sensing, for example in data acquisition for urban areas. This technique can be considered as a good complement to the existing well known and well studied photogrammetry methods. In photogrammetry, optical stereo images to reconstruct the surface of the photographed zone. In this thesis we reconstruct the surface by interpolating the laser scanning data. It is certainly possible to combine the both acquisition techniques while seeking for the more accurate results. Later in this chapter we will consider the principal differences between photogrammetry and laser scanning.

Airborne laser scanner is an active sensing system that uses a laser beam as the sensing carrier [Wehr, Lohr, 1999]. Airborne laser scanning produces irregularly

spaced 3D points of an area over which a flight is performed. These points provide the elevation values of the terrain and of the objects rising from the ground, like buildings and vegetation.

The technique is determined by three main components (Figure 2.1): the laser rangefinder (LRF), the INS and the DGPS (Differential Global Positioning System). The GPS is a navigation system which uses signals transmitted from 21 satellites orbiting the Earth in 6 orbital planes to provide the location of a receiver antenna anywhere on or above ground [Morshed, 2000]. The transmitted radio signals contain information on the ionosphere transmission parameters and positions of the satellites at the transmission time from which the location of the receiver can be referenced to the satellite orbits. These orbits have been determined to accuracies of better than 1 m by Earth stations. Given the speed of the signal and the time of its propagation, the distance from the GPS receiver and a satellite can be calculated. The three-dimensional position of the receiver is located via intersection of three spheres. Each sphere has a satellite as its center and a radius equal to the distance from the satellite to the receiver [Kaplan, 1996]. Using DGPS means having a reference ground station on the Earth. This station has known 3D coordinates and it receives the signals from the GPS satellites. The coordinates of the receiver are then adjusted using the time delay calculated with the ground station. That improves the precision. Accelerometers and gyroscopes are used in INS in order to determine the attitude of an aircraft. The laser scanner and the GPS/INS system have different measurement frequencies. Therefore in most cases at the exact time of a range measurement no directly measured position and attitude is available and interpolations are necessary [Haala et al., 1996].

Airborne laser scanning components include [Baltsavias, 1999c]:

- an LRF, that contains the laser, transmitting and receiving optics, the signal detector, amplifier, time counter and necessary electronic components;

- computer, operating system and software for control of the on-line data acquisition;

- storage media for laser, GPS, INS and possibly some other data;

- GPS and INS;

- ground reference GPS station;

- software for mission planning and for various stages of postprocessing;

- optionally, other sensors, for example, video and digital cameras.

The basic idea is to get polar coordinates of a point hit by a laser beam. The direction of the beam is calculated by combining the angle of the scanning system with the aircraft angles, given by the INS. The laser rangefinder measures the distance between the aircraft and the laser point. Most of the airborne laser scanning systems
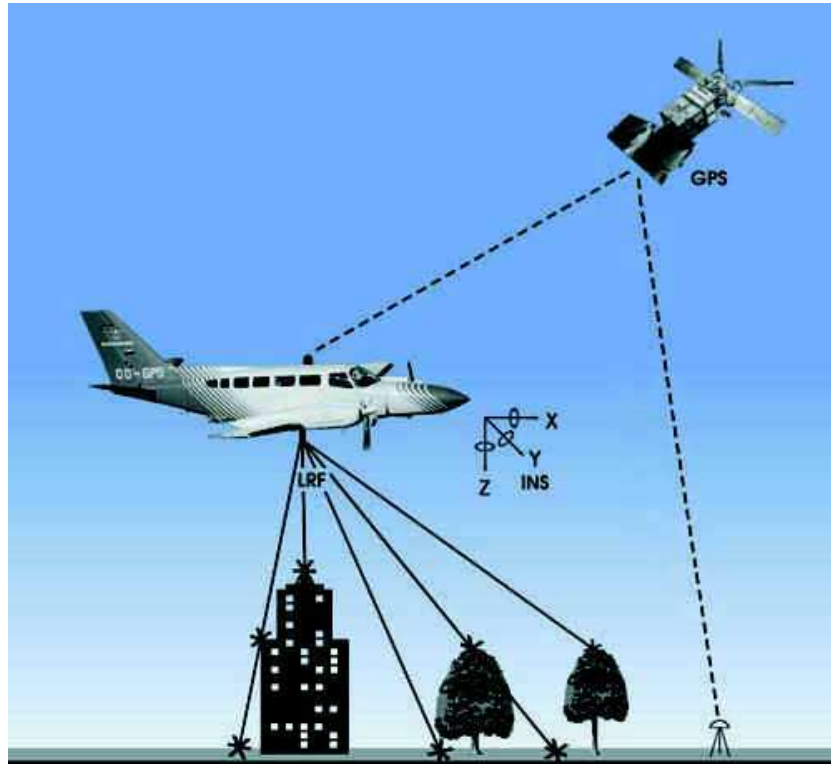
Figure 2.1: Airborne laser scanning acquisition principle (©Eurosense).

are using pulsed laser. In this case the distance between the aircraft and the laser point is

$$R = c\frac{t}{2},$$

where c is the speed of light, the time t is given by a time interval counter. The time is measured when the signal voltage has reached a predetermined threshold value. To avoid confusion in the pulses arriving at the time interval counter, it is usually a requirement that no pulse is transmitted until the echo of the previous pulse has been received [Baltsavias, 1999a]. The pulse rate depends on the laser scanning system and can differ from several kHz till 83 kHz (for the TopoSys system). The maximum range (and flying height) are limited by laser power and beam divergence, atmospheric transmission, target reflectivity, detector sensitivity. The position of a target hit by a laser is calculated using the transformations from one coordinate system to another, that is applying translation and rotation operators. At first, the coordinate system, centered at the laser firing point is rotated to compensate the angle of the laser beam. Then a rotation and transformation are performed to transform the laser coordinate system into the local INS system. After that a transformation from the local INS coordinate system to the local GPS coordinate system, centered on the GPS antenna, is performed. The last transformation is for getting the points in the WGS-84 coordinate system [Schenk, 2001]. An additional transformation may be done to convert the coordinates for a national system (for France - Lambert system).

Some technical parameters of airborne laser scanning systems [Baltsavias, 1999c]

are given in Table 2.1.

	Minimum value	Maximum value	Typical values
Scan angle (°)	14	75	20−40
Pulse rate (kHz)	5	83	5−15
Scan rate (Hz)	20	630	25−40
Flying height (m)	20	6100	500−1000 (for airplane)
GPS frequency (Hz)	1	10	1−2
INS frequency (Hz)	40	200	50
Beam divergence (mrad)	0.05	4	0.3−2
Across-track spacing (m)	0.1	≈10	0.5−2
Along-track spacing (m)	0.06	≈10	0.3−1
Angle precision (roll, pitch/heading) (°)	0.004/0.008	0.05/0.08	0.02−0.04/0.03−0.05
Range accuracy (cm)	2	30	5−15
Height accuracy (cm)	10	60	15−20
Planimetric accuracy (m)	0.1	3	0.3−1

Table 2.1: Overview of major technical parameters of airborne laser scanning systems.

The laser footprint is described by two angles γ and Θ shown in Figure 2.2. Received pulse energy depends on these two angles: $e(\gamma, \Theta)$. The range is $R(\gamma, \Theta)$ and the time of propagation $t(\gamma, \Theta) = \frac{2}{c}R(\gamma, \Theta)$. The reflected light at a position γ, Θ is $\rho(\gamma, \Theta)e(\gamma, \Theta)$, where ρ is the reflectivity of the target. The time response is

$$r(t) = \int_\gamma \int_\Theta \rho(\gamma, \Theta)e(\gamma, \Theta)\delta(t - \frac{2}{c}R(\gamma, \Theta))d\Theta d\gamma$$

.
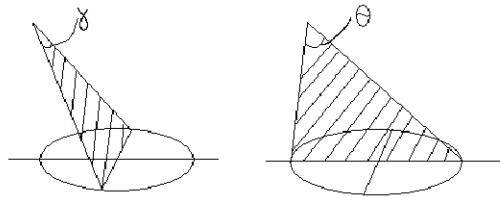
Figure 2.2: The two angles that describe a laser footprint.

A laser footprint on the ground has a diameter from 10 cm till 100 cm, depending on altitude and other factors [Mercer, 2001]. The minimum detectable object within the laser footprint does not depend on the object's size, but primarily on its reflectivity [Baltsavias, 1999a]. Often the beam meets two or more obstacles, especially in forest areas (Figure 2.3).

Then two or more reflections return to the rangefinder. Most of the systems can record these echoes or at least the first and the last pulse. Normally, the last pulse is

Figure 2.3: The first pulse comes from the top of the tree and the last one - from the ground (©TopoSys).

the one reflected from the ground and the first one comes from tops of trees or roofs of buildings. A laser pulse can penetrate partly into and possibly through the vegetation cover of the terrain. This potential of passing through forest canopies was the original motivation to study laser systems at the University of Stuttgart for the purpose of generating DTMs (Digital Terrain Models) of forest areas [Ackermann, 1999]. A DTM defines the ground surface without buildings and vegetation. Airborne laser scanning provides elevation values of the ground even in dense forests, especially if the footprint size is not too small. So a DTM can be produced easier and faster [Petzold et al., 1999].

To get strips of laser points, scanners use mirrors or fiber optics. Oscillating mirror technique (used in Eurosense company, for example) produces a z-line pattern of the laser points on the ground (Figure 2.4).
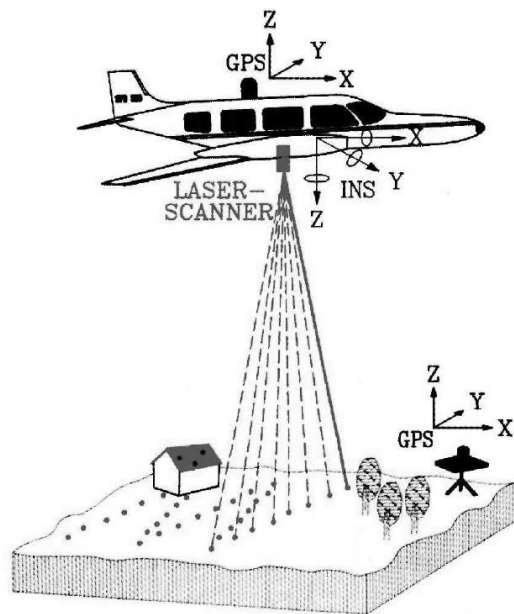
Figure 2.4: Laser scanning that produces a z-line pattern.

The TopoSys system uses fiber optics and produces a pushbroom measurement pattern resulting to parallel lines on the ground. For this system the point density on the flight direction is very high.

The most commonly used laser scanning systems are Optech ALTM, Saab TopEye,

Toposys and Azimuth [Baltsavias, 1999c].

The data acquired by airborne laser scanning is supposed to be evenly distributed regarding the planimetric coordinates of points. Though the density of the points varies considerably because the scanned strips overlap. It is done to avoid the gaps in the data shown in Figure 2.5. Also overlapping strips allow some quality control procedure since the same zone is scanned twice.
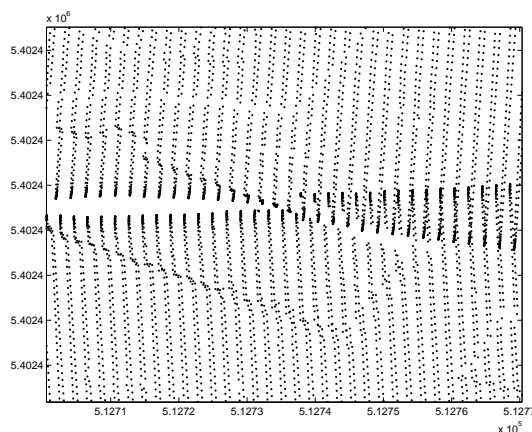
Figure 2.5: The sampling pattern of a real laser data: a gap in the data appears because two neighboring stips don't overlap.

With the development of laser scanning systems large amounts of data can be collected in a short time. For example, for the data of Amiens and its suburbs we have more the 72 million of points. Though we are only interested in the urban zone and we will interpolate only a part of it.

We dispose two real laser data sets for the experiments. The first data set was acquired on Brussels (Belgium) by the Eurosense company. They used an ALTM laser scanning system produced by the Optech company. Though the recent ALTM systems allow to acquire two echoes, the system used to scan the city of Brussels can register only one single echo. This acquisition system uses an oscillating mirror technique. It produces a sampling set formed by zig-zags. The second real data set is obtained on Amiens (France). The data acquisition is done by the TopoSys company and they use their own laser scanning technology. It has very high acquisition frequency (83 kHz) and uses fiber optics. The resulting sampling set is formed by parallel lines. The distance between points inside a line is several times smaller than the density between the lines. The distance between the lines is about 1.5 meters. A big part of the scanned area is covered twice by the laser scanning. Two echoes are received: the first and the last one. The last echo data is used for the experiments. The size of the laser beam in the both cases for Brussels and Amiens is about 30-50 centimeters.

2.3 Laser data accuracy and properties

The accuracy of 3D coordinates depends on many factors [Baltsavias, 1999a]. The main factors are the accuracy of the range, of the laser beam position and the accuracy of the laser beam direction. Since the results of laser scanning are usually in WGS84 (World Geodetic System 1984), the final results also depend on the accuracy of the transformation from WGS84 to the local coordinate system.

The range accuracy of pulse lasers depends on the ability to select the same relative position on the transmitted and received pulse in order to measure the time interval. Laser pulse waveforms for range measurement and waveform digitization is shown in Figure 2.6 [Bufton, 1989]. An example of the return pulse waveform for a zone
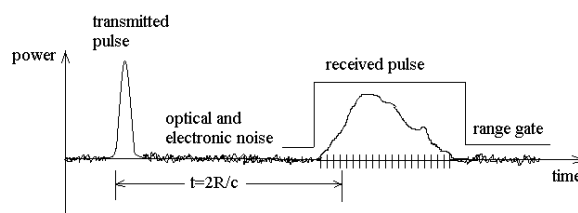
Figure 2.6: Laser pulse waveforms for the sent and received pulses.

with vegetation is given in Figure 2.7. It is obvious that recording and analyzing the
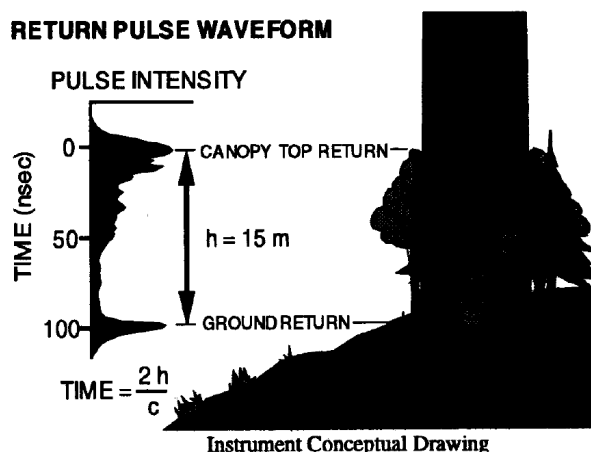
Figure 2.7: Return pulse waveform for airborne laser scanning vegetation [Blair et al., 1994].

waveform, instead of one or two echoes, will lead to much more precise information about the area hit by the laser beam. Another useful information for such analysis, especially for urban areas, will be the reflectivity of the objects on the ground.

The time interval measurement accuracy is limited by noise, signal strength and sensitivity of the threshold detector. The main factor here is the steepness of the received signal, that is the rise time of the pulse. Also important are the accuracy,

with which fixed time delays in the system are known, e.g. counter instability. The time counter has a resolution of approximately 0.1 ns (typical values are 0.05-0.2 ns), which would correspond to a range resolution of 1.5 cm. Among other factors, that affect the range accuracy, there are effects from the optical elements, properties of the detector, reflectivity and the form of the target.

Position accuracy depends mainly on the quality of the DGPS postprocessing. Other factors: GPS hardware, GPS satellite constellation during flight, number, distribution and distance of the ground reference station from the aircraft (values of 10-100 km have been reported), accuracy of offsets and misalignment between GPS and INS, and INS and laser scanner. Typically, with DGPS and postprocessing, accuracies of 5-15 cm can be achieved [Baltsavias, 1999a].

Attitude accuracy depends on the quality of the INS, the INS frequency, the method of postprocessing and integration with the GPS. The effect of attitude errors on the 3D accuracy increases with the flying height and the scan angle. Due to gyro drift and other errors INS forms the weakest part of the system since it is characterized by a good short term but a poor long term stability [Lemmens, 1997]. Orientation, position and range are to be taken at the same time in order to produce accurate data. If there is a time offset and this is not known precisely, it will cause a variable error.

The height accuracy of the airborne laser scanning data is about 5-20 cm and is 2-5 times better than the planimetric one. These are the estimations for a rather flat surface. With increase of terrain slope and roughness both planimetric and height errors increase: the height accuracy deteriorates to 0.5-1 m [Baltsavias, 1999b].

Scan angle also influences the accuracy. The angle may vary for different systems and applications from several degrees to ±30 [Ackermann, 1999]. The distance between laser points on the ground depends on the flying height, on the scan angle, acquisition system and can be from several centimeters till several meters (Figure 2.8).

(a)   (b)
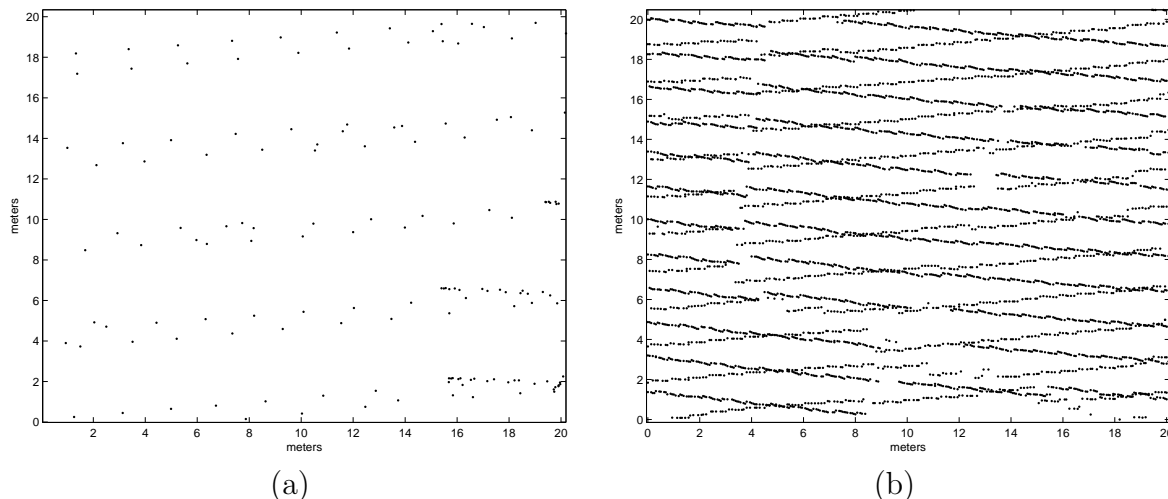
Figure 2.8: Planimetric coordinates of (a) laser points acquired using oscillating mirror technique (b) two strips overlap for the data taken using fiber optics.

The density of points is normally higher along scan lines than between them. Laser

45

scanning data is captured in strips with sufficient overlap to ensure that no gaps appear between the strips. The width of strips can be between 70 m and 800 m, depending on the flying height of the platform and on the system used [Behan, 2000]. If there are two strips that overlap, then elevation values of the laser points for the same area may not coincide, especially when the ground surface is not flat (Figure 2.9). In general,

(a) (b)
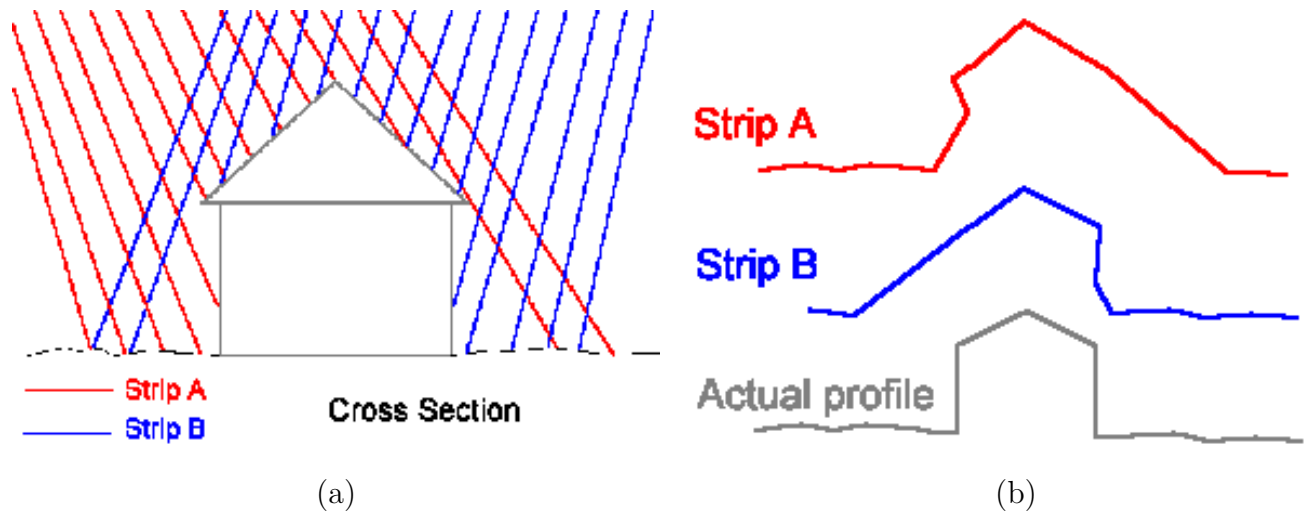
Figure 2.9: (a) Two strips overlap (b) laser data profiles in the overlap region (source: TU Delft).

airborne laser scanning systems are considered to be highly automated, with short data processing time and high precision [Ackermann, 1999, Murakami et al., 1998].

The output data is given by a text file that contains X,Y and Z coordinates of the acquired points. X and Y coordinates do not lie on a regular grid. This means that the data can't be presented as an image as long as no interpolation is performed. The laser data can be visualized like three-dimensional points or triangulated and then visualized (Figure 2.10).

As for a laser altimeter in earth orbit, ice and terrain topography can be measured at sub-meter vertical resolution and approximately 100 m horizontal separation with 50-100 m diameter laser footprint. Ice and terrain roughness can be measured via laser pulse waveform analysis [Bufton, 1989].

2.3.1 Comparison with photogrammetry

The major differences between photogrammetry and airborne laser scanning are the following [Baltsavias, 1999b]: passive versus active sensing; sensors with perspective geometry versus point sensors with polar geometry; full area coverage versus pointwise sampling; indirect versus direct encoding of 3D coordinates; geometrically high quality images with multispectral capabilities versus no imaging; and ability for airborne laser scanning to 'see' object much smaller than the footprint (small openings below vegetation, power lines, etc.). All other differences are a consequence of the above
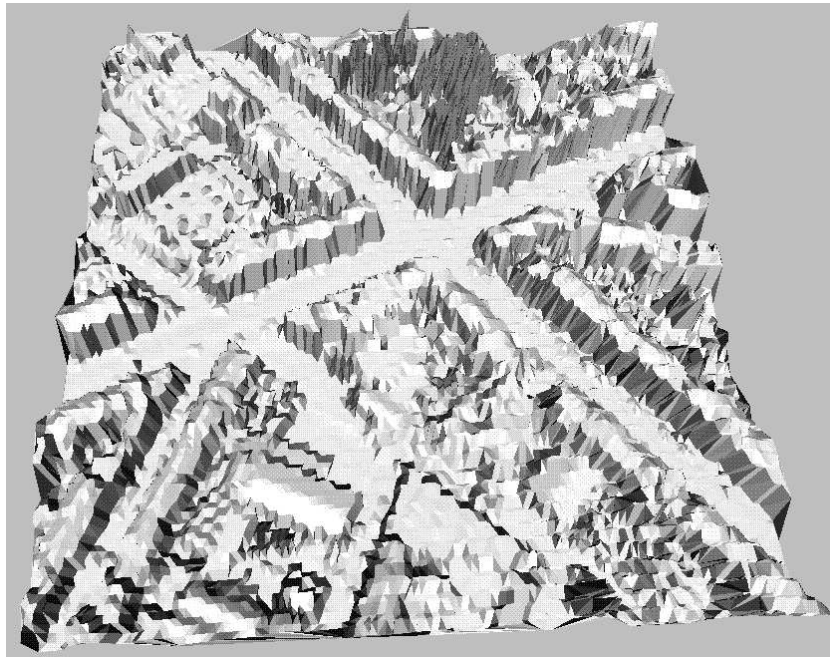
Figure 2.10: Triangulated laser scanning data of Brussels (©Eurosense).

mentioned ones. The advantage of using airborne laser scanning for DEM (Digital Elevation Model) generation is that, being produced by active systems, they are insensitive to illumination shadows. Furthermore, laser images are already geocoded, that is no orthoimage generation is necessary.

Density and distribution of raw measurements is a decisive factor with respect to DEM quality. With manual and matching photogrammetric measurements, one could measure theoretically as dense as possible. For airborne laser scanning the smallest reasonable grid spacing is assumed to be a half of the laser footprint. The grid sizes for both photogrammetry and laser scanning depend on the height of flight during which the data was acquired. In this regard the two technologies are more or less equivalent. In practice, manual photogrammetric measurements never need to be that dense, while matching usually delivers less dense results than those of airborne laser scanning.

As for the error budget and accuracy, the comparison between photogrammetry and airborne laser scanning is not easy to make [Baltsavias, 1999b]. In manual photogrammetric measurements, the height accuracy, assuming an image measurement accuracy of 15 micrometers for an image of average quality and texture, mainly depends on the flying height and the accuracy of the sensor orientation. With airborne laser scanning, there are much more factors that can influence the results. Thus making derivation of theoretical accuracy models, prediction of the achieved accuracy and error propagation much more complicated. Furthermore, with passive optical sensors the behavior of planimetry and height is quite independent of each other and can be analyzed separately. In addition, with airborne laser scanning the error budget has a substantial constant term which in photogrammetry is lower. Accuracy with passive

optical sensors is also more homogeneous within the image format, while with airborne laser scanning, attitude errors lead to a rapid height accuracy decrease with increasing scan angle, especially for high flying height.

With increasing terrain slope and roughness, the height accuracy of airborne laser scanning deteriorates to 0.5-1 m for 1000 m flying height. Airborne laser scanning becomes more accurate than photogrammetry for terrain slopes less than 30%. Ignoring the effect of terrain slope and target reflectivity on the laser accuracy, the expected height accuracy from a laser scanner consists coarsely of a fairly constant error of 5-20 cm (mainly due to GPS and ranging) and an error of 0.5-2 cm per 100 m of flying height for typical attitude errors and a scan angle of 30% (in reality the height error is not linear but rather exponential; for medium to large scan angles, it increases rapidly with increasing flying height). Photogrammetry also has a constant term assumed to lie at 2-5 cm and an additional error of about 1.6 cm per 100 m of flying height. Comparing the accuracy values for identical flying height in the range 400-1000 m, the photogrammetric accuracy is on the average slightly better than the airborne laser scanning one, although the latter can in good cases be more accurate. It is in the higher flying heights where laser could outperform photogrammetry, if attitude determination is accurate enough and the received target reflection is sufficient.

In photogrammetry, planimetry is typically more accurate than height, while with airborne laser scanning 2-6 times less accurate. Such planimetric errors will also severely influence the height accuracy of urban areas.

2.4 Applications of laser data

Satellite laser altimeters are used for high-resolution measurements of ice sheet topography, landform topography and cloud-top height on a global basis [Bufton, 1989].

The most important applications of airborne laser scanning include the following ones [Baltsavias, 1999b]:

- Mapping the surfaces with very little or no texture or poor definition. There, image matching delivers very poor results, and manual measurements are also poor and slow and cumbersome. Examples include ice or snow surfaces, sand (coasts, dunes, desserts), swamps and wetlands.

- Mapping of forests and vegetated areas. Airborne laser scanning systems can provide measurements on the ground. The penetration rate mainly depends on type of trees (deciduous or coniferous) and season. Useful results, depending also on the terrain roughness, can be achieved even with penetration rates of 20-30%. Experimental systems of NASA using a very large laser footprint (10-30 m) have achieved results in dense tropical forests with a ground obstruction of 95%. In addition, through appropriate data processing, both ground and tree height can be determined. Airborne laser scanning systems that record first and last echoes or even more than two echoes of each pulse, can more easily provide tree and ground height and those with more than two echoes can, in addition, measure

a vertical object profile, thus enabling derivation of other important parameters like biomass estimation, tree type, etc.

- Mapping of long, narrow features. This includes road mapping, planning and design, powerline corridor planning, coastal erosion monitoring, coastal zone management, riverways and water resources and traffic management, mapping of railway lines, pipelines, etc. Since airborne laser scanning systems have a narrower swath in comparison to optical sensors, they are more cost-effective in capturing the information needed for such applications.

- High point density, high accuracy mapping applications like monitoring of open pits, flood mapping, mapping of local infrastructures (airports, for example), oil and gas exploration.

- Mapping of very small objects, for example, power lines, which are hardly visible in optical images, or whose measurement cannot be automated. This application is possible when the laser scanning system is well calibrated.

- Fast response applications. Since airborne laser scanning provides digital range measurements, this information can be quickly converted to 3D coordinates. It can be important in some cases, for example, involving natural disasters. This application as well as several others may require automated classification, in other words - filtering, of clouds of points acquired by airborne laser scanning [Sithole, Vosselman, 2004].

- DEM generation of urban regions for urban planning, roof-top heights for communication antennas, etc. Since airborne laser scanning provides very dense and accurate measurements, detection, reconstruction and modeling of 3D objects with sharp discontinuities, especially buildings, is possible [Wang, 1998, Axelsson, 1999, Haala, Brenner, 1999].

The quality of a DEM depends on [Lemmens, 1997]:

- amount of outliers and undesired terrain objects;

- accuracy of the individual points;

- interpolation method to compute heights at wanted locations from the measured points;

- point density (the sampling distance should sufficiently well correspond to the terrain relief fluctuations).

2.5   Conclusion

The airborne laser scanning is explained in this chapter. The interpolation methods, described later in this thesis, will be applied to two real data sets acquired by this

technique. We are interested in the laser scanning acquisition method, because it characterizes the nature of our data. In this regard, it makes sense to investigate the accuracy of laser scanning which is closely connected to the hardware performance in the laser scanning system. Studying laser scanning we realize that at present no conclusions can be made about the surface inside a laser beam. A measurement we get comes from the laser beam that often has an elliptical form, but it is not clear what object inside the beam caused this measurement: inside the same beam we may have several objects of different height and different reflectivity. So one of the accuracy limits of laser scanning data is the size of the beam. Other limits come from the performance of the hardware and the type of the surface to scan. Post-processing of the data after the flight is also important. A new generation of laser altimeters additionally records the shape of the returning pulse. This waveform carries information on the reflecting objects (terrain, vegetation, etc.) within the pulse diameter. In this chapter we present an approximate shape of the waveform as we realize that its analysis will lead to better accuracy and therefore to better interpolation results.

We will perform several interpolation methods on two airborne laser scanning data sets and we will present and analyse the results in this thesis. As we have seen in this chapter, the first echoes of laser scanning come from the top parts of the vegetation and the last echoes - from the ground. We will take it into account for the data of Amiens and will use only the second echoes. It will allow us to avoid the vegetation in the data and so to be closer to the reference used for this zone, because the reference contains no vegetation.

Chapter 3

Interpolation for airborne laser data of urban areas

3.1 Introduction

Many interpolation methods are adapted for image interpolation. The methods for irregularly spaced data interpolation are not that numerous and we will consider some of them in this chapter. Both of the applications of this thesis demand irregularly spaced data interpolation methods. For the laser data on urban areas we need a method that allows discontinuities on the surface. These discontinuities will represent the edges of the buildings and therefore will delimit streets and buildings. Simple and fast approaches that can give such surfaces are nearest neighbor interpolation and triangle-based linear interpolation. We describe them in this chapter. We also present an energy minimization approach which allows to impose the desired properties on the surface to find. Since we know the characteristic properties of an urban area, we choose the appropriate potential functions and we adapt the cost function for the irregularly spaced samples. In this chapter we also describe kriging - the method developed in geostatistics for spatial data interpolation. We will mostly benefit from this method later, when we deal with the cosmic microwave background anisotropies measurements.

The chapter is organized in the following way. In the beginning we present the general approaches to the spatial data interpolation. Then we describe the methods that we will apply in the following chapters to the real data. The methods are presented by increasing their complexity. We start by the nearest neighbor interpolation, then we describe triangle-based linear interpolation and kriging, and we finish by the energy minimization method. Several issues are considered for the energy minimization. We define two kinds of neighborhoods - one for the data samples and one for the pixels on a regular grid. Then we formulate the expression for the cost function that will be minimized. The choices for potential functions and for the optimization algorithm are then discussed. Each of the presented methods is illustrated by simple examples on a synthetic model of an urban area. It gives the general idea about the advantages and drawbacks of the methods before their application to the real data.

3.2 General approaches

Originally, the data, obtained by airborne laser scanning, is scattered, and the task is to put it on the regular grid. We consider square regular grid, although a triangular grid also exists. Some essential aspects of ideal interpolation can be summed up by the following generalizations [Watson, 1992].

1. The interpolated surface fits the data to a nominated level of precision, that is, it agrees with the individual data points to within arbitrary, user prescribed, limits.

2. Each interpolated value depends only on a local subset of data, and the members of this subset are determined solely by the configuration of the data situated near the interpolation point. Such a restriction is necessary to prevent the masking or submerging of low amplitude surface forms by more dominated features, and prevent widespread propagation of an error in a datum. This insures that the generated surface is stable in the sense that a small change in any datum cannot cause a large change in the surface.

3. The interpolation method can be applied to all configurations and density patterns of data. It is in order to have consistency of interpretation, for example, between two data sets of the same region but with different sampling patterns.

The choice of interpolation approaches is very broad, but dealing with irregularly scattered points upon urban areas restricts the variety of possible solutions. There are two reasons for it: one needs to have a method, adapted for a scattered initial data and preserving discontinuities and slopes of a surface.

As described in [Watson, 1992], there are two interpolative approaches - fitted functions and weighted averages.

Fitted function methods first determine the parameters of an analytic bivariate function that represents a regional, or local, aggregate of data influences. Then, using these parameters, the function is evaluated at a given location to obtain the height of the representative surface. Fitted function interpolation techniques utilize surfaces that can be described by a set of coefficients in a polynomial function of geographical coordinates. These surface parameters usually are extracted by solving a system of linear equations expressing the combined influences of the data and the criteria controlling the fit of the polynomial function. Once the parameters, which in a sense are a summary of the data, have been determined, they may be applied to a series of locations for explicit evaluations of the surface. Fitting a function can impose a prescribed general behavior on the surface to override anomalous, or noisy, data. Therefore, fitting a function is a smoothing approach, that is not very suitable for urban areas, where edges, i.e. discontinuities, contain critical information, since they delimit streets and buildings.

The alternative approach, to obtain a representative surface height at a given location, is by directly summing the data influences that are within range; these are

weighted average methods. This approach uses a direct summation of data influences at each interpolation point, without using an intermediate parametric surface. The weight applied to each datum is the evaluated influence, relative to the interpolation point, for that datum. A set of weights must be computed for each interpolation point. Conceptually, the difference between the two approaches is that weighted average methods emphasize local detail whereas fitted functions methods summarize global behavior. Computationally, weighted average representative surfaces require more time per interpolation point than do fitted function surfaces. On the other side, fitted functions tend to overshoot in situations where a sharper curve established by weighted averages would give a more conservative surface. A principal advantage in computing a weighted average surface is that local details, implied by the small-scale trends in the data, can be developed to a degree of surface complexity not possible for a parametric surface with a reasonable number of parameters. This approach also is applicable to data sets of unlimited size because each computation involves only moderately sized subsets of data. Most importantly, weighted average methods produce surfaces that are dominated by local trends in the data.

Triangle-based linear interpolation, nearest neighbor interpolation and kriging can be considered as well-known methods for scattered data interpolation. Since the problem of 3D scattered data interpolation is ill-posed, it makes sense to introduce a regularized solution imposing desirable properties on the resulting surface. An energy minimization approach is proposed which allows to get a surface model corresponding to urban areas. In the following sections we will give the details on these methods.

3.3 Nearest neighbor interpolation

The simplest approach is nearest neighbor interpolation. At first, the given data must be triangulated. Triangulation of the spatial data is the way how to put the data in order to prepare them for some interpolation methods or, simply, visualize the data. In a triangulation every region, except for the external region, is a triangle. The Delaunay triangulation of a set $V = \{x_i\}$ of r points on the plane is usually defined in terms of another geometric structure, the Voronoi (Thiessen) tesselation, which describes the proximity relationship among the points V [Preparata et al., 1985, Rauth, 1998]. The Voronoi tesselation of a set V of r points is a subdivision of the plane into r convex polygonal regions, called Voronoi polygons, each associated with a point x_i of V. The Voronoi polygon of x_i is the set of points of the plane which lie closer to x_i than to any other point in V. A Voronoi tesselation always is unique and unbounded, because the x_i on the perimeter are unbounded. The Delaunay graph of V is a plane graph T, whose edges join pairs of points x_i, x_j, $i \neq j$, such that x_i and x_j are Voronoi neighbors (Figure 3.1).

Then we superimpose the regular grid, on which the interpolated values should lie (Figure 3.2).

For each node of the grid we find the triangle which contains this node. The value of height of this node is the height value of nearest vertex. The resulting surface is
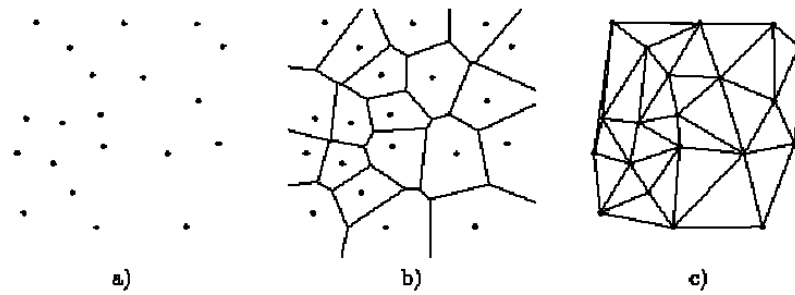
Figure 3.1: a) scattered points, b) Voronoi tesselation, c) Delaunay triangulation.
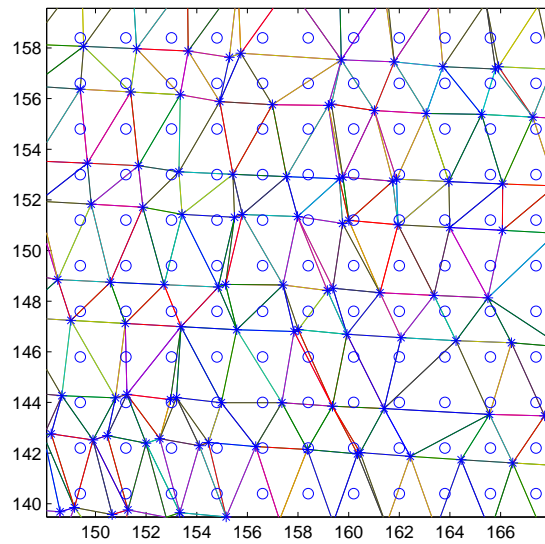
Figure 3.2: Scattered points of laser data (represented by stars) and nodes of a regular grid (represented by circles). Delaunay triangulation is performed on the laser data.

composed by flat zones (Voronoi polygons) divided by sharp transitions.

It actually means that during the triangle-based nearest neighbor interpolation the pixel takes the value of the closest vertex of the triangle which contains the pixel. When the samples are evenly distributed, then such a vertex will be the closest neighbor in most of the cases. But if the samples are organized in a particular way, for example the sampling set of the Amiens laser data is composed by lines, then the closest vertex may not be the closest sample as it will be illustrated in Figure 3.3. We will use the
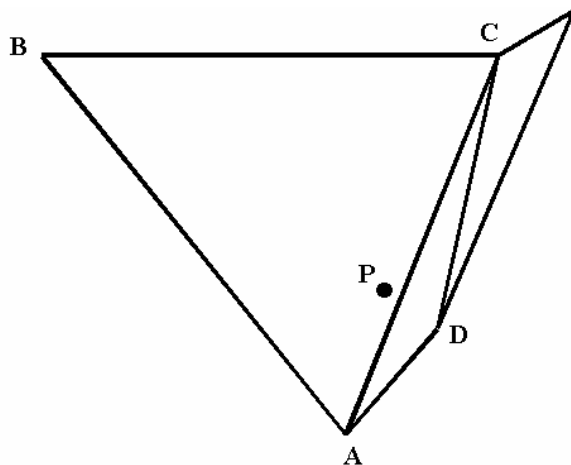
Figure 3.3: Point P is in the triangle ABC, but the closest neighbor for this point is D.

triangle-based nearest neighbor interpolation for the data of Brussels and the nearest neighbor interpolation based just on the distances between the pixel and data samples for the data of Amiens.

We have generated a synthetic model of an urban area (Figure 3.4) which will help us to check the performance of the interpolation methods, presented in this chapter. The proportions of a real urban zone are kept for this model. We estimated the approximate proportions from the digital elevation models of Brussels and Amiens, which will be presented in the following chapter. We designed the synthetic model taking into account differences in the shapes of roofs, in the heights of buildings and in the widths of streets. The synthetic model is designed through the equations of lines and planes. Therefore it is possible to get this model with any resolution. We generate the data to interpolate in the following way. At first we extract a piece of the real laser scanning data of Brussels, we need only x and y coordinates (Figure 3.5). The more detailed description of this data can be found in the following chapter. Knowing the altitude for any pair of x and y coordinates, we can sample our synthetic model according to the real laser data. The synthetic model, sampled according to the laser data of Brussels, is shown in Figure 3.6.

Figure 3.7 shows the result of the nearest neighbor interpolation on the synthetic model when the size of the pixel is 1.5 meters. Figure 3.8 shows the reference model generated with the same pixel size. We can easily see that the nearest neighbor interpolation distorts edges of the buildings. If a pixel, that should represent a roof,
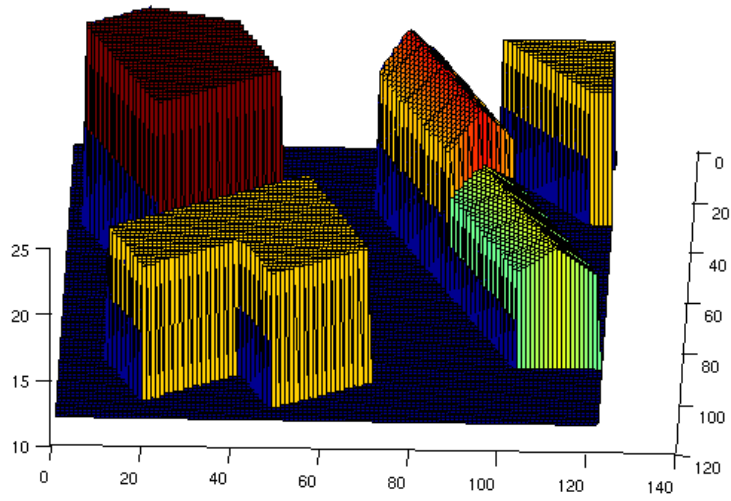
Figure 3.4: Synthetic model of an urban area.
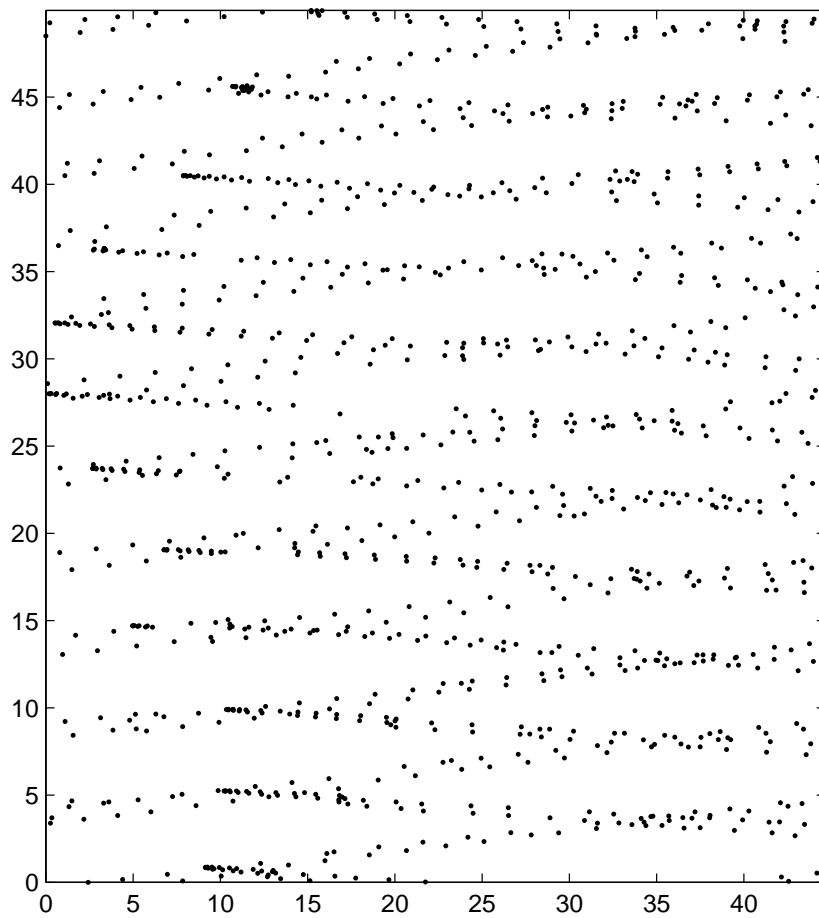
Figure 3.5: x versus y coordinates for a piece of the laser data acquired on Brussels.
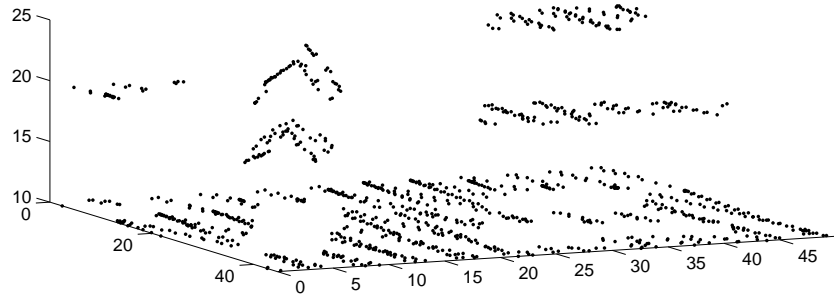
Figure 3.6: Plot of the 3D points for the synthetic model sampled according to the real laser scanning data of Brussels.
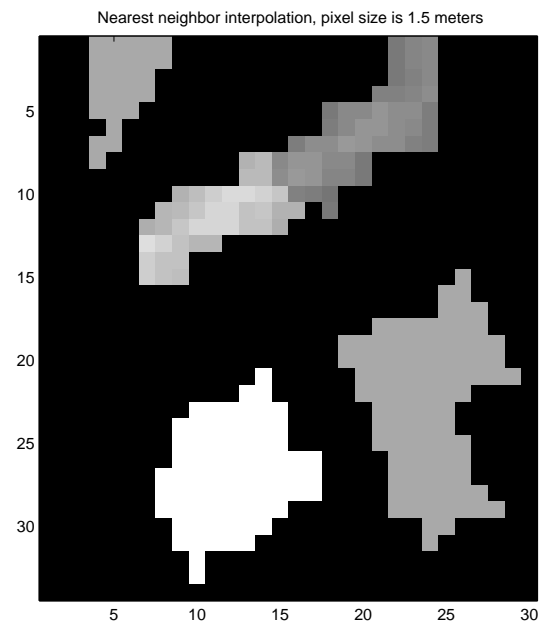
Figure 3.7: Nearest neighbor interpolation on the synthetic model.
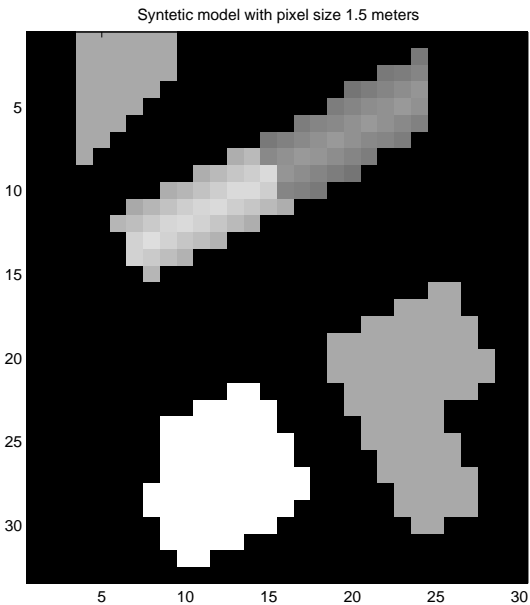
Figure 3.8: Synthetic model with the pixel size 1.5 meters.

has the nearest neighbor on the ground, then this pixel will take the altitude value of this nearest sample, and so it will represent the ground instead of representing the roof. This is the way how we loose some pixels from the roofs of the buildings. In the same manner some pixels get the altitude values of roofs while they should represent the ground. This explains the distortions of edges by the nearest neighbor interpolation. Another observation that we can make is the fact that nearest neighbor interpolation does not let us using all the samples available, especially when the samples compose lines. Only the value of the closest sample point will be taken into account.

We do not adapt the imposed regular grid to the original irregular one. It means that we don't optimize the distance between the nodes of the two grids. For some particular cases it is possible, but in the general framework of this thesis we consider our data to be on irregular grid and it is normally difficult to extract a structure from the data, because the scan lines overlap and the direction of movement of the plane (or satellite - for CMB measurements) changes.

In the following section we will consider triangle based linear interpolation since we suppose it to give more realistic representation of an urban area. This interpolation leads to a piece-wise linear surface, composed by planes determined by the triangles.

3.4   Triangle-based linear interpolation

When the data is triangulated, then interpolating of the planar surface of a triangle can only require applying barycentric coordinates to the data at the vertices of the triangle [Watson, 1992]. This is a weighted average method and the elevation of the interpolated surface at some interpolation point (x, y) within the triangle is

$$L(x, y) = \sum_{i=1}^{3} W_i f(x_i, y_i),$$

where the weight W_i is the ith barycentric coordinate of the interpolation point with respect to the triangle, and $f(x_i, y_i)$ is the observed value at the data point (x_i, y_i). The sum of the barycentric coordinates always is one for any interpolation point. Calculating of barycentric coordinates is shown below. Any interpolation point X, within the triangle IJK, subdivides it as shown in Figure 3.9.
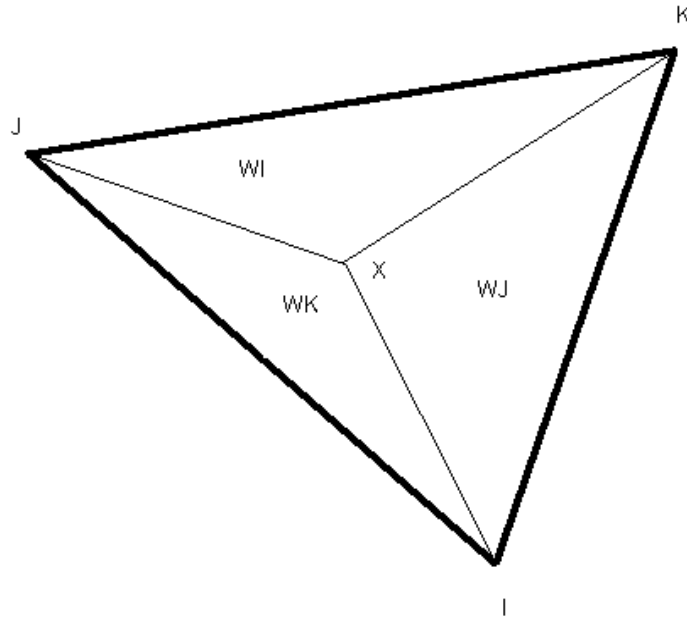
Figure 3.9: Barycentric local coordinates

The areas of these subtriangles, XIJ, XJK and XKI, each calculated as fractions of the area of the triangle IJK, are the barycentric coordinates of the interpolation point for each opposite vertex, respectively. Each coordinate refers to the data point that is opposite that subtriangle so that WK, the coordinate with respect to data point K, is proportional to the area of XIJ in Figure 3.9. A calculating of barycentric local coordinates for the point X with respect to the triplet IJK is following:

$$WI = ((J_x - X_x) * (K_y - X_y) - (K_x - X_x) * (J_y - X_y))/Det_{IJK}$$

$$WJ = ((K_x - X_x) * (I_y - X_y) - (I_x - X_x) * (K_y - X_y))/Det_{IJK}$$

$$WK = ((I_x - X_x) * (J_y - X_y) - (J_x - X_x) * (I_y - X_y))/Det_{IJK}$$

where subscripts x and y are the Cartesian coordinates and

$$Det_{IJK} = (J_x - I_x) * (K_y - I_y) - (K_x - I_x) * (J_y - I_y).$$

Because it is piecewise linear, the surface formed by this method has a discontinuous slope at the edges of each triangular facet.

Figure 3.10 shows the result of the triangle-based linear interpolation on the synthetic model, sampled according to the real laser data. We can observe that, unlike
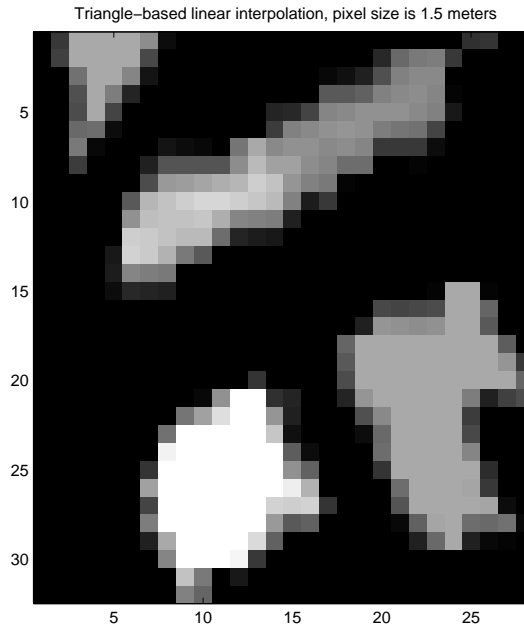
Figure 3.10: Triangle-based linear interpolation on the synthetic model.

the interpolation by the nearest neighbor, on the edges of the buildings there are pixels that have average values between the ground and the roof. The reason for it is the planar interpolation: for example, if the pixel is situated in the triangle, which has two vertices that are the samples taken from the roof and one vertex which is the sample of the ground, then the pixel will get the value of the linear combination of these three pixels. The resulting value of such a pixel will be neither on the roof nor on the ground, it will be in between. That is why we can see a kind of smoothing effect as the result of the triangle-based linear interpolation. Otherwise, this interpolation is quite good for most of the simple shapes of roofs.

It should be noticed that triangle-based linear interpolation provides the value of the pixel calculated using the three vertices of the triangle containing the pixel. These three vertices are not necessarily the three closest points to the considered pixel. Delaunay triangulation is used for this interpolation.

There exist some other methods for irregularly spaced spatial data interpolation [Watson, 1992]. Recently the method by spline functions has received a lot of attention in image processing [Unser, 1999]. Kriging - the method described below, is linked to the interpolation by spline functions [Billings et al., 2002] and leads to smooth surfaces.

3.5 Kriging

Kriging is a geostatistical method first mentioned by Krige and developed by Matheron [Journel et al., 1978, Cressie, 1991, Rauth, 1995, Rauth, 1998]. The idea is to regard all measurements z_i as a realization of a random process and to analyze the spatial behavior of the corresponding parameters. Normally, it is supposed that the expected value of the random function $Z(u)$ is constant all over the domain D and that the covariance of two random variables corresponding to two locations depends only on the vector h separating these two points:

$$E[Z(u)] = m \ \ for \ all \ u \in D,$$

and

$$E[(Z(u+h) - m)(Z(u) - m)] = Cov(h).$$

For ordinary kriging it is supposed that the mean value of the data is unknown.

The first step is the analysis of the spatial variability expressed by a function called variogram γ, which is defined as half the averaged squared difference between pairs of data points separated by the distance h. The variogram (also referred as semi-variogram) can be calculated from the data according to

$$\gamma(h) = \frac{1}{2N(h)} \sum_{N(h)} (v_i - v_j)^2,$$

where v_i, v_j are the data point values and $N(h)$ is the number of data point pairs approximately separated by h.

The experimental variogram is then replaced by a theoretical one (Figure 3.11), often by a spherical model:

$$\gamma(h) = \begin{cases} 0, & h = 0 \\ C_0 + C(1.5(\frac{h}{a}) - 0.5(\frac{h}{a})^3), & 0 < \frac{h}{a} \leq 1 \\ C_0 + C, & \frac{h}{a} > 1 \end{cases}$$

The model variogram is generally chosen to match the experimental one as close as possible (Figure 3.12).

The variogram $\gamma(h)$ is the key to the flexibility of kriging [Groenigen, 2000]. The theoretical variogram is described by a mathematical expression, relating the difference in the dependent values of two points a distance h apart. A model variogram equation has three parameters: scale (C), nugget effect (C_0) and range (a). These parameters are illustrated graphically [Carter et al., 1997] in Figure 3.13.

The scale is the maximum difference in possible for two points with a nonzero distance between them. The nugget effect gives the difference value as the distance between two points tends to zero. The sill is the sum of the scale and nugget effect. If the stationary conditions are met, i.e. there is no underlying trend in the data, then there will be a separation distance above which the variation is constant. This distance is denoted as the range of the variogram.
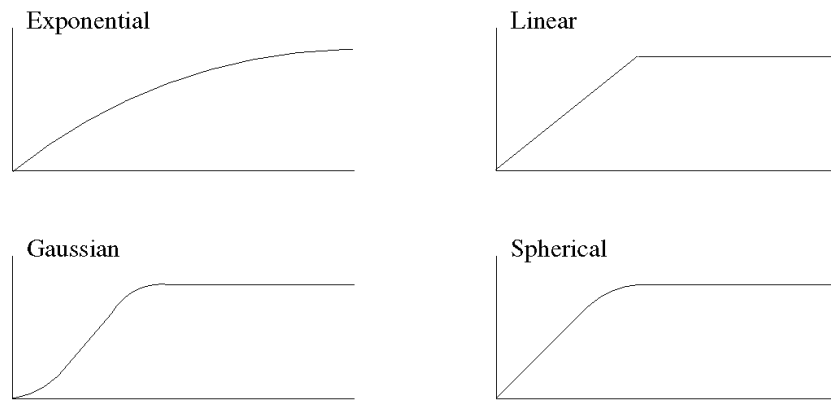
Figure 3.11: Shapes of some commonly used model variograms.
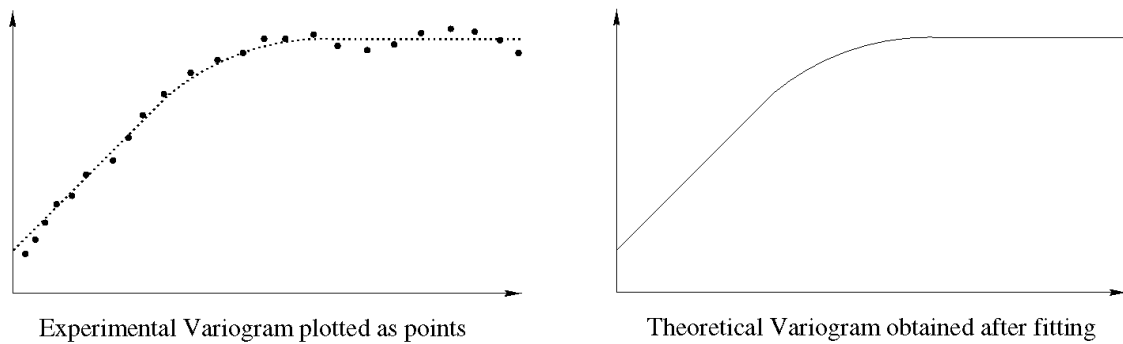
Figure 3.12: Fitting the theoretical variogram to the experimental one.
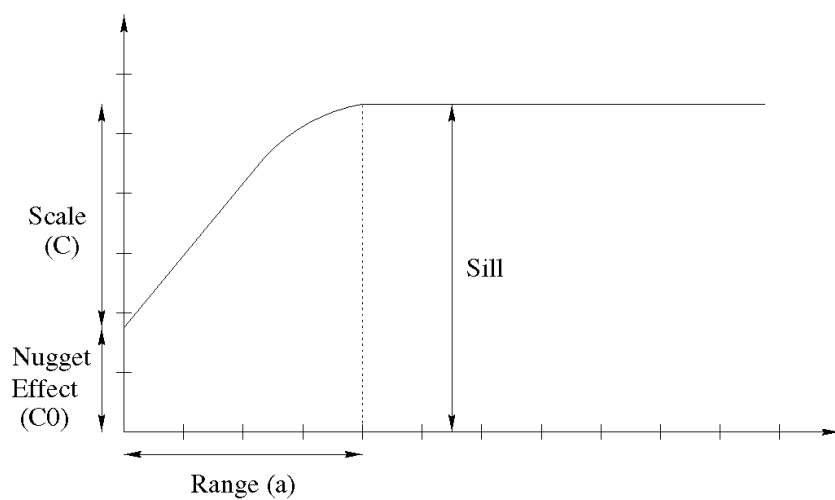
Figure 3.13: A typical model variogram. The parameters used in the mathematical expressions describing variograms are illustrated.

Ordinary kriging is known as best linear unbiased estimator [Pham et al., 1999, Pham et al., 2000]. It is linear because its estimates are based on weighted linear combinations of available data. It is unbiased since it tries to have the mean error to be zero. It is best because the error variance is minimized.

Let $\hat{v}_p$ be an estimated value at location x_p based on a weighted linear combination of available samples at locations x_i, $i = 1, ..., n$:

$$\hat{v}_p = \sum_{i=1}^{n} w_i v_i.$$

The error will be

$$\epsilon_p = \hat{v}_p - v_p,$$

where v_p is the true value. The variance of the estimation error can be computed as

$$Var(\epsilon_p) = Var(v_p - \hat{v}_p)$$

or

$$Var(\epsilon_p) = Var(v_p) - 2Cov(v_p, \hat{v}_p) + Var(\hat{v}_p),$$

giving

$$Var(\epsilon_p) = Var(v_p) - 2\sum_{i=1}^{n} w_i Cov(v_i, v_p) + \sum_{i=1}^{n}\sum_{j=1}^{n} w_i w_j Cov(v_i, v_j).$$

Let σ_e^2, σ^2, σ_{ip} and σ_{ij} stand for $Var(\epsilon_p)$, $Var(v_p)$, $Cov(v_i, v_p)$ and $Cov(v_i, v_j)$ respectively. Then the previous expression can be rewritten as

$$\sigma_e^2 = \sigma^2 + \sum_{i=1}^{n}\sum_{j=1}^{n} w_i w_j \sigma_{ij} - 2\sum_{i=1}^{n} w_i \sigma_{ip}.$$

To satisfy the unbiased condition,

$$\sum_{i=1}^{n} w_i = 1.$$

The optimization technique of Lagrange multipliers is applied to minimize the variance σ_e^2 of the error, which is subject to the unbiased condition:

$$L = \sigma_e^2 + 2\lambda(\sum_{i=1}^{n} w_i - 1)$$

$$\sum_{i=1}^{n} w_i - 1 = 0,$$

where λ is a Lagrange multiplier.

Setting the partial first derivatives of the function L to zero with respect to λ and the weights, after $n + 1$ differentiations, the set of weights that minimize the error variance can be obtained as

$$\begin{cases} \sum_{j=1}^{n} w_j \sigma_{ij} + \lambda = \sigma_{ip}, & i = 1, ..., n \\ \sum_{i=1}^{n} w_i = 1. \end{cases}$$

This system of equations is called the ordinary kriging system [Pham et al., 2000]. In order to be consistent with the variogram symbols, let $\sigma_{ij} = \gamma_{ij}$ and $\sigma_{ip} = \gamma_{ip}$. The system can be rewritten in a matrix form:

$$[A]\{w\} = \{b\}$$

where

$$[A] = \begin{bmatrix} \gamma_{11} & \gamma_{12} & ... & \gamma_{1n} & 1 \\ \gamma_{21} & \gamma_{22} & ... & \gamma_{2n} & 1 \\ . & . & ... & . & . \\ \gamma_{n1} & \gamma_{n2} & ... & \gamma_{nn} & 1 \\ 1 & 1 & ... & 1 & 0 \end{bmatrix},$$

and $[A]$ is symmetrical and its diagonal elements are zeros;

$$\{w\} = \{w_1 \ \ w_2 \ \ ... \ \ w_n \ \ \lambda\}^T,$$

and

$$\{b\} = \{\gamma_{1p} \ \ \gamma_{2p} \ \ ... \ \ \gamma_{np} \ \ 1\}^T.$$

In case of large data sets one uses only a small subset of the samples in the neighborhood of the point to be estimated. This splits the problem into subproblems and keeps computational expenses reasonably low. The biggest advantage of kriging is the fact that the spatial behavior of the resulting surface can be controlled via the variogram. The main disadvantage is the strong influence of the variogram, which in most of the cases has to be fitted interactively. The parameters of the theoretical variogram can be received by observing the experimental one. It is also possible to fit the function of the theoretical variogram to the experimental one through analytical formulas, minimizing the error between the two variograms: theoretical and experimental one [Cressie, 1991]. If there is no precise information a-priori on the surface which has to be interpolated, then one can verify through the form of the experimental variogram whether the hypotheses of kriging are preserved. Since we know the formulas of the theoretical variograms, we can check if the experimental variogram has an approximately the same form or not. For the experiments we take ordinary kriging. This version of the methods supposes that the surface to interpolate is a random stochastic process of the second order with an unknown mean value.

Kriging methods are used not only for statistical interpolation of images [Leung et al., 2001], but also for irregular image subsampling [Stoffel et al., 2001].

The performance of kriging depends on the sampling set. The method presented above is supposed to work on the evenly distributed points in the sampling set. We show it on the synthetic model of an urban area. We sample this model according to two sampling sets: the sampling set of the data of Brussels (Figure 3.5) and the sampling set of the data of Amiens (Figure 3.14). Then we compute the experimental
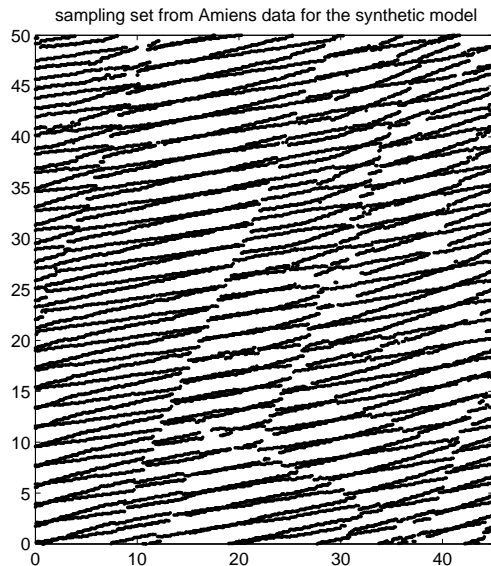
Figure 3.14: x versus y coordinates for a piece of the laser data acquired on Amiens.

variograms for the both sets of data. They look very similar and so the parameters for kriging obtained from both variograms will be practically the same (Figure 3.15), as it should be, because the original synthetic model was the same for both sampling sets. The following parameters are chosen from the visual observation of the variograms:
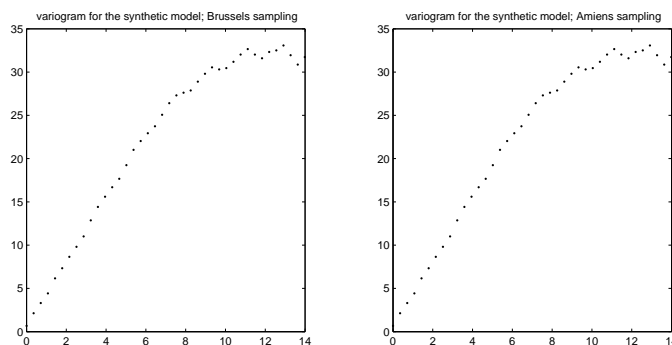
Figure 3.15: Variograms for the synthetic model sampled according to the Brussels laser data (left) and Amiens laser data (right).

range - 10; sill - 32; nugget - 0. The spherical theoretical variogram is taken. We perform kriging on the neighborhood and we take the square window 10×10 meters

for the model sampled by the laser data of Brussels and the square window 1×1 meters for the model sampled by the laser data of Amiens. The results of kriging are presented on Figure 3.16. Kriging produces smooth surfaces as we can see from the
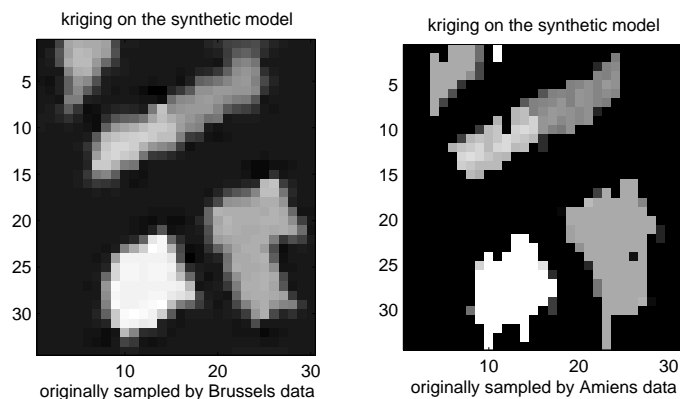
Figure 3.16: Kriging for the synthetic model sampled according to the Brussels laser data (left) and Amiens laser data (right).

result on the synthetic model sampled by the Brussels laser data. The distortions, which are obvious from the results on the Amiens sampling set, are caused by the problem of the choice of the neighborhood. The sampling set of the Amiens data is not favorable for kriging and makes it very difficult to get acceptable results without major changes in the strategy of the neighborhood choice.

In the following chapter we will apply kriging to the real data sets: two sets of laser data and the simulated CMB data. It is to be noticed, that the hypotheses of kriging are well verified for the CMB anisotropies measurements and therefore good results can be obtained with kriging as we will see in the experimental results on this data.

The following section describes the energy minimization method for spatial data interpolation. We especially concentrate on this method for urban areas interpolation, because, unlike the previously described approaches, this method allows to impose the desired properties on the surface to find. We will describe these properties and the details of the method.

3.6 Energy minimization approach

A problem is considered to be well-posed in the sense of Hadamard, if the solution of this problem exists, it is unique and stable: small changes in the input data will not lead

to large changes of the result [Chalmond, 2000]. An example of an inverse problem can be image enlargement. In this case the enlargement is presented as the inverse problem of image reduction [Calle, 1999]. Resampling of irregularly spaced data also can be considered as an ill-posed problem. Regularization methods are applied to such kind of problems to ensure the computation of a meaningful solution. These methods impose some constraints on the solution. The constraints are often related to the a-priori knowledge about the result to be obtained [Blanc-Féraud, 2000, Kybic et al., 2002].

Image discontinuity-preserving restoration and interpolation is often based on the total variation minimization [Rudin et al., 1992, Guichard et al., 1998, Dibos et al., 2000]. One of methods for image restoration with edge preserving is based on energy minimization approach [Geman et al., 1992, Blanc-Féraud, 2000, Blanc-Féraud et al., 1995, Charbonnier, 1994]. In this approach a solution is a surface which minimizes a cost function, i.e. which minimizes an energy. An expression for energy has two terms:

- data-fidelity term, which penalizes variations between a surface and experimentally measured data

- regularization term, which penalizes surfaces if they don't have properties defined a priori.

The optimization of such an energy, in the general case, is too expensive. One generally chooses to introduce assumption of markovianity which makes it possible to ensure that a minimum can be obtained as sum of local terms (this seems reasonable in our case, since it is probable that the quality of reconstruction of a roof of building does not concern the geometry of other distant buildings).

F is said to be a Markov random field on the set S with respect to a neighborhood system N if and only if the following two conditions are satisfied [Li, 1995]:

1) $P(f) > 0 \; \forall f \in F$ (positivity);

2) $P(f_i | f_{S-\{i\}}) = P(f_i | f_{N_i})$ (Markovianity),
   where f - is a configuration of F, corresponding to a realization of the field.

During the reconstruction, one makes iterative calculations of the surface so that a minimum of energy is obtained. Several elements are significant for the method: the definition of the neighborhood considered around each point, the definition of the terms of energy and the corresponding potentials, finally a method to decrease an energy.

The interpolation method based on the energy minimization, described below, does not require any previous data resampling. It has been one of our major goals: to develop a method which takes the original data and produces the output which should be as close as possible to the sampled surface. We try to avoid as much as possible any pre- or post-processing. So the initialization for the energy minimization can be just noise. Though taking a surface consisting of interpolated data will help to avoid some local minima during the energy minimization with non-convex potential functions. For convex potential functions the initialization does not matter.

3.6.1 Definition of neighborhood

There are following requirements for the irregularly spaced data neighborhood definition [Watson, 1992].

1. The selection method should not allow excessively large or small subsets. If the selected subset is large, the combined effect will tend to submerge the local details. On the other hand, if a subset is too sparse, there will not be enough information to obtain a robust and stable surface.

2. The subset should be distributed uniformly around the interpolation point as nearly as possible.

3. Individual data points should not mask other data in the subset. This occurs when two or more data are in line with the interpolation point. Subsets need to be selected so that the maximum of local information can be extracted.

There are mainly three selection criteria for the neighborhood on the irregularly spaced data: fixed number, fixed area, natural neighbors [Watson, 1992]. We will describe each of them.

The first method of selection is the selection by the fixed number. This method causes the running subset to always be the same size. Therefore this selection criterion approaches the problem of excessively large, or insufficiently small, subsets. However, the unsatisfactory effect is that the nearest fixed number of scattered data often are not arranged evenly around the interpolation point in regions where the density of data is changing. Therefore, effects due to uneven distribution of data about the interpolation point remain, and this method is particularly susceptible to problems of masking of nearby data by more distant data. Selecting a subset with a fixed number of data is suitable only when the data are distributed evenly over the region.

By the criterion of the fixed distance, subsets are selected on the basis of fixed distance by including every datum that is closer than some fixed distance from the interpolation location. All the data within a circular region centered on the interpolation location belong to the subset. This approach works well for data that are uniformly and regularly spaced so that subsets are nearly always the same or similar size. However, whenever the data are more dense in one region of the data set than in another, this approach tends to select too many in the densest region, and too few in the sparse area. Preferably, the fixed distance may be varied, according to local density of data, to prevent excessively large or small subsets. This, however, requires monitoring of either density or number of data obtained in subsets. If the samples are more densely spaced in one direction than another, fixed distance subsets may include too many data and still not provide an adequate local subset with respect to the sparse direction. Fixed area subsets are a conceptual variation of fixed distance that allows an anisotropic subset to be selected. The use of fixed distance subsets implies that all the data within a circular window are included in the subset. To allow for data that are unequally dense in some directions, a variation on fixed distance allows the number of data in the running subset to be controlled by the size and shape of the window that

includes the subset data. The window containing the data to be included in the subset may be rectangular, or elliptical. The orientation of the rectangle, or ellipse, is chosen so that the maximum and minimum widths correspond to the directions of least and greatest density of data. The ratio of width to length for these windows should be similar to the ratio of directional densities, so this approach remains unsuitable if the data density is strongly anisotropic or this ratio varies.

When the samples in data sets are distributed unevenly, the size and shape of the region covered by the subset need to be adjusted to suit the local configuration of data locations, and this is done by natural neighbor subsets. The natural neighbors are determined by the Voronoi diagram. Such a subset adjusts automatically if necessary for the irregular data distributions. It is also possible to use k-order Voronoi neighbors [Zhao et al., 2002] as it is shown in Figure 3.17.
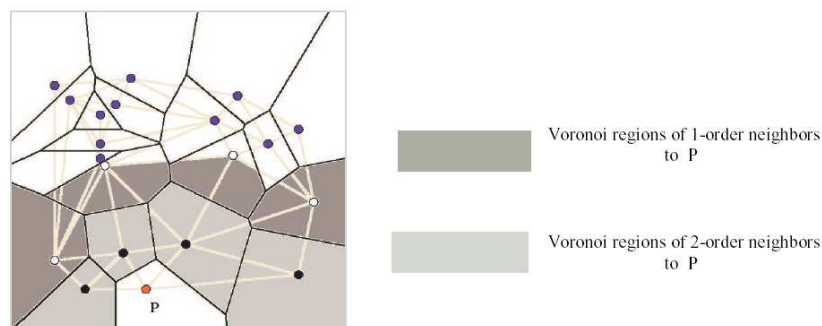
Figure 3.17: First order and second order Voronoi neighbors of point P [Zhao et al., 2002].

We use the fixed distance criterion for the choice of neighboring data samples. Let observed data samples be $\{z(x_k, y_k)\}$ at positions (x_k, y_k) for $k = 1, ..., K$. We are looking for samples $u(i, j)$ on a regular grid (i, j).

The neighborhood consists of points inside a circle, which includes 8 nearest points on the regular grid (Figure 3.18). So the neighborhood of each point is

$N(i, j) = M(i, j) \cup P(i, j),$

where

$M(i, j) = \{(i', j') : dist((i', j'), (i, j)) \leq r\}$

$P(i, j) = \{(x_k, y_k) : dist((x_k, y_k), (i, j)) \leq r\},$

$dist((x, y), (i, j)) = \sqrt{(x - i)^2 + (y - i)^2}$ - a distance between two points.

The radius r is chosen to encompass the 8 nearest neighbors on a regular grid. The indexes of the points $z(x_k, y_k)$ which are in the neighborhood of a regular grid point (i, j):

$K(i, j) = \{k : (x_k, y_k) \in P(i, j)\}.$
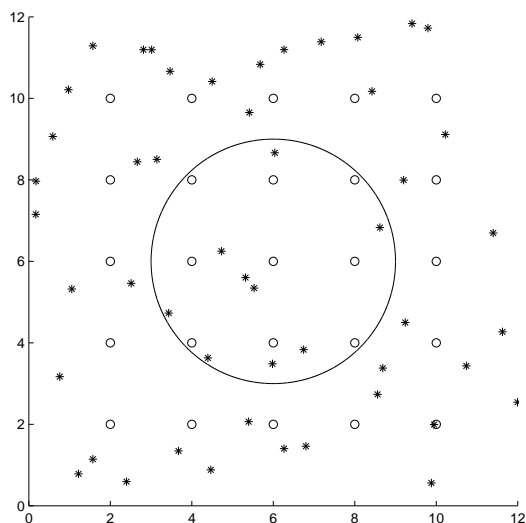
Figure 3.18: Definition of the neighborhood of a pixel: the neighborhood is represented by all the points located inside the circle. The stars represent the irregularly distributed original data (set $P(i,j)$), the circles are the regular points (set $M(i,j)$) which one wants to determine.

3.6.2 Expression for the cost function

The form of the energy generally consists of 2 terms, data-fidelity term and regularization-term [Geman et al., 1995]. For our problem, we have chosen a following cost function:

$$F(u) = \sum_{i,j} \left(\sum_{K(i,j)} \psi \left(\frac{z(x_k, y_k) - u(i,j)}{\text{dist}((x_k, y_k), (i,j))} \right) + \alpha \sum_{M(i,j)} \varphi \left(\frac{u(i', j') - u(i,j)}{\text{dist}((i', j'), (i,j))} \right) \right),$$

where ψ and φ - potential functions, the multiplier α gives a weight to the regularization term. The first summation (on i and j) will be made on all the points of the regular grid. The second summation (on the set K) is done on all the points of the irregular grid inside the circle of neighborhood of the current point i,j (Figure 3.19).
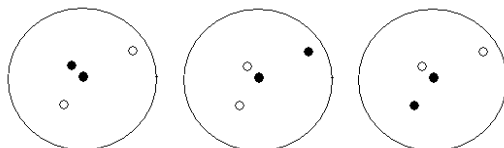
Figure 3.19: Cliques considered for the neighborhood over the irregular grid of the laser data points (the current pixel of the regular grid is in the center of the circle, white circles determine the pixels in the neighborhood, black ones form a clique).

The third summation is done on the 8 neighbors of the current point i,j (Figure 3.20).

Sometimes the position of a laser point may coincide with a node of the regular grid. In this case the denominator of the data-term will become zero. In order to
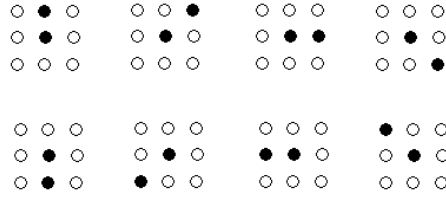
Figure 3.20: Cliques considered for the neighborhood over the regular grid (the current pixel is in the middle, white circles determine the pixels in the neighborhood, black ones form a clique).

avoid division by zero, one can add a constant, which is much smaller than 1, to this denominator. The solution $\hat{u}$ will be a surface which minimizes the cost function:

$$\hat{u} = \arg\min F(u).$$

The cost function $F(u)$ can be considered as the variational approach for the inverse problem [Blanc-Féraud, 2000, Nikolova, 2004]. It can also be presented as an anisotropic diffusion by partial differential equation [Blanc-Féraud, 2000]. In this case a set of images is considered, parameterized by the variable of time t. And the evolution of f is studies as a function of t through a partial differential equation. It will lead to the minimization of a function, which consists of two terms, like the energy presented above: the data-term and the regularization term. As it is described in [Blanc-Féraud, 2000], the data term is the squared difference between the observed image and the surface to find, and the regularization term is a potential function whose argument is the total variation of the gradient of the sought surface. The regularization coefficient, which determines the strength of the imposed properties on the surface, will appear as the time t. The potential functions, proposed for the anisotropic diffusion in the literature, are not convex. On the contrary to this representation, we do not limit ourselves by the only choice of the quadratic function for the data term, we will explore different choices of the potential functions for the data-term of the energy to minimize. It concerns also the regularization term of our energy function: we will consider both convex and not convex potential function, even though in the case of anisotropic diffusion the preference is given to the functions which are not convex. Indeed, using concave potential functions should lead to better edge preserving, but in the same time it may complicate the optimization procedure.

3.6.3 Potential functions

The choice of the potential functions φ and ψ is supposed to lead us to the best solution which is determined by features of altimetric reconstruction in urban environment. Let us express some common-sense remarks about urban environment.

1. A lot of surfaces are horizontal (or about): streets, pavements, terraces, gardens and yards, etc.

2. Other surfaces are flat, but oblique, in particular the sides of the roofs.

3. Many discontinuities have to be found in the vertical ortho-photographic projection which we want to make of the city, the frontages in particular. Nevertheless, these surfaces can give measurements which do not correspond the real model because of the angle of scanning of the laser which can hit the frontages or cling on convex objects: balconies, canopies, etc.

4. Finally, a small number of objects do not correspond to any of these models. It happens for vegetation, vehicle surfaces of car parks where these vehicles are gathered in a very dense way.

A lot of studies have been done to determine potential functions for filtering images while recovering edges [Nikolova, 2000, Charbonnier et al., 1997, Bouman et al., 1993, Blanc-Féraud, 2000]. Some potential functions are convex, some are not. They can be smooth or non-smooth at the origin. Spatially adaptive potential functions have been developed for noisy images [Park et al., 2000].

We limit our interest to four choices for potential functions. Each of them, except for total variation, has a parameter to tune (denoted by β).

Huber function (Figure 3.21(a)):

$$\varphi(t) = t^2 I(|t| < \beta) + (\beta^2 + 2\beta||t| - \beta|)I(|t| \geq \beta) \tag{3.1}$$

where I(p)=1 if p is true and I(p)=0 otherwise. This function is supposed to preserve slopes on the surface.

Total variation function (Figure 3.21(b)):

$$\varphi(t) = |t|. \tag{3.2}$$

Since this function is non-smooth at zero, it causes steplike zones on the surface [Nikolova, 2000]. Using the total variation potential function for the regularization term is a common choice when a surface with discontinuities is needed [Acar et al., 1994]. The total variation potential function, i.e. the modulus, for the regularization term leads to a surface composed of flat zones which are separated by sharp boundaries. In general, total variation methods for image restoration were introduced by Rudin and Osher [Rudin et al., 1992]. In these methods the regularization is a L_1-norm of the derivatives of the unknown signal. Such regularizations have been observed to produce "blocky estimates". It is established that strongly homogeneous zones in the resulting surface are both recovered from noisy data and preserved intact from small variations of the data, if the potential function is nonsmooth at zero [Nikolova, 2000].

Generalized Gaussian function (Figure 3.22(a)):

$$\varphi(t) = |t|^\beta \quad 1 \leq \beta \leq 2. \tag{3.3}$$

Truncated quadratic function (Figure 3.22(b)):

$$\varphi(t) = min\{t^2, \beta\}. \tag{3.4}$$
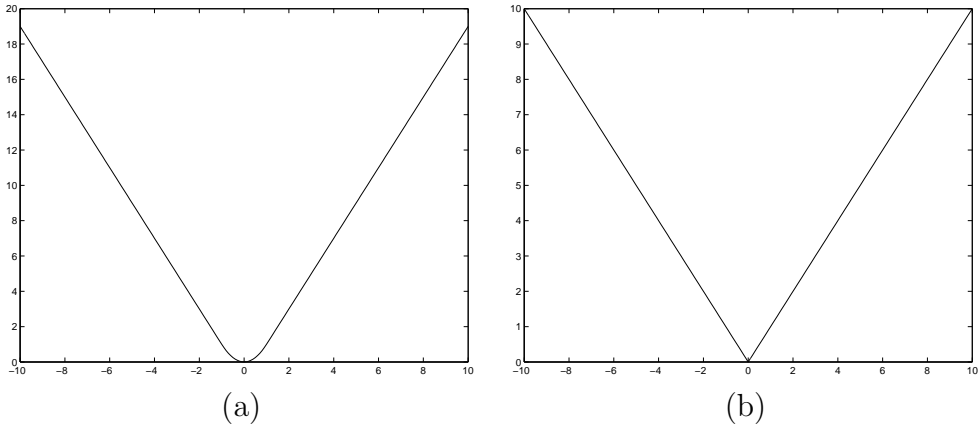
Figure 3.21: (a) Huber and (b) total variation function.
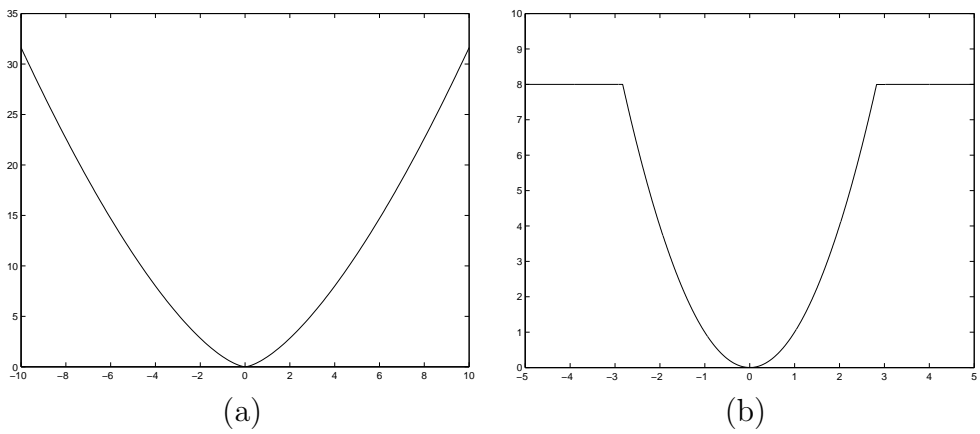
Figure 3.22: (a) generalized Gaussian and (b) truncated quadratic function.

It is a common choice to take a smooth function as a potential function for the data-term. Most often the quadratic function is taken. Recently it has been proved that the choice of a non-smooth potential function for the data-term may be useful in order to eliminate outliers or impulse noise. This choice also leads to the exact fitting for the most of the original data [Nikolova, 2002, Nikolova, 2004].

3.6.4 Optimization algorithm

In order to find an optimum of the cost function several algorithms may be used [Li, 1995]. These algorithms may be classified in two groups - deterministic and stochastic ones [Charbonnier, 1994]. The problem is that the energy function can have local minima, if a potential function is not convex. While the best solution is in the global minimum, some algorithms lead to a local one. This is the case when a deterministic algorithm is applied for minimizing a non-convex function. The result of such a minimization will depend on an initialization. If the initial surface is close to the global maximum, it is possible to recover a good solution. iterated conditional modes (ICM) [Li, 1995] and graduated nonconvexity [Nikolova, 1999] algorithms are deterministic and often used for cost function minimization in image processing [Charbonnier, 1994].

The ICM algorithm requires only the knowledge of the cost function in a local neighborhood. It was used in our case and it has the following steps.

1. Initialization of the surface;

2. For each point

   - compute cost function values for all possible values the surface can have
   - attribute to the point the value which minimizes the cost function

3. Stop calculations if there are no changes at step 2; otherwise - come back to step 2.

ICM algorithm is a relatively fast optimization technique which unfortunately does not converge towards the global optimum unless the initial point is close from it. Another very known technique is simulated annealing which theoretically gives a global optimum. This algorithm is a stochastic optimization algorithm. It is based on an analogy with a physical process of cooling for metals and freezing for liquids. A parameter that represents a temperature is introduced, and according to the theory it should decrease very slow. When the temperature is high enough, there is the probability of choosing not the values that minimize the cost function, but the ones that maximize it. It insures avoiding local minima. Simulated annealing is considerably more expensive in calculation time [Picard et al., 1995].

Among other available minimization algorithms are graduated non-convexity algorithm, half-quadratic regularization and graph cuts method. The graduated non-convexity algorithm [Charbonnier, 1994] starts by minimizing a convex criterion and

the non-convexity is introduced gradually during the process of minimization. This technique leads to a local minimum. The half-quadratic regularization uses the Legendre transform in order to represent a concave function by two convex ones. Then the iterative gradient-based minimization is performed on these convex functions. This method is developed in [Charbonnier, 1994]. Graph cuts method is the newest approach proposed for energy minimization. It is based on combinatorial optimization and allows to change several values of the sought surface in the same time. It is also shown that this method converges faster than simulated annealing to a better local minimum. This method is presented in [Boykov et al., 2001].

For our energy function we choose the ICM method: in the case of convex potential function it will lead us to the global minimum and for the concave ones with a good initialization we will get a local minimum which is good enough. Most of the functions we have to minimize are convex, though not necessarily having derivatives at the origin.

3.6.5 Example on the synthetic model

The result of the interpolation based on energy minimization is in Figure 3.23. The
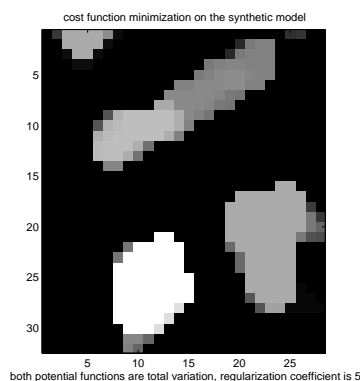
Figure 3.23: Energy minimization result on the synthetic model sampled according to the laser data of Brussels; pixel size is 1.5 meters, regularization coefficient $\alpha = 5$.

performance of the regularization is more obvious when we decrease the size of the pixel, that is we impose a more dense regular grid (Figure 3.24). We can see that energy minimization leads to the better preservation of edges. The radius for the circle, inside which the data samples are searched, is taken to be equal to 1.41 meters. It corresponds to the circle including 8 nearest neighboring pixels for the regular grid size 1.5 meters. It leads to having practically no pixel without data samples in their neighborhood.

For the examples, presented above, we take the result of the linear interpolation as the initialization of the surface for the optimization algorithm. The algorithm should always converge to the same solution as long as convex potential functions are used in the cost function. It means that actually the surface can be initialized by noise or by zeros at every pixel. We will demonstrate the results of energy minimization
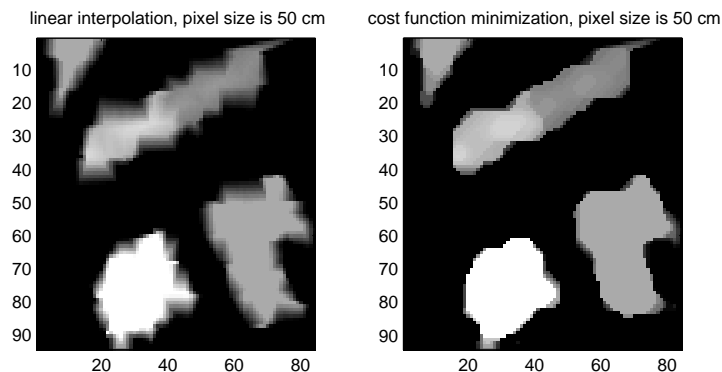
Figure 3.24: Left image: triangle-based linear interpolation. Right image: energy minimization, regularization coefficient $\alpha = 5$. For both images the synthetic model is sampled according to the laser data of Brussels; pixel size is 50 cm.

on different initial surfaces in the following chapter. When we take the result of the linear interpolation as an initial surface, then we have a good starting point for the minimization algorithm and the solution should be found quicker.

3.7 Conclusion

The choice of interpolation approaches is very broad, but dealing with irregularly scattered points upon urban areas restricts the variety of possible solutions. There are two reasons for it: one needs a method, adapted for a scattered initial data and preserving discontinuities and slopes of a surface. Two kinds of interpolation (linear and nearest neighbor interpolation) are done by using Delaunay triangulation of original data. Triangle-based linear interpolation applies barycentric coordinates to the data at the vertices of the triangle. We don't consider interpolation of higher orders, because it is known to produce smooth surfaces which will not represent properly an urban area. Kriging is a geostatistical method, which considers all the elevation values as samples from a realization of a stationary random process and analyses the spatial behavior of the corresponding parameters. This approach also can be applied to the laser data.

Since the problem of 3D scattered data interpolation is ill-posed, it makes sense to introduce a regularized solution imposing desirable properties on the resulting surface. One of methods for image restoration with edge preserving is based on energy minimization approach. In this approach a solution is a surface which minimizes a cost function, i.e. which minimizes an energy. An expression for energy has two terms:

a data-fidelity term and a regularization term. The regularization term is weighted by a multiplier so that the larger is the multiplier the more regularized the resulting surface will be. Several elements are significant for the method: the definition of the neighborhood considered around each point, the definition of the terms of energy and the corresponding potentials, and a method to minimize an energy. For each point of a regular grid, where one wants to get an elevation value, two kinds of neighborhood are introduced. The first one consists of eight nearest neighbors on the regular grid, the second neighborhood has all the scattered points inside a circle, which contains eight nearest regularly spaced points. We consider four choices for potential functions: total variation, generalized Gaussian, Huber and truncated quadratic function. The quadratic potential function is often used for regularization, but it imposes a smoothness constraint on the resulting surface. A discontinuous surface can be achieved with the requirement that the solution be of bounded variation rather than smooth. This means using the total variation potential function. Generalized Gaussian and Huber function have edge-preserving properties too. These functions are convex and it ensures finding the global minimum of the cost function. The truncated quadratic function leads to smoothing as long as the gradient values are lower then a threshold. When the gradient is larger then the threshold, no penalties are introduces. And so the edges are preserved. To start, the same functions for both data and regularization terms will be taken. To minimize the cost function the iterated conditional modes algorithm is used. The energy minimization is supposed to lead to surfaces well representing urban areas, where edges contain important information because they delimit buildings and streets.

In this chapter we described the methods that we have chosen for the interpolation of the airborne laser data. The results of these methods, applied to the real data sets, are presented in the following chapter. We also will apply these methods, as well as binning, described in the last chapter, for the simulated data of cosmic microwave background anisotropies.

Chapter 4

Experimental results on laser data

4.1 Introduction

In this chapter we present the experimental results on two real sets of airborne laser scanning data. We apply the methods described in the previous chapter: nearest neighbor interpolation, linear interpolation, kriging and energy minimization method.

The first data set that we consider is the data of Brussels acquired by the Eurosense company. We describe the data and then apply the methods mentioned above. We have a reference image for the considered area and it will allow us to evaluate the quality of the obtained results.

The second data set is acquired the TopoSys company with a different laser scanning technique. It is the data of Amiens, and we also have a reference image for this town. So we are interested in applying the interpolation methods to this data in order to verify how the performance of these methods is linked to the properties of surfaces representing urban areas. Having two data sets acquired by different laser scanning systems, with different precision, will let us evaluate the methods not depending on one particular data set.

4.2 Data of Brussels

4.2.1 Data description

The airborne laser scanning data of Brussels, taken for the experiments, was acquired over the area shown in Figure 4.1.

The size of the area covered by the laser scanning data is 200×200 meters. The laser data over this area contains 15288 points. The laser points form a zigzag scanning pattern (4.2).

Figure 4.3 shows that the laser points are irregularly distributed: x coordinates of the laser points are plotted versus y coordinates (in meters). The range of altitudes is from 14 to 42 meters. The values of about 14 meters represent the ground. Large

Figure 4.1: The aerophoto of the studied area of Brussels: source Eurosense.

Figure 4.2: Laser scanning data points form zigzags.
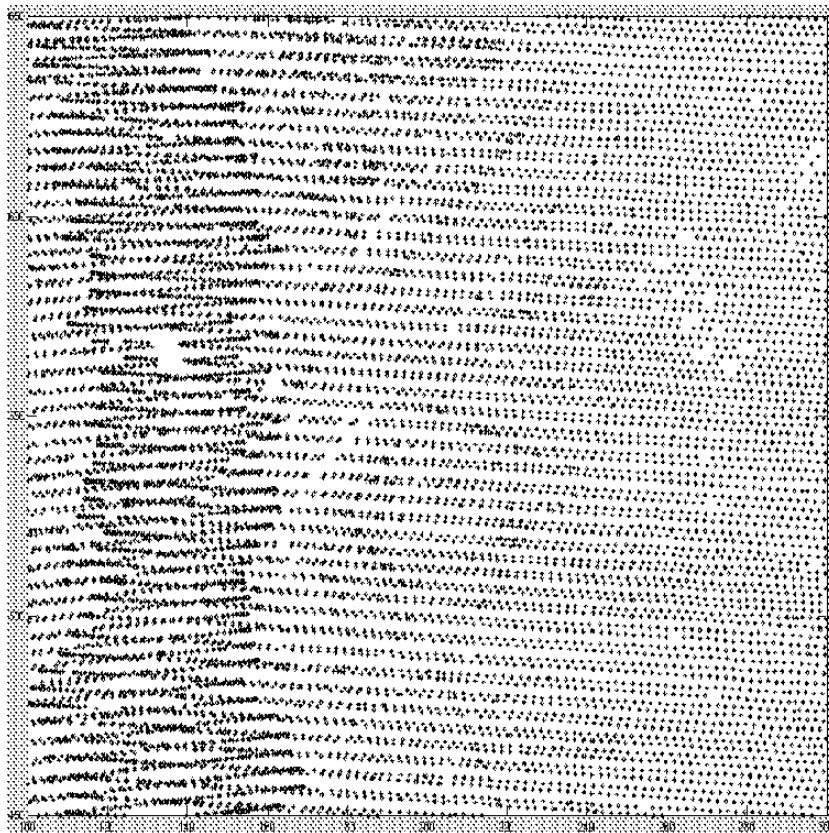
Figure 4.3: The primary irregular grid.

values of altitudes correspond to the roofs and the tops of trees. The histogram of the altitude values is in Figure 4.4.
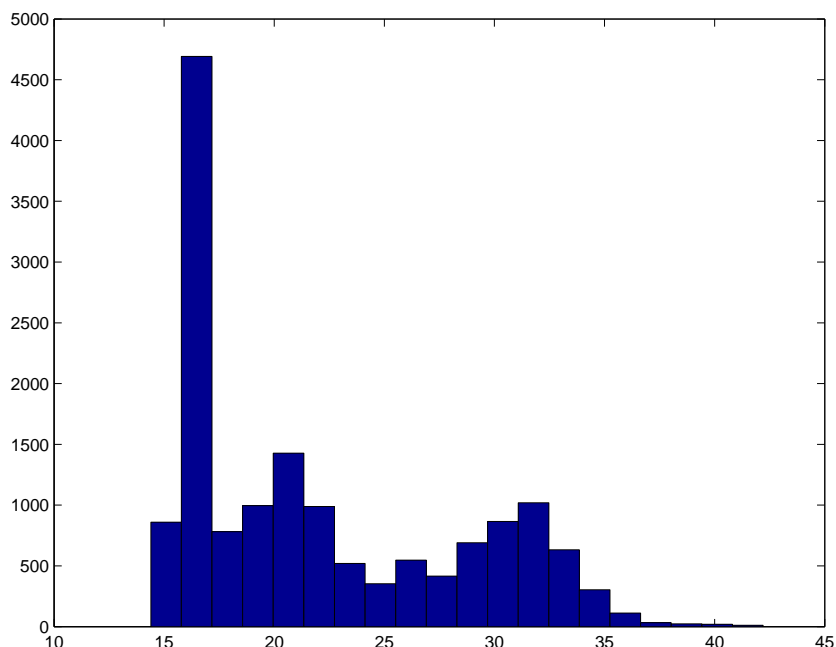
Figure 4.4: Histogram of the altitude values of Brussels laser scanning data.

The peak of the histogram shows the laser points that are on the ground: roads and pavements. The heights of most of the buildings and vegetation are lower than 20 meters. Laser scanning points are also visualized on Figure 4.5, where colors represent altitudes.

The density of primary laser data is about 1 point per 3,24 m^2. The value 3,24 m^2 will thus be taken as a grid size for regular sampling. It corresponds to a sampling on the grid with a step 1,8 m.

Now, when we have given a description of the laser scanning data of Brussels, we apply the interpolation methods to this set of data. We start by the nearest neighbor interpolation and the results are presented below.

4.2.2 Nearest neighbor interpolation

The results of the nearest neighbor interpolation are in Figures 4.6 - 4.7. Figure 4.6 represents altitude values as gray levels. The colorbar on the right side of an image shows the correspondence between the gray levels and the height. The larger is the altitude assigned for a pixel, the lighter is its color on the image.

The drawback of nearest neighbour interpolation is that the surface is very discrete, there are no slopes, and changes between groups of values are very steep. It is especially obvious when the density of a regular grid is higher than the density of laser points.

In the following section we present the results of the linear interpolation.
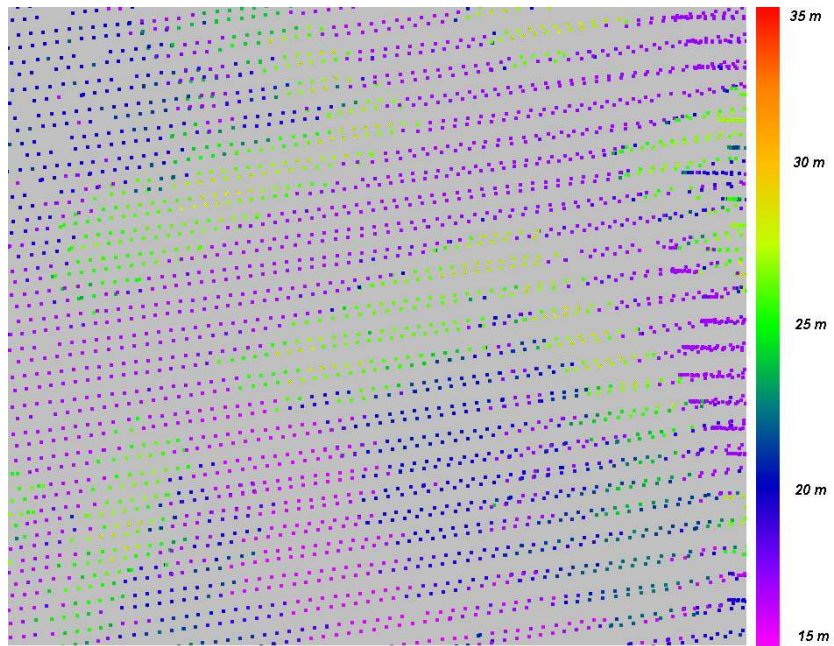
Figure 4.5: Laser scanning points, colors represent altitude values (green points are on the roofs, blue - on the ground).
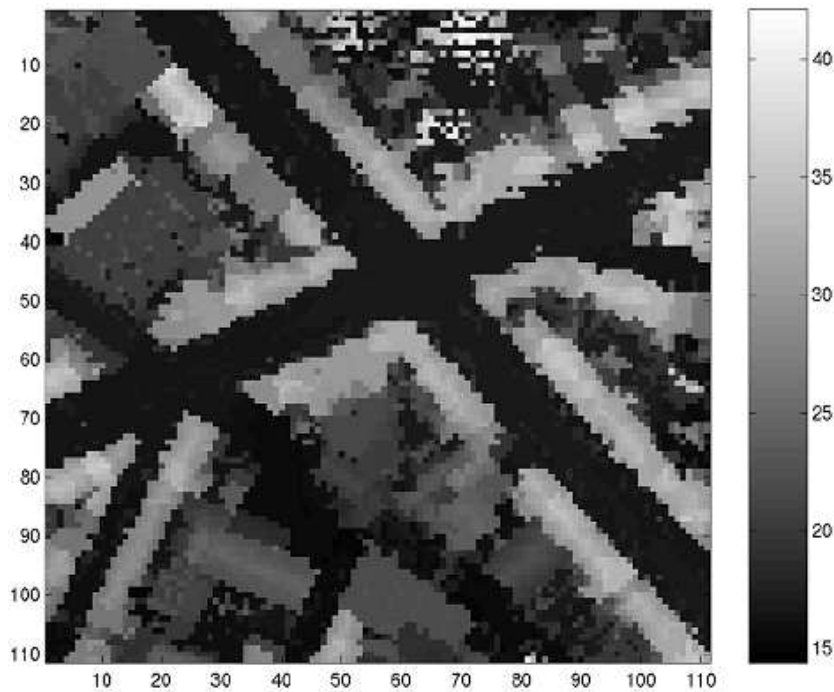
Figure 4.6: Result of nearest neighbor interpolation based on Delaunay triangulation of initial data (site of Brussels, data of Eurosense).
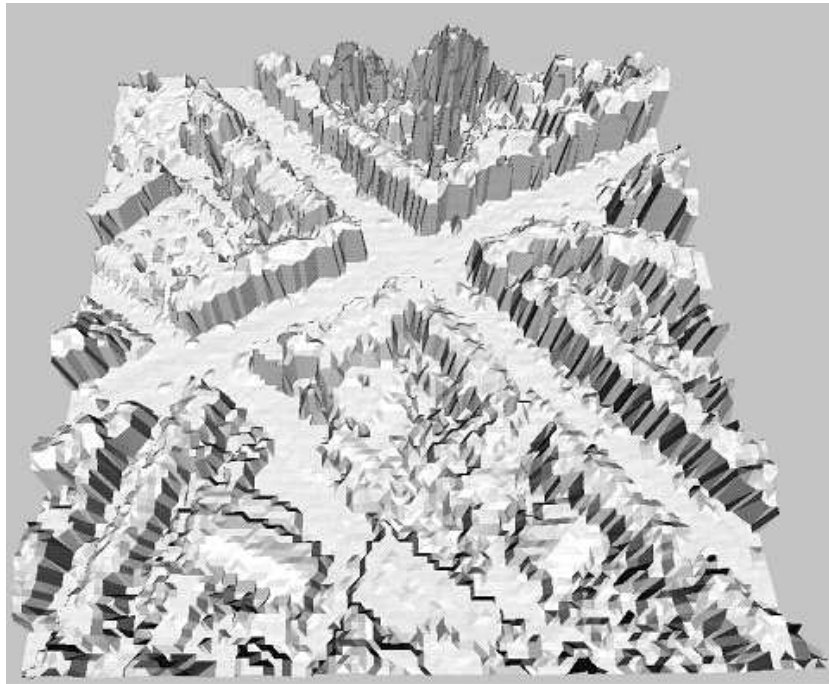
Figure 4.7: 3D model of the nearest neighbor interpolation result.

4.2.3 Linear interpolation

Triangle-based linear interpolation results are in 4.8 - 4.9.

The linear interpolation results look quite realistic, but there are problems with edges. The edges are distorted and smoothed.

In the following section we describe how kriging is applied to the data.

4.2.4 Kriging

Spherical variogram is taken to adapt the parameters for kriging. This type of variogram is often used in different applications. This variogram is less smooth than Gaussian or exponential ones. Linear variogram can also be used, though it is not expected to change the results considerably. First an experimental variogram was calculated from the laser data, then the parameters were chosen so that they correspond to this experimental variogram. Initially, the parameters of the theoretical variogram are chosen from the visual observation of the experimental one. While running kriging on the data set, singular matrices occur sometimes. That creates a problem with matrix inversion and therefore it is desirable to have a set of variogram parameters that helps to avoid singular matrices. That is why the parameters obtained from the experimental variogram were a bit tuned. For the spherical variogram used to perform kriging, the range is equal to 25, nugget is 4 and sill is 40. The experimental variogram and the corresponding theoretical one are in 4.10. Only the left part of the variogram is shown in this figure. The variogram values which correspond to distances between
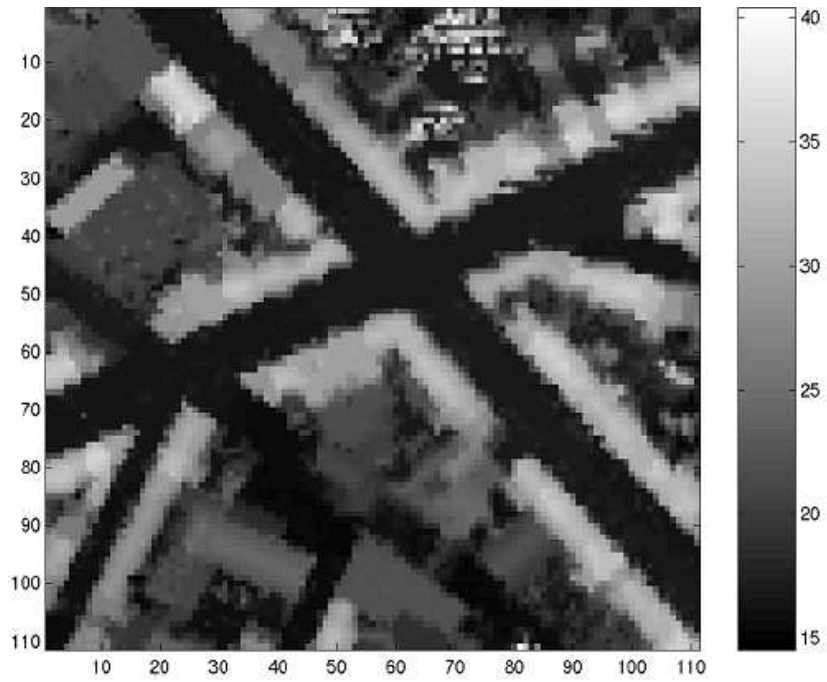
Figure 4.8: Triangle-based linear interpolation result.
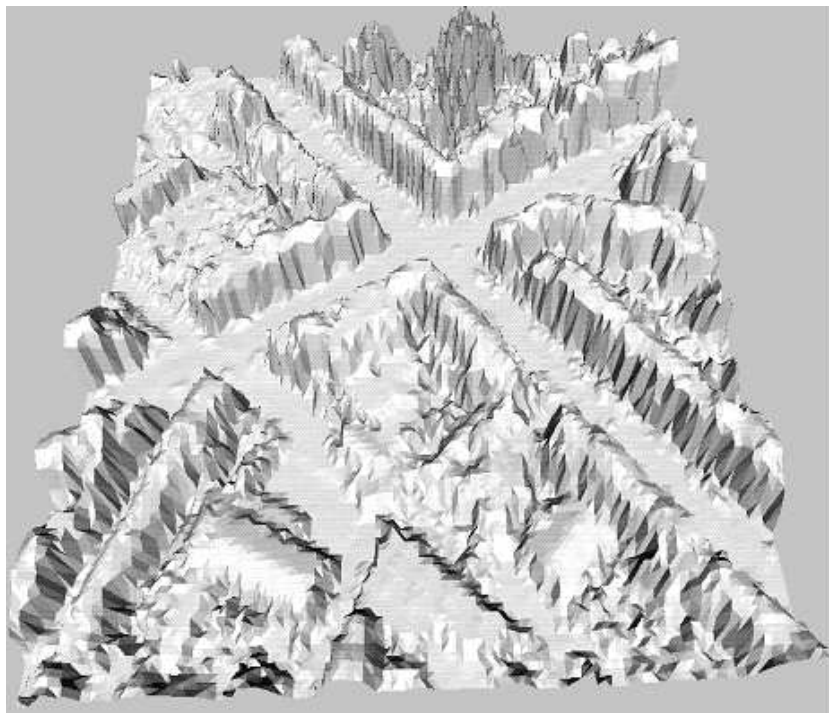
Figure 4.9: 3D model of the triangle-based linear interpolation result.

points larger than 110 meters are not presented. The influence of such distant point on each other doesn't matter, because in order to calculate a value in a grid point, we use only values that lie in a neighborhood of the current point. So not all the data points are used, only local ones are considered. The neighborhood size for each pixel
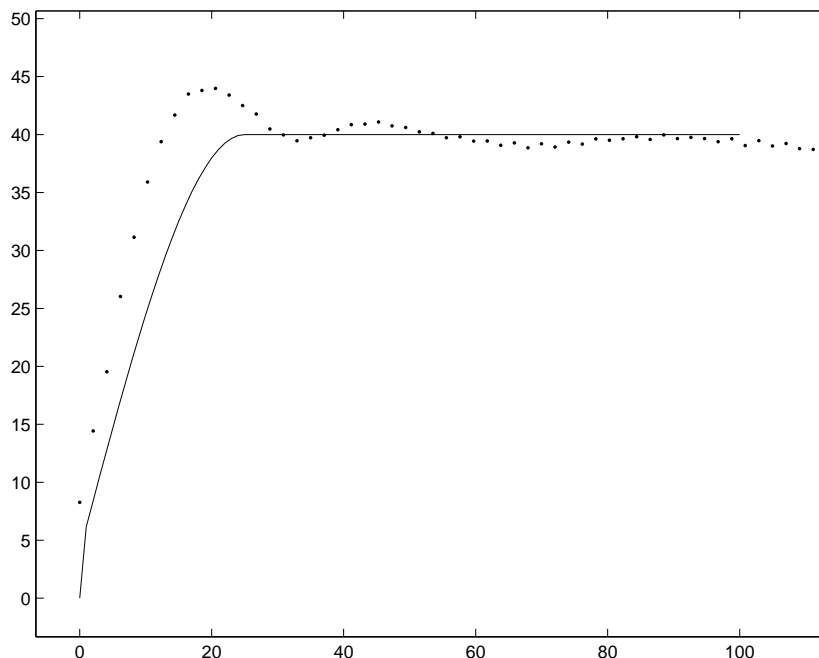
Figure 4.10: Experimental variogram (points) and the theoretical spherical variogram.

is a square 10×10 meters. There are around 20-50 samples that fall in each neighborhood. The resulting surfaces are in 4.11 - 4.12. Kriging gives smooth areas. We use ordinary kriging method. We can see that kriging is not well adapted for the surfaces representing urban areas. It can be noticed already from the experimental variogram whose form does not correspond to a theoretical one. The software for performing ordinary kriging was developed in the TSI department of the ENST.

The following section is devoted to the comparison between the results, obtained above on the real set of laser scanning data of Brussels, and the reference. We describe the reference and make the comparison.

4.2.5 Comparison of results

Obviously, the quality of results is not to be determined only visually. Correlation values with ground truth can be used as quality measures in this case. The Digital Elevation Model (DEM), obtained from high resolution optical images, is taken as a reference here (Figures 4.13 and 4.14) [de Joinville, 2001, Fradkin et al., 1999]. For some points of this reference the altitude values are not determined. These points have black color in Figure 4.13. The reasons for not having the elevation values are the following. At first, the stereo-photos of the area are taken. Then a correlation method is applied to calculate the elevation values. In the sites where the correlation
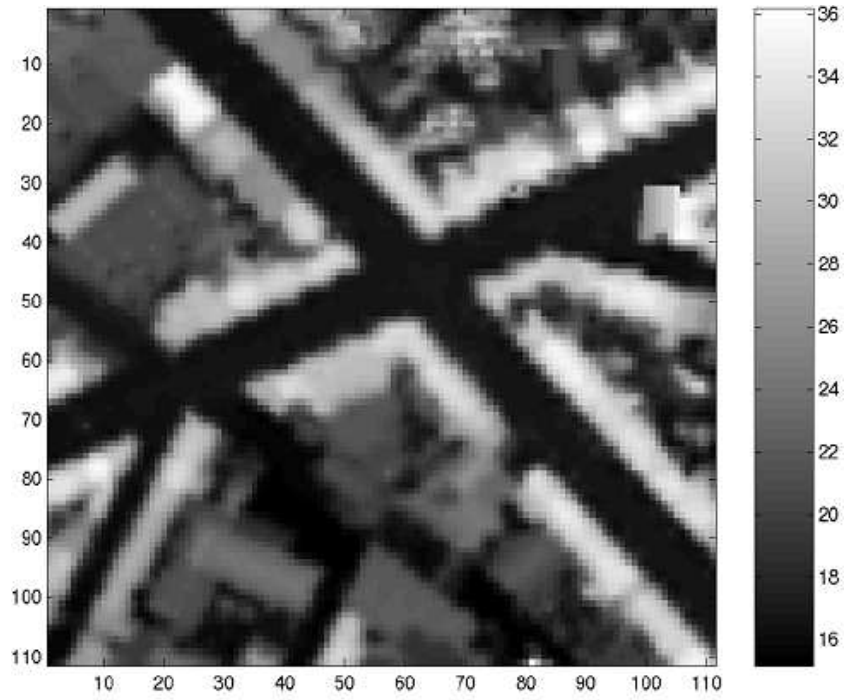
Figure 4.11: Kriging result with a spherical model of variogram.
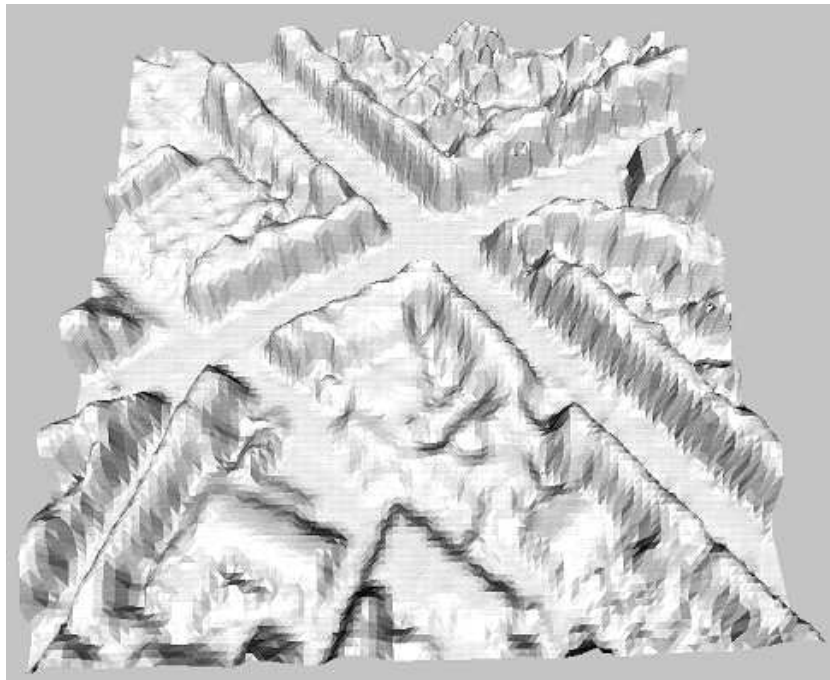
Figure 4.12: 3D model of the kriging result with a spherical model of variogram.

method fails, the elevation is unknown. At second, plane fitting is performed over the parts of the received surface [Roux et al., 1999]. If a fitted plane is considered to be reliable, then the resulting elevation values will belong to this plane. If it is unreliable, no interpolation is made. Since in the areas of vegetation it is difficult to fit a plane, it leads to many undetermined elevation values there. This area is on the top of the image in 4.13.
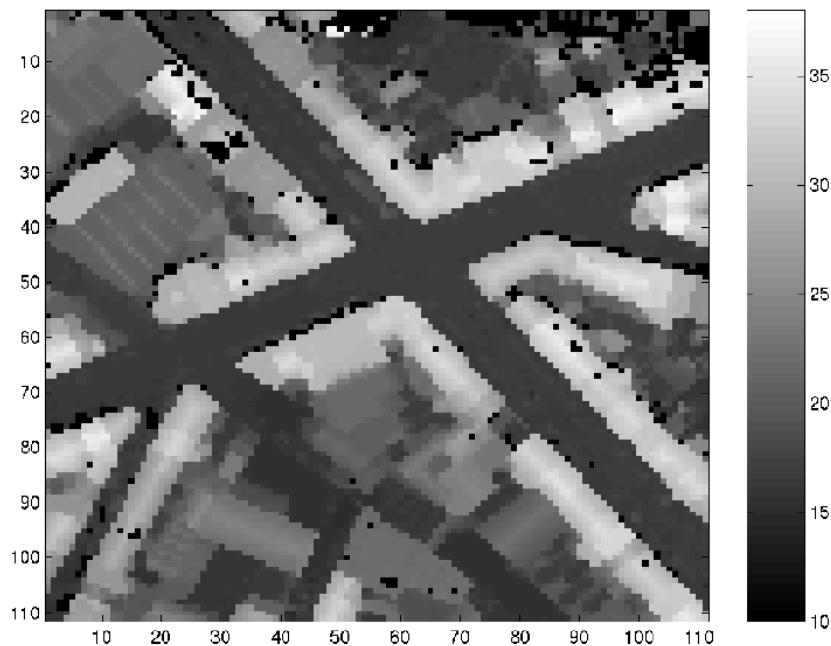
Figure 4.13: DEM obtained from stereo photos. The sampled version to adapt the resolution (1.8 meters) for comparisons. Black color corresponds to pixels where altitude values are not determined.

If we put z values of original scattered laser data on one axis and corresponding the same locations z values of the DEM on another axis, then we get Figure 4.15. In the ideal case this Figure must show a line $y = x$.

The image in Figure 4.16 represents in levels of gray the altitude values of the laser data versus the altitude values of the reference DEM: the darker is a points, the more times it was hit while plotting the laser data z values versus the DEM z values. The values along the colorbar indicate how mane times a point fell on a site of the image.

Subtracting the reference DEM from the linear interpolation result, the problems on the edges is obvious (Figure 4.17).

The large errors that appear on the top part of the image are due to the vegetation. The reference DEM has a smooth surface in this part, while the laser data penetrates the vegetation and the resulting surface is very irregular: some points lie on the ground, some - on the tops of trees.

A correlation coefficient is calculated between two vectors: a vector X of the DEM elevation values and a vector Y of a resultant surface elevation values:
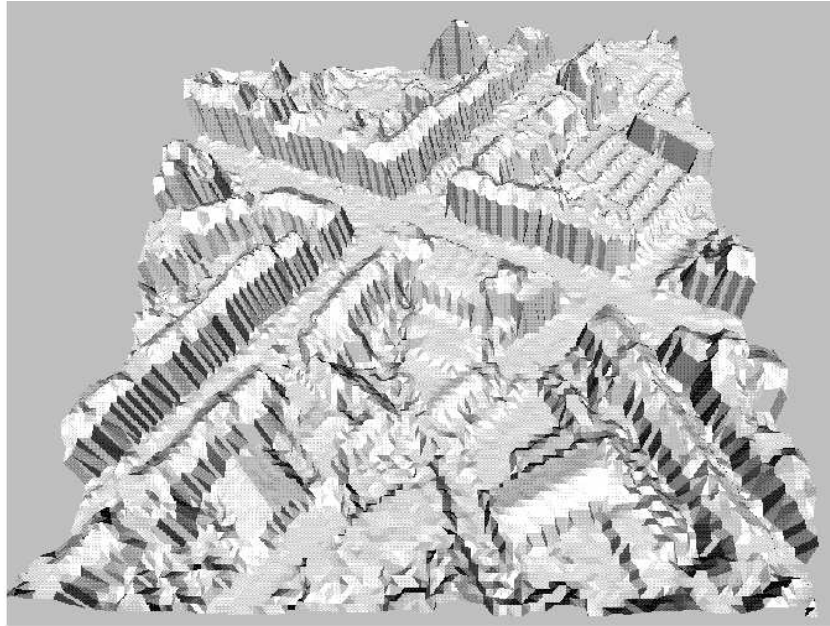
Figure 4.14: 3D reference DEM model.
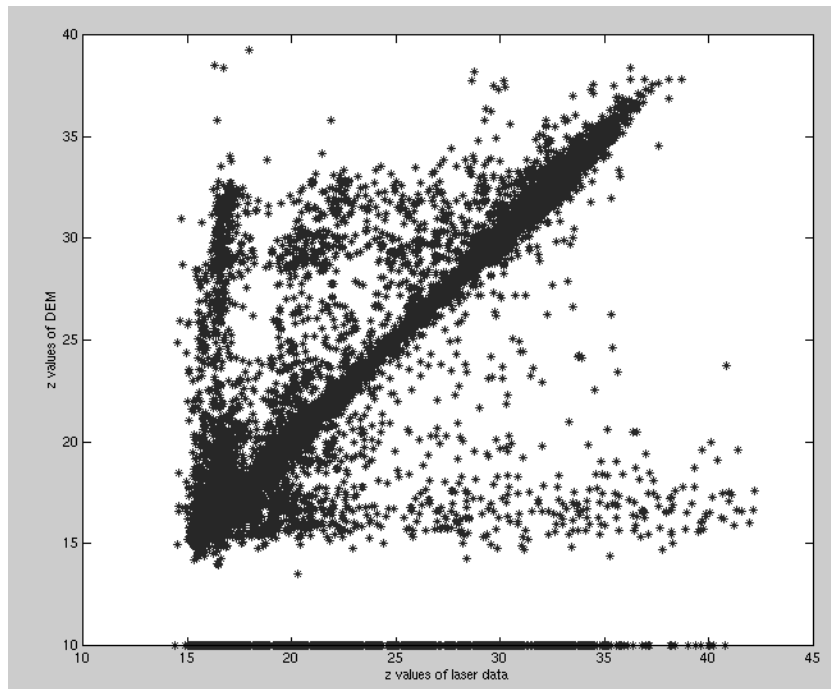
Figure 4.15: Original z values of the laser data versus z values of the DEM, 15288 points (the points on the horizontal axis mean the points for which there is no information in the DEM) The correlation between the two data sets is 0.6740.
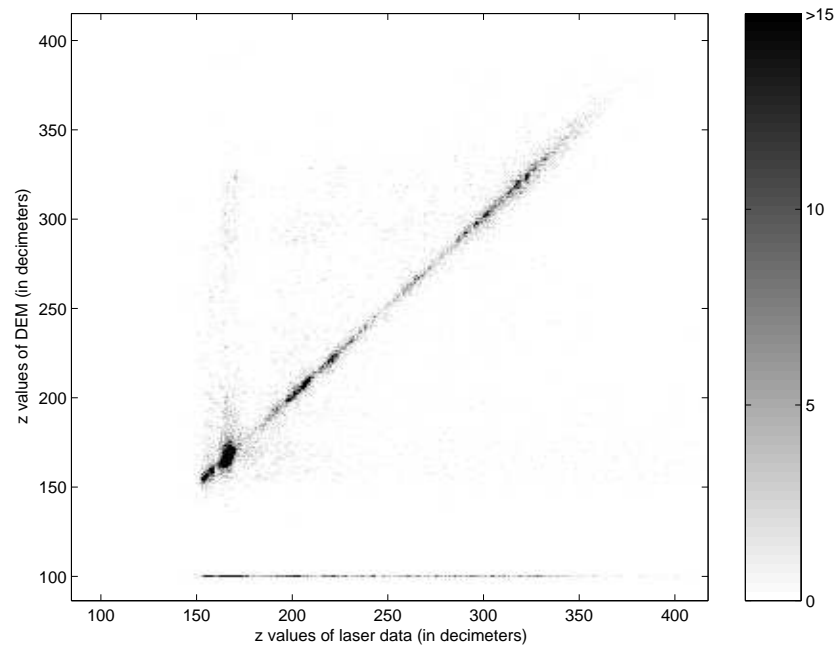
Figure 4.16: Original z values of the laser data versus z values of the DEM, in gray scale.
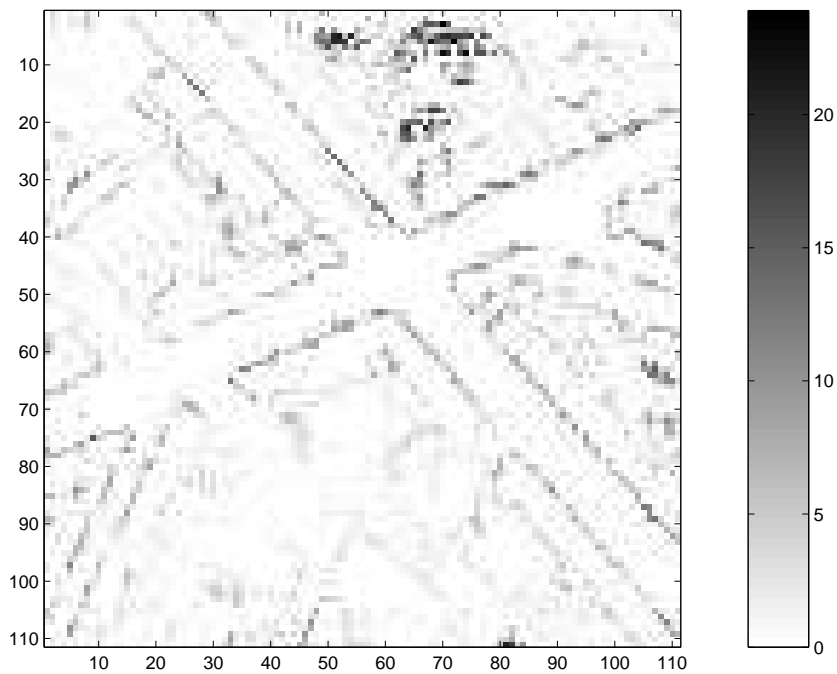
Figure 4.17: The absolute values of the difference between the reference DEM and the linear interpolation result.

$$z_x = \frac{X - \bar{X}}{std(X)}, \quad z_y = \frac{Y - \bar{Y}}{std(Y)}$$

$$r = \frac{< z_x z_y >}{N - 1}$$

where $\bar{X}$, $\bar{Y}$ - mean values of the vectors X and Y respectively, $std(X)$, $std(Y)$ - their standard deviations, N - a number of elements in a vector, r - a correlation coefficient. A perfect correspondence between interpolated measurements and the DEM should lead us to a coefficient r equal to 1.

The resolution of the DEM is 10cm. The resolution of a resultant surface is 1m 80cm. In order to get values of the DEM for comparison we do the following. For each point of a resultant surface we find a corresponding point of the DEM. Then a value for comparison will be a median value of all the points inside the window 5x5 pixels on the DEM. There are some points where the DEM doesn't provide any information (Figure 4.13) (absence of textures on very uniform surfaces or hidden parts during the construction of the DEM). In the first case, the median value makes it possible to correct this absence, in the second (too large zones) the point is ignored in the correlation calculation.

We also noticed that the area of study contained 2 different zones:

- the large part of the image has buildings in an urban zone,

- but in the part of the area located in the top of the image, closer to the right side, has vegetation with much more irregular geometry.

This second zone is of a less interest for the study we made a study with and without this zone.

In the following section we apply the energy minimization method and compare the results with the reference. We evaluate this method relatively to the previous results obtained by using the well known approaches: nearest neighbor interpolation, linear interpolation and kriging.

4.2.6 Energy minimization method

In the beginning of making experiments we supposed the multiplier α for the regularization term to be less or equal to 1 (in order to stay close to original data). The cost function is:

$$F(u) = \sum_{i,j} \left(\sum_{K(i,j)} \psi \left(\frac{z(x_k, y_k) - u(i,j)}{\text{dist}((x_k, y_k), (i,j))} \right) + \alpha \sum_{M(i,j)} \varphi \left(\frac{u(i', j') - u(i,j)}{\text{dist}((i', j'), (i,j))} \right) \right),$$

To start, we took both potential functions the same: $\psi = \varphi$. We initialized the optimization algorithm with different surfaces:

- white noise,

- results of triangle-based linear interpolation,

- results of nearest neighbour interpolation,

- results of kriging.

The method of optimization will be the ICM for its more reduced calculating time. A significant parameter in this algorithm is the choice of the step in altitude (the height discretisation). A too small step significantly increases the calculations since it is necessary to calculate the potential function for all these altitudes. A too coarse step leads to a too schematic description of the buildings but can also produce false minima. We chose a step of 50 cm, quite compatible with the required space resolution. For these initial surfaces, we obtained the following results of correlation.

Initialization	On the complete test area	Only on the area with buildings
White noise	0.0170	0.0177
Linear interpolation	0.9060	0.9311
Nearest neighbour interpolation	0.8627	0.8989
Kriging	0.9193	0.9406

Table 4.1: Initializations of the optimization and the correlation values between them and the DEM.

We can see that kriging gives better results than the linear interpolation, the nearest neighbor interpolation is worse. We also can see that the zone of vegetation has tendency to degrade the correlation.

Figures 4.18-4.21 show results for various α values for the complete area (with vegetation).

The horizontal line determines the best correlation between the DEM and an initialization surface (it is kriging for all the figures) in order to see if energy minimization approach outperforms the classical ones or not. A curve located below this line indicates that optimization degrades the initial solution. Results for the same area but without vegetation (only for the area with buildings) are in Figures 4.22-4.25.

From the pictures we can see that the larger is α, the better results we get. So we continue increasing α. We take linear interpolation results as an initial surface, because they give better output according to previous plots. The parameter for the truncated quadratic function must be adjusted. So for the following results it is equal to 50. It means that if the difference between heights of two points is larger than approximately 5 meters, then the penalty introduced by the truncated quadratic potential function will not increase. Results are presented in Figures 4.26, 4.27.

For the generalized Gaussian function we take $\beta = 1.2$, because it gives better correlation results than other values of β. We can see the results for four potential functions, where truncated quadratic function gives the best results for the complete
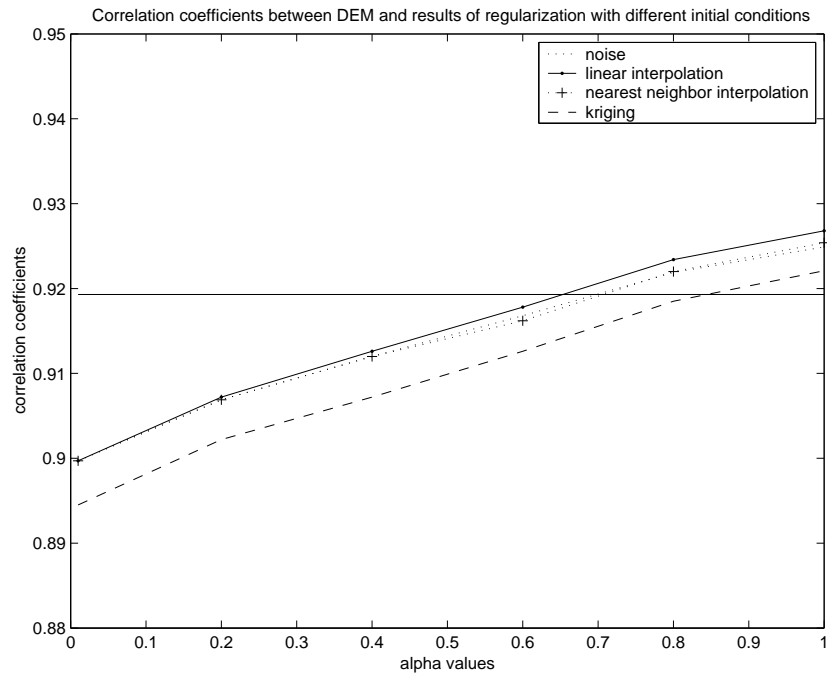
Figure 4.18: Results for Huber potential function (parameter is equal to 1)
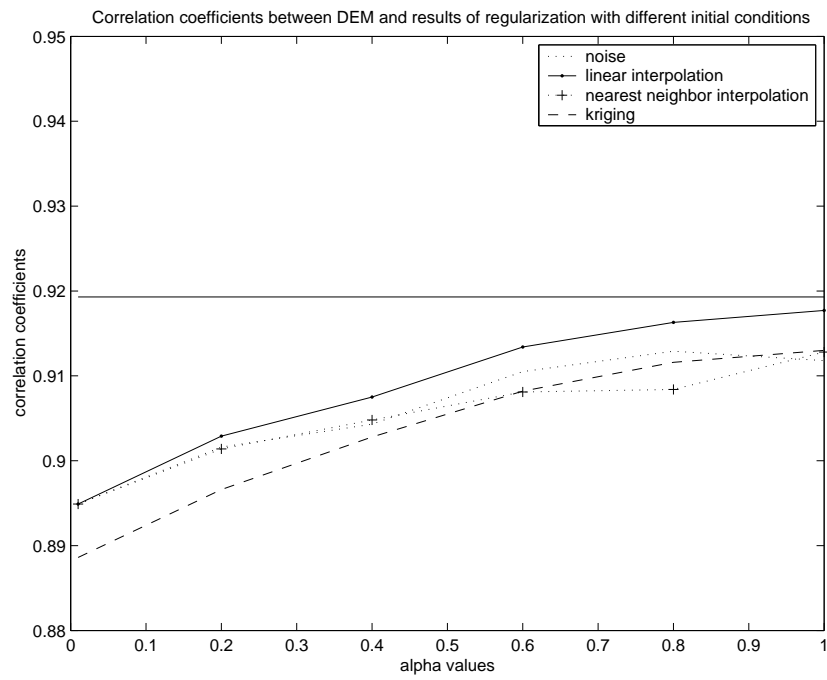
Figure 4.19: Results for total variation potential function
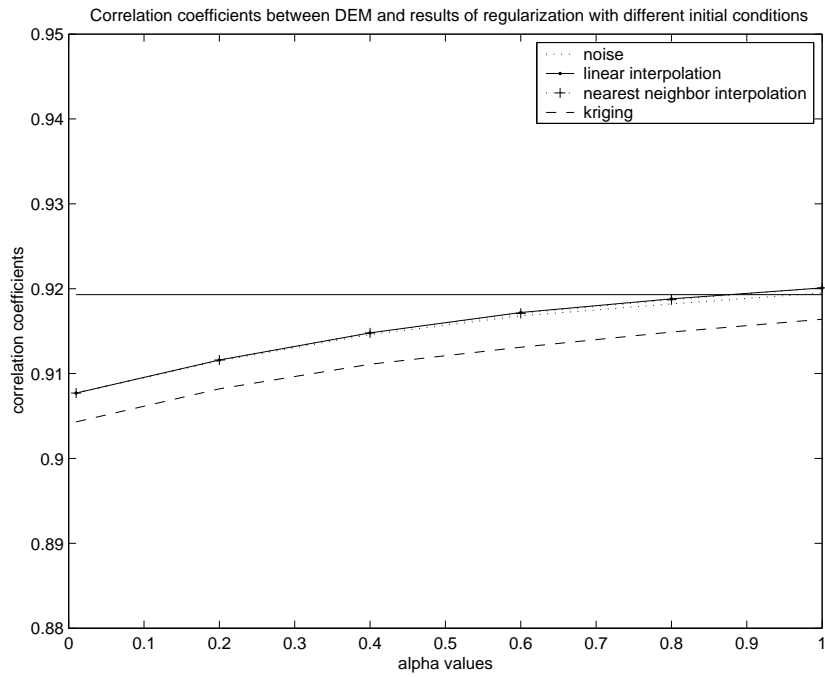
Figure 4.20: Results for generalized Gaussian potential function (parameter is equal to 1,5)
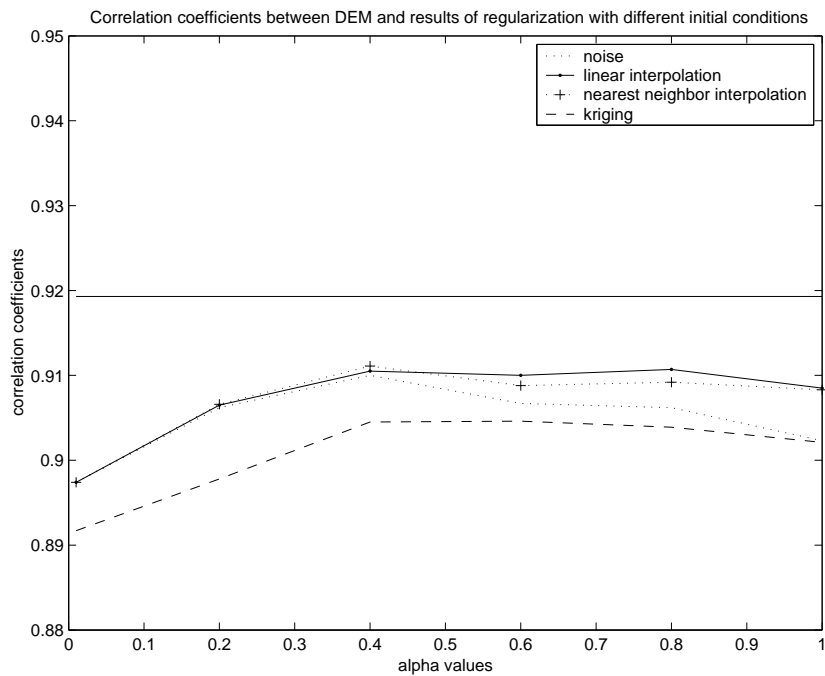
Figure 4.21: Results for truncated quadratic potential function (parameter is equal to 1)
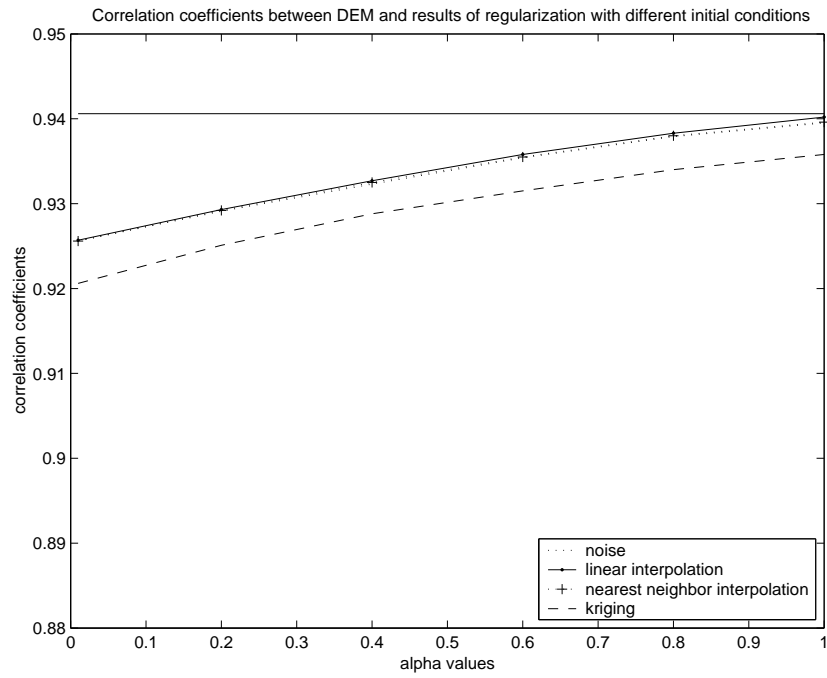
Figure 4.22: Results for Huber potential function (parameter is equal to 1)
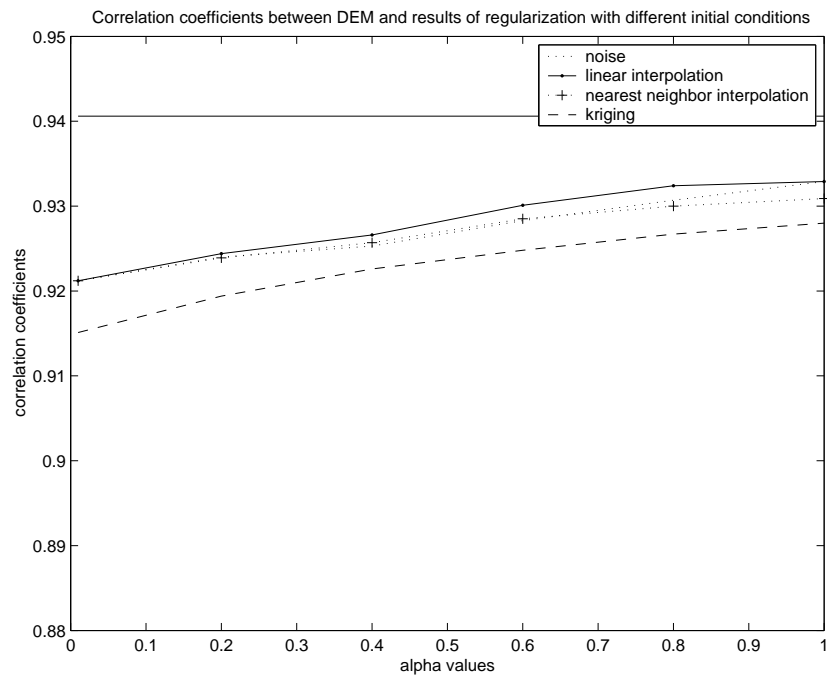
Figure 4.23: Results for total variation potential function
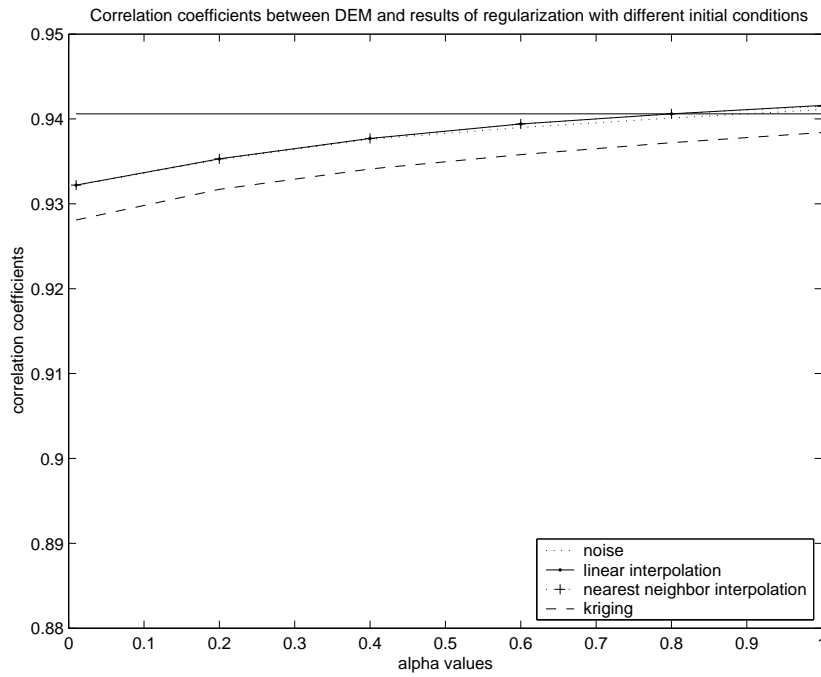
Figure 4.24: Results for generalized Gaussian potential function (parameter is equal to 1,5)
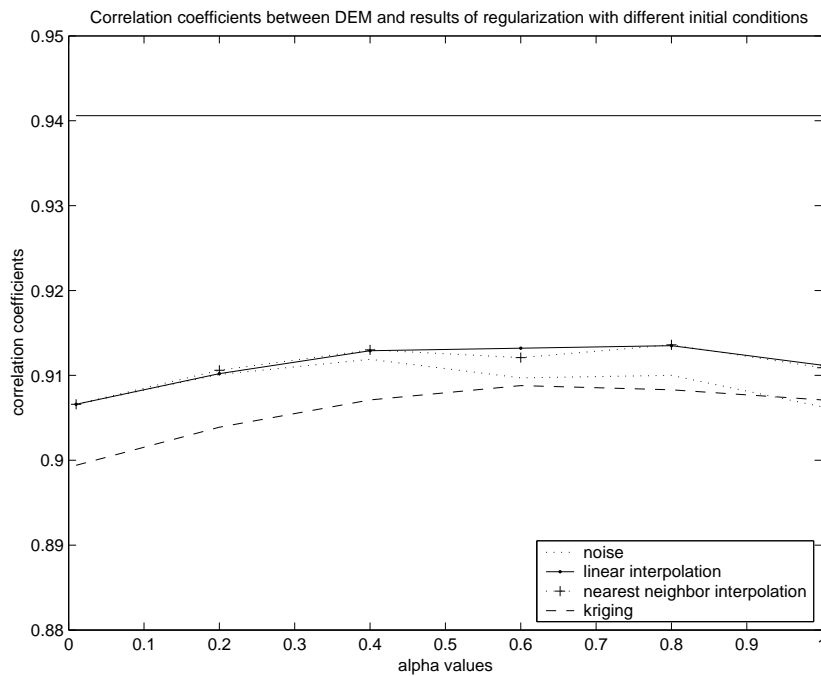
Figure 4.25: Results for truncated quadratic potential function (parameter is equal to 1)
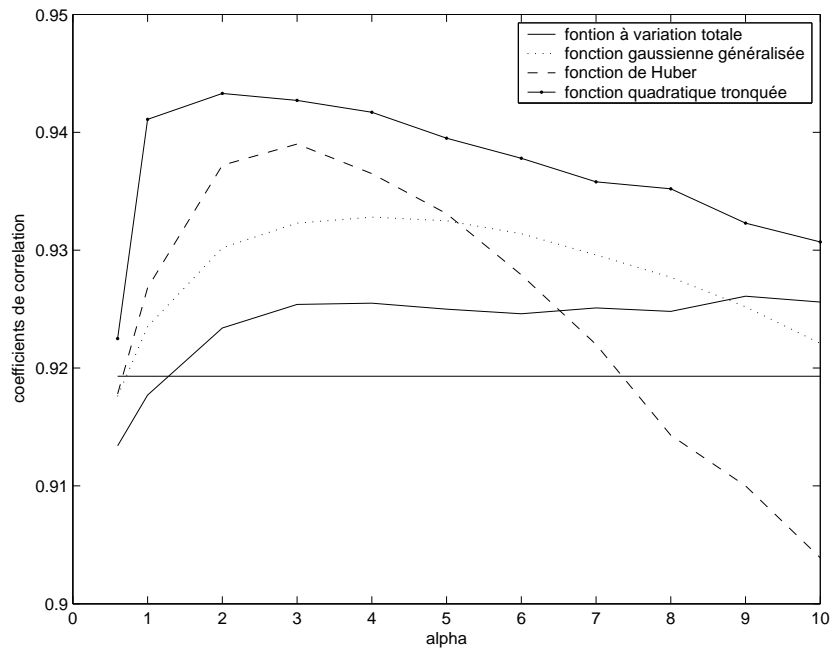
Figure 4.26: Search for an optimum α for the area with vegetation.
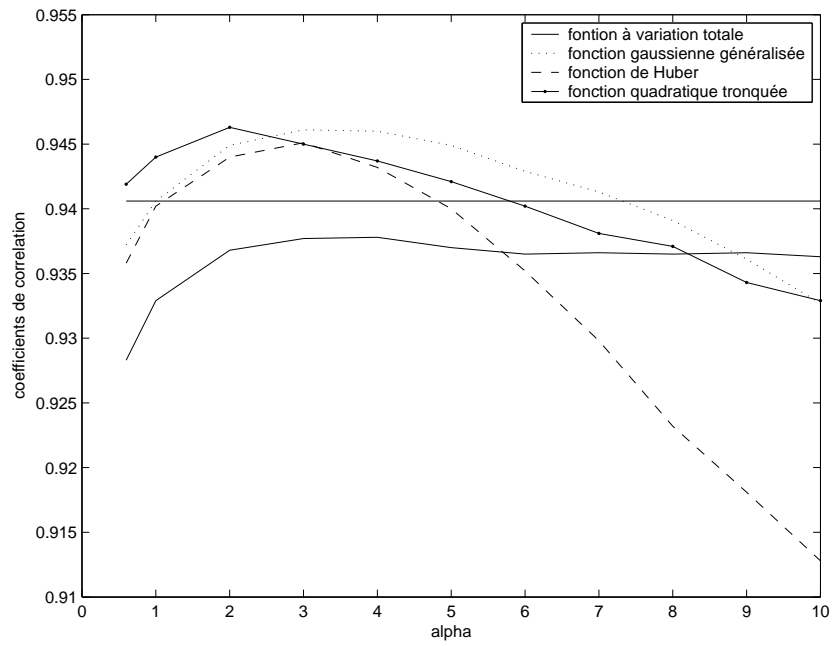
Figure 4.27: Search for an optimum α for the area without vegetation.

area and generalized Gaussian and truncated quadratic functions are better for the area without vegetation. Huber potential function is the most sensitive to the change of the coefficient α, whereas total variation function gives worse results, but guaranteed for a very broad set of parameters.

Taking the results that correspond to the maximums of the curves, when α is equal to 2 or 3 (Figures 4.26, 4.27) are in Figures 4.28 - 4.31.
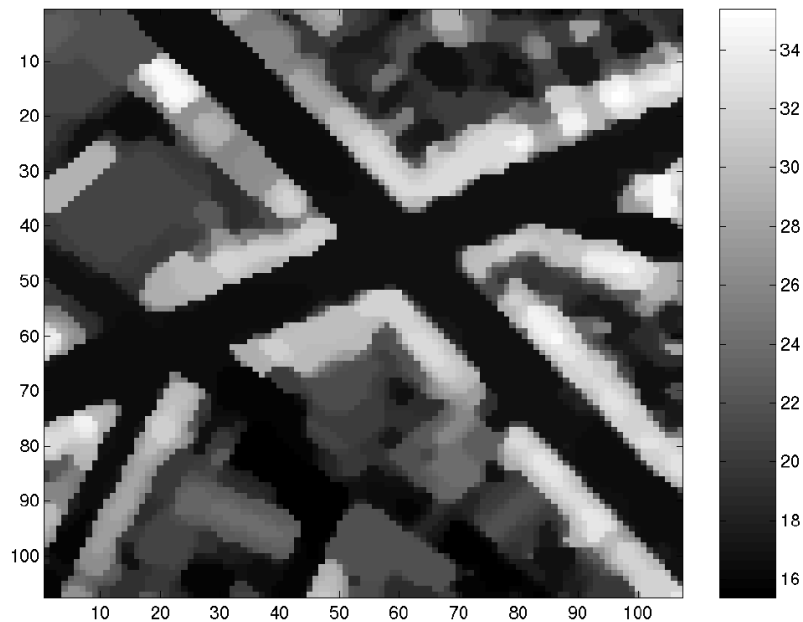
Figure 4.28: Both potential functions are total variation.

The common choice for the data-term potential function is quadratic function. We have tried each of the four potential functions for the regularization term, having the quadratic function for the data-term, but the results do not outperform the ones presented above. The 3D model with colors, projected from an optical photo on the result with truncated quadratic function and $\alpha = 2$ is in Figure 4.32.

In the following section we repeat the experiments, which are done on the data of Brussels in this chapter, applying the interpolation methods to the second real data set - the laser scanning data of Amiens.
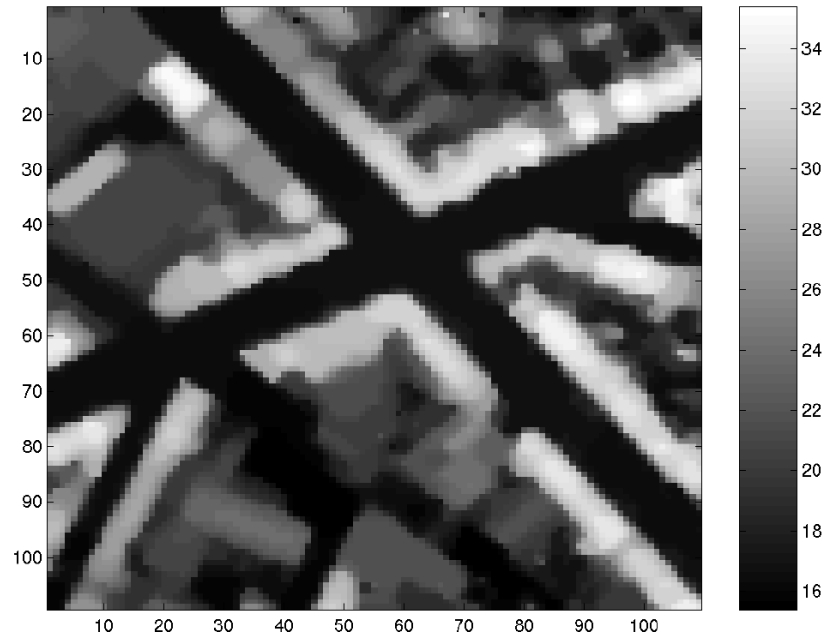
Figure 4.29: Both potential functions are generalized Gaussian.
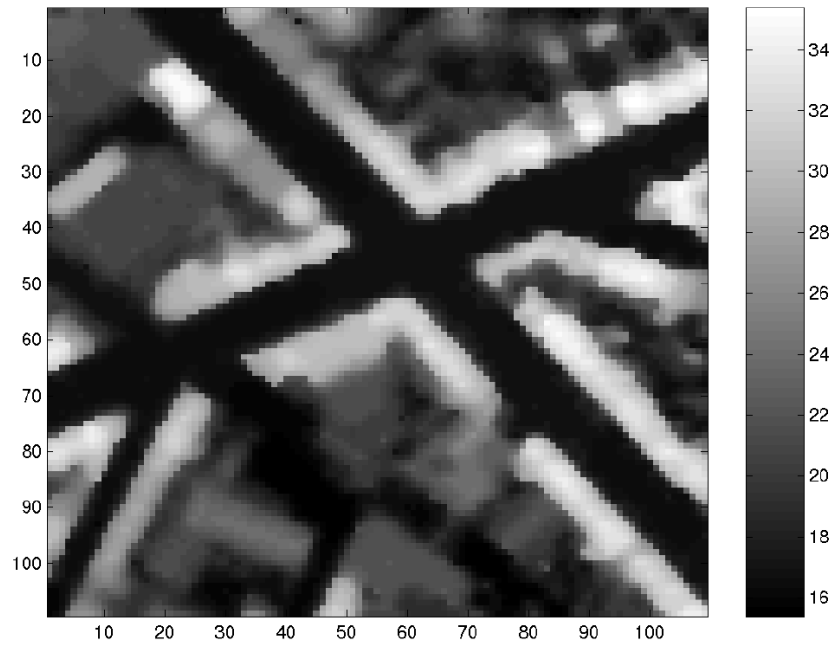
Figure 4.30: Both potential functions are Huber functions.
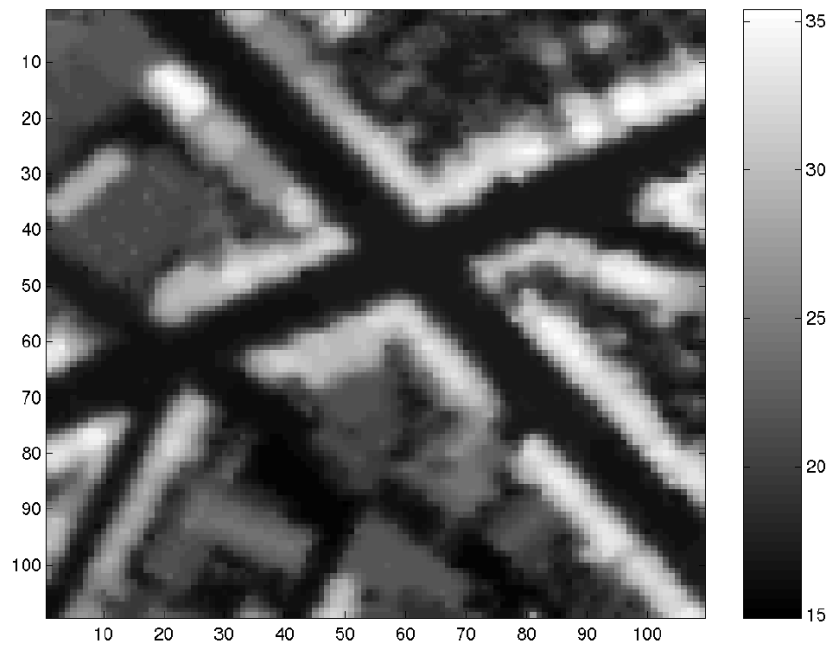
Figure 4.31: Both potential functions are truncated quadratic.

Figure 4.32: 3D model with colors: energy minimization result, potential functions - truncated quadratic, $\alpha = 2$.

4.3 Data of Amiens

4.3.1 Data and ground truth description

The Toposys company, using laser scanning system with fiber optics, has acquired the laser data of Amiens. The laser data used for the experiments is taken over the area in Figure 4.33.

Figure 4.33: The orthophoto of the studied area of Amiens, resolution is 40 cm.

The interpolation is performed on the zone of 140×140 meters. There are 193990 laser scanning points in this area. The altitude values vary from 27.6 to 54.6 meters. The histogram of the altitude values is in Figure 4.34.

The first peak of the histogram is due to the points that lie on the ground. The second peak appears because of the buildings and vegetation. Laser points form parallel lines Figure 4.35.

The density of points along lines is much higher than across them: the distance between lines is about two meters, and the distance between points in a line is some centimeters. So the points are spaced very irregularly. For a big part of the area, the scanning strips overlap (Figure 4.36, 4.37).

The size of the grid for interpolation corresponds to the average density of the laser points and it is 40cm. Previously, a DEM of the same area was made in IGN
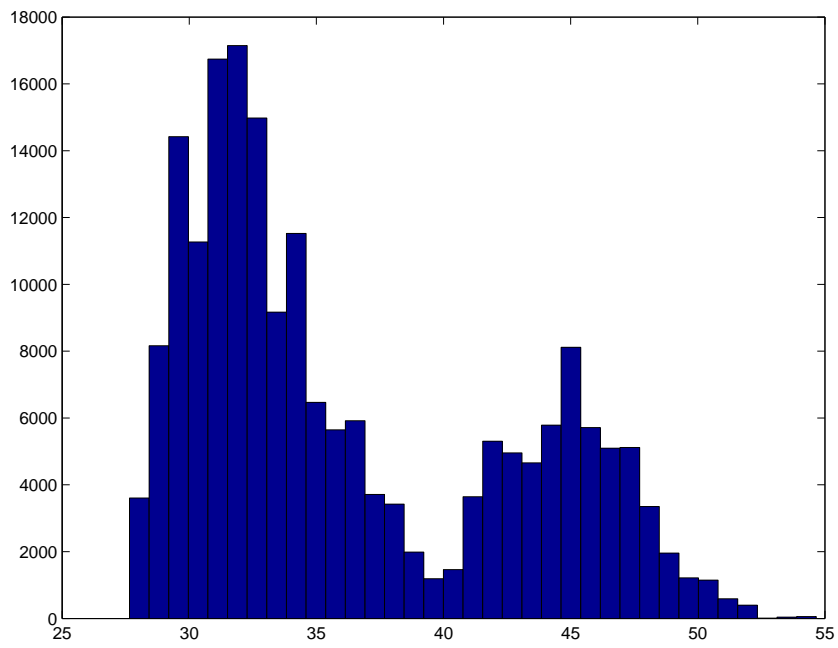
Figure 4.34: Histogram of altitude values for Amiens laser scanning data.
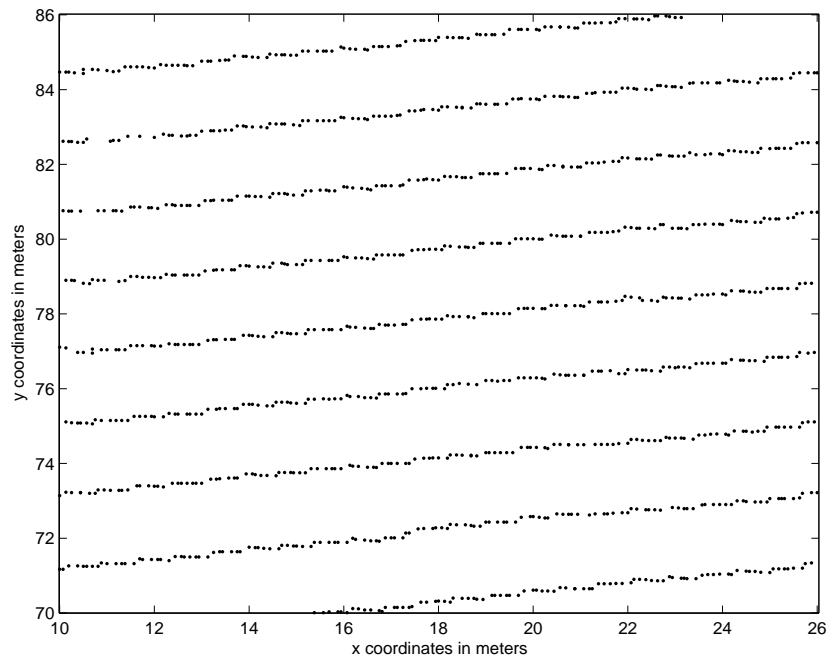
Figure 4.35: Laser scanning points form parallel lines.
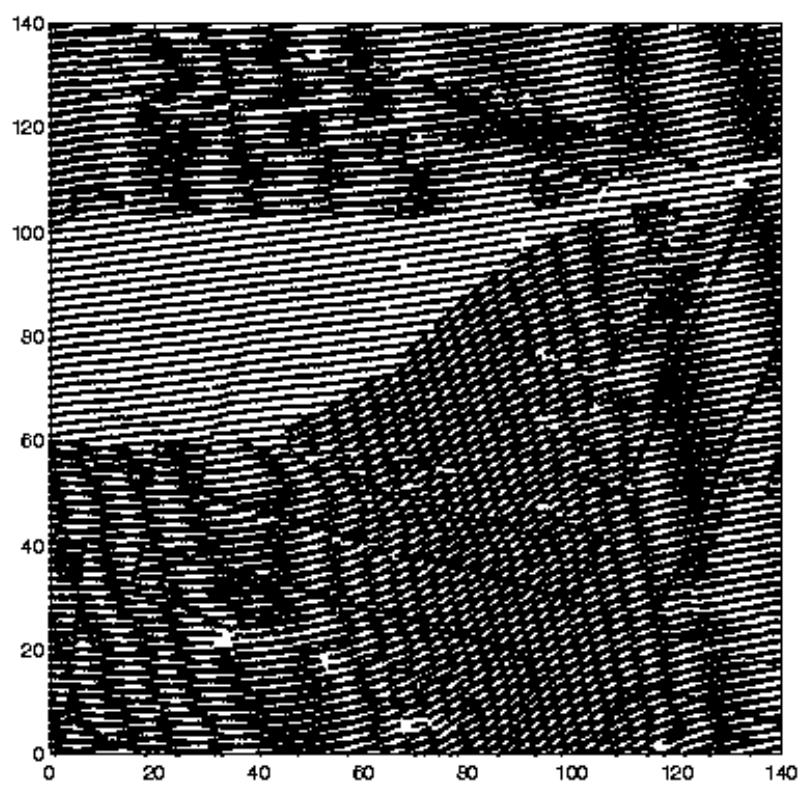
Figure 4.36: Laser scanning points over the studied zone of Amiens.
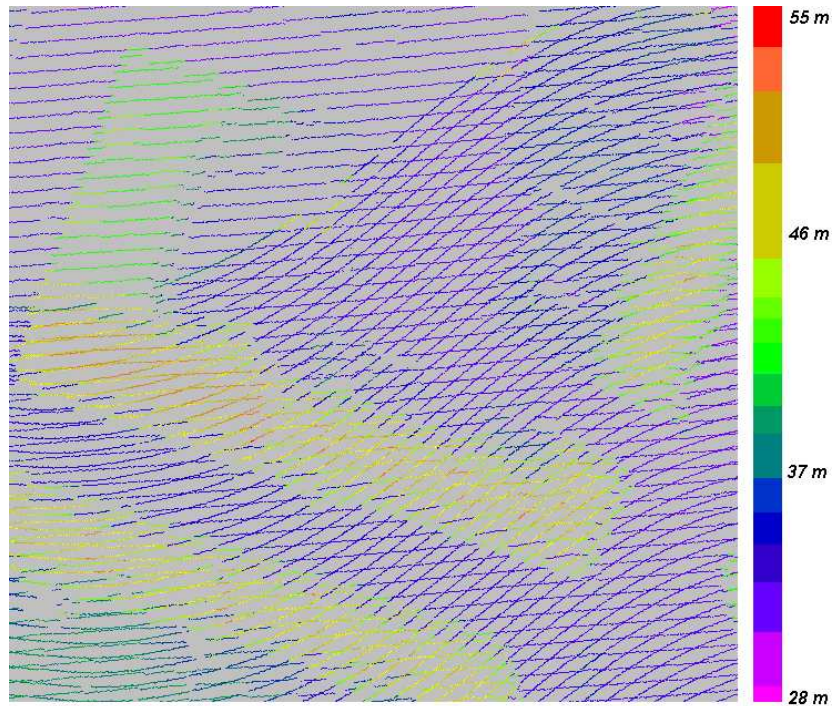
Figure 4.37: Laser scanning points over a piece of the studied zone (colors represent altitude values).

(Institut Géographique National). It was done using the information on building edges [de Joinville, 2001]. This DEM served us as the reference model. It contains only buildings and pavements, there is no vegetation there (4.38).

The reference DEM corresponds to the laser data quite well. The correlation coefficient between the laser data and the reference is 0.9372 (Figure 4.39, 4.40).

Considering the evaluation of results for the laser data of Brussels, the correlation coefficient, as the evaluation of quality, prefers smooth surfaces. So for the quality evaluation for the data of Amiens two measures are considered: mean absolute error and correlation coefficient. Root mean square error gives results proportional to the ones of the correlation coefficient. That is why it is not presented here. The mean absolute error (MAE) between two vectors X and Y is calculated using the formula

$$MAE = \frac{1}{N} \sum_{i=1}^{N} |x_i - y_i|.$$

4.3.2 Classical interpolation approaches

Considering the classical interpolation methods, triangle-based linear interpolation gives better results than nearest neighbor interpolation (Figure 4.41) or kriging (Figure 4.42). The distribution of points is not favorable for kriging, neither for calculating the experimental variogram nor for the interpolation. If a large size of a neighborhood for kriging is taken, then the result is too smooth, but small neighborhoods don't
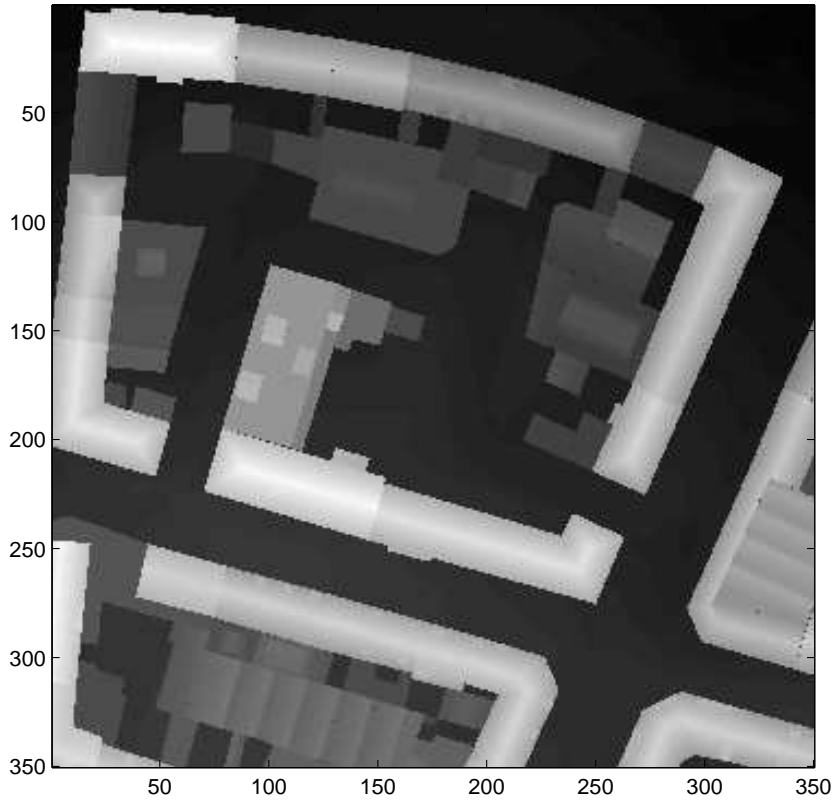
Figure 4.38: DEM used as a reference for Amiens.
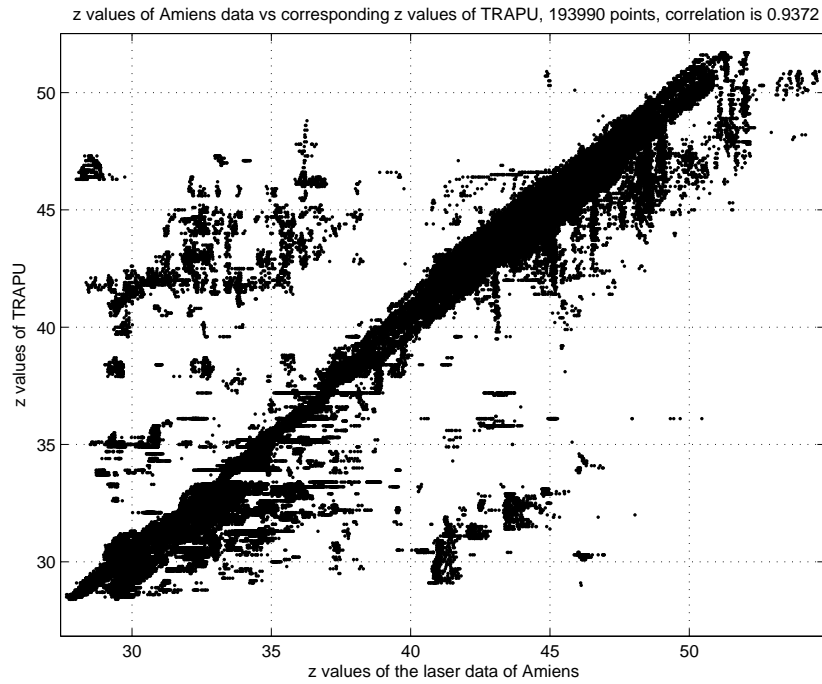
Figure 4.39: Laser points versus the reference values. The correlation between the two data sets is 0.9372.
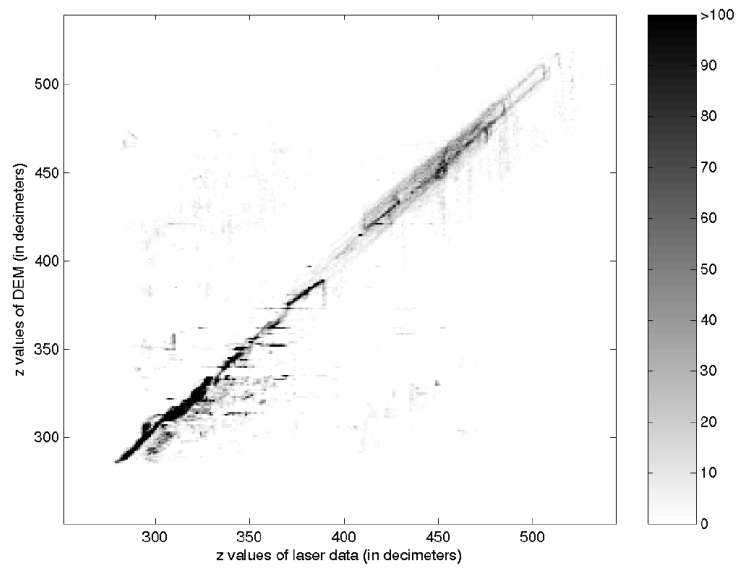
Figure 4.40: Laser points versus the reference values. The darker is a point, the more times it was hit while plotting z values of laser data versus z values of the reference.
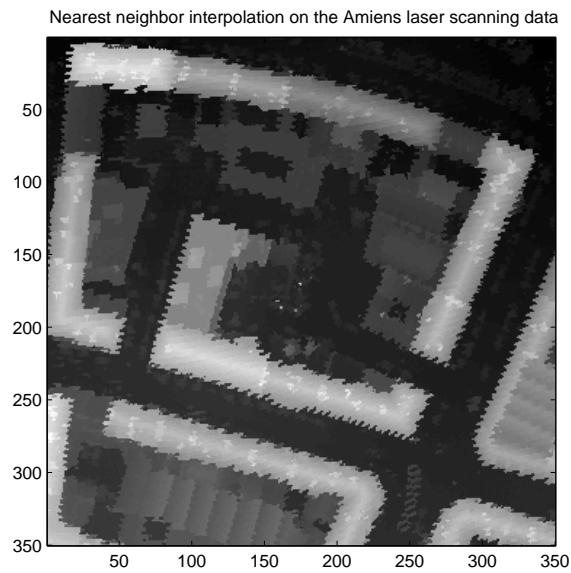
Figure 4.41: Nearest neighbor interpolation on the laser scanning data of Amiens.
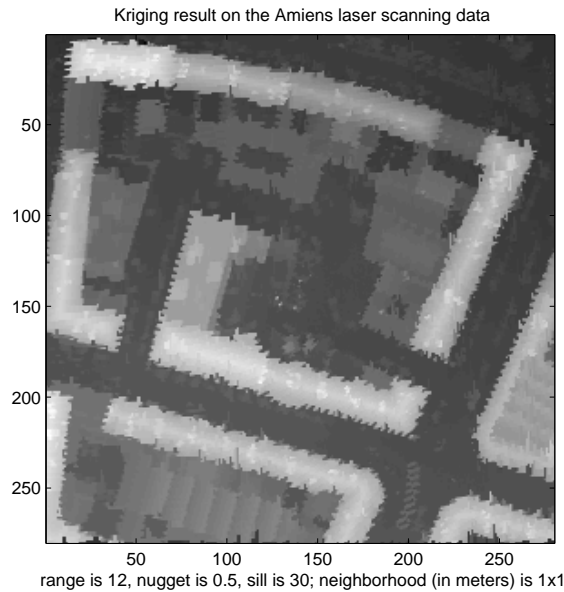
Figure 4.42: Kriging on the laser scanning data of Amiens.

contain enough information and lead to distorted images.

For the data of Amiens there are two echo pulses available, that is first and last echoes of the laser. Only the last echo pulses were considered for interpolation, because the first echo pulses contain more information on the vegetation which is not present on the reference model. The correlation coefficient for the linear interpolation result (Figure 4.43) is 0.9460, the mean absolute error is 1.0198 meters. Since the reference DEM was done some years before the laser scanning data acquisition, there are some parts of buildings that appeared meanwhile, and they contribute to the error value.

4.3.3 Energy minimization method and comparison of results

To perform the energy minimization method, the solution is initialized with the result of the triangle-based linear interpolation. The step for the ICM algorithm is 20 cm. In this case the choice of the neighbourhood size for the laser data was more important than the choice of a potential function for the regularization term. Data values in different directions are required, therefore for each pixel the values in a circle with the radius 1 m are taken. The radius that corresponds to the 8 nearest neighbors on the regular grid should be 0.57 m, but in this case a large part of pixels doesn't have any laser data points in the neighborhood. The correlation coefficients for different values of α are in Figure 4.44.

The mean absolute error is in Figure 4.45.

The horizontal line shows the linear interpolation result.

According to the correlation coefficient, the generalized Gaussian function provides the best result (Figure 4.46), and the Huber potential function is the best (Figure 4.47)
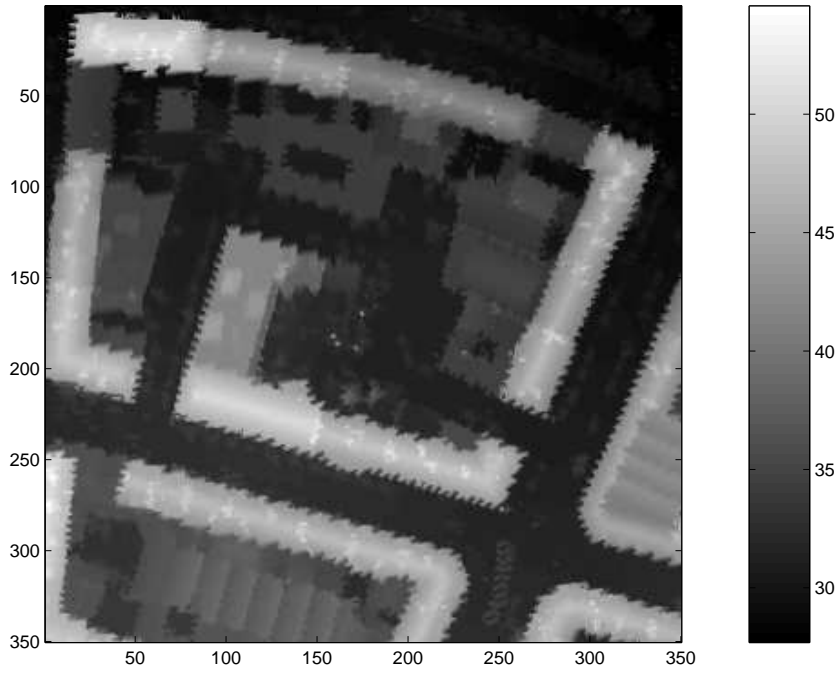
Figure 4.43: Triangle-based linear interpolation.
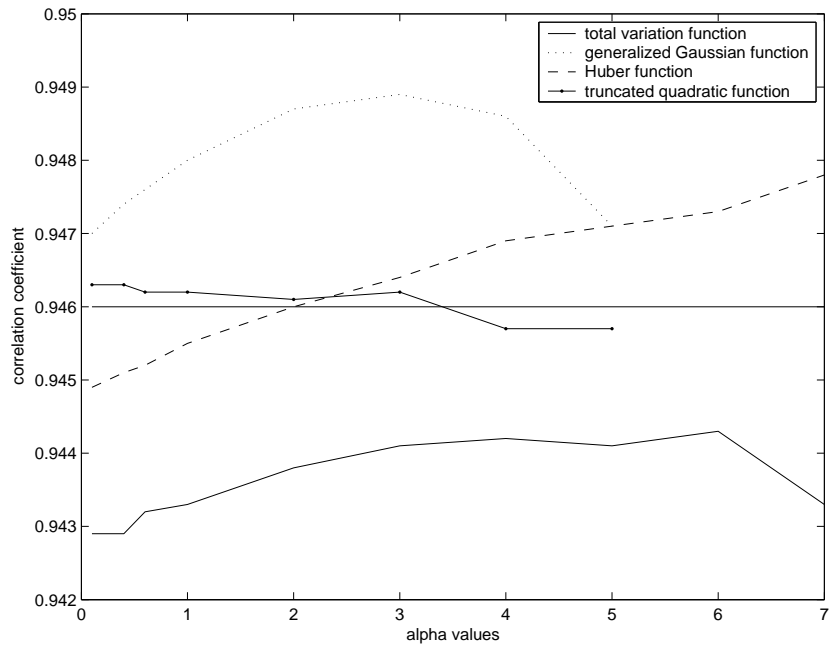
Figure 4.44: Search for an optimum α value for the data of Amiens.
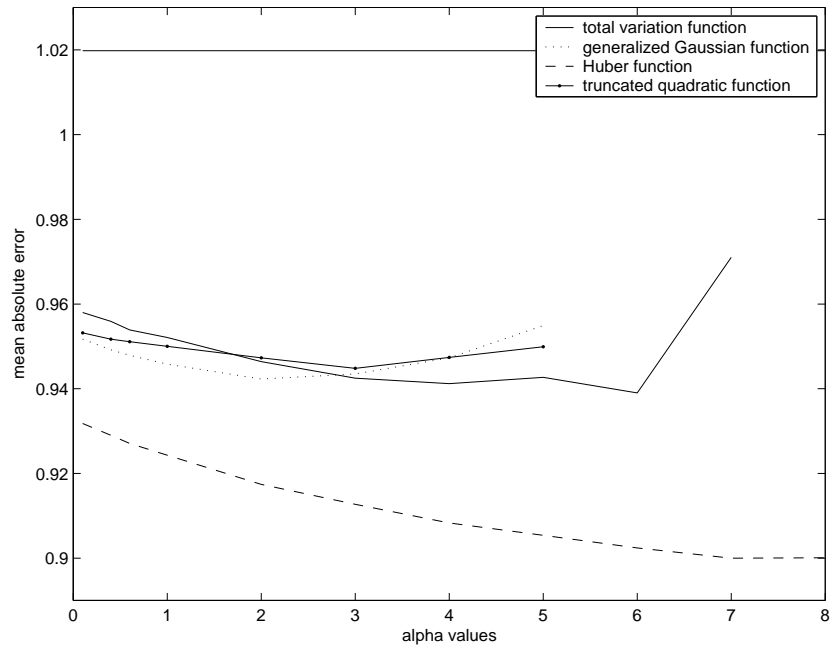
Figure 4.45: Search for an optimum α value for the data of Amiens.

according to the mean absolute error.

The best result according to the mean absolute error is visually better than the one preferred by the correlation coefficient.

The effect of the regularization can be seen in Figures 4.48 - 4.51. In Figures 4.49 - 4.51 solid line represents the profile of the resulting surface after interpolation, and the points are the laser scanning data samples. The linear interpolation distorts edges because of the triangulation made on the points situated around the discontinuities.

The colors projected on the result of energy minimization with Gaussian potential functions is in Figure 4.52

potential functions are generalized Gaussian
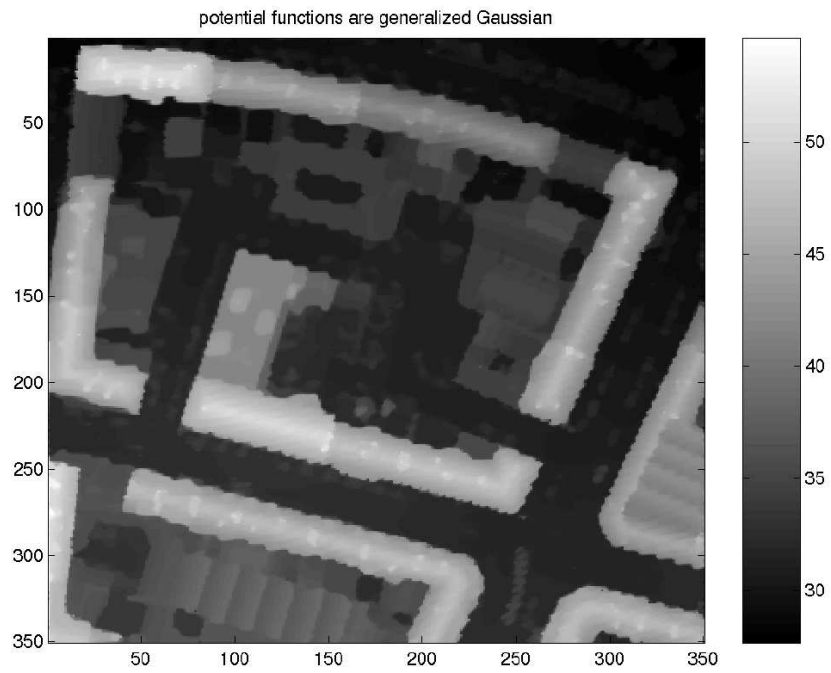
Figure 4.46: Both potential functions are generalized Gaussian - the best result according to the correlation coefficient.

potential functions are Huber functions
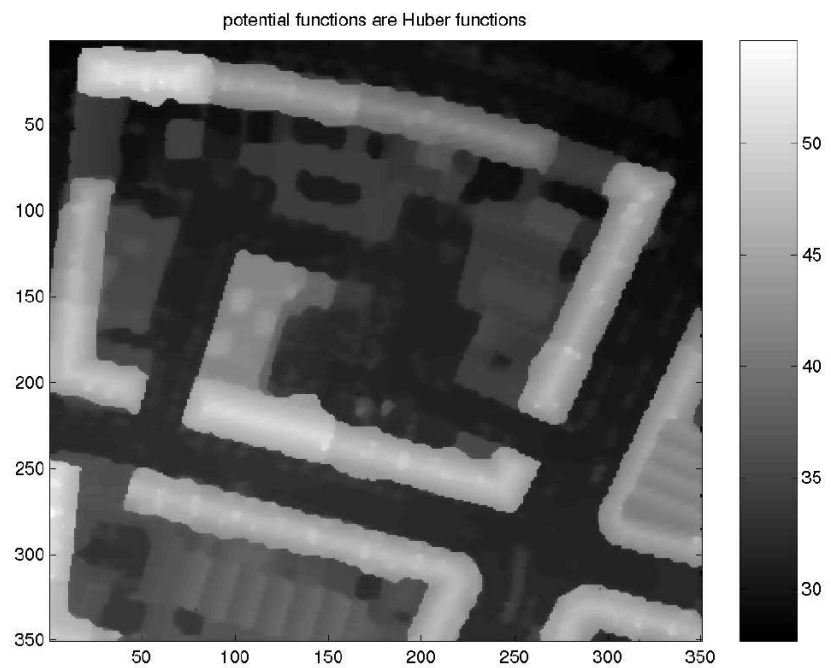
Figure 4.47: Both potential functions are Huber functions - the best result according to the mean absolute error.
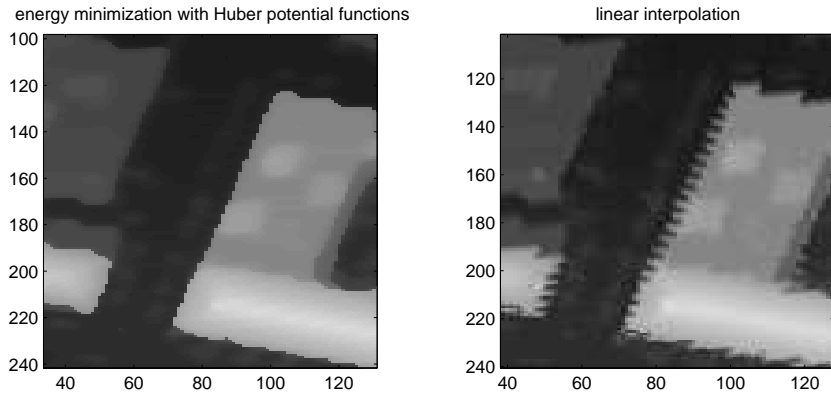
Figure 4.48: The effect of the regularization on a piece of the data of Amiens.
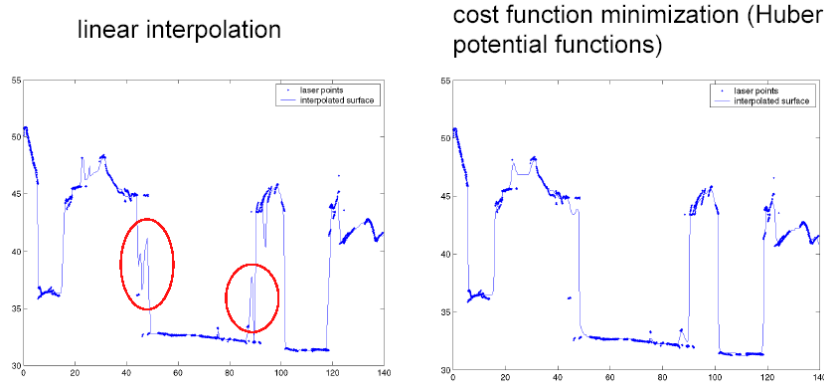
Figure 4.49: Left image - profile of the linear interpolation result; right image - profile of the surface obtained by energy minimization. The distortions of the edges or buildings are eliminated by applying the energy minimization to the laser scanning data.
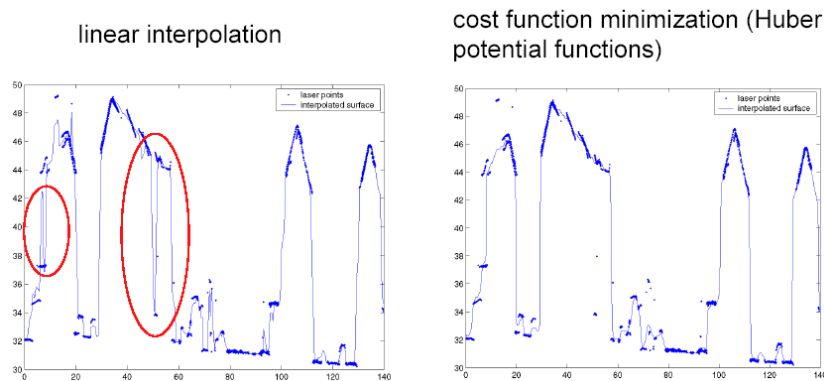
Figure 4.50: Left image - profile of the linear interpolation result; right image - profile of the surface obtained by energy minimization. The distortions of the edges or buildings are eliminated by applying the energy minimization to the laser scanning data.

110
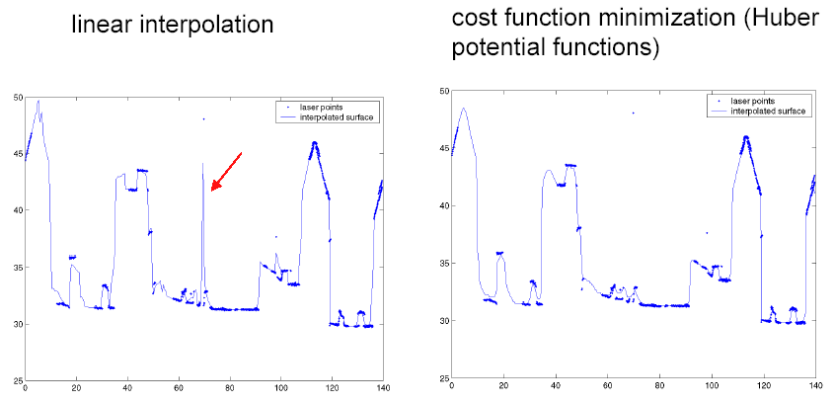
Figure 4.51: Left image - profile of the linear interpolation result; right image - profile of the surface obtained by energy minimization. The outliers are suppressed by applying the energy minimization to the laser scanning data.
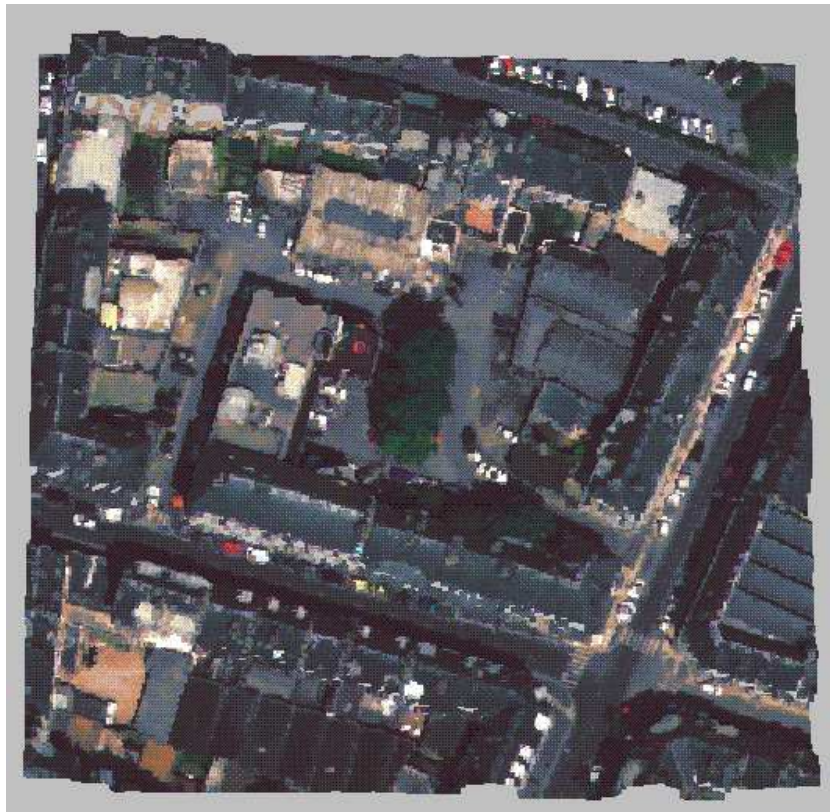
Figure 4.52: A result for Amiens as 3D model with colors.

4.4 Conclusion

The well-known interpolation methods for scattered data were applied for the laser scanning data over urban areas. There are two different data sets (Brussels and Amiens) for the tests: the distribution, the density of the laser points and the scanning system are different for them. For the Brussels data the result of kriging is the best according to the correlation coefficient. The correlation coefficient as a quality measure chooses smooth surfaces as the best ones. So while treating the data of Amiens, two quality measures are utilized: correlation coefficient and mean square error. For Amiens, triangle-based linear interpolation outperforms nearest neighbor interpolation kriging. Most of the distortions in the interpolation results are obviously on the edges. We can see that kriging does not lead to satisfactory results, the hypotheses of this method are not verified on surfaces representing urban areas.

Taking into account the drawbacks of the classical methods, we propose an energy minimization approach. The results with the same potential functions for the both data- and regularization-term are presented, though more experiments were made. It is because other compositions of potential functions or different parameters for each term of the energy didn't lead to better results. The choice of potential functions as well as their parameters obviously determine the quality of reconstruction. Different initializations for the optimization algorithm were tried, but they didn't influence the results too much. In general, initialization is important when the truncated quadratic function is used, because this function is not convex. Choice of a strong parameter of regularization (for example, when it is equal to 3) improves the quality criterion of correlation. It happens because often there are more than 8 laser points in the neighborhood of the pixel, and then a strong regularization coefficient is needed to compensate their influence on the result and to regularize the surface. Also the value of the regularization parameter depends on the choice of potential functions for the data-term and regularization-term. As for the choice of the neighborhood, it is important to have data points in several directions. Fixed distance approach, proposed here, can be substituted by a neighborhood based on Delaunay triangulation of the laser data.

We also saw that the potential functions guided the reconstruction well towards theoretically foreseeable specific profiles (Figure 4.53). The theoretical properties of
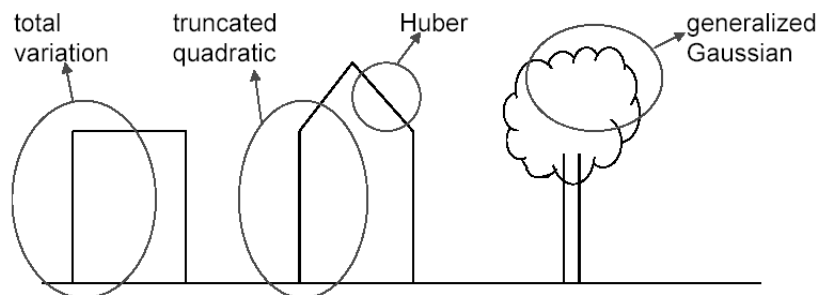

Figure 4.53: Preferable choices of potential functions on urban areas.

the potential functions have been confirmed during our experiments. The total varia-

tion potential function is working well when one wants to get a surface composed of strongly homogeneous zones divided by sharp edges. In the case of an urban area it is a building with a flat roof. Truncated quadratic potential function helps to preserve edges, and the parameter of truncation is of a great importance. Huber function performs well on the slopes and therefore it is a good choice for roofs of most of buildings. Generalized Gaussian function produces the smoother solutions the larger is its parameter. The model of the cost function adopted today does not make it possible however to control locally the type of a solution. It would certainly be useful to be able to vary the criterion locally.

A visual observation of the reconstructed images shows that the correlation prefers surfaces a little too smoothed whereas the human observer is less disturbed by local noises if the transitions are strictly respected. That is why we propose the mean absolute error to measure the quality of the results.

The quality of the results is supposed to increase when both echoes are used: the first and the last one. These echoes will provide more laser points around edges. As far as the quality of the results is concerned, we should mention that the references we use to verify it are not perfect representations of the studied areas. Evaluation of the quality of such a reference itself is also an issue of research [de Joinville, 2001]. The reference image that we have for Brussels is obtained by a plane fitting technique which makes the roofs to be simpler than they are in the reality (Figure 4.54). The

Figure 4.54: Roofs of buildings in an urban area.

model contains some distortions in the area of vegetations. As for the data of Amiens, the reference we have is also simplified and not containing vegetation. It is obtained from the some polygons which delimit the edges of buildings [de Joinville, 2001].

In the following two chapters we will describe the CMB data properties and the acquisition technique as well as the interpolation results obtained by using the same

methods as the ones applied for the laser data. We will use binning as the reference method in order to evaluate the performance of the interpolation approaches described earlier in this thesis and applied to the laser data in this chapter.

Chapter 5

Cosmic microwave background

5.1 Introduction

Previously we considered the irregularly spaced data interpolation for the airborne laser scanning data. The second application considered in the thesis is the Cosmic Microwave Background (CMB) anisotropies measurements interpolation. In this chapter we consider the nature of the data as well as the acquisition techniques. The description of the Archeops and Planck instruments, and the results presented in the next chapter, are a part of the large project aiming to produce the most precise and complete CMB measurements ever accomplished.

The Archeops experiment is supposed to test the equipment which will be used for the Planck satellite mission. We present a short overview of these two instruments, because they let us understand how the measurements are acquired and what kind of noise is supposed to be present in them.

We will also describe the simulated CMB anisotropy measurements made according to the Archeops acquisition technique. This set of data will be used for testing the interpolation methods in the next chapter.

5.2 CMB radiation

The CMB radiation constitutes one of the most powerful tools of cosmology. This photon radiation is a relic from a hot and dense past of the universe, produced at the Big Bang and freely propagated 300000 years after it [Barreiro, 2000]. In the framework of Big Bang theory, the universe started with the hot and dense phase about 15 billion years ago and cooled down while expanding. As the universe expands, the temperature decreases and drops to about $3000K$ (2727℃), allowing free electrons and protons to form neutral atoms. At this time, known as decoupling, the universe becomes transparent, the photons can freely propagate, giving rise to the CMB. It is supposed that after the decoupling there was no interaction between matter and the CMB radiation. With time the temperature of the CMB has dropped and now is $T_0 = 2.73K$ (-270℃). This temperature is almost perfectly isotropic, the

anisotropies being about one part to 100000. Measuring the properties of these temperature anisotropies will constrain drastically the seeds for structure formation as well as the cosmological parameters describing the matter content, the geometry and the evolution of our universe. The accuracies, required for precision tests of the cosmological models and measurements of the cosmological parameters, are such that it is necessary to separate the contribution of several distinct astrophysical sources, all of which emit radiation in the frequency range used for CMB observations, i.e. the 10 GHz - 800 GHz range [Delabrouille et al., 2002]. The separation of astrophysical components is possible essentially because the components have distinct emission spectra as a function of radiation wavelength. Subtraction of slow drifts and the straylight problem are also important issues for CMB anisotropies experiments [Delabrouille, 2001].

The existence of the CMB was first predicted by Gamow and his collaborators in 1948, when studying the light-element synthesis in the primordial universe. They predicted that this relic radiation should still be ubiquitous today, with a temperature of about $5K$ (-268℃). In 1964 the discovery of the CMB was made by Penzias and Wilson. They detected a noise in their antenna with a temperature of about $3K$ (-270℃) coming from all directions in the sky and being very uniform. The temperature of the CMB has been measured by the FIRAS (Far Infrared Absolute Spectrophotometer) instrument on board of the COBE (Cosmic Background Explorer) satellite to be $T_0 = 2.728 \pm 0.004K$. These measurements were done by NASA (National Aeronautics and Space Administration) in 1989 [Henrot-Versillé, 2003]. The prediction and the subsequent detection of the CMB is one of the strongest supports for the Big Bang model.

Since the CMB freely propagated after the decoupling time, it carries information about how the universe was much time ago. The fact that the CMB is very homogeneous, means that so was the primitive universe. However, the matter in our universe clusters on a wide range of scales, forming all the structures we see today. If all theses structures were formed via gravitational instability, those density fluctuations should already be present at early times, leaving their imprint as temperature anisotropies in the CMB.

The temperature anisotropies of the CMB are described by a 2-dimensional random field $\frac{\Delta T}{T}(\vec{n}) \equiv \frac{T(\vec{n}) - T_0}{T_0}$, where $\vec{n}$ is a unit vector on the sphere. It is usual to expand the field in spherical harmonics.

There have been many ground based, balloon-borne and satellite experiments to measure the CMB anisotropies. They acquired data at different resolutions and different frequencies. Among ground based experiments there are APACHE, CAT, Python, VLA and others. Balloon-borne experiments: Archeops, ARGO, BAM, BOOMERanG, FIRS, MAX, MAXIMA, MSAM, QMAP, TopHat [Barreiro, 2000]. In 2001 NASA has launched the WMAP (Wilkinson Microwave Anisotropy Probe) satellite to measure the CMB anisotropies [Bennett et al., 2003]. The WMAP satellite has provided much more detailed data comparing to the COBE (see Figure 5.1 - from the web-page of NASA: http://map.gsfc.nasa.gov/). The ESA (European Space Agency) project for the Planck satellite is to be completed in 2007. Both satellites are meant to provide full sky covering measures.
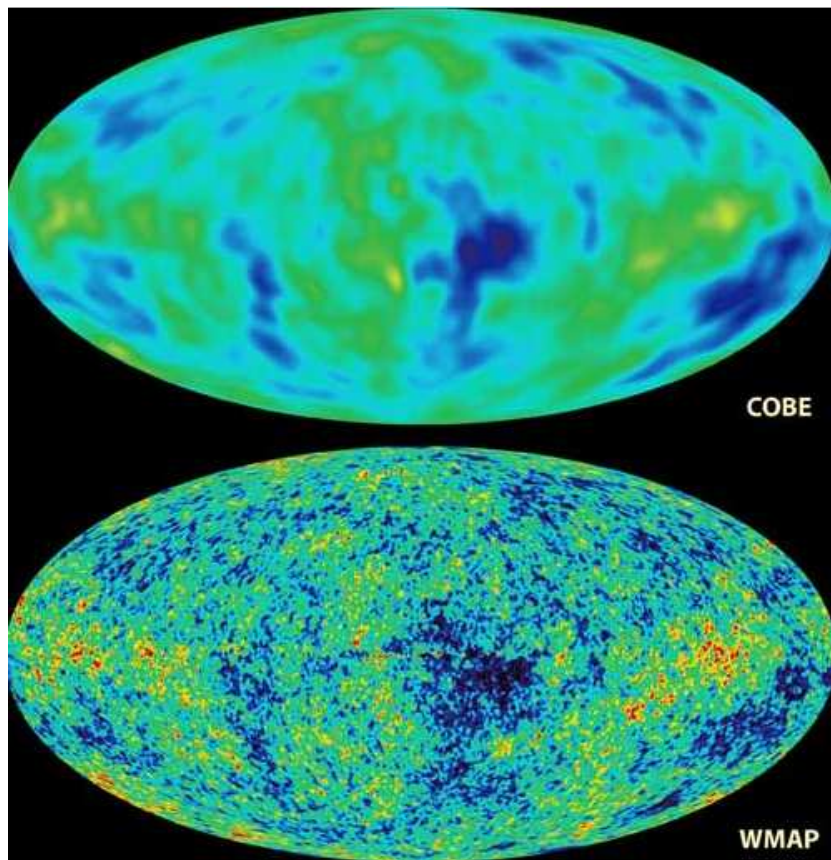
Figure 5.1: COBE and WMAP sky maps of CMB anisotropies (from the web-page of NASA: http://map.gsfc.nasa.gov/).

5.3 Archeops experiment

Archeops is a balloon-borne instrument dedicated to measuring CMB temperature anisotropies at high angular resolution (about 8 arcminutes) over a large fraction (about 30%) of the sky in the millimeter domain. To achieve this, the 1.5 meter diameter telescope (Figure 5.2) is suspended below a stratospheric balloon, pointing 45 degrees from vertical, and spun at about 2 rotations per minute [Hamilton, 2001]. The general design of Archeops is based on Planck High Frequency Instrument (HFI) technology [Benoît et al., 2002]. With this scanning strategy, as much as one third of
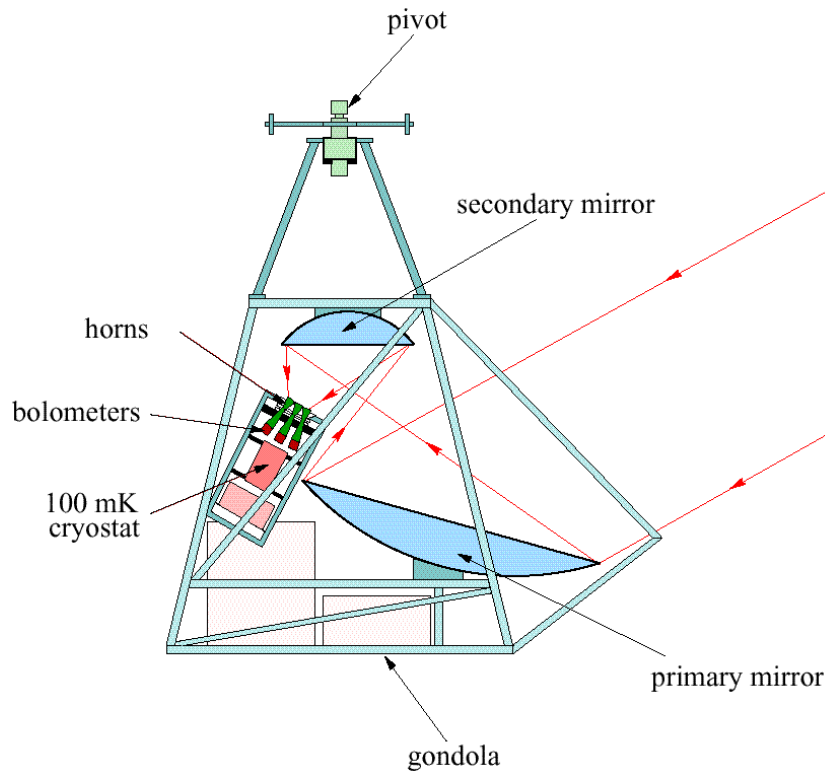
Figure 5.2: Archeops instrument (from [Hamilton, 2001]).

the sky can be covered during a 12 hour flight. After a test flight from Sicily to Spain in 1999, the instrument has flown 3 times from Kiruna (Sweden) to Russia. Winter night flights from above the Arctic Circle are necessary to avoid the combined effects of the Moon and Sun. In February 2002, the flight from Kiruna lasted during 19 hours, providing 12 hours of scientific data at an altitude of 33 km. Observations of a single night cover a large fraction of the sky as the circular scans (Figure 5.3) drift across the sky due to the rotation of the Earth.

The detectors, that are capable to measure the temperature differences on the sky of one part in 100000, are bolometers. They measure the temperature change of a crystal cooled to one tenth of a degree above absolute zero ($-273.15°C$) by a special cooling system. The frequency bands are centered at 143 GHz, 217 GHz, 353 GHz and 545 GHz [Benoît et al., 2003].
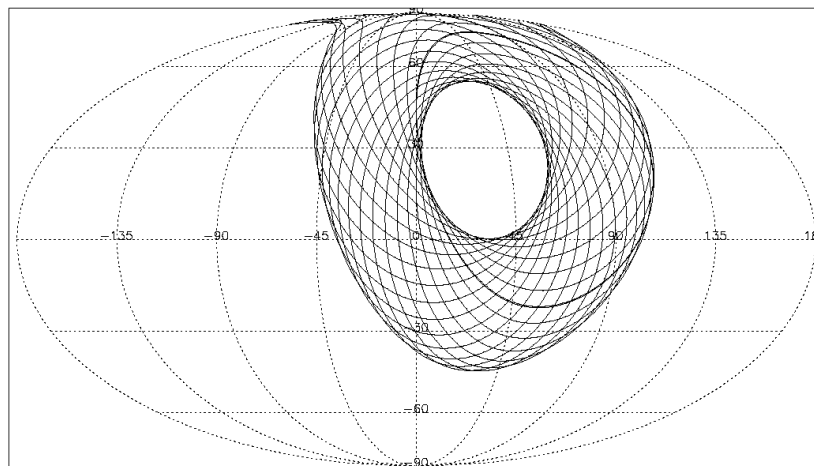
Figure 5.3: Typical Archeops sky coverage: each line represents a circle, the time separation between the circles is 1 hour [Amblard, 2001].

Several data products are being prepared from Archeops data: timelines, maps of the sky, maps of components, spatial power spectra [Delabrouille et al., 2004].

The goals of Archeops are twofold:

- from the scientific point of view, it has to provide CMB temperature anisotropies at high angular resolution, and it will add some precision to the calculation of the CMB anisotropies power spectrum, used for determining cosmological parameters [Benoît et al., 2003];

- from the technical side, Archeops is a test for Planck HFI, because it uses very similar hardware, has similar scanning strategy and data processing.

5.4 Planck mission

The Planck mission is to be launched by ESA in 2007 and it has been designed primarily for the ultimate mapping of CMB temperature anisotropies. The Planck satellite is constituted by two different instruments: the Low Frequency Instrument (LFI) and the High Frequency Instrument (HFI). The LFI will measure the microwave sky at frequencies 30-100 GHz. The HFI will cover frequencies 100-900 GHz [Barreiro, 2000]. Planck will provide multifrequency all-sky maps an angular resolution of about 4.5 arcminutes and a sensitivity $\frac{\Delta T}{T} \sim 2 \times 10^{-6}$. A study has been done in order to select an optimal scanning strategy for the Planck mission (Figure 5.4).

Planck will observe the sky from the L2 Sun-Earth Lagrange point, in a very stable thermal environment, away from sources of spurious radiation due to the Earth, the Moon, and the Sun. The scanning is made along large circles at a rate of 1 rotation per minute. The full sky should be covered in slightly more than 6 months [Delabrouille, 2004]. As mentioned in [Delabrouille et al., 1998], a good scan strategy should meet, as much as possible, the following requirements:
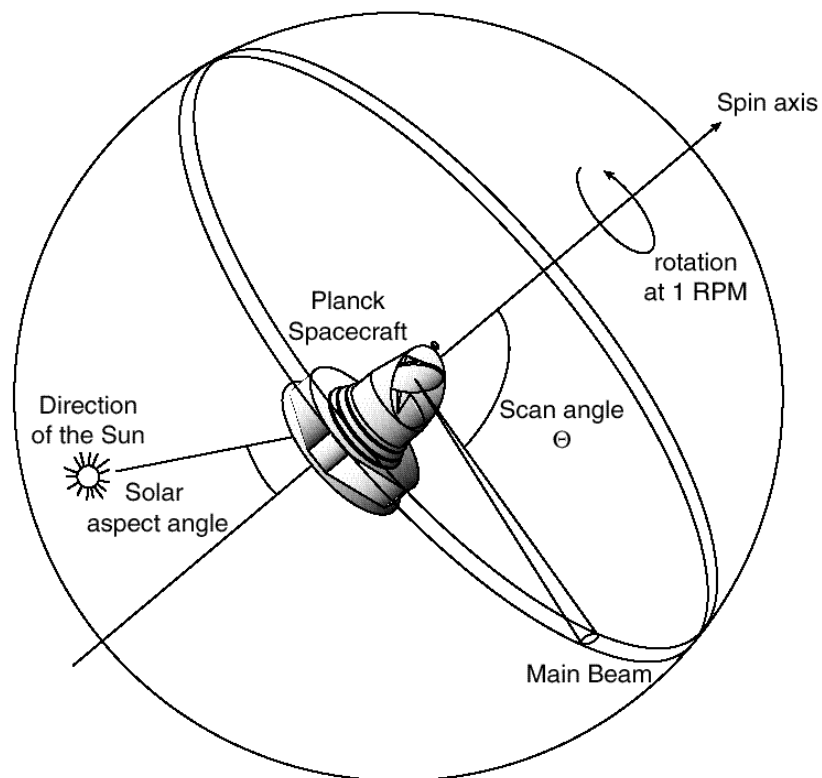
Figure 5.4: Planck scanning strategy: the trajectory of the field of view of one single detector is shown [Delabrouille et al., 2002].

- redundancy and robustness - there should be enough redundancy to test and correct for the presence of systematic effects in the data such as sidelobe stray signals, in order to obtain after processing the cleanest maps possible and reliable error estimation; the scan strategy should be such that the inversion of the data (i.e. obtaining full sky maps from the data streams and useful cosmological and astrophysical information from the maps) is possible even if a few days of data are lost or if one detector fails during the mission;

- sky coverage - Planck should provide full sky maps;

- adaptability - it should be possible if necessary to select the best scan strategy in the light of the information gathered during the verification phase after injection at L2.

- minimization of systematics - as much as possible the scan strategy should minimize the level of signal contamination by such systematic effects in the data streams;

A fundamental requirement in the new generation of high resolution Cosmic Microwave Background imaging experiments is a strict control of systematic errors. Some of these errors are of celestial origin, while others will be generated by periodic fluctuations of the satellite environment. These environment instabilities will cause fluctuations in the measured signal output thus generating correlated effects in the reconstructed maps [Mennella et al., 2002]. Spin synchronous fluctuations are not damped by the measurement redundancy, while spin resonant fluctuations, instead, are such that for every pixel the average fluctuation after N consecutive measurements is zero.

5.5   Data description

The simulated data is considered to be close to the real Archeops data in the sense of scanning strategy. The data is composed of simulated normalized CMB fluctuations and 1000 point sources of a medium size. There is also one large point source in the data. Though the real cosmological measurements are considered to be made on a sphere and therefore are determined using angles, we consider Cartesian coordinates. The simulated measurements are presented in the same way as the laser scanning data. There are three columns: x coordinates, y coordinates and measures.

Figure 5.5 shows x coordinates plotted versus y coordinates of the data. From this plot one can see the lines formed by the scanning pattern. The histogram of the measurement values is in Figure 5.6. Most of the measurements are in the interval between -2.5 and 4. The total amount of points is 47914, and only 13 of them exceed the value of 4: they correspond to the large point source in the data. The data points are visualized in Figure 5.7.

The real measurements of Archeops are affected by noise. This is modeled by adding a Gaussian noise with the standard deviation equal to 1. The resulting data is shown in Figure 5.8.
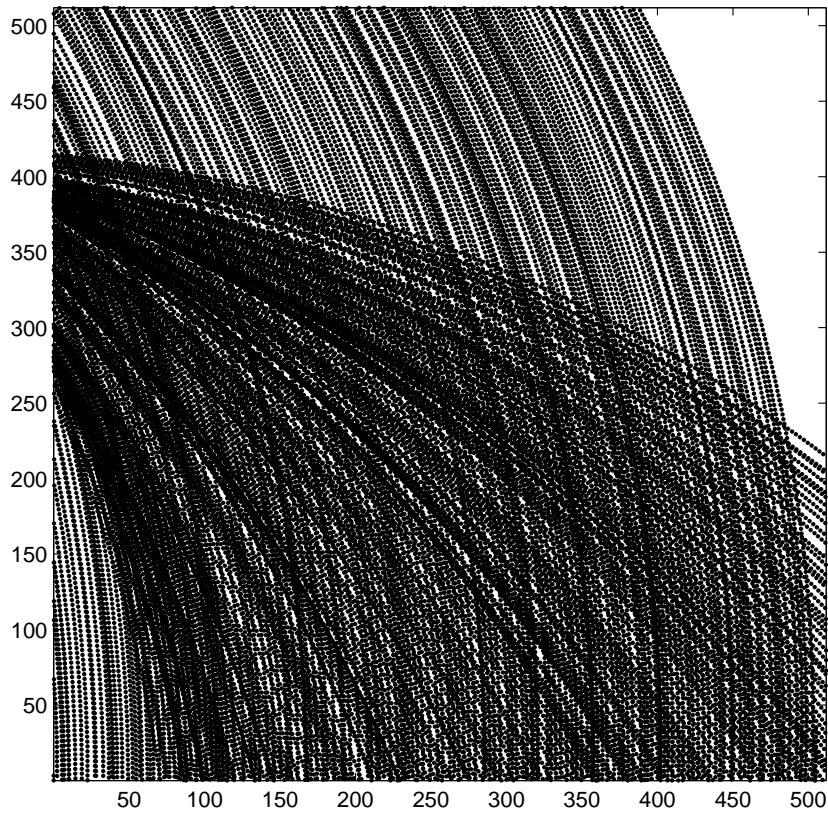
Figure 5.5: Simulated CMB measurements: x coordinates versus y coordinates.
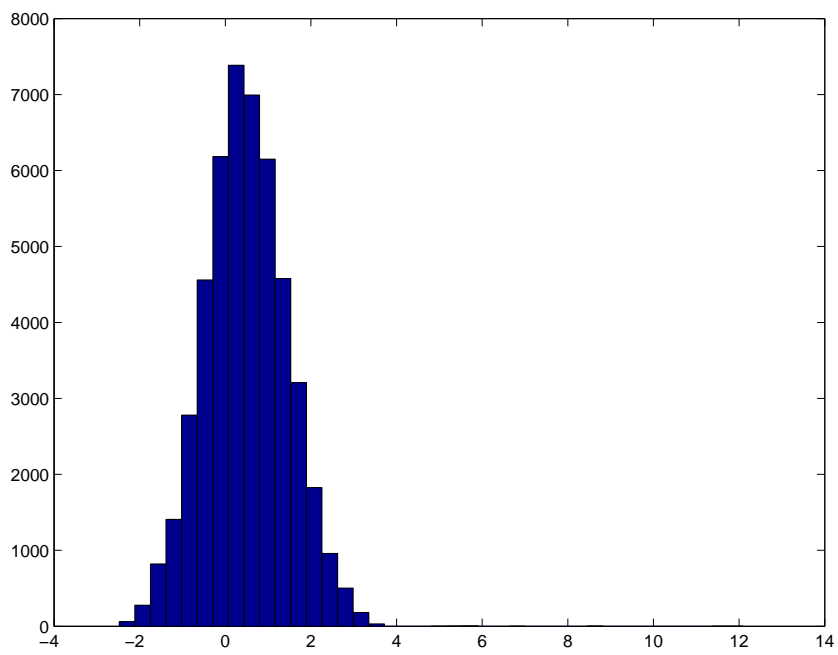
Figure 5.6: Histogram of the measurements.

122
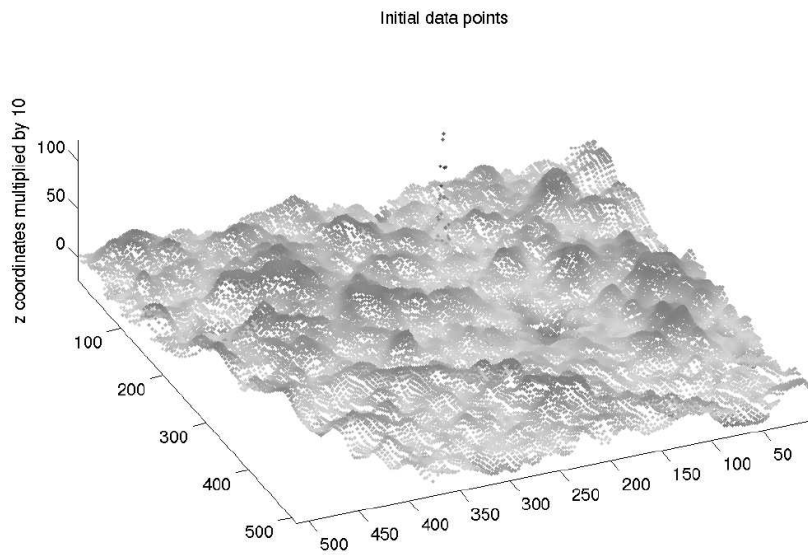
Figure 5.7: Simulated measurements.
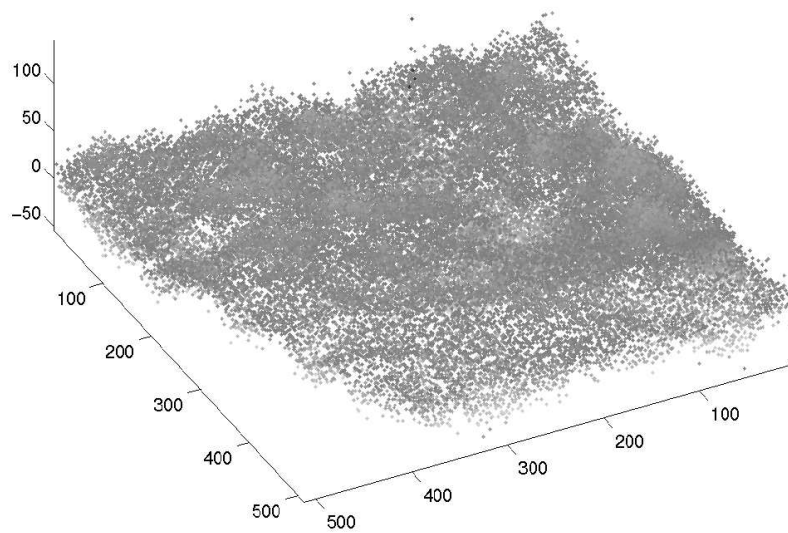
Figure 5.8: Simulated measurements with noise.

In the following chapter we will present the experiments with the simulated CMB data. Our goal is to determine the method, best suited for the interpolation of the data.

Chapter 6

Experiments on simulated CMB data

6.1 Introduction

The processing of the CMB anisotropies measurements often needs the data on the regular grid. Here we present several techniques that may be used for the CMB measurements interpolation. We are interested in several aspects. At first, the density of the measurements is not constant: for some regions it is much higher than for the others. The simulated data contains such different regions and allow to make conclusions on the methods performance depending on the density of measurements. At second, we would like to choose the best interpolation method according the root mean square error (RMSE) for the region with high sampling density and for the one with the varying density of sampling. Apart from the methods applied in our previous work to the laser data, we also consider binning. This is our reference method and we compare it with the others. Binning is very simple and fast interpolation which is often used in astronomy. So it is interesting to consider it and to find out in which cases which method is better. Binning will be presented in Section 6.2.4. At third we will try two data sets - with and without noise. The case with noise is closer to the real measurements expected from the Plank mission.

6.2 Interpolation methods

The tasks set for the experiments with the simulated CMB data will differ on two points:

- density of the original data set;

- presence or absence of noise.

Therefore three different tasks will be the following.

Task 1. For x values from 0 to 255 and for y values in the same interval, make an image 64×64, 128×128 and 256×256. More than a half of the data will fall outside of the considered area. In this case the interpolation will be performed over an area with high density of the measures. This task should be performed on the data without noise (Figure 5.7).

Task 2. For x and y coordinates varying between 0 and 511, make an image with the size 128×128, 256×256 and 512×512. This task considers the complete zone, with low density of measures in some regions. This task should also be performed on the data without noise.

Task 3. The requirements are the same as in the second task, but the data is noisy (Figure 5.8).

6.2.1   Nearest neighbor interpolation

The results of the nearest neighbor interpolation, corresponding to the first task, are in Figures 6.1 - 6.3.
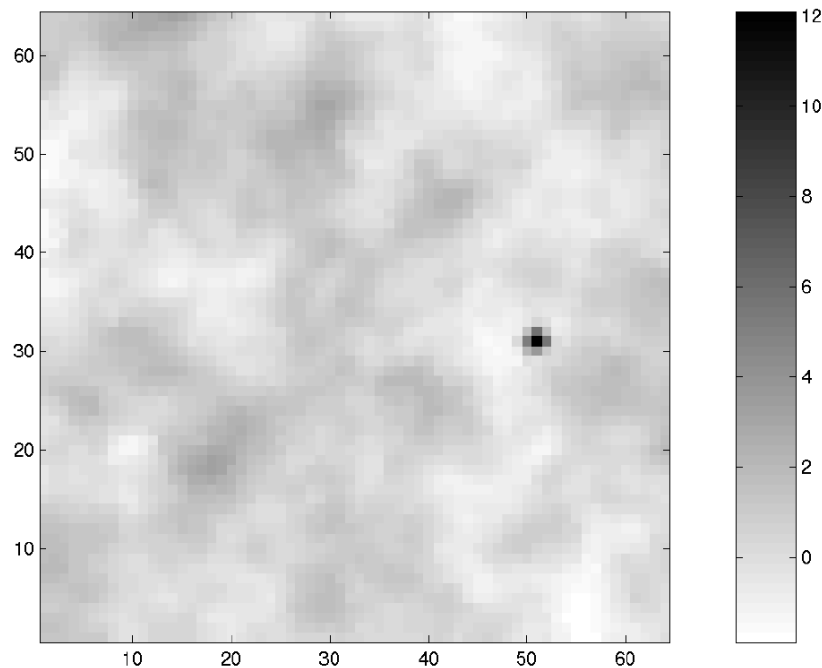
Figure 6.1: Nearest neighbor interpolation, x and y vary between 0 and 255, pixel size is 4 units.

The results, corresponding to the second task, are in Figures 6.4 - 6.6.

The upper right part of the images is not covered by measurements, therefore it should not be considered for quality evaluation of the results. It is obvious especially from the interpolation results on the smaller area (when x and y are between 0 and 255), that the higher is the resolution the more distortion is introduced by the nearest
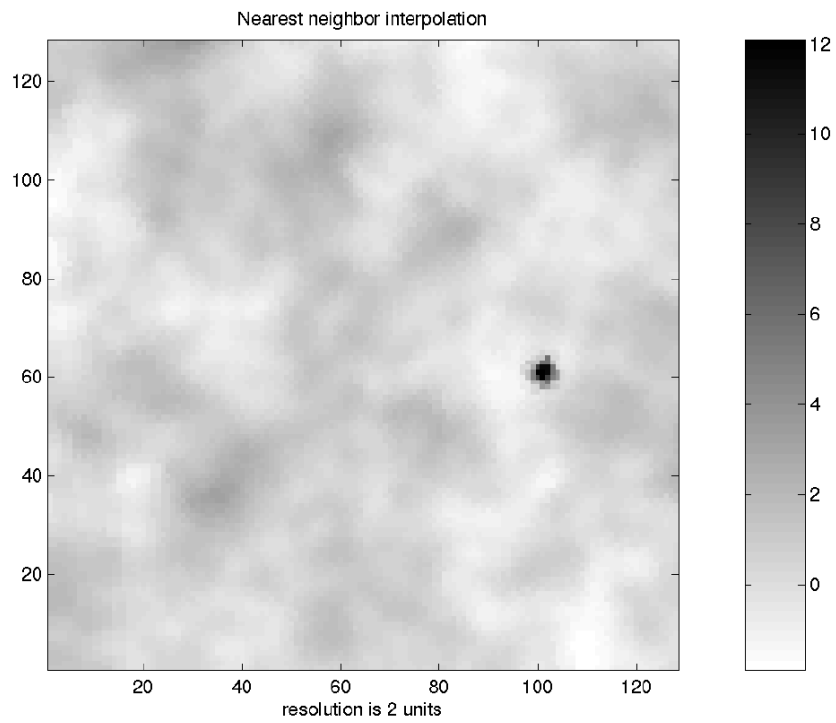
Figure 6.2: Nearest neighbor interpolation, x and y vary between 0 and 255, pixel size is 2 units.
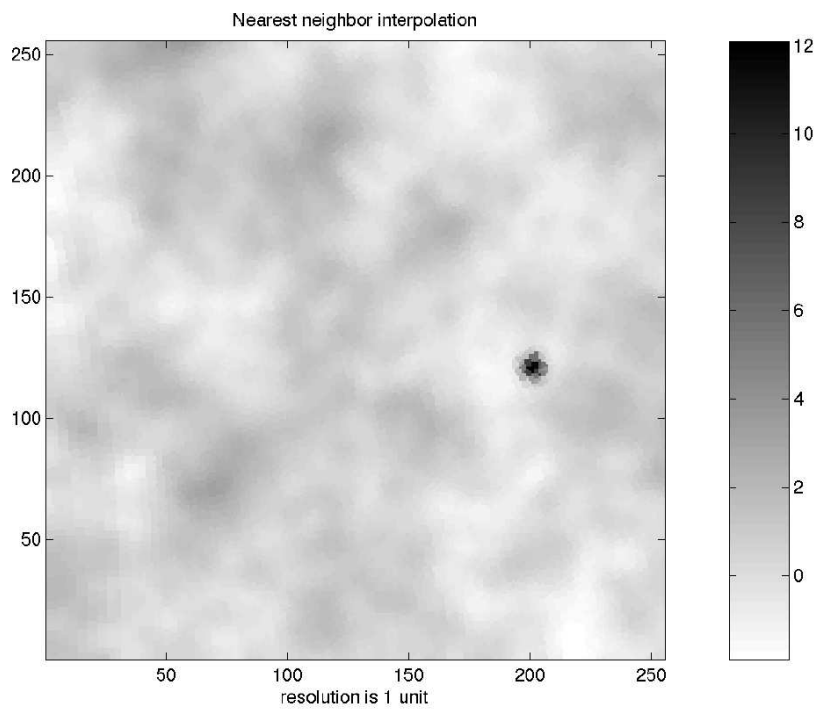
Figure 6.3: Nearest neighbor interpolation, x and y vary between 0 and 255, pixel size is 1 unit.

127
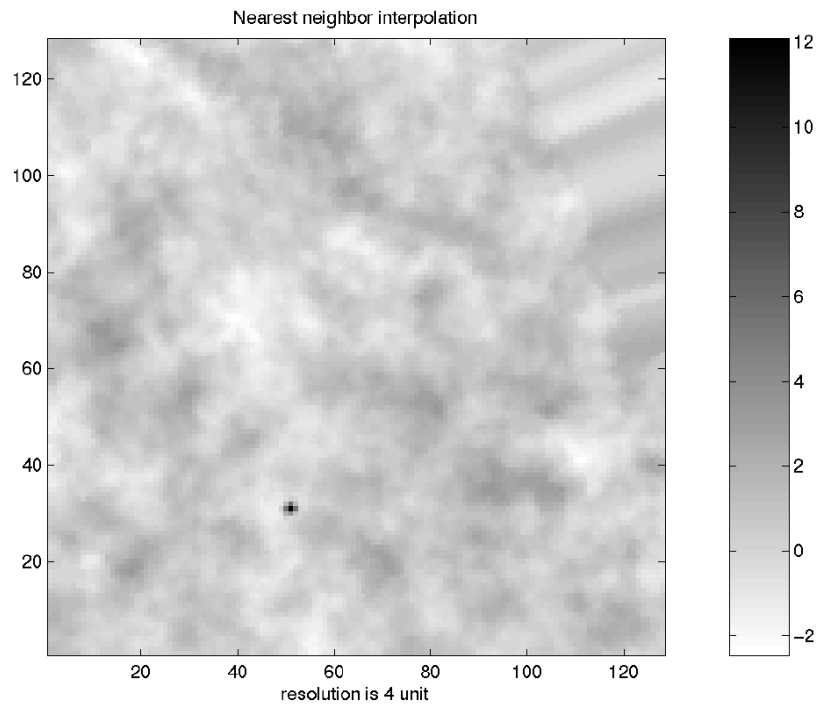
Figure 6.4: Nearest neighbor interpolation, x and y vary between 0 and 511, pixel size is 4 units.
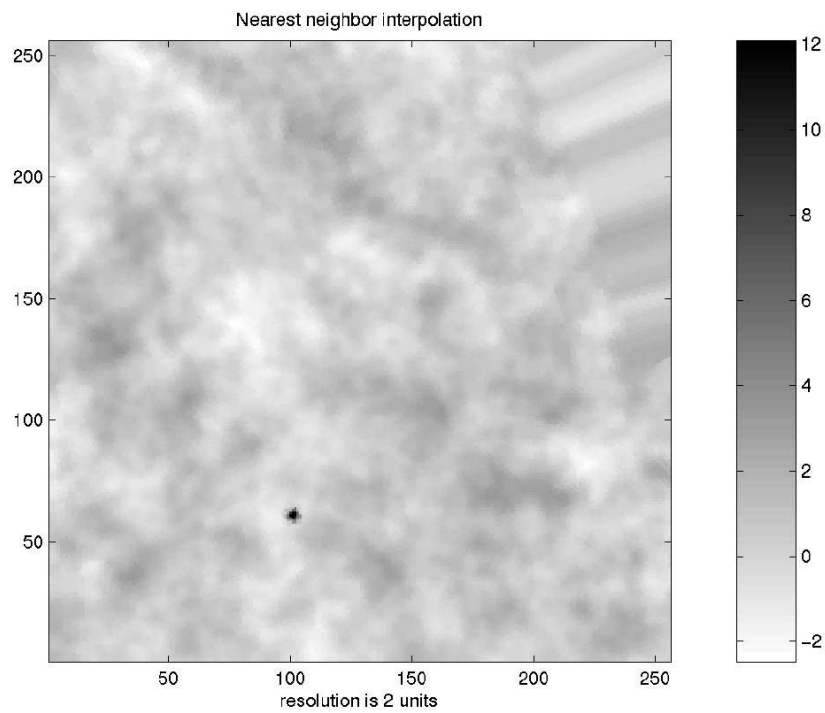
Figure 6.5: Nearest neighbor interpolation, x and y vary between 0 and 511, pixel size is 2 units.

128
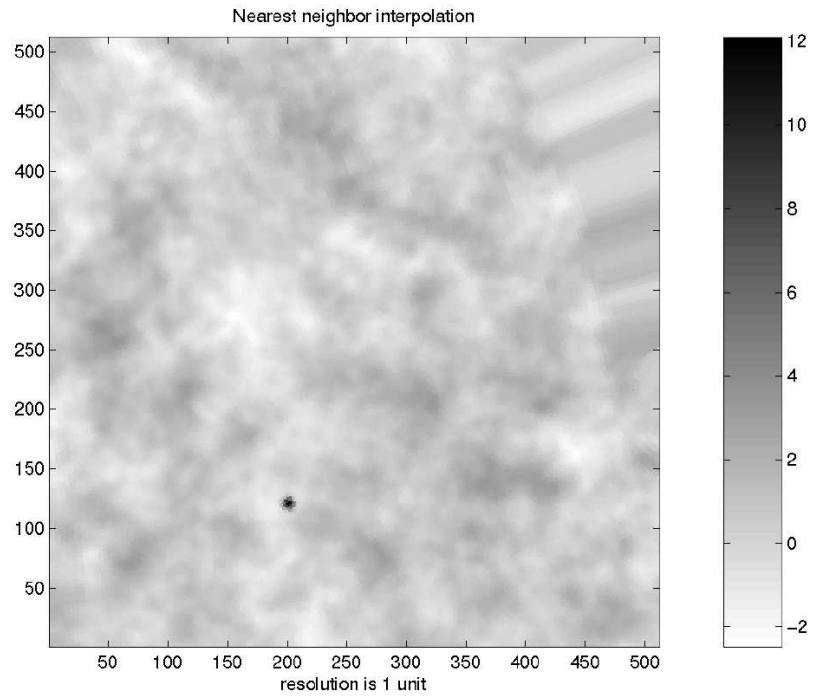
Figure 6.6: Nearest neighbor interpolation, x and y vary between 0 and 511, pixel size is 1 unit.

neighbor interpolation. This interpolation is not suitable for the noisy data, because it is not able to avoid the effects of noise (Figure 6.7).
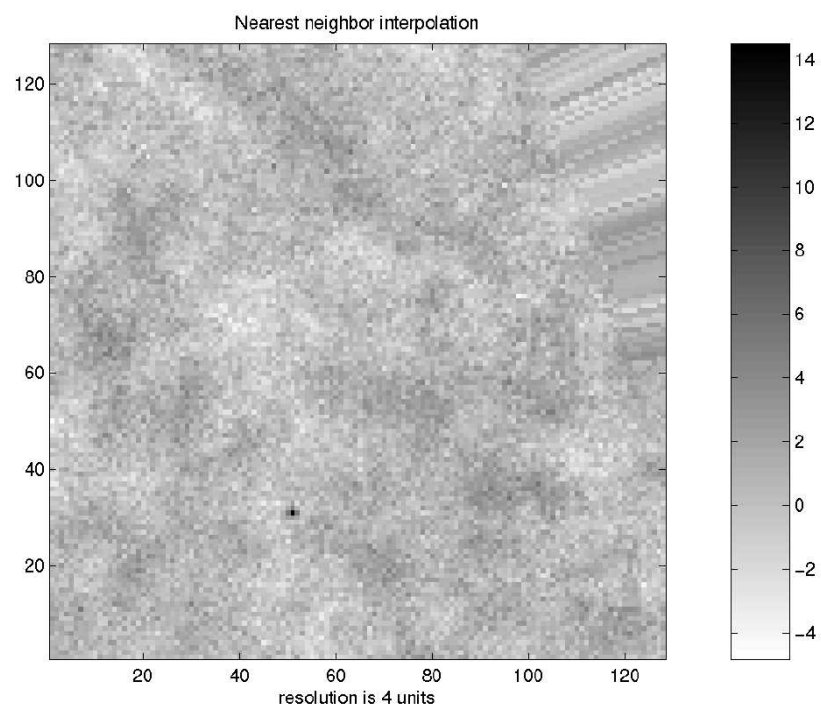
Nearest neighbor interpolation

resolution is 4 units

Figure 6.7: Nearest neighbor interpolation on the noisy data, x and y vary between 0 and 511, pixel size is 4 units.

6.2.2 Triangle-based linear interpolation

The results of the triangle-based linear interpolation are in Figures 6.8 - 6.11.
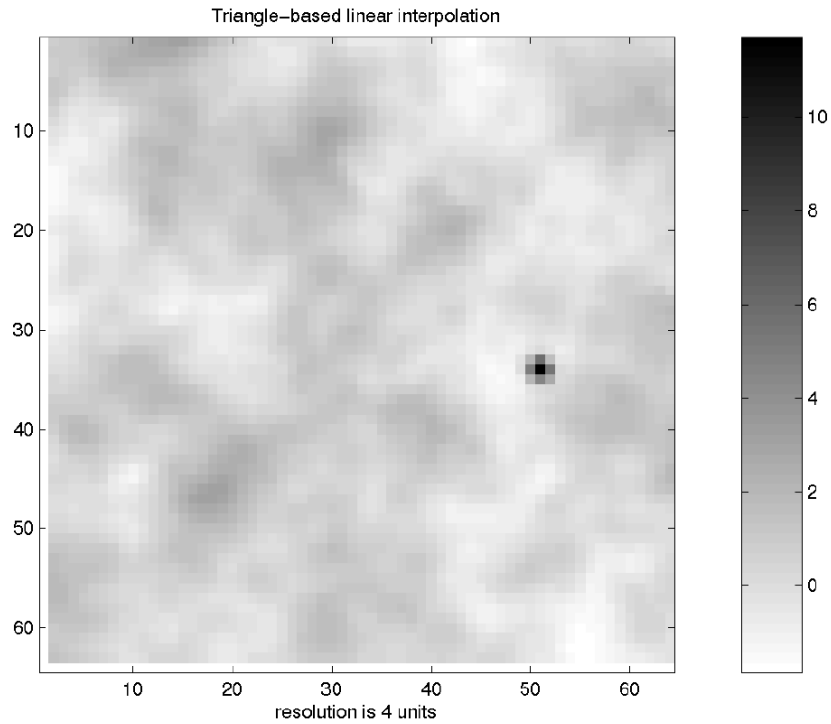
Figure 6.8: Linear interpolation, x and y vary between 0 and 255, pixel size is 4 units.

These images are smoother than the ones of the nearest neighbor interpolation. But triangle-based linear interpolation doesn't give good results on the noisy data (Figure 6.14).
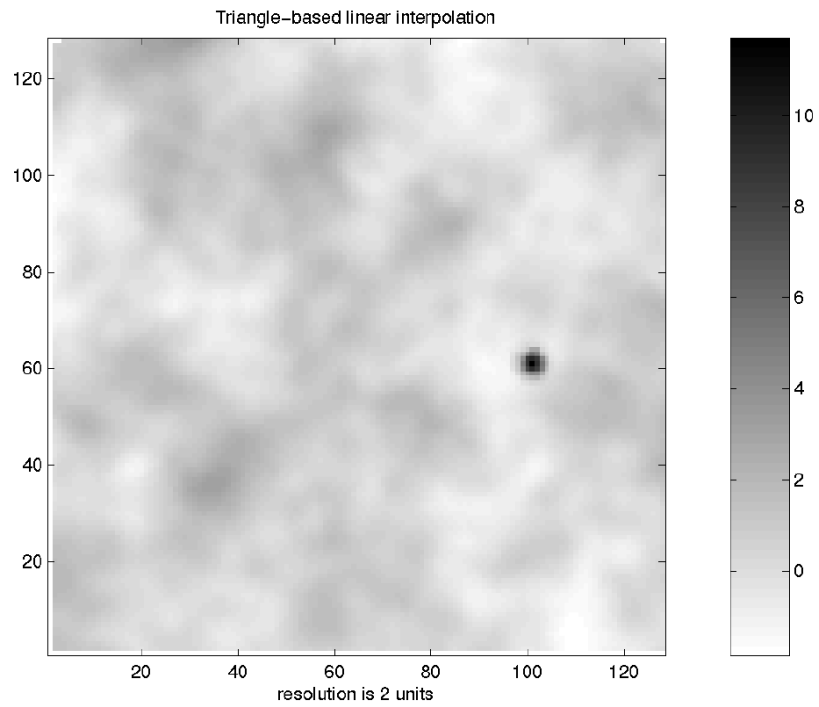
Figure 6.9: Linear interpolation, x and y vary between 0 and 255, pixel size is 2 units.
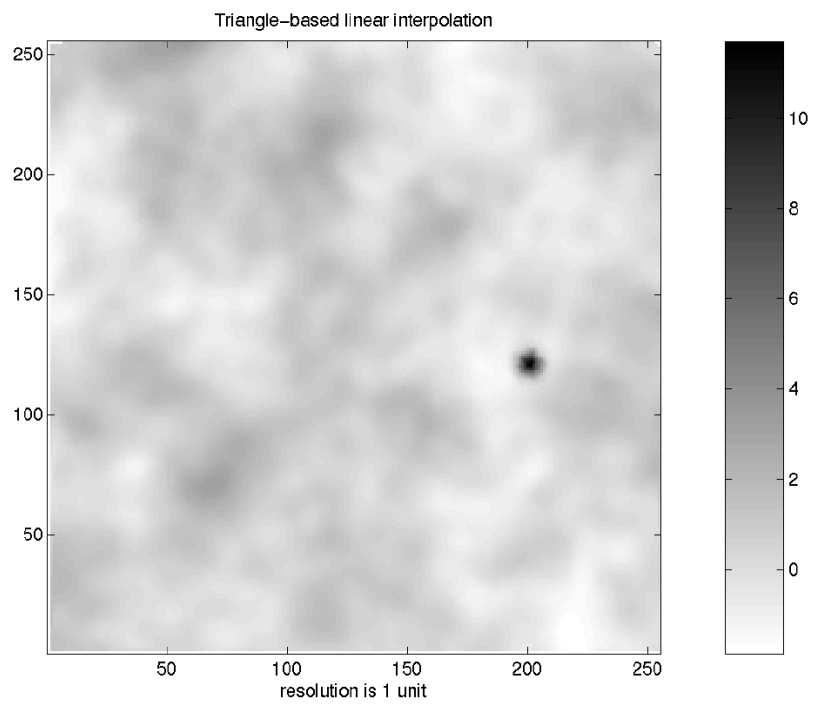
Figure 6.10: Linear interpolation, x and y vary between 0 and 255, pixel size is 1 unit.

132
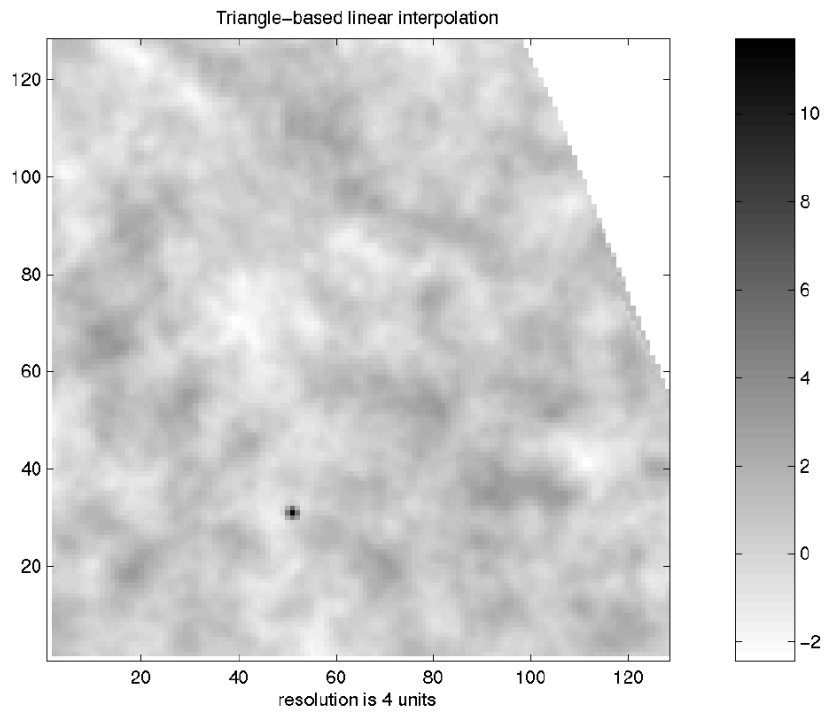
Figure 6.11: Linear interpolation, x and y vary between 0 and 511, pixel size is 4 units.
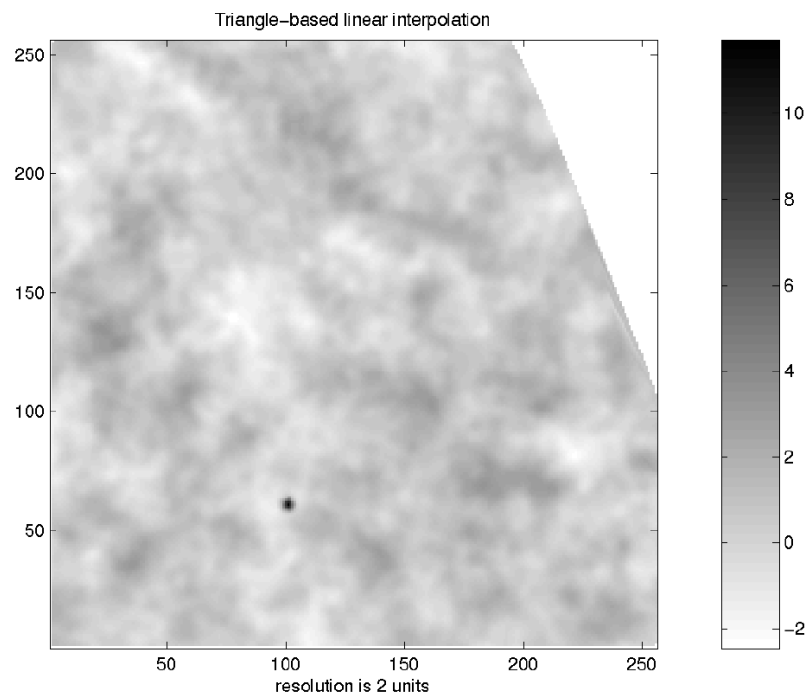

Figure 6.12: Linear interpolation, x and y vary between 0 and 511, pixel size is 2 units.
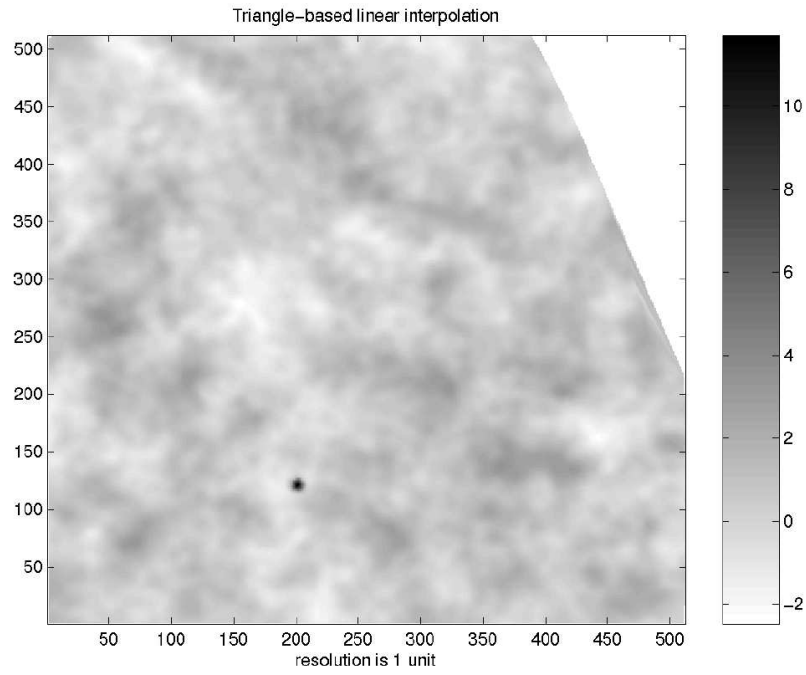
Figure 6.13: Linear interpolation, x and y vary between 0 and 511, pixel size is 1 unit.
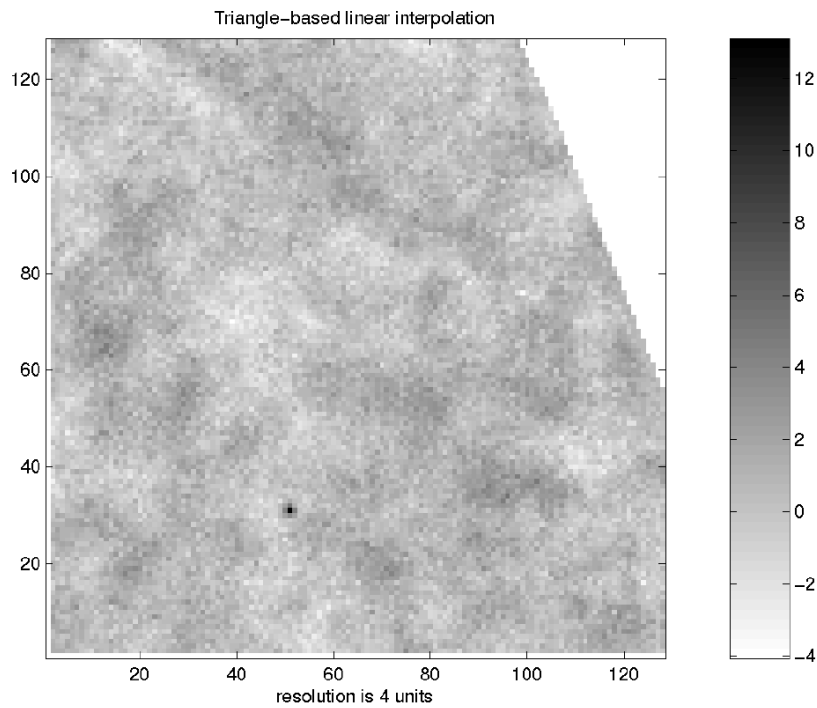

Figure 6.14: Triangle-based interpolation on the noisy data, x and y vary between 0 and 511, pixel size is 4 units.

6.2.3 Kriging

Most of the research on the nature of the CMB anisotropies characterizes them as a stationary random process of the second order. So the assumptions for kriging are well verified for the CMB data. For the calculation of the experimental variogram and for the implementation of the ordinary kriging we use the software developed in the TSI department of ENST.

Before using kriging it is necessary to determine the three parameters of the variogram. So the experimental variograms are calculated first. Figure 6.15 shows first halves of the experimental variograms, for the simulated data divided on 4 parts.
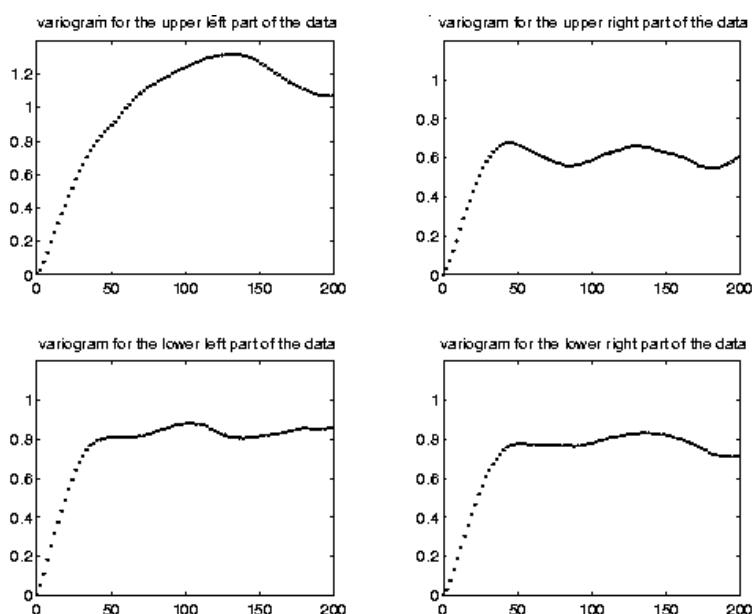

Figure 6.15: First halves of the experimental variograms for the simulated data without noise.

The lower left part of the data contains the large point source. From Figure 6.15 we can see that this point source doesn't change the statistics of the area considerably. The kriging interpolation will be performed on neighborhoods. It means that for calculating a value at a regular grid point, only the neighboring data points will be considered, and not all the data points. It will speed up the calculations and make them more precise in the presence of large point sources. In the case of kriging on a neighborhood, only the beginning of the variogram curve is of interest, because this part of curve describes the statistics for the points that are close to each other, i.e. the points in a neighborhood. The spherical model of the variogram is chosen. The parameters, deduced from the experimental curves are: range is 45, nugget is 0 and sill is 0.81. Figure 6.16 shows the experimental variogram and the fitted theoretical one.

The size of the neighborhood is taken to be 10 by 10 units, because it allows having several data points around each regular grid point, even in the areas with low density of sampling.

solid line – spherical theoretical variogram, points – experimental variogram values

range is 45, nugget is zero, sill is 0.81
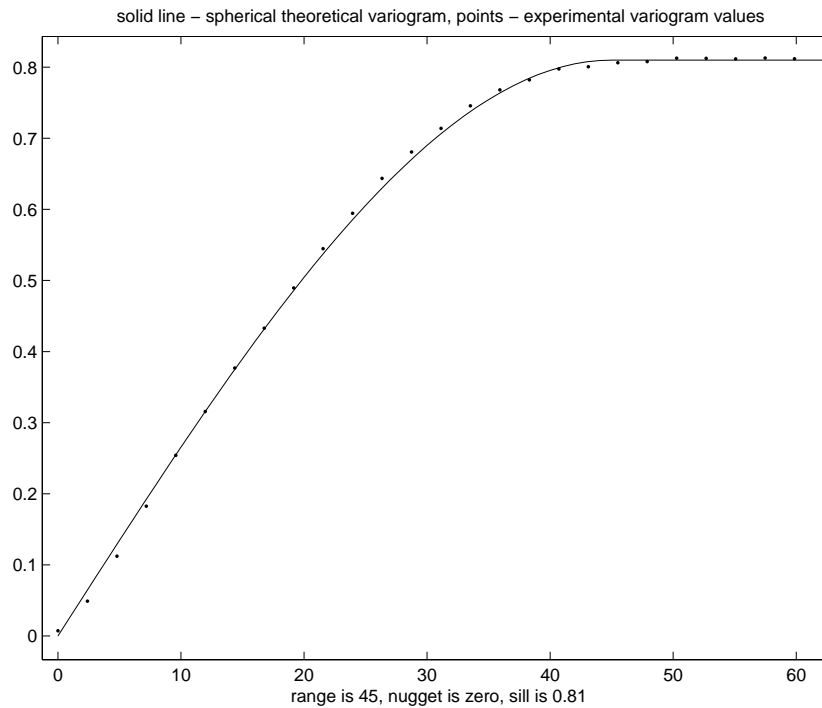
Figure 6.16: Experimental (points) and theoretical (solid line) spherical variograms.

In average there are around 17 measurements in each block that is defined by the neighborhood. It means that the matrix to inverse will have in general $18 * 18 = 324$ elements. The highest density of the considered data will lead to having 133 points in the neighborhood 10×10 units. Then the matrix to inverse will have 17956 elements.

Kriging results on the data without noise are in Figures 6.17 - 6.22.

For the noisy data the variogram will not be the same. Noise will make the value of nugget to be above zero (Figure 6.23). And it will lead to approximation of the data rather than interpolation. The variations lower than the nugget value can be neglected by the kriging algorithm as they will be considered as noise. The parameters chosen for the theoretical variogram for the noisy data are: range is 43, nugget is 1, sill is 1.8 (Figure 6.24).

The resulting images are in Figures 6.25 - 6.27.

For all the experiments ordinary kriging is used. From the kriging results on the noisy data it is evident that the algorithm suppresses noise. But from the colorbars on the right parts of the images one can see that the range of the values is no longer the same. The largest value for the data without noise was about 12, and the largest value for the noisy data after kriging is approximately 6. But it mainly concerns the large point source.
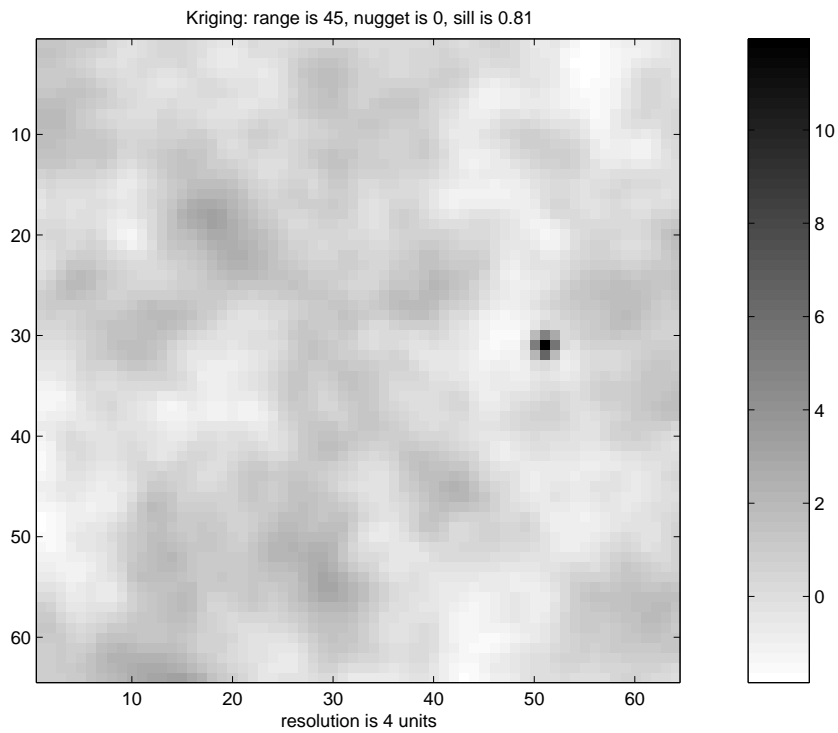
Figure 6.17: Kriging without noise, x and y vary between 0 and 255, pixel size is 4 units.
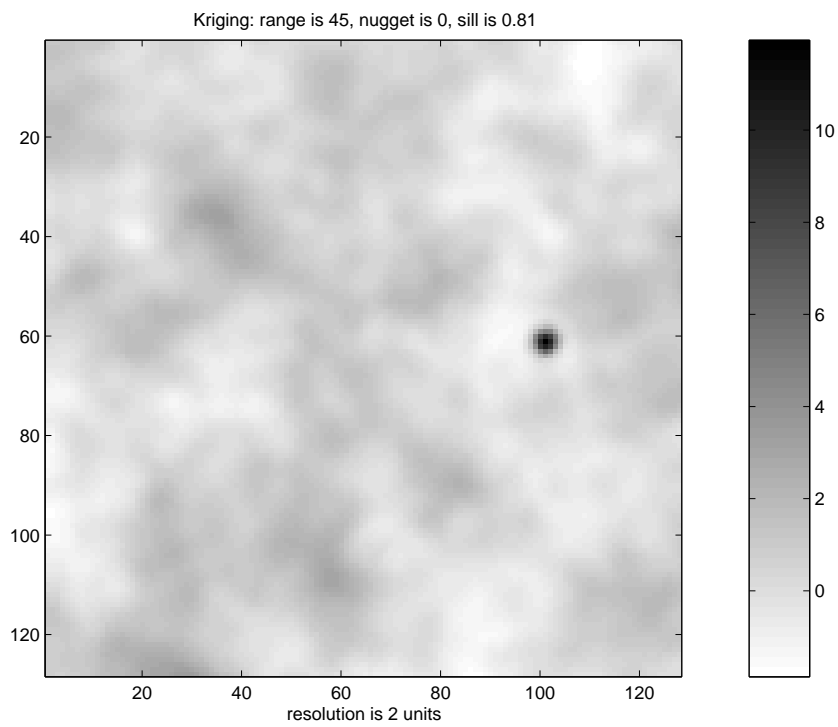
Figure 6.18: Kriging without noise, x and y vary between 0 and 255, pixel size is 2 units.
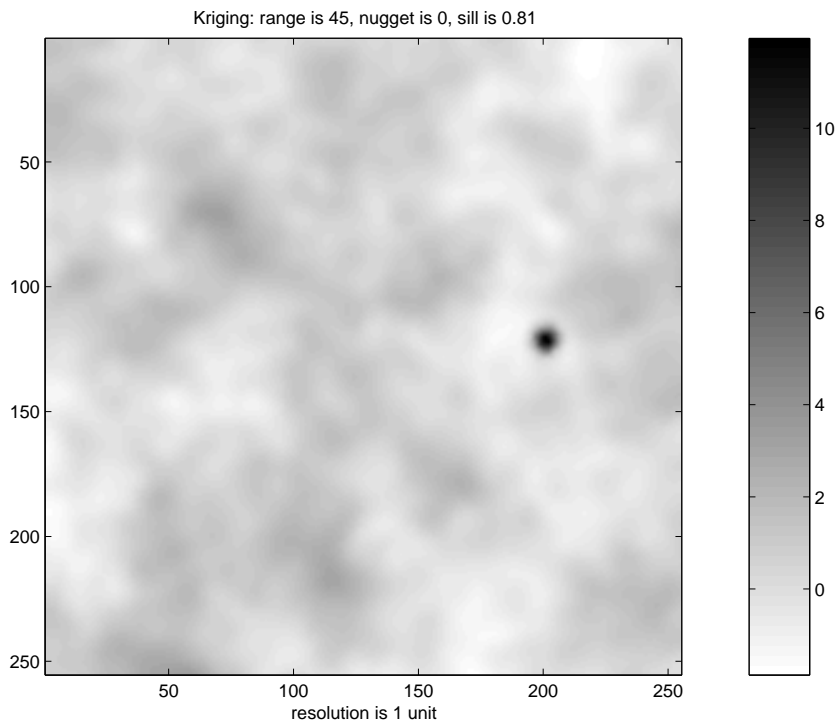
Figure 6.19: Kriging without noise, x and y vary between 0 and 255, pixel size is 1 unit.
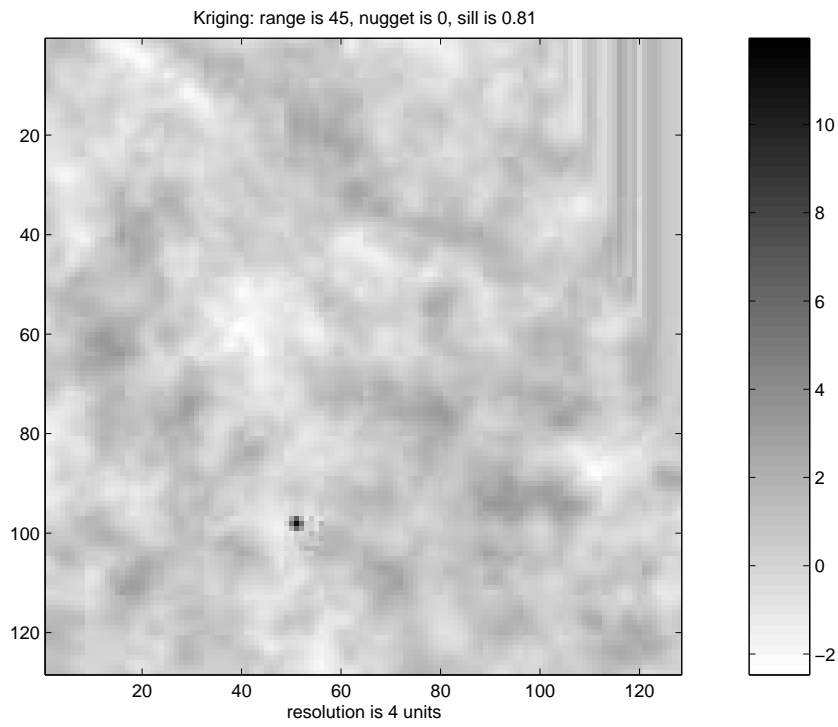
Figure 6.20: Kriging without noise, x and y vary between 0 and 511, pixel size is 4 units.
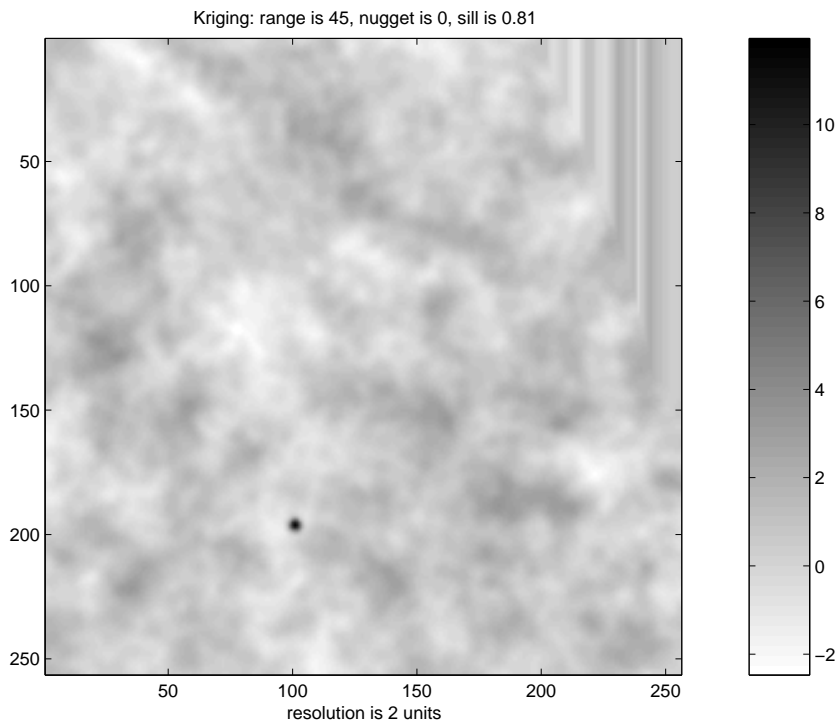
Figure 6.21: Kriging without noise, x and y vary between 0 and 511, pixel size is 2 units.
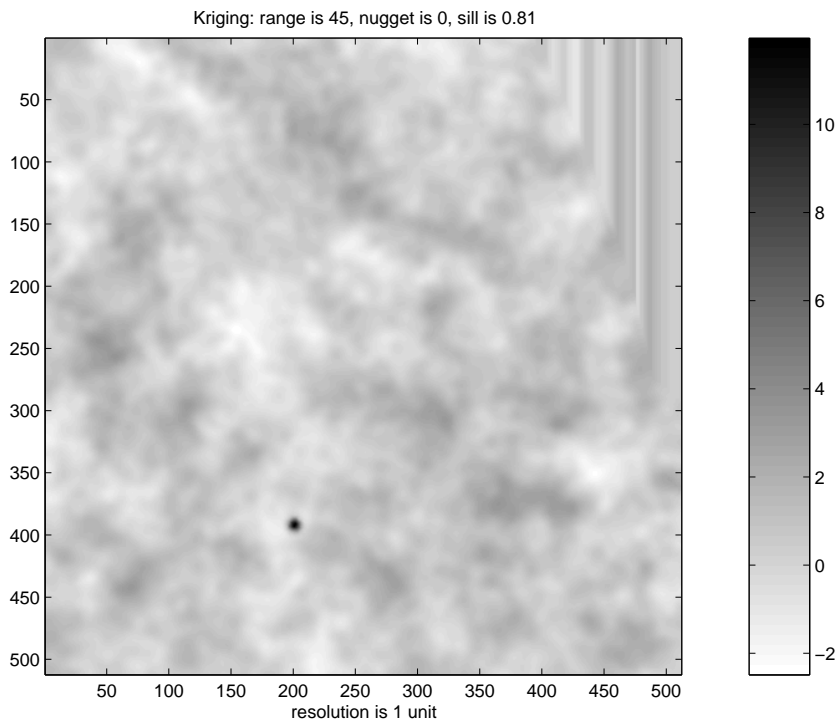
Figure 6.22: Kriging without noise, x and y vary between 0 and 511, pixel size is 1 unit.
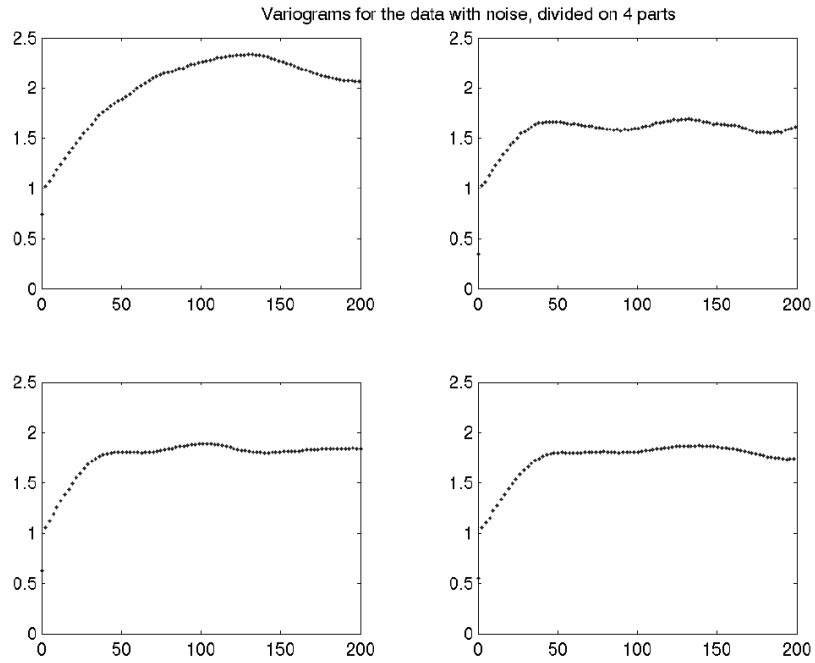
Figure 6.23: First halves of the experimental variograms for the simulated data with noise.
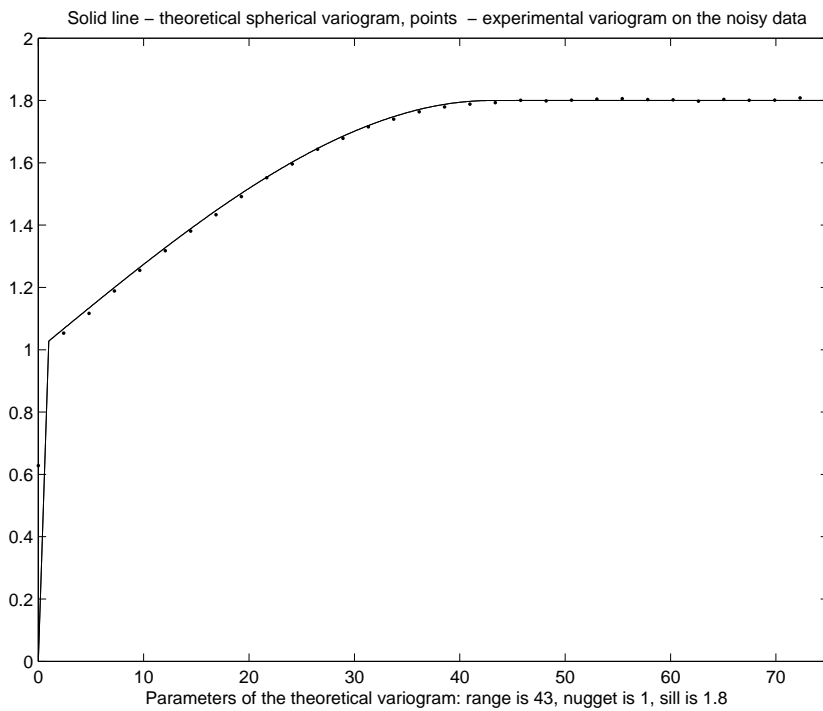
Figure 6.24: Experimental (points) and theoretical (solid line) spherical variograms.
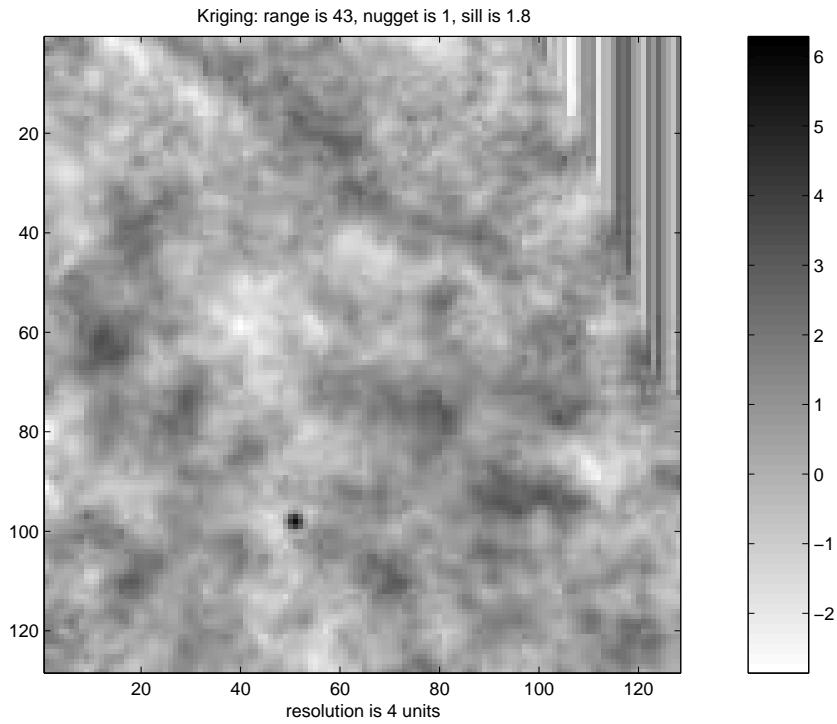
Figure 6.25: Kriging on the noisy data, x and y vary between 0 and 511, pixel size is 4 units.
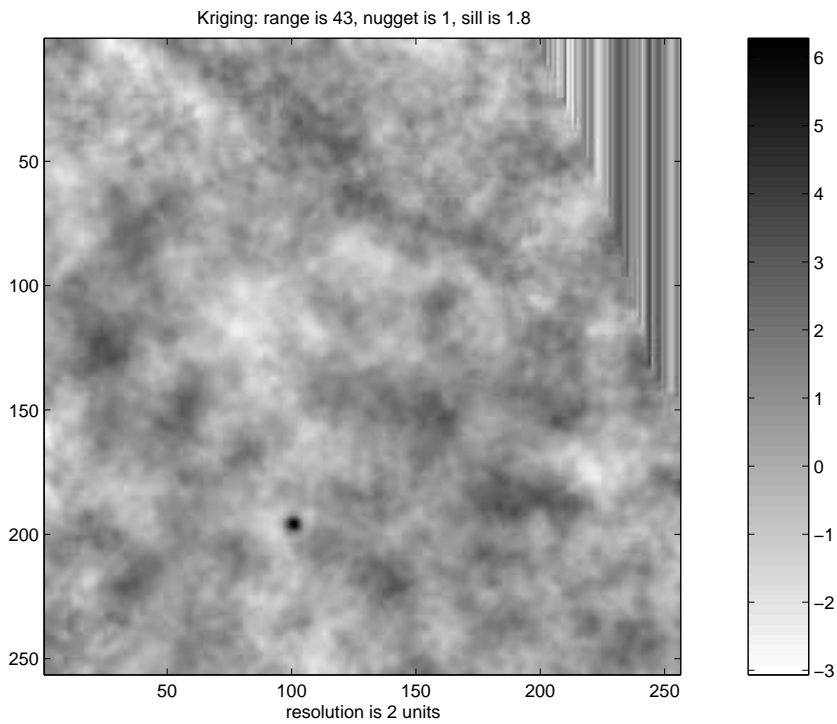
Figure 6.26: Kriging on the noisy data, x and y vary between 0 and 511, pixel size is 2 units.
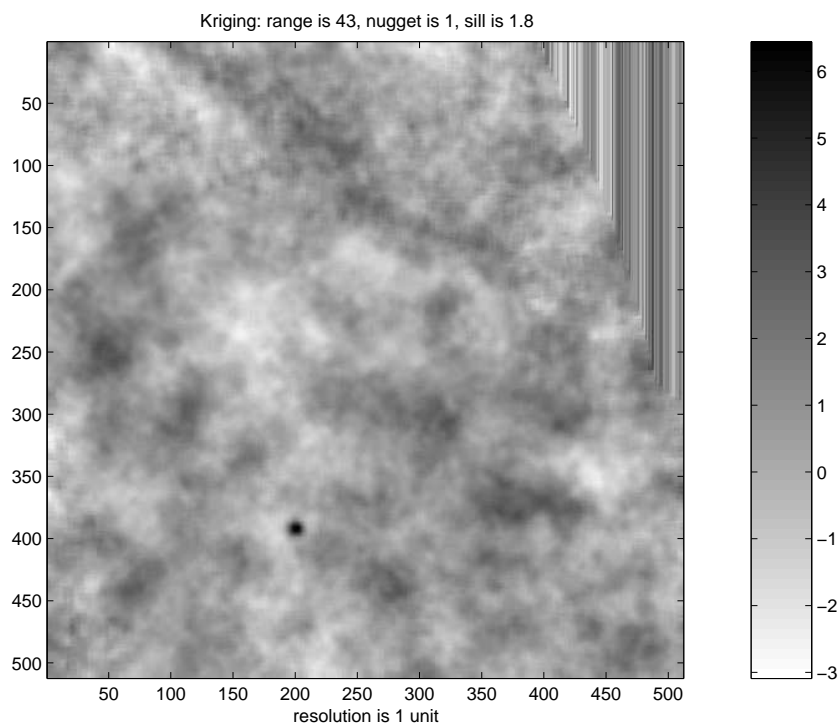
Figure 6.27: Kriging on the noisy data, x and y vary between 0 and 511, pixel size is 1 unit.

6.2.4 Binning

A common and simple approach, that is often used in astronomy, is binning. The method consists of averaging the data values inside each pixel. At first, one should find the data points situated inside the area of a pixel. The pixel takes the average of these points values. If there are no data points inside a pixel, then this pixel stays empty, no value is assigned to it. The higher is the sampling density, the more points will fall inside pixel's area, and the more precise will be the interpolation. Averaging helps to avoid the effects of noise, because it smoothes the surface. Figure 6.28 shows the amount of data points inside pixels of an image with 4 units pixel size.
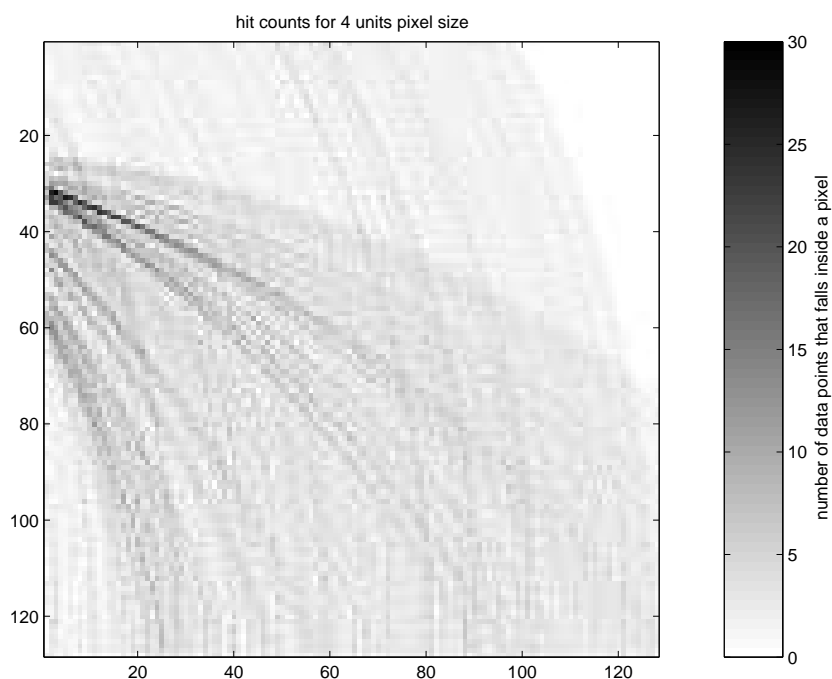
Figure 6.28: Hit counts when the resolution is 4 units.

If the pixel size is taken to be 2 units, then much less points fall inside pixels. And when the pixel size is 1 unit, then more than 80% of the pixels are empty. The pixels that have data points, assigned to them, have just one point. So in this case averaging is not possible. Figures 6.29 and 6.30 show results of binning. This means that binning reduces the image resolution.

The next section is devoted to the comparisons between the reference image and the obtained interpolation results. Since the data is simulated, we can trust the reference and be sure that the calculated errors are only due to the faults of an interpolation method.
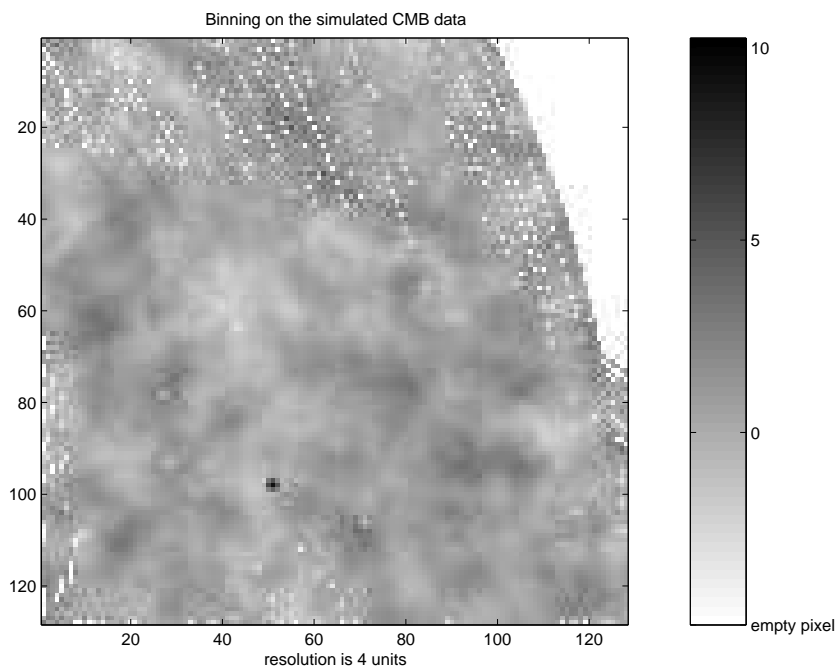
Figure 6.29: Binning, the resolution is 4 units.
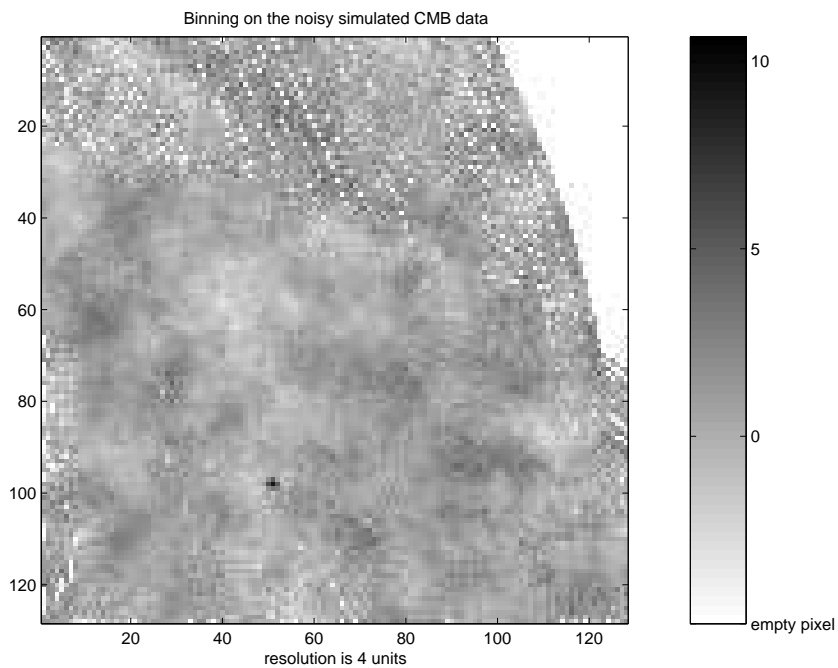
Figure 6.30: Binning on the noisy data, the resolution is 4 units.

6.3 Comparisons with the reference

Figure 6.31 represents the reference provided for the simulated data. The root mean

Reference image (sky map convolved with the sensor impulse response)
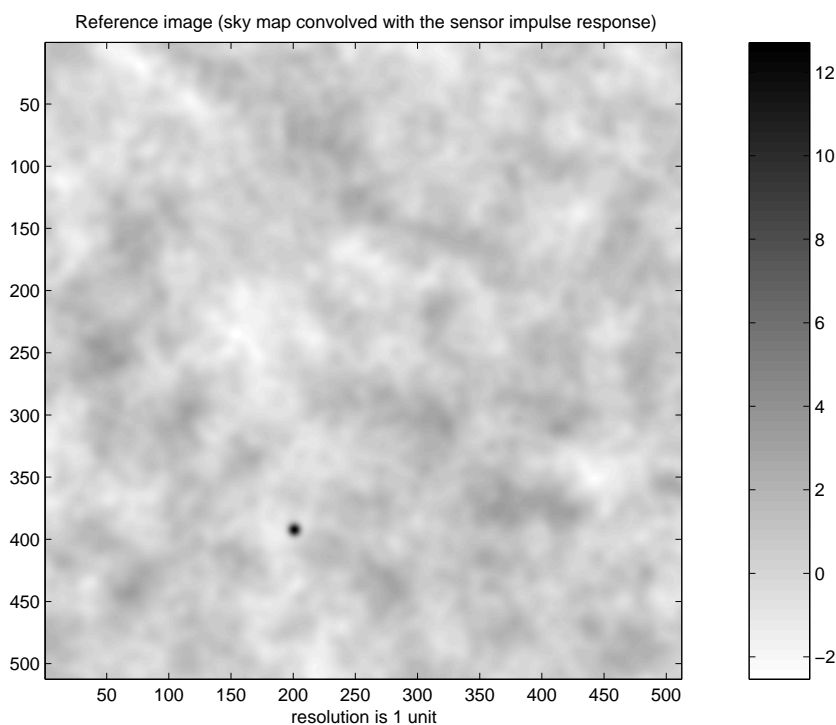
Figure 6.31: Reference for the simulated data.

square errors (RMSE) between the reference and interpolation results are in Tables 6.1 - 6.3.

Interpolation method	Resolution		
	1 unit	2 units	4 units
Binning	1.2809	0.0804	0.0903
Nearest neighbour	0.1103	0.1086	0.0968
Linear	0.0475	0.0445	0.0428
Kriging	0.0314	0.0310	0.0344

Table 6.1: RMSE between the reference and the results without noise when x and y coordinates vary between 0 and 255.

From the RMSE values it is obvious that kriging gives better results than the other three interpolation methods, but linear interpolation also gives good results when noise is low. It is true for the noisy data as well as for the data without noise. The performance of binning becomes better if the size of the pixel increases, when one treats the data with noise. It happens because the larger is pixel, the more data points will fall inside it. Then the averaging is done on more samples, and it suppresses

Interpolation method	Resolution		
	1 unit	2 units	4 units
Binning	1.2749	0.0682	0.0732
Nearest neighbour	0.0966	0.0958	0.0926
Linear	0.0586	0.0570	0.0573
Kriging	0.0323	0.0315	0.0320

Table 6.2: RMSE between the reference and the results when x and y coordinates vary between 0 and 512.

Interpolation method	Resolution		
	1 unit	2 units	4 units
Binning	0.9836	0.9238	0.6827
Nearest neighbour	1.0110	1.0112	1.0048
Linear	0.7152	0.7146	0.7085
Kriging	0.2930	0.2928	0.2900

Table 6.3: RMSE between the reference and the results on the noisy data, x and y coordinates vary between 0 and 512.

the noise, because of the gaussian probability of noise, averaging provides an optimal filtering. It is possible that binning gives quite good results when the pixel size is larger. For example, considering the interpolation results for the data with noise, we can see that the best result according to the RMSE error is produced by kriging. The RMSE in this case is equal to 0.2900 when the regular grid size is 4 units. The same value of the RMSE is obtained for binning when the regular grid size is 13 units. It means that if the pixels are more than three times larger, then we can get the comparable quality of binning. However, in this case it is certain to destroy large point sources and small scale fluctuations in the data. Kriging has an advantage over binning, because of using weighted average of the data and because the weights depend on the data statistics. Figure 6.32 is the comparison between the reference, kriging and linear interpolation results on the data with noise.

Figures 6.33 and 6.34 show the search for the optimal size of the neighborhood for kriging. It is done in order to check whether the choice made previously was correct. The neighborhood is a square, the length of the side was taken to be 10 units. The criterion for this choice was to have approximately 8 neighbors, desirably in different directions, for each regular grid point. We can see that is a valid choice when the data has no noise. However, considering the noisy data, it is better to enlarge the neighborhood to suppress the effect of noise. The larger is the neighborhood, the more time it takes to perform kriging, especially on high sampling density areas.

The quality of binning results obviously depends on the density of data points per regular grid pixel. The Figures 6.35 and 6.36 demonstrate it. In both cases - with and without noise - we can see that averaging on 10 or more pixels often leads to the smaller errors than the ones of kriging. So binning can outperform kriging only when
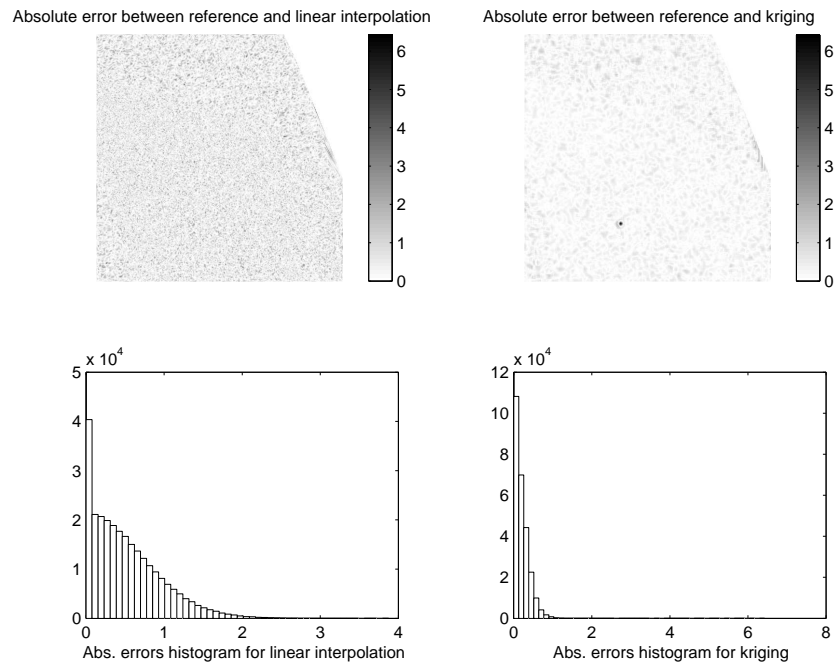
Figure 6.32: Absolute errors and their histograms for linear interpolation (left column of images) and kriging (right) on the data with noise; resolution is 1 unit.
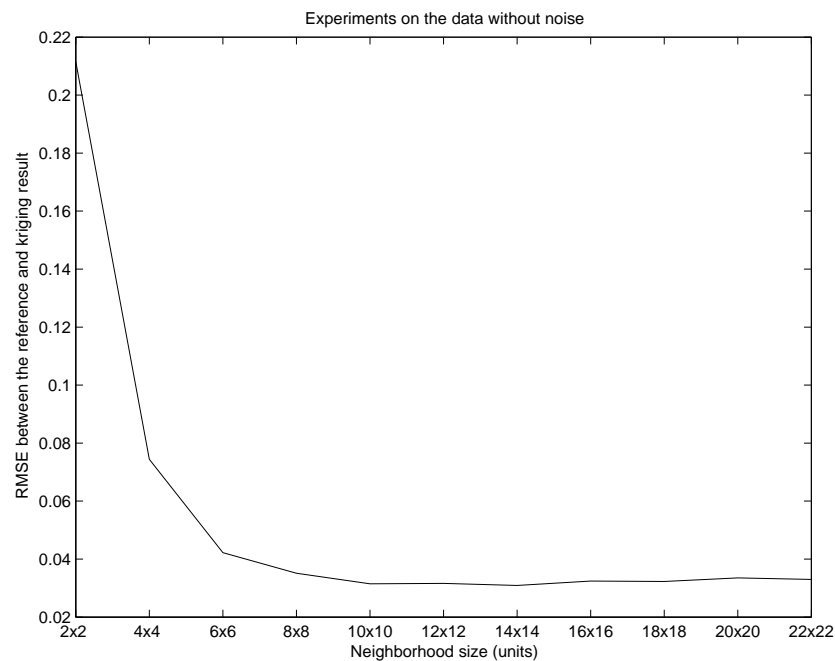
Figure 6.33: Search for the optimal neighborhood size for kriging; the data is without noise. The 10×10 window size is sufficient for an excellent reconstruction.
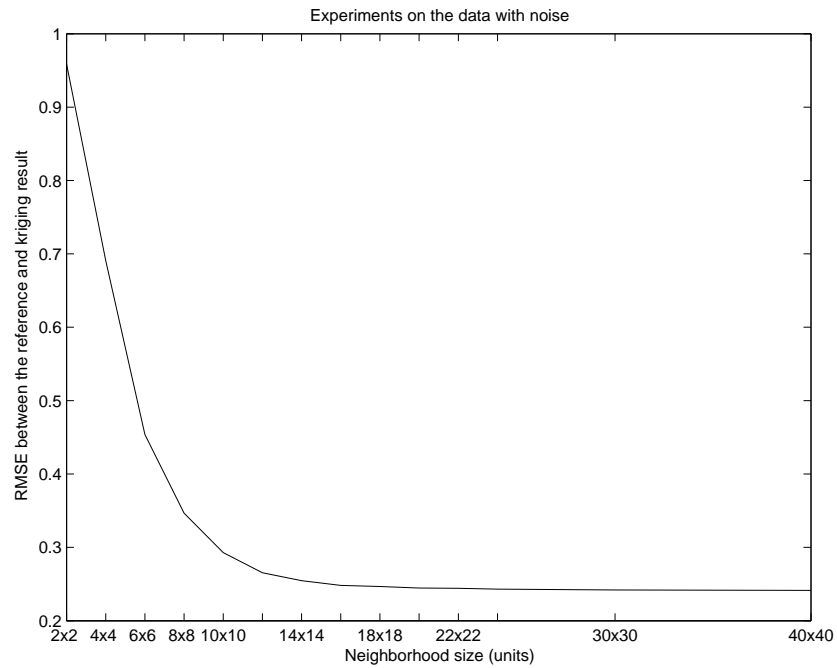
Figure 6.34: Search for the optimal neighborhood size for kriging; the data is with noise. The 10×10 window size is not sufficient for an optimal reconstruction.
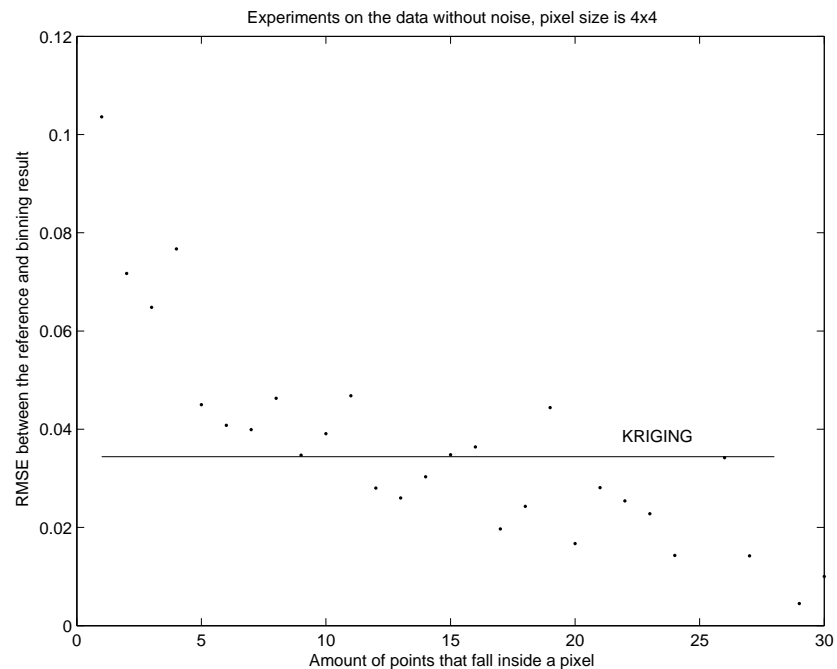
Figure 6.35: Hit counts versus RMSE for binning interpolation. The horizontal line represents the RMSE value for kriging (with 10×10 window size) with the same pixel size on the same data.
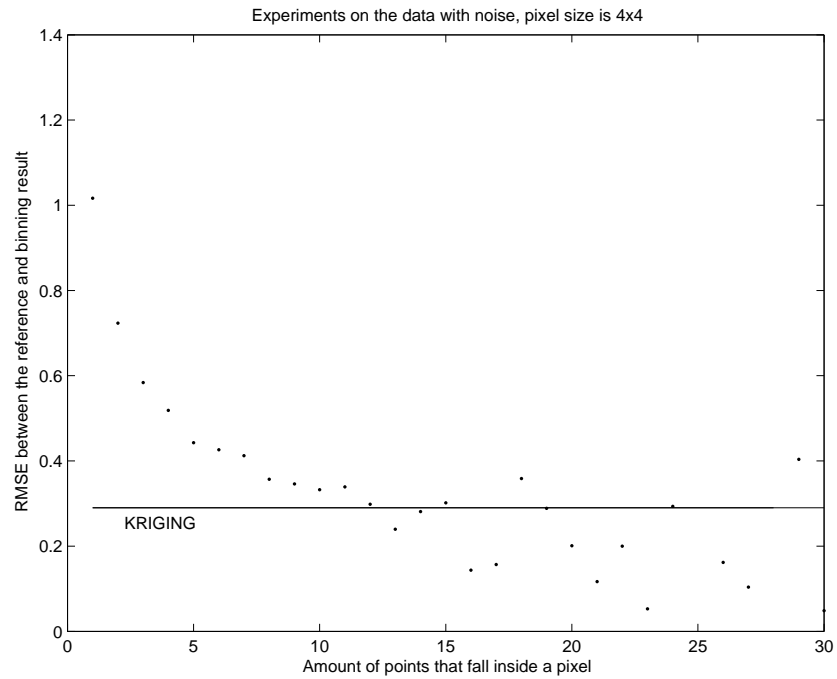
Figure 6.36: Hit counts versus RMSE for binning interpolation for the data with noise. The horizontal line represents the RMSE value for kriging with the same pixel size on the same data.

the density of points is quite high.

The application of the energy minimization technique to the simulated CMB data interpolation is illustrated in the next section.

6.4 Energy minimization

The considered data has been obtained by adding point sources to the simulation of CMB anisotropies and by smoothing the result by the convolution with an expected impulse response of the sensor. It means that the surface, obtained in this way, doesn't have discontinuities. So the result of the interpolation of such data should lead to a smooth result, as long as deconvolution is not done. That is why we take the energy function to minimize the square differences:

$$F(u) = \sum_{i,j} \left(\sum_{K(i,j)} \psi \left(\frac{z(x_k, y_k) - u(i,j)}{\text{dist}((x_k, y_k), (i,j))} \right) + \alpha \sum_{M(i,j)} \varphi \left(\frac{u(i', j') - u(i,j)}{\text{dist}((i', j'), (i,j))} \right) \right),$$

where $\psi(t) = \varphi(t) = t^2$. This cost function is Tikhonov regularization and it has been successfully applied to the CMB maps [Vio et al., 2003]. Though in [Vio et al., 2003] the regularization is used for CMB maps deconvolution, the initial data is considered on a regular grid.

We applied energy minimization method for the simulated CMB data with noise, when the pixel size is 4 units. The surface to find is initialized with the results of the linear interpolation, though it is of no importance, because the both potential functions are convex. It means that there is the only one global minimum that will be reached with the ICM optimization method as well as with any gradient based approach. Changing the α coefficient for the regularization term and comparing the obtained images with the reference, we get the plot in Figure 6.37.

The results (Figure 6.37) show that the method outperforms binning, linear and nearest neighbor interpolation, but cannot eliminate the noise as well as kriging does: the RMSE for kriging is about 0.29 on the same area. Figure 6.38 shows the comparison for the kriging and energy minimization images.

We can see that the energy minimization method gives the results that are worse than kriging. So kriging is the method that deserves more analysis and investigation as it is done in the next section.
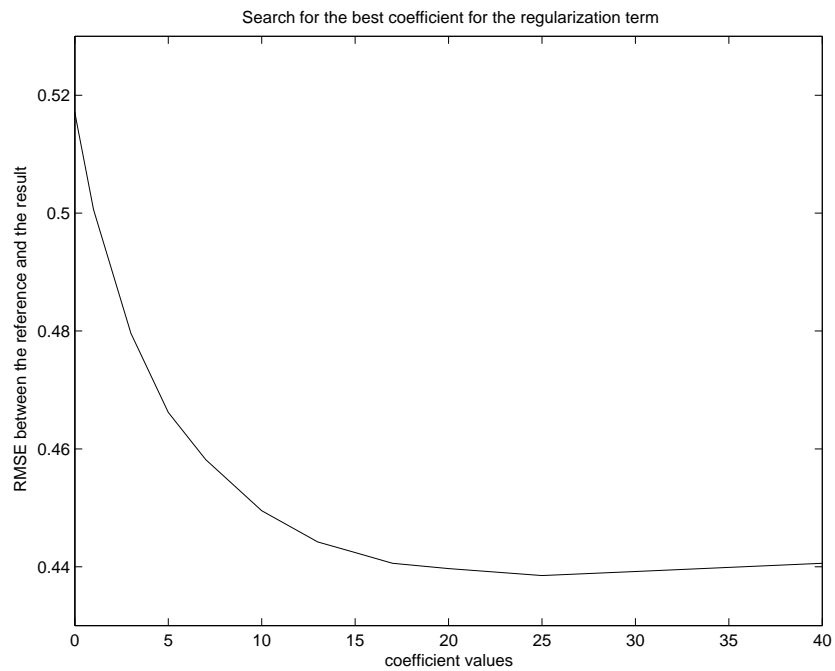
Figure 6.37: Search for an optimal regularization term coefficient α for the noisy CMB data interpolation.
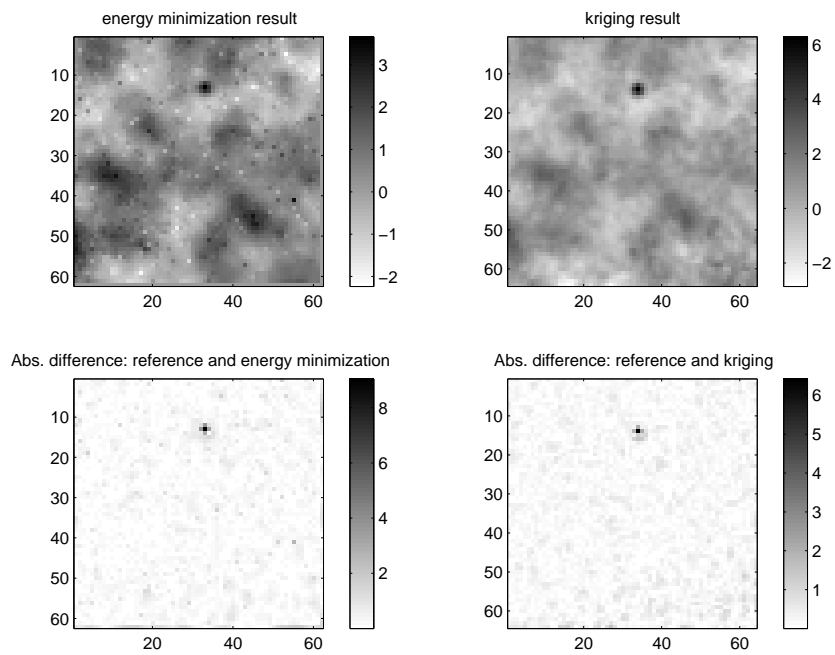

Figure 6.38: Right column: energy minimization. Left column: kriging. Pixel size is 4 units.

6.5 Kriging versus binning: performance analysis

From the previous results it is obvious that kriging outperforms several other methods that we tried. The reference method - binning - works worse especially in the cases of small grid sizes, i.e. high resolution. Though we considered the simulated data with and without noise, now we would like to limit our interest on the case of the noisy data. The main reason for it is that the data with noise corresponds much more to the real measurements. In the same time the random noise that we add to our data is Gaussian, and probably can be considered as a very simple model of noise. For the real data the noise will have a systematic component and it can make it more difficult to deal with.

From the experiments presented above we can see that when there is no noise in the data, then kriging or linear interpolation is a good choice. Linear interpolation is a bit worse than kriging according to the RMSE error, but it is much easier and faster method.

As for the noisy data interpolation, kriging is the best, but binning can improve its performance if the size of the pixel is enlarged. The goal of performance analysis between binning and kriging is the detailed study if these methods applied to the simulated CMB data. This study takes into account two parameters: the level of noise and the size of the pixel. We take the white noise with zero mean and we use five different values for the standard deviation: 0.2; 0.4; 0.6; 0.8; 1. When the standard deviation of noise is 1, it is the case for the Archeops acquisition system. We also vary the pixel size in order to see how it influences the interpolation results.

The parameters of the theoretical spherical variograms are found by analysing the experimental values of variograms. The theoretical variograms plotted versus experimental ones are shown in Figures 6.39 - 6.42, 6.24.

In general, the parameters of the theoretical variogram are easy to predict in the case of simulated data. The value of range does not depend on the noise considerably. The value of nugget is approximately the variance of the noise, so one has to square the standard deviation to obtain it. The value of sill will change according to the nugget effect. Kriging is performed on neighborhoods, each neighborhood is a block 10×10 units. That is why the theoretical variogram is adjusted only for the first half of the experimental one: the points which are far apart will not be taken into account while performing kriging.

Figures 6.43 - 6.47 demonstrate the RMSE measured between the reference and kriging or binning interpolation results for different sizes of the pixel. Solid line represent kriging, dashed - binning.

It is easy to see that the larger is the size of pixel, the better is the binning result. The important advantage of kriging is that its performance does not depend on the choice of the resolution for the image. The stronger is the noise, the larger pixel size is needed in order to get binning results as good as the ones of kriging. In fact, binning reaches kriging only in the case of very large pixels. The resolution should drastically degrade before these both methods perform equally good. This degradation of the resolution depends on the standard deviation of noise. But even for the case with
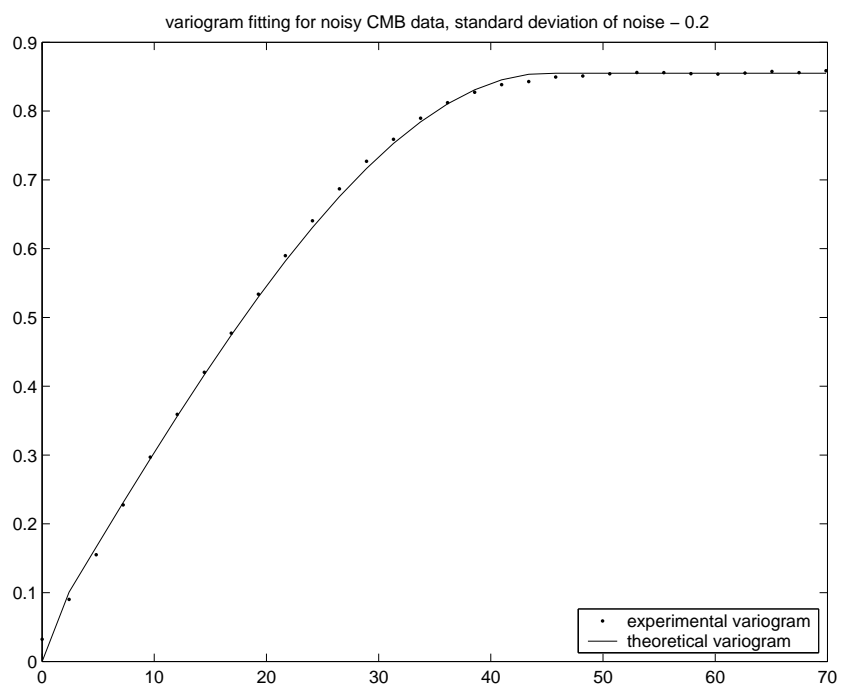
Figure 6.39: Fitting the theoretical spherical variogram: dotted line - experimental variogram, solid line - theoretical variogram. The standard deviation of noise is 0.2. Theoretical variogram is built with the following parameters: range is 45, nugget is 0.035, sill is 0.85.
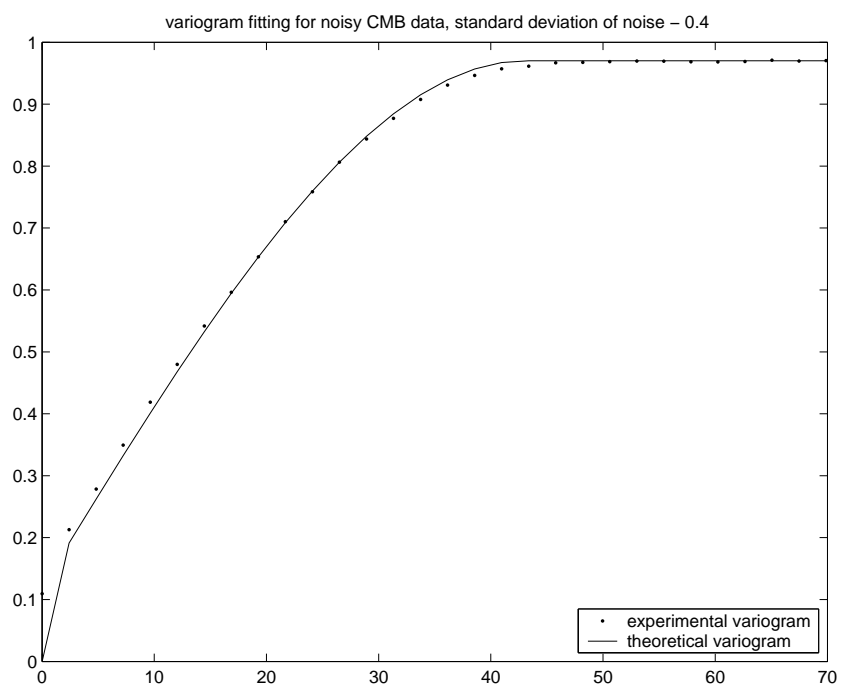
Figure 6.40: Fitting the theoretical spherical variogram: dotted line - experimental variogram, solid line - theoretical variogram. The standard deviation of noise is 0.4. Theoretical variogram is built with the following parameters: range is 43, nugget is 0.12, sill is 0.97.
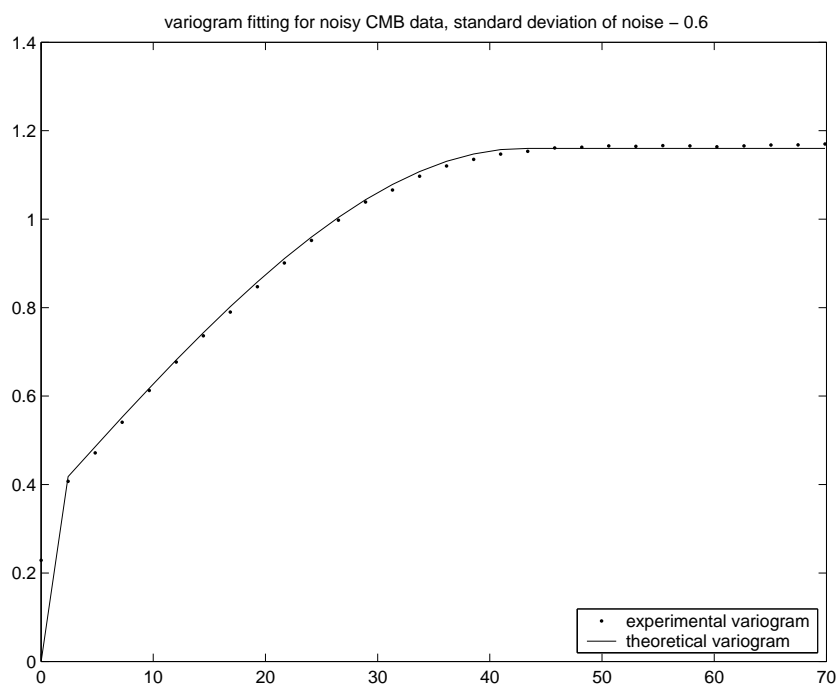
Figure 6.41: Fitting the theoretical spherical variogram: dotted line - experimental variogram, solid line - theoretical variogram. The standard deviation of noise is 0.6. Theoretical variogram is built with the following parameters: range is 43, nugget is 0.35, sill is 1.16.
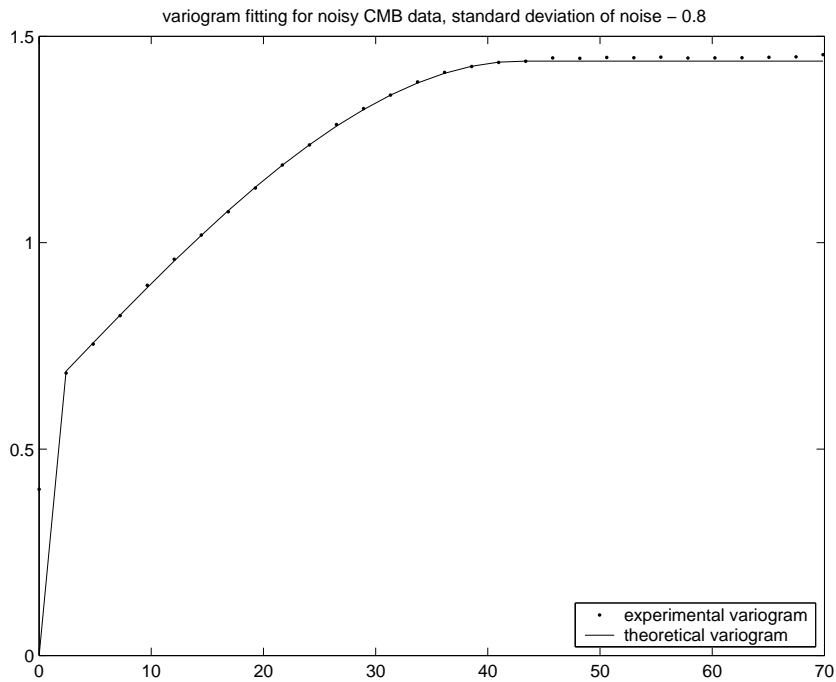
Figure 6.42: Fitting the theoretical spherical variogram: dotted line - experimental variogram, solid line - theoretical variogram. The standard deviation of noise is 0.8. Theoretical variogram is built with the following parameters: range is 43, nugget is 0.62, sill is 1.44.
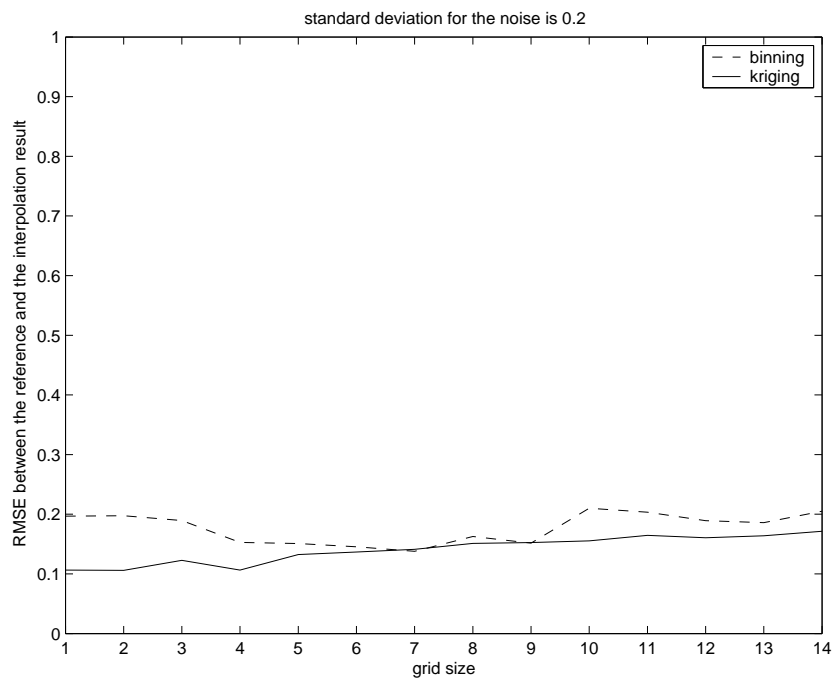
Figure 6.43: Kriging versus binning performance, standard deviation of noise is 0.2.
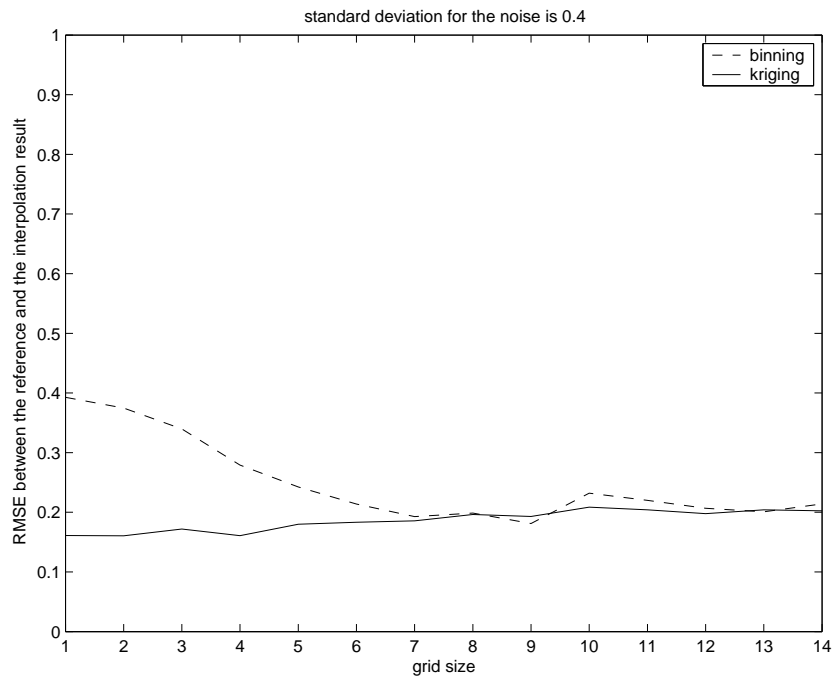
Figure 6.44: Kriging versus binning performance, standard deviation of noise is 0.4.
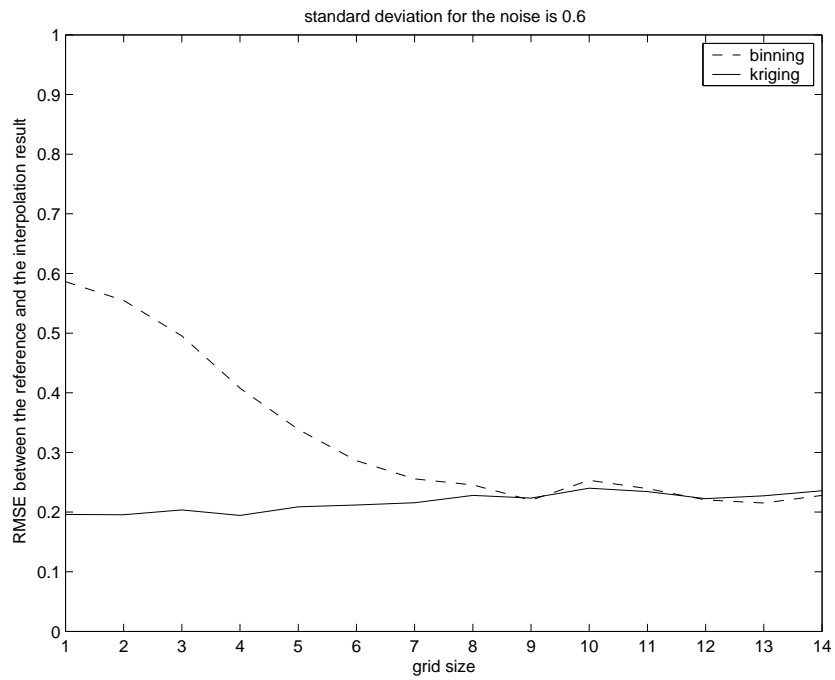
Figure 6.45: Kriging versus binning performance, standard deviation of noise is 0.6.
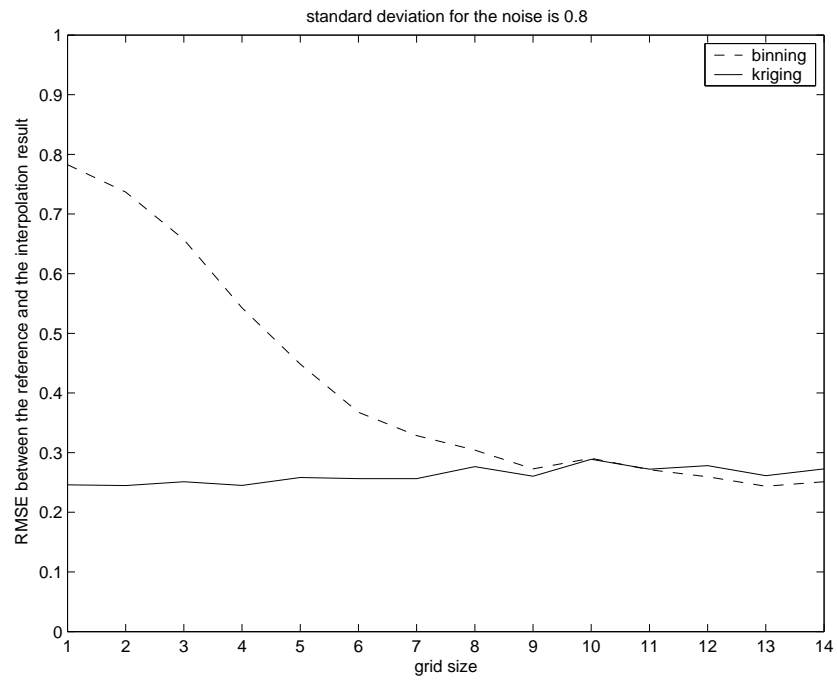
Figure 6.46: Kriging versus binning performance, standard deviation of noise is 0.8.
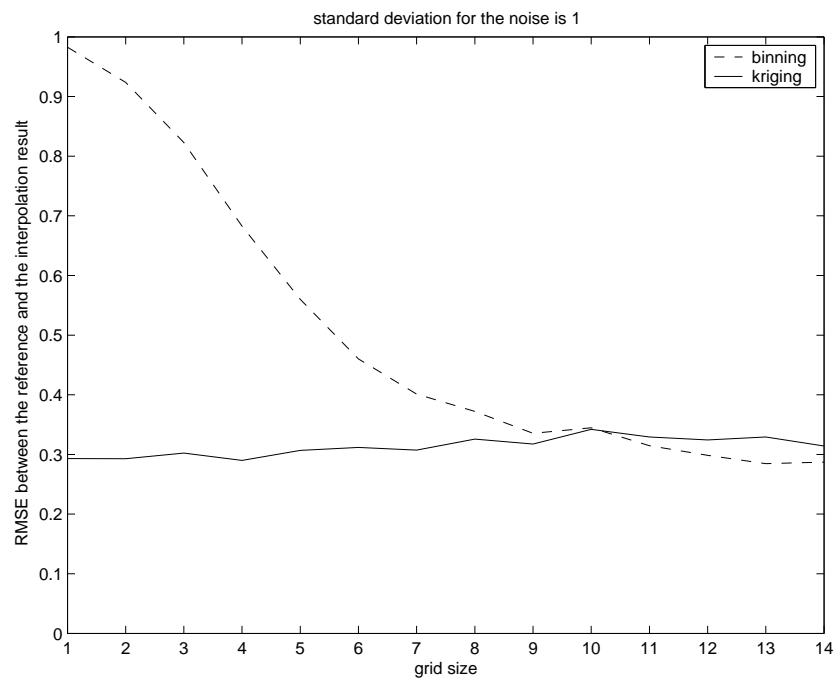
Figure 6.47: Kriging versus binning performance, standard deviation of noise is 1.

158

quite a small standard deviation of noise the size of the grid should be at least 7 units, then binning is as good as kriging. And the grid size is 10 units when both methods start having the same performance in the presence of strong noise.

From the practical point of view, the size of the grid equal to 7 or to 10 is much too coarse. If one wants to have the size of the grid the same as the average density of the original scattered CMB data, then it should be approximately 3 units.

6.6 Conclusion

Several methods can be used for the interpolation of the CMB anisotropies. These measurements are irregularly distributed 3D points. In practice, they are affected by noise and by other radiation sources. We have considered the simulated data, composed by the CMB anisotropies and point sources. Two cases are taken: with and without noise.

Four interpolation methods are tried on the data without noise. These methods are: binning, nearest neighbor interpolation, linear interpolation and kriging. At first, these methods were used on an area where the sampling density is relatively constant and high. At second, the whole data was considered, in this case the density of points varies considerably from one part of the data to another. As a conclusion, it can be noticed that the performance of the methods doesn't depend on the points density changes: kriging outperforms the other three approaches in the both cases. Obviously, the quality of the results is better when the density of points is higher. Apart from kriging, linear interpolation also gives good results. The advantage of kriging is the good results it provides. The disadvantage is that this method needs the preliminary treatment of the data in order to get the parameters of the variogram. Linear interpolation can be faster and simpler but it will be less precise. The nearest neighbor interpolation and binning give worse results than kriging and linear interpolation. For the experiments described above, the pixel size is taken to be 1, 2 and 4 pixels. When the pixel size is larger, binning is expected to give better results, especially it is valid for the noisy data.

For the data with noise we tried the four methods described above and also the cost function minimization for the data interpolation. Adding the noise made the problem more complicated, especially because the range of the noise is almost as large as the range of the data. In this case an interpolation technique should be able to decrease the effect of noise as much as possible. The best results are obtained with the kriging technique, because it allows take the noise into account through the parameters of the variogram. The satisfactory results are also obtained with the cost function minimization, when it performs Tikhonov regularization while interpolating the data. Since the sensor impulse response is considered to be known, this cost function can be adapted for the deconvolution. The disadvantage of the cost function minimization is the use of the coefficient for the regularization term. The change of this coefficient will change the results. For the CMB data it is crucial, because the interpolation is only a intermediate step in the data processing. The resulting CMB maps are used for power spectra estimation and other calculations, for which the precision is important.

After completing the experiments mentioned above, we noticed that good results can be obtained with kriging. The advantage of kriging over energy minimization is that the parameters for kriging are obtained by the analysis of the experimental variogram, that is obtained from the original data, while the coefficient for the regularization term in the energy expression is the parameter to tune. Taking binning as the reference method often used in astronomy for interpolation, we make a detailed comparison between this method and kriging. We find that these two methods can

be equally good when the regular grid size of the image to find is very coarse. Otherwise, for acceptable grid sizes kriging outperforms binning, especially in the presence of noise. The modelling of noise is necessary since it will be present in the real measurements.

Conclusions

Many theoretical and applied problems deal with interpolation and resampling of irregularly spaced 3D data. In the framework of the thesis we consider some theoretical and practical issues for two applications in the remote sensing domain:

- airborne laser data interpolation over urban areas;

- determination of the CMB (cosmic microwave background).

Theoretical aspects of irregularly spaced data resampling are the subject of current research. The basics for the theory is developed in the theorems of Shannon and Papoulis. Most of the theoretical works as well as interpolation methods are for bandwidth-limited signals and images.

Before interpolating the data, we have studied their acquisition techniques, accuracies and properties. Though the resulting distribution of points on XY plane is not much different for laser data and CMB anisotropies measurements, the acquisition techniques differ a lot.

It is considered that the laser data has a good accuracy and practically no noise. On the contrary, the CMB data is very much affected by noise and foreground radiations. Also, CMB data is a result of convolution of the sky map with the sensor impulse response.

The expected properties of the surface to reconstruct should be taken into consideration as well as the acquisition techniques. For the airborne laser data interpolation, we consider the problem to be ill-posed, and we adapt a cost function for the irregularly spaced data. Since the edges of the buildings in urban areas form strong discontinuities, we use edge preserving potential functions. Minimization of such a cost function leads to the sought surface. The results of this approach were compared to some well-known methods for irregularly spaced data interpolation, namely linear interpolation, nearest neighbor interpolation and kriging. These methods were outperformed by the cost function minimization, because it imposed the desired properties on the resulting surface. We used correlation and mean absolute error to verify that. The visual quality of the results, preferred by the mean absolute error, is better, while correlation criterion chooses smooth surfaces. The experiments were made on two different real data sets. For these two data sets the scanning strategy and the density of points were different.

Adapting the cost function for the airborne laser data interpolation, we present the choice of the neighborhood, results with different potential functions and we try

different values of coefficients for the regularization term. We have studied excessively the influence of the choice of potential functions on the properties of the reconstructed surface which represents an urban area. We have used the recent theoretical results on the choice of the potential functions for the data-term in the cost function. We propose using a Huber function for the data-term or using just the same function for both data- and regularization terms. For laser data the classical choice of the quadratic function for the data-term will not lead to satisfactory results on urban zones.

Except for the well-known nearest neighbor, linear interpolation methods and kriging, we also try binning method and the cost function minimization for the simulated CMB anisotropies measurements. These measurements are smooth, as long as no deconvolution is made. So in this case Tikhonov regularization was made on the noisy data. Kriging was not applied before to the interpolation of the CMB data and we proved that this method gives good results. Kriging on a fixed neighborhood allows quick performance on large data sets - it is an advantage for the real data interpolation. Though kriging outperforms the cost function minimization, the cost function can be adapted for deconvolution and interpolation in the same time. In this case it is better to use a truncated quadratic function for the regularization term in order to reconstruct the point sources.

Our experience with the several interpolation methods for irregularly spaced data led to the following conclusions:

- nearest neighbor interpolation is suitable as long as the density of the imposed regular grid is lower than the density of the original irregularly spaced data; the data has to have no noise; the advantage of this method is its speed and simplicity;

- triangle-based linear interpolation works well when the density of the grid points is less or equal to the original data density;

- kriging is based on the variogram parameters, that makes it necessary to estimate them before using the method; the parameters estimation is often done manually, though it is possible to make it automatic; unlike the two previous methods, kriging can cope with noise, because the nugget parameter introduces the information about the noise in the algorithm;

- binning is often used in astronomy, it averages the values of the data inside each pixel and so can decrease the noise; the disadvantage is that the density of data points should be at least ten times higher than the density of the regular grid in order to get good results; it is also desirable for binning to have evenly distributed data points;

- cost function minimization has a disadvantage of tuning the coefficient for the regularization term, this parameter depends on the potential functions, when not the same one is used for the data term and the regularization term, and on the choice of neighborhood - more study has to be done about that; the advantages of the method are its flexibility and capacities for interpolating different kinds

of surfaces using different potential functions; in the cost function the gradient values of the data points are not explicitly present, a future work can be on incorporating them in the model.

Making the experiments with the cost function minimization for the airborne laser scanning data, we have learnt the following:

- the values of the coefficient for the regularization term should be equal to 1 or higher to get good results;

- irregularly spaced data points around a regular grid point were initially chosen to be inside the circle that includes the eight nearest regular grid points; the experiments showed that such a neighborhood is a good choice when:

    1) the density of the regular grid points is approximately the density of the data points;

    2) the data points are evenly distributed on the XY plane;

- when one of the two requirements, mentioned above, is not met, then we proposed another definition of the neighborhood - it should include data points from different directions relatively to a current considered regular grid point; this conclusion is made after the experiments with the airborne laser scanning data of Amiens, where the data points form parallel lines, and the density of points along a line is many times higher than across lines;

- the advisable size of the neighborhood should be approximately equal to the distance between the scanning lines, this distance can be calculated even before the data acquisition, taking into account the technical parameters of the laser scanning system and the expected speed of a plane or a helicopter to be used.

Improving the presented results of laser data interpolation is possible in several directions. Considering the cost function minimization technique, the future work can be the following. The definition of the neighborhood can be changed: one can take data points that are neighbors of a regular grid point according to the Voronoi diagram. The first advantage of such a choice is the anisotropy of the chosen data points and the second advantage is that the model will have one parameter less: there is no need to fix the size of the neighborhood, it will change automatically for each location according to the proximity of data points. Another adjustment can be in changing the cost function so that the choice of potential functions will depend on local gradient estimation of the data points. One can also use different potential functions in different directions inside a clique, trying to reinforce the discontinuities of the surface. Another form and size of the cliques may be considered in order to introduce some obvious geometric properties of urban areas, such as straight lines. Apart from the cost function based interpolation, one can consider wavelet functions regarding their use for surface interpolation preserving discontinuities. Another way to try is

to take into account the structure present in many sampling sets and to use methods that profit from this fact. Iterative median filtering is also a good perspective for the future work. It is a simple and fast technique which is known to have the properties of anisotropic diffusion. It will help to preserve discontinuities. The results of linear interpolation on the laser data can be better if the triangulation of Delaunay on the edges of the buildings is improved using stochastic geometry.

As for the CMB data, the indications for future work include the adaptation of the cost function as well as trying some other methods. For the methods, that we tried for the CMB data, it is interesting to study the dependence of their performance from the standard deviation of the additive noise. It concerns the performance of kriging and cost function minimization. Further, the cost function can be adapted for making deconvolution while interpolating the data: the convolution with the impulse response of the sensor should be done for the sought surface used in the data term. Such a modification allows taking into consideration the elliptical shape of the response, which is important for the real CMB anisotropies measurements. The CMB data can be considered as a sum of the smooth surface, representing the CMB anisotropies, and the surface that consists of point sources. Imposing different constraints on each of these two surfaces can improve the results. There are also some reconstruction methods for randomly sampled band-limited signals, they can be applied to the CMB data as well. But in this case the signal should preferably be sampled at the Nyquist rate at average.

The goal of the experiments with CMB data interpolation is to get a method that works for spherical coordinates. The real CMB data is considered to be on the sphere. The methods, presented in the thesis, work on local small patches of the data. In such cases the sphere can be approximated by a plane.

The general conclusion is that we formulated the irregularly spaced data resampling as an ill-posed inverse problem, and we received good results applying the appropriate mathematical model.

Bibliography

[Acar et al., 1994] R. Acar, C. Vogel, "Analysis of bounded variation penalty methods for ill-posed problems", *Inverse Problems*, Vol. 10, No. 6, pp. 1217-1229, 1994.

[Ackermann, 1999] F. Ackermann, "Airborne laser scanning - present status and future expectations", *ISPRS Journal of Photogrammetry and Remote Sensing*, 54, pp. 64-67, 1999.

[Almansa, 2002] A. Almansa, "Échantillonnage, interpolation et détection. Applications en imagerie satellitaire.", *Ph.D. thesis, École Normale Supérieure de Cachan*, 260 pages, 2002.

[Almansa et al., 2001] A. Almansa, S. Jaffard, B. Rougé, "Perturbed sampling in satellite images and reconstruction algorithms", *Proceedings of GRETSI 2001*, 3 pages, 2001.

[Amblard, 2001] A. Amblard, "Archeops: CMB anisotropies measurement from large to small angular scale", *COSMO-01 Workshop, Rovaniemi, Finland*, 9 pages, 2001.

[Axelsson, 1999] P. Axelsson, "Processing of laser scanner data - algorithms and applications", *ISPRS Journal of Photogrammetry and Remote Sensing*, 54, pp. 138-147, 1999.

[Baltsavias, 1999a] E.P. Baltsavias, "Airborne laser scanning: basic relations and formulas", *ISPRS Journal of Photogrammetry and Remote Sensing*, 54, pp. 199-214, 1999.

[Baltsavias, 1999b] E.P. Baltsavias, "A comparison between photogrammetry and laser scanning", *ISPRS Journal of Photogrammetry and Remote Sensing*, 54, pp. 83-94, 1999.

[Baltsavias, 1999c] E.P. Baltsavias, "Airborne laser scanning: existing systems and firms and other resources", *ISPRS Journal of Photogrammetry and Remote Sensing*, 54, pp. 164-198, 1999.

[Barreiro, 2000] R. B. Barreiro, "The cosmic microwave background: state of the art", *New Astronomy Reviews*, Vol. 44, pp. 179-204, 2000.

[Behan, 2000] A. Behan, "On the matching accuracy of rasterised scanning laser altimeter data", *ISPRS Congress 2000*, Amsterdam, Vol. XXXIII, Part B2, pp. 75-82, 2000.

[Bennett et al., 2003] C. L. Bennett, M. Halpern, G. Hinshaw et al., "First Year Wilkinson Microwave Anisotropy Probe (WMAP) Observations: Preliminary Maps and Basic Results", *Astrophysical Journal*, Vol. 148, pp. 1-43, 2003.

[Benoît et al., 2002] A. Benoît, P. Ade, A. Amblard et al., "Archeops: a high resolution, large sky coverage balloon experiment for mapping CMB anisotropies", *Astroparticle Physics*, Vol. 17, pp. 101-124, 2002.

[Benoît et al., 2003] A. Benoît, P. Ade, A. Amblard et al., "Cosmological constraints from Archeops", *Astronomy & Astrophysics*, Vol. 399, pp. L25-L30, 2003.

[Benoît et al., 2003] A. Benoît, P. Ade, A. Amblard et al., "The cosmic microwave background anisotropy power spectrum measured by Archeops", *Astronomy & Astrophysics*, Vol. 399, pp. L19-L23, 2003.

[Billings et al., 2002] S. D. Billings, R. K. Beatson, G. N. Newsam "Interpolation of geophysical data using continuous global surfaces", *Geophysics*, Vol. 67, No. 6, pp. 1810-1822, 2002.

[Blanc-Féraud, 2000] L. Blanc-Féraud, "Sur quelques problèmes inverses en traitement d'image", Habilitation à diriger des recherches, Université de Nice-Sophia Antipolis, France, 2000.

[Blanc-Féraud et al., 1995] L. Blanc-Féraud, P. Charbonnier, G. Aubert, M. Barlaud, "Nonlinear image processing: modeling and fast algorithm for regularization with edge detection", *Proceedings of the International Conference on Image Processing*, Vol. 1, pp. 474-477, 1995.

[Blair et al., 1994] J. B. Blair, D. B. Coyle, J. L. Bufton, D. J. Harding. "Optimization of an Airborne Laser Altimeter for Remote Sensing of Vegetation and Tree Canopies", *Proceedings of IGARSS '94*, Vol. II, pp. 939-941, 1994.

[Bouman et al., 1993] C. Bouman, K. Sauer, "A generalized Gaussian image model for edge-preserving MAP estimation", *IEEE Trans. on Image Processing*, Vol. 2, issue 3, pp. 296-310, 1993.

[Boykov et al., 2001] Y. Boykov, O. Veksler, R. Zabih, "Fast approximate energy minimization via graph cuts", *IEEE transactions on Pattern Analysis and Machine Intelligence (PAMI)*, Vol. 23, No. 11, pp. 1222-1239, 2001.

[Bufton, 1989] J. L. Bufton, "Laser altimetry measurements from aircraft and spacecraft", *Proceedings of the IEEE*, Vol. 77, No. 3, pp. 463-477, 1989.

[Calle, 1999] D. Calle, " Agrandissement d'images par synthèse de similarités et par induction sur un ensemble", Ph.D. thesis, Université Joseph-Fourier - Grenoble I, France, 1999.

[Carter et al., 1997] G. Carter, U. Shankar, "Creating rectangular bathymetry grids for environmental numerical modelling of gravel-bed rivers", *Appl. Math. Modelling*, Vol. 21, pp. 699-708, 1997.

[Cenker et al., 1991] C. Cenker, H. G. Feichtinger, H. Steier. "Fast iterative and non-iterative reconstruction of band-limited functions from irregular sampling values", *International Conference on Acoustics, Speech, and Signal Processing ICASSP-91*, Vol. 3, pp. 1773-1776, 1991.

[Chalmond, 2000] B. Chalmond, "Eléments de modélisation pour l'analyse d'images", *Springer*, 2000.

[Charbonnier, 1994] P. Charbonnier, "Restauration d'image: régularisation avec prise en compte des discontinuités", Ph.D. thesis, Université de Nice-Sophia Antipolis, France, 1994.

[Charbonnier et al., 1997] P. Charbonnier, L. Blanc-Féraud, G. Aubert, M. Barlaud, "Deterministic edge-preserving regularization in computed imaging", *IEEE Trans. on Image Processing*, Vol. 6, No. 2, pp. 298-311, 1997.

[Cheung, 1993] K. F. Cheung, "A multidimensional extension of Papoulis' generalized sampling expansion with the application in minimum density sampling", in R. J. Marks II, editor, *Advanced Topics in Shannon Sampling and Interpolation Theory*, Springer-Verlag, pp. 85-119, 1993.

[Cressie, 1991] N. A. Cressie, "Statistics for spatial data", *A Wiley-Interscience publication*, 1991.

[Daubechies et al., 1999] I. Daubechies, I. Guskov, P. Schröder, and W. Sweldens. "Wavelets on Irregular Point Sets", *Phil. Trans. R. Soc. Lon. A*, Vol. 357, No. 1760, pp. 2397-2413, 1999.

[Delabrouille, 2001] J. Delabrouille, "Issues and methods for CMB anisotropy data reduction", *New Astronomy Reviews*, Vol. 45, pp. 313-320, 2001.

[Delabrouille, 2004] J. Delabrouille, "Measuring CMB polarisation with the Planck mission", *Astrophysics and Space Science*, Vol. 290, pp. 87-103, 2004.

[Delabrouille et al., 2004] J. Delabrouille, P. Filliatre, "An update on Archeops: flights and data products", *Astrophysics and Space Science*, Vol. 290, pp. 119-134, 2004.

[Delabrouille et al., 2002] J. Delabrouille, G. Patanchon and E. Audit, "Separation of instrumental and astrophysical foregrounds for mapping cosmic microwave background anisotropies", *Monthly Notices of the Royal Astronomical Society*, Vol. 330, Issue 4, pp. 807-817, 2002.

[Delabrouille et al., 1998] J. Delabrouille, J.-L. Puget, J.-M. Lamarre and R. Gispert, "Scanning strategies for the Planck mission", *invited talk at the workshop "The Cosmic Microwave Background and the Planck Mission", Santander, Spain*, 7 pages, 1998.

[Dibos et al., 2000] F. Dibos and G. Koepfler, "Global total variation minimization" *SIAM Journal on Numerical Analysis*, Vol. 37, No. 2, pp. 646-664, 2000.

[Feichtinger et al., 1991] H. G. Feichtinger, C. Cenker, M. Herrmann. "Iterative algorithms in irregular sampling: A first comparison of methods", *Conf. ICCCP'91*, Phoenix, AZ, USA, pp. 483-489, 1991.

[Feichtinger et al., 1993] H. G. Feichtinger, K. Gröchenig. "Error Analysis in Regular and Irregular Sampling Theory", *Applicable Analysis*, Vol. 50, pp. 167-189, 1993.

[Feichtinger et al., 1992] H. G. Feichtinger, K. Gröchenig, "Iterative reconstruction of multivariate band-limited functions from irregular sampling values", *SIAM J. Math. Anal.*, Vol. 23, No. 1, pp. 244-261, 1992.

[Feichtinger et al., 1994] H. G. Feichtinger, K. Gröchenig, "Theory and Practice of Irregular Sampling", in Benedetto J. and Frazier M., editors, *Wavelets: Mathematics and Applications*, CRC Press, pp. 305-363, 1994.

[Feichtinger et al., 1995] H. G. Feichtinger, K. Gröchenig, T. Strohmer. "Efficient numerical methods in non-uniform sampling theory", *Numerische Mathematik*, Vol. 69, pp. 423-440, 1995.

[Feichtinger et al., 1994] H. G. Feichtinger, T. Strohmer. "Recovery of missing segments and lines in images", *Digital Image Recovery and Synthesis*, Vol. 33/10 of Optical Engineering, pp. 3283-3289, 1994.

[Ferreira, 1995] P. J. S. G. Ferreira, "Nonuniform sampling of nonbandlimited signals", *IEEE Signal processing letters*, Vol. 2, No. 5, pp. 89-91, 1995.

[Fradkin et al., 1999] M. Fradkin, M. Roux, H. Maître and U. M. Leloglu, "Surface Reconstruction from Multiple Aerial Images in Dense Urban Areas", *IEEE Conference on Computer Vision and Pattern Recognition*, Vol. 1, pp. 262-267, 1999.

[Geman et al., 1992] D. Geman and G. Reynolds, "Constrained Restoration and the Recovery of Discontinuities" *IEEE Trans. Pattern Anal. Machine Intell.*, Vol. 14, pp. 367-383, 1992.

[Geman et al., 1995] D. Geman and C. Yang, "Nonlinear image recovery with half-quadratic regularization" *IEEE Trans. on Image Processing*, Vol. 4, No. 7, pp. 932-946, 1995.

[Groenigen, 2000] J. W. van Groenigen, "The influence of variogram parameters on optimal sampling schemes for kriging", *Geoderma*, Vol. 97, pp. 223-236, 2000.

[Guichard et al., 1998] F. Guichard, F. Malgouyres, "Total variation based interpolation", *Proceedings of the European Signal Processing Conference*, Vol. 3, pp. 1741-1744, 1998.

[Haala, Brenner, 1999] N. Haala, C. Brenner, "Extraction of buildings and trees in urban environments", *ISPRS Journal of Photogrammetry and Remote Sensing*, 54, pp. 130-137, 1999.

[Haala et al., 1996] N. Haala, M. Cramer, J. Kilian, "Sensor fusion for airborne 3D data capture", *Second International Airborne Remote Sensing Conference and Exhibition*, Vol. I, San Francisco, California, pp. 344-353, 1996.

[Hamilton, 2001] J.-Ch. Hamilton, "Archeops, mapping the CMB sky from large to small angular scales.", *Proceedings of TAUP2001 conference, LNGS, Italy*, 6 pages, 2001.

[Henrot-Versillé, 2003] S. Henrot-Versillé, "Archeops' results on the cosmic microwave background", *Proceeding of the Moriond ElectroWeak 2003 conference*, 6 pages, 2003.

[Jerri, 1977] A. J. Jerri, "The Shannon sampling theorem - its various extensions and applications: a tutorial review", *Proceedings of the IEEE*, Vol. 65, No. 11, pp. 1565-1596, 1977.

[Jerri, 1993] A. J. Jerri, "Error analysis in the application of generalizations of the sampling theorem", in R. J. Marks II, editor, *Advanced Topics in Shannon Sampling and Interpolation Theory*, Springer-Verlag, pp. 219-298, 1993.

[de Joinville, 2001] O. de Joinville, "Evaluation de la qualité d'une cartographie urbaine à l'aide d'images aériennes à haute résolution", Ph.D. thesis, TSI Department, ENST Paris, France, 2001.

[de Joinville, 2003] O. de Joinville, "Le levé laser aéroporté : techniques, applications et recherche", Bulletin d'Information de l'IGN n 74, pp. 37-52, 2003.

[Journel et al., 1978] A. G. Journel, C. J. Huijbregts, "Mining Geostatistics", *Academic Press*, 1978.

[Kaplan, 1996] E. D. Kaplan, "Understanding GPS: principles and applications", *Boston, MA: Artech House*, 1996.

[Kybic et al., 2002] J. Kybic, T. Blu, M. Unser, "Generalized sampling: a variational approach - part II: applications" *IEEE Trans. on Signal Processing*, Vol. 50, No. 8, pp. 1977-1985, 2002.

[Lemmens, 1997] M. J.P.M. Lemmens, "Accurate height information from airborne laser-altimetry", *Proceedings of International Geoscience and Remote Sensing Symposium*, Singapore, pp. 423-426, 1997.

[Leung et al., 2001] W.-Y. V. Leung, P. J. Bones, R. G. Lane, "Statistical interpolation of sampled images" *Optical Engineering*, Vol. 40, No. 4, pp. 547-553, 2001.

[Li, 1995] S. Li, "Markov Random Field Modeling in Computer Vision", *Springer*, 1995.

[Marks, 1991] R.J. Marks II, "Introduction to Shannon Sampling and Interpolation Theory", *Springer-Verlag*, 1991.

[Martin, 1998] R. J. Martin, "Irregularly sampled signals: theories and techniques for analysis", *Ph.D. thesis, University College London*, 158 pages, 1998.

[Marvasti, 1993] F. Marvasti, "Nonuniform sampling", in R. J. Marks II, editor, *Advanced Topics in Shannon Sampling and Interpolation Theory*, Springer-Verlag, pp. 121-156, 1993.

[Marvasti and Jain, 1986] F. Marvasti, A. K. Jain, "Zero crossings, bandwidth compression, and restoration of nonlinearly distorted band-limited signals", *Journal of the Optical Society of America A* , Vol. 3, No. 5, pp. 651-654, 1986.

[Mennella et al., 2002] A. Mennella, M. Bersanelli, C. Burigana et al., "PLANCK: systematic effects induced by periodic fluctuations of arbitrary shape", *Astronomy & Astrophysics*, Vol. 384, pp. 736-742, 2002.

[Mercer, 2001] B. Mercer, "Combining LIDAR and IfSAR: What can you expect?", *Photogrammetric Week 2001*, Dieter Fritsch and Rudolf Spiller, editors, Stuttgart, pp. 227-237, 2001.

[Morshed, 2000] A.H. Morshed, "Laser Altimetry and Its Application in Geographic Scanning", *17th National Radio Science Conference*, Minufiya, Egypt, pp. 298-311, February 2000.

[Murakami et al., 1998] H. Murakami, K. Nakagawa, T. Shibata, E. Iwanami, "Potential of an airborne laser scanner system for change detection of urban features and orthoimage development", *IAPRS*, Stuttgart, Vol. 32, Part 4, pp. 422-427, 1998.

[Nikolova, 2004] M. Nikolova, "A variational approach to remove outliers and impulse noise", *Journal of Mathematical Imaging and Vision*, Vol. 20, pp. 99-120, 2004.

[Nikolova, 2002] M. Nikolova, "Minimizers of cost-functions involving non-smooth data-fidelity terms. Application to the processing of outliers", *SIAM Journal on Numerical Analysis*, Vol. 40, No. 3, pp. 965-994, 2002.

[Nikolova, 2000] M. Nikolova, "Local strong homogeneity of a regularized estimator", *SIAM J. Appl. Math.*, Vol. 61, No. 2, pp. 633-658, 2000.

[Nikolova, 1999] M. Nikolova, "Markovian Reconstruction Using a GNC Approach" *IEEE Trans. on Image Processing*, Vol. 8, No. 9, pp. 1204-1220, 1999.

[Papoulis, 1977] A. Papoulis, "Generalized sampling expansion", *IEEE Transactions on Circuits and Systems*, Vol. CAS-24, No. 11, pp. 652-654, 1977.

[Park et al., 2000] S. C. Park, M. G. Kang, "Noise-adaptive edge-preserving image restoration algorithm" *SPIE Optical Engineering*, Vol. 39, No. 12, pp. 3124-3137, 2000.

[Petzold et al., 1999] B. Petzold, P. Reiss, W. Stössel, "Laser scanning - surveying and mapping agencies are using a new technique for the derivation of digital terrain models", *ISPRS Journal of Photogrammetry and Remote Sensing*, 54, pp. 95-104, 1999.

[Pham et al., 1999] T. D. Pham, M. Wagner, "Fuzzy kriging filter for image restoration ", *Knowledge-Based Intelligent Information Engineering Systems, 1999. Third International Conference*, pp. 333-336, 1999.

[Pham et al., 2000] T. D. Pham, M. Wagner, "Image restoration by fuzzy convex ordinary kriging", *International Conference on Image Processing, 2000*, Vol. 1, pp. 113-116, 2000.

[Picard et al., 1995] R. Picard and A. Pentland, "Temperature and Gibbs image modeling" Media Laboratory, Perceptual Computing 254, MIT, Cambridge, MA, 1995.

[Preparata et al., 1985] F. P. Preparata, M. I. Shamos, "Computational geometry: an introduction", *Springer*, 1985.

[Rauth, 1995] M. Rauth, "Application of 2D methods for scattered data approximation to geophysical data sets", *Proc. Conf. SampTA'95*, Jurmala, Latvia, pp. 38-43, 1995.

[Rauth, 1998] M. Rauth, "Gridding of Geophysical Potential Fields from Noisy Scattered Data", Ph.D. thesis, Department of Geophysics, University of Vienna, Austria, 1998.

[Roux et al., 1999] M. Roux, M. Fradkin and H. Maître, "Urban Areas Description using Multiple Aerial Images ", *SFPT Special Issue on 3D Geospatial Data Production: Meeting Application Requirements*, Vol. 153, pp. 36-45, 1999.

[Rudin et al., 1992] L. Rudin, S. Osher, E. Fatemi, "Nonlinear total variation based noise removal algorithms" *Physica D*, Vol. 60, pp. 259-268, 1992.

[Schenk, 2001] T. Schenk, "Modeling and analyzing systematic errors in airborne laser scanners", *Technical Notes in Photogrammetry No 19*, The Ohio State University, 46 pages, 2001.

[Schmidt, 1997] W. J. Schmidt, "On reconstruction of images from structured sampling sets: classification, morphology, TILS, POCS and applications", *Master's thesis, Dept. of Mathematics, University of Vienna*, 179 pages, 1997.

[Shannon, 1949] C. E. Shannon, "Communication in the presence of noise", *Proceedings of the IRE*, Vol. 37, No. 1, pp. 10-21, 1949.

[Sithole, Vosselman, 2004] G. Sithole, G. Vosselman. "Experimental comparison of filter algorithms for bare-Earth extraction from airborne laser scanning point clouds", *ISPRS Journal of Photogrammetry and Remote Sensing*, 59, pp. 85-101, 2004.

[Stark, 1993] H. Stark, "Polar, spiral, and generalized sampling and interpolation", in R. J. Marks II, editor, *Advanced Topics in Shannon Sampling and Interpolation Theory*, Springer-Verlag, pp. 185-218, 1993.

[Stoffel et al., 2001] A. Stoffel, A. Zergaïnoh, C. Kulcsár, J.-P. Astruc, "The importance of edges in irregular subsampling" *International Symposium on Signal Processing and its Applications (ISSPA)*, pp. 565-568, 2001.

[Strohmer, 1991] T. Strohmer. "Irregular sampling, frames and pseudoinverse", *Master's thesis, Dept. of Mathematics, University of Vienna*, 84 pages, 1991.

[Strohmer, 1997] T. Strohmer, "Computationally attractive reconstruction of bandlimited images from irregular samples", *IEEE Transactions on Image Processing*, Vol. 6, No. 4, pp. 540-548, 1997.

[Sweldens, 1997] W. Sweldens. "The lifting scheme: a construction of second generation wavelets", *SIAM Journal on Mathematical Analysis*, Vol. 29, No. 2, pp. 511-546, 1998.

[Unser, 2000] M. Unser, "Sampling - 50 years after Shannon", *Proceedings of the IEEE*, Vol. 88, No. 4, pp. 569-587, 2000.

[Unser, 1999] M. Unser, "Splines: a perfect fit for signal and image processing", *IEEE Signal Processing Magazine*, Vol. 16, No. 6, 1999.

[Unser, 1994] M. Unser, A. Aldroubi. "A general sampling theory for noniddeal acquisition devices", *IEEE Transactions on Signal Processing*, Vol. 42, No. 11, pp. 2915-2925, 1994.

[Unser et al., 1998] M. Unser, J. Zerubia, "A generalized sampling theory without band-limiting constraints", *IEEE Transactions on Circuits and Systems II: Analog and Digital Signal Processing*, Vol. 45, No. 8, pp. 679-692, 1998.

[Vaidyanathan, 2001] P. P. Vaidyanathan, "Generalizations of the sampling theorem: seven decades after Nyquist", *IEEE Transactions on Circuits and Systems I: Fundamental Theory and Applications*, Vol. 48, No. 9, pp. 1094-1109, 2001.

[Vio et al., 2003] R. Vio, J. Nagy, L. Tenorio et al., "Digital Deblurring of CMB Maps II: Asymmetric Point Spread Function", *Astronomy & Astrophysics*, Vol. 408, pp. 835–843, 2003.

[Wang, 1998] Z. Wang, "Extracting building information from LIDAR data", *ISPRS Proceedings of Commission III Symposium on Object Recognition and Scene Classification from Multispectral and Multisensor Pixels*, Columbus, Ohio, Vol. 32 Part 3/1, pp. 279-284, 1998.

[Watson, 1992] D. F. Watson, "Contouring: a guide to the analysis and display of spatial data", *Pergamon Press*, 1992.

[Wehr, Lohr, 1999] A. Wehr, U. Lohr, "Airborne laser scanning - an introduction and overview", *ISPRS Journal of Photogrammetry and Remote Sensing*, 54, pp. 68-82, 1999.

[Zhao et al., 2002] R. L. Zhao, J. Chen, Z. L. Li, C. M. Gold, "A Voronoi k-order approach for digital elevation model (DEM) interpolation", *International Archives of the Photogrammetry, Remote Sensing and Spatial Information Sciences*, 34(5W3) (on CD-ROM). Accessed August 10th, 2004. Available at: http://www.acrors.ait.ac.th/kunming/proceedings.htm.

[Zinger et al., 2002] S. Zinger, M. Nikolova, M. Roux, and H. Maître, "3D resampling for airborne laser data of urban areas", *ISPRS Symposium PCV'02, Graz (Austria)*, vol. XXXIV, part 3A, pp. 418-423, 2002.

[Zinger et al., 2003] S. Zinger, M. Nikolova, M. Roux, and H. Maître, "Rééchantillonnage de données 3D laser aéroporté en milieu urbain", *ORASIS 2003, Congrès Francophone de Vision par Ordinateur, Gérardmer (France)*, pp. 75-82, 2003.